

Some pages of this thesis may have been removed for copyright restrictions.

If you have discovered material in Aston Research Explorer which is unlawful e.g. breaches copyright, (either yours or that of a third party) or any other law, including but not limited to those relating to patent, trademark, confidentiality, data protection, obscenity, defamation, libel, then please read our [Takedown policy](#) and contact the service immediately (openaccess@aston.ac.uk)

METHYL CHLORIDE PURIFICATION FOR THE SILICONE INDUSTRY

JAI BIPIN LAD

Doctor of Philosophy

ASTON UNIVERSITY

JULY 2015

© Jai Bipin Lad, 2015

Jai Bipin Lad asserts his moral right to be identified as the author of this thesis.

This copy of the thesis has been supplied on condition that anyone who consults it is understood to recognise that its copyright rests with its author and that no quotation from the thesis and no information derived from it may be published without appropriate permission or acknowledgement.

METHYL CHLORIDE PURIFICATION FOR THE SILICONE INDUSTRY

JAI BIPIN LAD

Doctor of Philosophy

THESIS SUMMARY

This study experimentally investigated methyl chloride (MeCl) purification method using an in-house designed and built volumetric adsorption/desorption rig. MeCl is an essential raw material in the manufacture of silicone however all technical grades of MeCl contain concentrations (0.2 - 1.0 % wt) of dimethyl ether (DME) which poison the process. The project industrial partner had previously exhausted numerous separation methods, which all have been deemed not suitable for various reasons. Therefore, adsorption/desorption separation was proposed in this study as a potential solution with less economic and environmental impact. Pure component adsorption/desorption was carried out for DME and MeCl on six different adsorbents namely: zeolite molecular sieves (types 4 Å and 5 Å); silica gels (35-70 mesh, amorphous precipitated, and 35-60 mesh) and granular activated carbon (type 8-12 mesh). Subsequent binary gas mixture adsorption in batch and continuous mode was carried out on both zeolites and all three silica gels following thermal pre-treatment in vacuum. The adsorbents were tested as received and after being subjected to different thermal and vacuum pre-treatment conditions. The various adsorption studies were carried out at low pressure and temperature ranges of 0.5 - 3.5 atm and 20 - 100 °C.

All adsorbents were characterised using Brunauer Emmett Teller (BET), thermogravimetric analysis (TGA), scanning electron microscopy (SEM) and energy dispersive x-ray analysis (EDXA) to investigate their physical and chemical properties. The well-known helium (He) expansion method was used to determine the empty manifold and adsorption cell (AC) regions and respective void volumes for the different adsorbents. The amounts adsorbed were determined using Ideal gas laws via the differential pressure method. The heat of adsorption for the various adsorbate-adsorbent (A-S) interactions was calculated using a new calorimetric method based on direct temperature measurements inside the AC. Further adsorption analysis included use of various empirical and kinetic models to determine and understand the behaviour of the respective interactions. The gas purification behaviour was investigated using gas chromatography and mass spectroscopy (GC-MC) analysis. Binary gas mixture samples were syringed from the manifold

and AC outlet before and after adsorption/desorption analysis through manual sample injections into the GC-MS to detect and quantify the presence of DME and ultimately observe for methyl chloride purification. Convincing gas purification behaviour was confirmed using two different GC columns, thus giving more confidence on the measurement reliability.

From the single pure component adsorption of DME and MeCl on the as received zeolite 4A subjected to 1 h vacuum pre-treatment, both gases exhibited pseudo second order adsorption kinetics with DME exhibiting a rate constant nearly double that of MeCl thus suggesting a faster rate of adsorption. From the adsorption isotherm classification both DME and MeCl exhibited Type II and I adsorption isotherm classifications, respectively. The strength of bonding was confirmed by the differential heat of adsorption measurement, which was found to be 23.30 and 10.21 kJ mol⁻¹ for DME and MeCl, respectively. The former is believed to adsorb heterogeneously through hydrogen bonding whilst MeCl adsorbs homogeneously via van der Waal's (VDW) forces. Single pure component adsorption on as received zeolite 5A, silica gels (35-70, amorphous precipitated and 35-60) resulted in similar adsorption/desorption behaviour in similar quantities (mol kg⁻¹). The adsorption isotherms for DME and MeCl on zeolite 5A, silica gels (35-70, amorphous precipitated and 35-60) and activated carbon 8-12 exhibited Type I classifications, respectively. Experiments on zeolite 5A indicated that DME adsorbed stronger, faster and with a slightly stronger strength of interaction than MeCl but in lesser quantities. On the silica gels adsorbents, DME exhibited a slightly greater adsorption capacity whilst adsorbing at a similar rate and strength of interaction compared to MeCl. On the activated carbon adsorbent, MeCl exhibited the greater adsorption capacity at a faster rate but with similar heats of adsorption.

The effect of prolonged vacuum (15 h), thermal pre-treatment (150 °C) and extended equilibrium time (15 min) were investigated for the adsorption behaviour of DME and MeCl on both zeolites 4A and 5A, respectively. Compared to adsorption on as received adsorbents subjected to 1 h vacuum the adsorption capacities for DME and MeCl were found to increase by 1.95 % and 20.37 % on zeolite 4A and by 4.52 % and 6.69 % on zeolite 5A, respectively. In addition the empirical and kinetic models and differential heats of adsorption resulted in more definitive fitting curves and trends due to the true equilibrium position of the adsorbate with the adsorbent.

Batch binary mixture adsorption on thermally and vacuum pre-treated zeolite 4A demonstrated purification behaviour of all adsorbents used for MeCl streams containing DME impurities, with a concentration as low as 0.66 vol. %. The GC-MS analysis showed no DME detection for the tested concentration mixtures at the AC outlet after 15 or 30 min, whereas MeCl was detectable in measurable amounts. Similar behaviour was also observed when carrying out adsorption in continuous mode. On the other hand, similar studies on the other adsorbents did not show such favourable MeCl purification behaviour.

Overall this study investigated a wide range of adsorbents (zeolites, silica gels and activated carbon) and demonstrated for the first time potential to purify MeCl streams containing DME impurities using adsorption/desorption separation under different adsorbent pre-treatment and adsorption operating conditions. The study also revealed for the first time the adsorption isotherms, empirical and kinetic models and heats of adsorption for the respective adsorbent-surface (A-S) interactions.

In conclusion, this study has shown strong evidence to propose zeolite 4A for adsorptive purification of MeCl. It is believed that with a technical grade MeCl stream competitive yet simultaneous co-adsorption of DME and MeCl occurs with evidence of molecular sieving effects whereby the larger DME molecules are unable to penetrate through the adsorbent bed whereas the smaller MeCl molecules diffuse through resulting in a purified MeCl stream at the AC outlet. Ultimately, further studies are recommended for increased adsorption capacities by considering wider operating conditions, e.g. different adsorbent thermal and vacuum pre-treatment and adsorbing at temperatures closer to the boiling point of the gases and different conditions of pressure and temperature.

I would like to dedicate this thesis to my family, especially my parents whom have supported me unconditionally throughout. Without your patience, understanding and most of all love this would not have been possible.

ACKNOWLEDGEMENTS

OM NAMAH SHIVAYA

ॐ नमः शिवाय

First and foremost I am indebted to the Divine Holy Trinity: Brahma, Vishnu and Shiva.

I would like to express my sincerest gratitude to my supervisor and guru Dr Yassir Makkawi for his relentless support, expert guidance, understanding and inspiration throughout my research. Without him I would never have had the opportunity to fulfil my dream of someday becoming a doctor. I attribute a large part of this work to him, without him this would not have been possible. I could not have wished for a better, kinder, supportive and admirable supervisor.

I would like to thank Dow Corning Limited for allowing me to undertake such an interesting and exciting project with such potential. I would like to give my sincere thanks to Dr Simon Acey for his continued support, supervision and confidence in me over the course of the research especially during difficult times; it was a pleasure working with you. My additional thanks go to Dave Crosby for his support over the project.

My deepest thanks to a friend and former MEng supervisor Dr Daniel Nowakowski for his counsel, support and assistance during difficult times, technically and practically. I would like to give my thanks to former and current associate supervisors Dr James Titiloye and Prof. Karen Wilson, for their support at times of need and use of their analytical equipment.

My additional thanks go to Surila Darbar for her advice, support and assistance at difficult times in the laboratory. Fellow PhD colleges and post doctorates for their knowledge, support and assistance from time to time. Without our shared experiences this journey would be incomplete.

Finally I would like to give the utmost gratitude to my family and friends for supporting and encouraging me continuously throughout all my studies.

LIST OF CONTENTS

THESIS SUMMARY	ii
ACKNOWLEDGEMENTS	vi
LIST OF CONTENTS	vii
LIST OF PUBLICATIONS	xii
NOMENCLATURE.....	xiii
LIST OF FIGURES	xviii
LIST OF TABLES	xxiii
CHAPTER I: INTRODUCTION, AIM AND OBJECTIVES	25
1.1 Problem at hand	25
1.2 Company expectation.....	26
1.3 Proposed problem solution.....	26
1.4 Objectives.....	28
1.5 Description of thesis chapters	29
CHAPTER II: LITERATURE REVIEW.....	31
2.1 General background on dimethyl ether (DME) and methyl chloride (MeCl)	32
2.1.1 Dimethyl ether (DME)	32
2.1.2 Methyl chloride (MeCl)	32
2.2 Adsorption.....	33
2.3 Adsorption fundamentals	34
2.3.1 Adsorbate-adsorbent (A-S) interactions.....	36
2.3.2 Factors affecting adsorption.....	38
2.3.3 Adsorbent structure and functional groups	39
2.4 Types of adsorbents.....	40
2.4.1 Silica gel.....	41
2.4.2 Activated carbon	42
2.4.3 Zeolites	43
2.4.4 Activated alumina	45
2.5 Adsorption equilibria and isotherms	46

2.5.1	Langmuir model	49
2.5.2	Freundlich model	50
2.5.3	Sips model.....	50
2.5.4	Tóth model	51
2.5.5	Brunauer Emmett Teller (BET) model.....	51
2.5.6	Adsorption potential.....	51
2.5.7	Dubinin equations	52
2.6	Adsorption kinetics and models.....	53
2.6.1	Pseudo first order model	54
2.6.2	Pseudo second order model.....	54
2.6.3	Elovich model	55
2.6.4	Intraparticle diffusion (IPD) model.....	55
2.6.5	Intraparticle diffusion (IPD) versus surface resistance layering	56
2.7	Heat of adsorption	56
2.8	Industrial applications of adsorption/desorption separation.....	58
CHAPTER III: EXPERIMENTAL.....		59
3.1	Literature review	59
3.1.1	Experimental adsorption analysis.....	59
3.1.2	Volumetric adsorption: system and void volumes (V_0).....	60
3.2	Experimental	63
3.2.1	Apparatus for adsorption.....	63
3.2.2	Adsorbate gases.....	66
3.2.3	Adsorbents	68
3.3	Estimation of empty manifold (V_M) and adsorption cell (AC) volumes	70
3.3.1	Helium (He) expansion method	70
3.3.2	Determination of particle (glass beads) density	72
3.4	Estimation of the void volume (V_0) in the adsorption cell (AC)	73
3.5	Pure component adsorption/desorption.....	74
3.5.1	Sievert method	75

3.5.2	Differential pressure method.....	76
3.5.3	Determination of adsorption and desorption isotherms	77
3.5.4	Calorimetric heat of adsorption.....	78
3.6	Results and discussion.....	81
3.6.1	Experimental determination of the empty manifold and adsorption cell (AC) volumes	81
3.6.2	Empty adsorption cell (AC) validation for pure component dimethyl ether (DME) and methyl chloride (MeCl) adsorption	82
3.6.3	Experimental void volume (V_0) determination.....	82
CHAPTER IV: CHARACTERISATION OF ADSORBENTS.....		85
4.1	Background and literature review	85
4.1.1	Adsorbent characterisation techniques.....	85
4.1.2	Determination of porosity: mercury intrusion porosimetry (MIP) and Brunauer Emmett Teller (BET) analysis	85
4.1.3	Scanning electron microscopy (SEM) and energy dispersive x-ray analysis (EDXA)	86
4.1.4	Thermogravimetric analysis (TGA).....	87
4.1.5	Fourier transform infra-red (FTIR)	89
4.1.6	Gas chromatography and mass spectrometry (GC-MS) analysis.....	90
4.2	Results and discussion.....	92
4.2.1	Brunauer Emmett Teller (BET) analysis.....	92
4.2.2	Scanning electron microscopy (SEM) and energy dispersive x-ray analysis (EDXA)	93
4.2.3	Thermogravimetric (TGA) analysis	96
4.2.4	Gas chromatography and mass spectrometry (GC-MS) analysis.....	100
4.3	Summary	101
CHAPTER V: PURE COMPONENT DME AND MECL ADSORPTION/DESORPTION ON DIFFERENT ADSORBENTS.....		102
5.1	Introduction.....	102
5.2	Literature review	103

5.2.1	Reported studies on dimethyl ether (DME) and methyl chloride (MeCl) adsorption/desorption separation	103
5.2.2	Adsorption/desorption using zeolites	104
5.2.3	Adsorption/desorption using silica gels	109
5.2.4	Adsorption/desorption on other adsorbents.....	112
5.2.5	Theoretical comparison: dimethyl ether (DME) versus methyl chloride (MeCl)	113
5.3	Results and discussion.....	117
5.3.1	Pure component adsorption/desorption of dimethyl ether (DME) and methyl chloride (MeCl) on zeolites 4A and 5A	117
5.3.2	Pure component adsorption/desorption of dimethyl ether (DME) and methyl chloride (MeCl) on silica gels	136
5.3.3	Pure component adsorption/desorption of dimethyl ether (DME) and methyl chloride (MeCl) on activated carbon.....	149
5.3.4	Overall sorption error	156
5.4	Summary	158
CHAPTER VI: EFFECT OF PRE-TREATMENT AND EQUILIBRIUM TIME ON ADSORPTION ISOTHERMS.....		160
6.1	Introduction.....	160
6.2	Results and discussion.....	161
6.2.1	Effect of vacuum, thermal pre-treatment and longer equilibrium to pure component DME and MeCl adsorption isotherms on zeolites 4A and 5A	161
6.3	Summary	178
CHAPTER VII: BINARY ADSORPTION OF MECL: DME MIXTURES ON DIFFERENT ADSORBENTS		180
7.1	Binary gas adsorption literature	180
7.1.1	Reported dimethyl ether (DME) and methyl chloride (MeCl) desorption	182
7.1.2	Reported dimethyl ether (DME) conversion to methyl chloride (MeCl)	183
7.2	Experimental	183
7.2.1	Gas chromatography and mass spectrometry (GC-MS) analysis.....	183
7.2.2	Quantification and calibration curves	184

7.2.3	Binary adsorption	186
7.2.4	Batch mode fixed bed binary adsorption.....	187
7.2.5	Continuous flow binary adsorption.....	188
7.3	Results and discussion.....	189
7.3.1	Calibration curves	189
7.3.2	Batch binary mixture expansion into an empty adsorption cell (AC).....	195
7.3.3	Continuous flow of a binary mixture into an adsorption cell (AC) filled with glass beads	196
7.3.4	Batch fixed bed binary gas adsorption	197
7.3.5	Continuous flow of binary mixtures.....	205
7.3.6	Desorption	219
7.4	Summary	221
CHAPTER VIII: CONCLUSIONS.....		223
CHAPTER IX: FUTURE WORK AND RECOMMENDATIONS		226
REFERENCES.....		229

LIST OF PUBLICATIONS

Published journal article

Lad, J.B. and Makkawi, Y.T. Adsorption of dimethyl ether (DME) on zeolite molecular sieves.
Chemical Engineering Journal, 2014. 256(0): p. 335-346

NOMENCLATURE

Abbreviations

A-A	Adsorbate-adsorbate interactions
A-Al	Adsorbate-Aluminium functional group interaction
A-H ₂ O	Molecular adsorbate-water interaction
AES	Auger electron spectroscopy
A-S	Adsorbate-solid/adsorbent interactions
A-Si	Adsorbate-Silanol functional group interaction
BET	Brunauer-Emmett-Teller
BJH	Barrett-Joyner-Halenda method
BSE	Back-scattered electrons
BSI	British Standards Institute
CMS	Carbon molecular sieves
DA	Dubinin-Astakhov method
DFB	Dual fluidised bed
DFT	Density Functional Theory method
DH	Dollimore Heal method
DME	Dimethyl ether / methoxymethane / methyl ether / CH ₃ OCH ₃
DME-DME	DME-DME molecule interaction
DME-H ₂ O	Molecular DME-water interaction
DR	Dubinn-Radushkevich method
EELS	Electron energy loss spectroscopy
EPSRC	Engineering and physical sciences research council
ESCA	Electron spectroscopy for chemical analysis
EXAFS	Extended x-ray absorptive fine structure
EDXA	Energy dispersive x-ray analysis
FHH	Frenkel-Halsey-Hill method
GAC	Granular activated carbon
GC-MS	Gas chromatography and mass spectrometry
HK	Horvath-Kawazoe method
INS	Ion neutron spectroscopy
IPD	Intraparticle diffusion
IR	Infra-red spectroscopy
IRA	Infrared reflection adsorption
ISS	Ion scattering spectroscopy
IUPAC	International Union of Pure and Applied Chemistry

LEED	Low energy electron diffraction
LPDME	Liquid phase dimethyl ether
LPG	Liquefied petroleum gas
MARS	Mechanically agitated slurry reactor
MeCl	Methyl chloride / chloromethane / CH_3Cl
MeCl-MeCl	MeCl-MeCl molecule interaction
MeCl-H ₂ O	Molecular MeCl-water interaction
MIP	Mercury intrusion porosimetry
MSDS	Materials safety data sheet
MTZ	Mass transfer zone
PAC	Powdered activated carbon
PSA	Pressure swing adsorption
PSD	Pressure swing desorption
RLEED	Reflection low energy electron diffraction
RMM	Relative molecular mass
SE	Secondary electrons
SEM	Scanning electron microscopy
SF	Saito-Foley method
SIMS	Secondary ion mass spectroscopy
SMB	Stimulated moving bed
STM	Scanning tunnelling microscopy
TCD	Thermal conductivity detector
TGA	Thermogravimetric analysis
TPD	Temperature programmed desorption
TPO	Temperature programmed oxidation
TPSA	Temperature-pressure swing adsorption
TSA	Temperature swing adsorption
TSD	Temperature swing desorption
VA	Variable area
VDW	Van der Waal's forces
VSA	Vacuum swing adsorption
XPS	X-ray photoelectron spectroscopy

Symbols and letters

\AA	Angstroms
A	Heat transfer area (m^2)
AC	Adsorption cell
b	Empirical parameter (Langmuir, Sips and Tóth models)
C	Concentration (mol L^{-1})
C_{act}	Actual concentration of mixture from calibration curve (vol. %)
C_{BET}	BET constant (-)
C_{h}	Constant for natural convection from a vertical heat plated (0.10)
C_{IPD}	IPD model constant (-)
$C_{\text{p g}}$	Specific heat capacity of adsorbate gas (kJ)
$C_{\text{p s}}$	Specific heat capacity of solid/adsorbent (kJ)
$C_{\text{p th}}$	Specific heat capacity of thermocouple rod (kJ)
C_{p}	Specific heat capacity ($\text{kJ kg}^{-1} \text{K}^{-1}$)
C_{pred}	Predicted concentration using Ideal gas laws (vol. %)
C_{s}	Concentration of adsorbate in solid phase (mol L^{-1})
E	Characteristic adsorption energy for DA equation (kJ mol^{-1})
e	Voidage (-)
$-E_{\text{a}}$	Activation energy (kJ mol^{-1})
F	Flowmeter (ml min^{-1})
g	Gravitational acceleration (m s^{-2})
Gr	Grashof's Number (-)
GC-Col-1	GC column which separates molecules through volatility
GC-Col-2	GC column which separates molecules through polarity
h	Heat transfer coefficient ($\text{W m}^{-2} \text{K}^{-1}$)
h_{c}	Cumulative calorimetric heat of adsorption (kJ mol^{-1})
k	Thermal conductivity ($\text{W m}^{-1} \text{K}^{-1}$)
k''_{ads}	Pseudo second order adsorption rate constant ($\text{mol kg}^{-1} \text{s}^{-1}$)
k'_{ads}	Pseudo first order adsorption rate constant (s^{-1})
k_{IPD}	IPD rate constant ($\text{mol kg}^{-1} \cdot \text{mol}^{-1/2}$)
K	Empirical parameter (Freundlich model)
L	Height of vertical surface (m)
m_{f}	Mass of adsorbent in the final stage using Sievert method (kg)
$m_{\text{g ads}}$	Mass of adsorbed adsorbate (kg)
$m_{\text{g free}}$	Mass of free non-adsorbed adsorbate (kg)
m_{i}	Mass of adsorbent (kg)

m_s	Mass of adsorbent / solid (kg)
MV	Manual valve
n_{ads}	Amount adsorbed (mol kg ⁻¹)
n/n_{max}	Fractional coverage (-)
n_s	Amount adsorbed in monolayer (mol kg ⁻¹)
Nu	Nusselt's number (-)
P	Pressure (psiA or atm)
P	Pressure gauge (psiA)
P/P_0	Relative pressure (-)
P_{AC}	Pressure in AC (psiA, atm)
P_{M}	Pressure in manifold (psiA, atm)
Pret-	Thermally pre-treated adsorbent at 150 °C in vacuum for 15 h
Pr	Prandtl's number (-)
P_r	Reduced pressure (atm)
Q_{diff}	Differential heat of adsorption (kJ)
q_e	Amount adsorbed at equilibrium (mol kg ⁻¹)
$Q_{\text{g ads}}$	Heat gained by adsorbed gas (kJ)
$Q_{\text{g free}}$	Heat gained by free non-adsorbed adsorbate (kJ)
Q_{g}	Heat gained by adsorbate in AC (kJ)
Q_{int}	Integral heat of adsorption (kJ)
Q_{loss}	Heat loss (kJ)
Q_s	Heat gained by adsorbent (kJ)
q_s	Theoretical isotherm saturation capacity (mol kg ⁻¹)
Q_{th}	Heat gained by the thermocouple rod (kJ)
R	Universal gas constant
R^2	Coefficient of determination (-)
Ra	Rayleigh's number (-)
t	Empirical fitting parameter (Freundlich, Sips and Tóth Models)
T_{AC}	Temperature in AC (°C / K)
t_{ads}	Adsorption time (s)
T_{amb}	Ambient room temperature (°C / K)
T_{b}	Temperature inside AC (°C / K)
T_{M}	Temperature in manifold (°C / K)
t_{max}	Time for maximum temperature peak from adsorption (s)
T_r	Reduced temperature (K)
T_{Ref}	Reference temperature

$T_{W \text{ inside}}$	Temperature of wall inside AC ($^{\circ}\text{C}$ / K)
V_0	Void volume (L)
VA	Variable area
V_{AC}	Volume of AC (L)
$V_{\text{adsorbent}}$	Volume of adsorbent (L)
V_{gb}	Volume of glass beads (L)
V_M	Volume of manifold (L)
VP	Vacuum pump (Torr. / atm)
V_s	Volume of solid (L)
z	Compressibility factor (-)
Z^0	Coefficient for compressibility factor determination (-)
Z^1	Coefficient for compressibility factor determination (-)

Greek symbols

α	Elovich initial adsorption rate constant ($\text{mol kg}^{-1} \text{ min}^{-1}$)
β_E	Related to the extent of surface coverage and $-E_a$, Elovich model (kg mol^{-1})
β_M	Affinity coefficient, related to the A-S interaction (-)
β_{Ra}	Thermal expansion coefficient (-)
γ	Constant for natural convection from a vertical heated plate (0.33)
ΔH_{ads}	Heat of adsorption (kJ mol^{-1})
Δn	Adsorption uptake (mol kg^{-1})
Δn^{ex}	Surface excess adsorption (mol kg^{-1})
ε	Adsorption potential (kJ mol^{-1})
μ	Dynamic viscosity ($\text{m}^2 \text{ s}^{-1}$)
ρ	Density (kg m^{-3})
ϕ_D	Dispersion energy (kJ mol^{-1})
$\phi_{F-\mu}$	Field dipole interaction (kJ mol^{-1})
ϕ_R	Close range repulsion (kJ mol^{-1})
ϕ_{SP}	Self-potential for A-A interactions (kJ mol^{-1})
ϕ_{total}	Total potential energy (kJ mol^{-1})
$\phi_{\delta \text{ F-Q}}$	Field gradient quadrupole interaction (kJ mol^{-1})
ω	Acentric factor (-)

LIST OF FIGURES

Fig. 1.1. Vapour liquid equilibrium curve for MeCl and DME	26
Fig. 1.2. Proposed MeCl purification using a DFB adsorption process.....	27
Fig. 2.1. Adsorption steps: adsorbate molecules interacting with an adsorbent surface and pores (Obtained from: [19]).....	35
Fig. 2.2. Silica gel surface: silanol groups forming hydrogen bonds.....	41
Fig. 2.3. Line representations of zeolite structures: a) sodalite cage or β -cage or truncated octahedron; b) type A zeolite “unit cell”; c) types X and Y, or faujasite; d) cation sites in type A (8 in I, 3 in II and 12 III sites per unit cell; e) cation sites in types X and Y (16 I, 32 I', 32 II, 32 II', 48 III and 32 III sites per unit cell) (Obtained from: Yang, [2])	45
Fig. 2.4. Types of adsorption isotherms according to the International Union of Pure and Applied Chemistry (IUPAC) (Obtained and modified from: [31])	47
Fig. 2.5. Individual steps of a simple heterogeneous A-S interaction (A_1 - A_2) carried out on a porous adsorbent (Obtained and modified from: [38])	53
Fig. 3.1. The different types of volumes associated with solid particles (Obtained from: [61]).	60
Fig. 3.2. The reported adsorption correction factor for experimental hydrogen adsorption on activated carbon using the Sieverts method (Obtained from: [68])	62
Fig. 3.3. Simplified process flow diagram for adsorption/desorption system volumes	63
Fig. 3.4. AC assembly and dimension drawing (Obtained and supplied: HEL group Ltd, UK)	64
Fig. 3.5. Image of experimental set-up	65
Fig. 3.6. Gas stations used to dose gaseous DME and MeCl to the adsorption/desorption rig ..	66
Fig. 3.7. Physical appearance of the different adsorbents used	68
Fig. 3.8. Reported static-bed void fraction as function of particle size (Reproduced from: [75])	74
Fig. 3.9. An example of the variation in temperature and pressure inside the AC during experimental DME adsorption on as received zeolite 5A subjected to 1 h vacuum pre-treatment	78
Fig. 3.10. An example of the experimentally calculated heat transfer for the adsorption of DME on as received zeolite 5A subjected to 1 h vacuum pre-treatment when $\theta = 0.75$	80
Fig. 3.11. The volume ratios for empty manifold and AC volumes, $x_1=V_M/V_{AC}$	81
Fig. 3.12. Empty AC isotherms at 20 °C for pure component a) DME and (b) MeCl	82
Fig. 3.13. a) The ratio of manifold volume to adsorbent void volume versus gas expansion pressure and b) adsorption isotherms at 20 °C for He, N ₂ , and Ar on zeolite 5A	83
Fig. 4.1. The different functional groups on silicas	88

Fig. 4.2. GC-MS illustration	90
Fig. 4.3. SEM images at low and high magnification for: a, b) 4A; c, d) 5A; e, f) Si35-60 and g, h) AC.....	94
Fig. 4.4. TGA for a) mass and b) derivative weight loss versus temperature for zeolites 4A and 5A.....	97
Fig. 4.5. TGA for a) mass and b) derivative weight loss versus temperature for Si35-70, SiAmor and Si35-60	99
Fig. 4.6. TGA for mass and derivative weight loss versus temperature for AC8-12.....	100
Fig. 5.1. Flow Diagram for separation & recovery of MeCl from vent streams of isobutane (Reproduced from: [69])	109
Fig. 5.2. Adsorption/desorption isotherms for DME at 248.2 K on A, 240; B, 500; C, 700 & D, 900 °C (Obtained from: [100]).....	110
Fig. 5.3. Schematic representation of adsorption structures of DME on Cu(111) and Ag(111) surfaces Obtained from: [105])	112
Fig. 5.4. Zeolite surface hydroxyls interacting molecularly with a water, DME and MeCl molecule	115
Fig. 5.5. Pure component DME and MeCl adsorption isotherms on 4A at 20 °C	117
Fig. 5.6. Pure component DME and MeCl adsorption isotherms on 5A at 20 °C	118
Fig. 5.7. Pure component empirical adsorption models for a) DME on 4A; b) MeCl on 4A; c) DME on 5A and d) MeCl on 5A.....	119
Fig. 5.8. Pure component adsorption uptake trends for DME and MeCl on a) 4A; b) 5A	120
Fig. 5.9. Adsorption isotherms fitted to Freundlich model at 20, 30 and 40 °C for pure component DME on a) 4A and (b) 5A and MeCl on c) 4A and d) 5A.....	122
Fig. 5.10. Dependence of the Freundlich model parameter, K , on temperature for pure component adsorption of a) DME and b) MeCl on 4A and 5A.....	123
Fig. 5.11. Adsorption and desorption isotherms for pure component a) DME and b) MeCl on 4A at 20 °C.....	124
Fig. 5.12. Adsorption and desorption isotherms for pure component a) DME and b) MeCl on 5A at 20 °C	124
Fig. 5.13. Pure component adsorption mechanisms for DME and MeCl on zeolite 4A where a) and c) represent intracrystalline diffusion controlled adsorption in a short time scale and b) and d) represent surface resistance layering in a long time scale at 2.0 atm and 3.0 atm.....	130
Fig. 5.14. Pure component adsorption mechanisms for DME and MeCl on zeolite 5A where a) and c) represent intracrystalline diffusion controlled adsorption in a short time scale and b) and d) represent surface resistance layering in a long time scale at 2.0 atm and 3.0 atm.....	132
Fig. 5.15. Differential heat of adsorption for pure component DME and MeCl on a) 4A and b) 5A with corresponding isotherms to show adsorbent saturation points.....	134

Fig. 5.16. Pure component adsorption isotherms for DME and MeCl on a) Si35-70, b) SiAmor and c) Si35-60	137
Fig. 5.17. Pure component adsorption uptake points for DME and MeCl on a) Si35-70, b) SiAmor and c) Si35-60	139
Fig. 5.18. Pure component adsorption mechanisms for DME and MeCl on Si35-70 where a) and c) represent intracrystalline diffusion controlled adsorption in a short time scale and b) and d) represent surface resistance layering in a long time scale at 2.0 atm and 3.0 atm	145
Fig. 5.19. Pure component adsorption mechanisms for DME and MeCl on SiAmor where a) and c) represent intracrystalline diffusion controlled adsorption in a short time scale and b) and d) represent surface resistance layering in a long time scale at 2.0 atm and 3.0 atm	146
Fig. 5.20. Pure component adsorption mechanisms for DME and MeCl on Si35-60 where a) and c) represent intracrystalline diffusion controlled adsorption in a short time scale and b) and d) represent surface resistance layering in a long time scale at 2.0 atm and 3.0 atm	147
Fig. 5.21. Differential heat of adsorption for pure component DME and MeCl on a) Si35-70; b) SiAmor and c) Si35-60	148
Fig. 5.22. Pure component DME and MeCl adsorption isotherms on AC8-12 at 20 °C	149
Fig. 5.23. Pure component adsorption and desorption isotherms at 20 °C for a) DME and b) MeCl on AC8-12	151
Fig. 5.24. Pure component adsorption mechanisms for DME and MeCl on AC8-12 where a) and c) represent intracrystalline diffusion controlled adsorption in a short time scale and b) and d) represent surface resistance layering in a long time scale at 2.0 atm and 3.0 atm	154
Fig. 5.25. a) Differential and b) integral heat of adsorption for pure component DME and MeCl on AC8-12 at 20 °C	155
Fig. 5.26. Experiment error bars for pure component DME adsorption isotherms at room temperature, 20 °C on a) 4A and b) 5A	157
Fig. 6.1. Effect of longer vacuum and thermal pre-treatment with combined longer vacuum, thermal pre-treatment and extended equilibrium time for the pure component adsorption isotherms of a) DME and b) MeCl on Pret-4A	162
Fig. 6.2. Effect of longer vacuum and thermal pre-treatment with combined longer vacuum, thermal pre-treatment and extended equilibrium time for the pure component adsorption isotherms of a) DME and b) MeCl on Pret-5A	164
Fig. 6.3. Pure component adsorption isotherms for DME and MeCl at 20 °C for 5 min versus 15 min equilibrium time on a) Pret-4A and b) Pret-5A	166
Fig. 6.4. Pure component empirical adsorption models at 20 °C for a) DME on Pret-4A; b) MeCl on Pret-4A; c) DME on Pret-5A and MeCl on Pret-5A	167
Fig. 6.6. Pure component adsorption mechanism for DME and MeCl on Pret-4A-15 where a) and c) represent IPD controlled adsorption in a short time scale and b) and d) represent surface resistance layering in a long time scale	174

Fig. 6.7. Adsorption mechanism for pure component DME and MeCl on Pret-5A-15 where a) and c) represent IPD controlled adsorption in a short time scale and b) and d) represent surface resistance layering in a long time scale.....	175
Fig. 6.8. Heat of adsorption for DME and MeCl where a) and c) represents differential heats and b) and d) represent integral heats for Pre-4A and Pret-5A.....	176
Fig. 7.1. An illustrative example of the DME fragmentation in a MS.....	185
Fig. 7.2. Locations of manual GC-MS sample points within experimental adsorption/desorption rig	186
Fig. 7.3. MeCl and DME peak separation using GC-Col-1	190
Fig. 7.4. DME shouldering on MeCl GC peak response using GC-Col-1	191
Fig. 7.5. MS calibration curve for DME on GC-Col-1	191
Fig. 7.6. MeCl and DME peak separation using GC-Col-2	193
Fig. 7.7. Actual concentration versus predicted concentration (vol. %) for a) GC and b) MS .	193
Fig. 7.8. GC calibration curve for GC-Col-2	194
Fig. 7.9. MS calibration curve for GC-Col-2.....	194
Fig. 7.10. Ratio of MeCl outlet peak response to the initial manifold peak response and DME concentrations at manifold and AC outlet following batch mode binary mixture expansion in an empty AC	195
Fig. 7.11. Ratio of MeCl outlet peak response to the initial manifold peak response and DME concentrations at manifold and AC outlet following a continuous flow of a binary mixture through an AC filled with glass beads.....	197
Fig. 7.12. DME concentration in manifold and AC outlet [left figures: a and c] and ratio of MeCl peak response at manifold and AC outlet to initial manifold peak [right figures: b and d] at different time intervals following batch fixed bed binary adsorption on Pret-4A-B1 and Pret-4A-B2	198
Fig. 7.13. a) DME concentration in manifold and AC outlet and b) ratio of MeCl peak response at manifold and AC outlet to initial manifold peak at different time intervals following batch fixed bed binary adsorption on Pret-Si35-70	204
Fig. 7.14. GC and MS spectrums for AC outlet concentration for Pret-4A-C1, a) after 1 min and b) after 7 min from commencement of binary mixture flow.....	206
Fig. 7.15. DME AC outlet concentration following continuous flow experiments of binary mixtures on Pret-4A where (a) C1 (b) C2 and (c) C3	207
Fig. 7.16. Ratio of MeCl outlet peak response to the initial manifold peak response following continuous flow experiments of binary mixtures on Pret-4A	208
Fig. 7.17. DME manifold concentration following continuous flow experiments of binary mixtures on Pret-4A	208

Fig. 7.18. GC and MS spectrums for AC outlet concentration for Pret-5A-C2, a) after 1 min and b) after 7 min from commencement of binary mixture flow.....	211
Fig. 7.19. DME manifold concentrations for two continuous flow run experiments on Pret-5A where (a) C1 and (b) C2.....	212
Fig. 7.20. MeCl MS AC outlet peak ratio to initial manifold peak following continuous flow of binary mixture on Pret-5A where (a) C1 and (b) C2.....	212
Fig. 7.21. DME AC outlet concentration following continuous flow experiments of binary mixtures on Pret-Si35-70	214
Fig. 7.22. Ratio of MeCl outlet peak response to the initial manifold peak response following continuous flow experiments of binary mixtures on Pret-Si35-70.....	214
Fig. 7.23. DME manifold concentration following continuous flow experiments of binary mixtures on Pret-Si35-70	215
Fig. 7.24. DME AC outlet concentration following continuous flow experiments of binary mixtures on Pret-SiAmor	216
Fig. 7.25. Ratio of MeCl outlet peak response to the initial manifold peak response following continuous flow experiments of binary mixtures on Pret-SiAmor.....	216
Fig. 7.26. DME manifold concentration following continuous flow experiments of binary mixtures on Pret-SiAmor	217
Fig. 7.27. MeCl MS AC outlet peak ratio to initial manifold peak (left y-axis) and DME outlet concentration following a continuous flow of binary mixture on Pret-Si35-60 (right y-axis)..	218
Fig. 7.28. TSD analysis from 20-100 °C for DME manifold concentration using Pret-4A.....	219
Fig. 7.29. PSD analysis for DME manifold concentration using Pret-4A	220

LIST OF TABLES

Table 2.1. Differences and similarities between physisorption and chemisorption	36
Table 2.2. Typical physical properties of commercial adsorbents (Reproduced from: [17])	40
Table 2.3. Physical properties of typical commercial activated carbons, [2]	42
Table 2.4. Gas sorption calculation mechanisms & models, [25, 31]	49
Table 3.1. Physical and chemical properties comparison table for DME and MeCl.....	67
Table 3.2. The physical properties of the adsorbents, as received from the supplier	69
Table 3.3. The experimentally obtained ratio of manifold volume to the respective adsorbent void volume (x_3)	84
Table 4.1. Surface analysis techniques and obtainable information (Reproduced from: [78]) ..	85
Table 4.2. BET surface area and pore distribution for adsorbents used	92
Table 4.3. EDXA data for all adsorbents	95
Table 5.1. Reported studies on DME adsorption on various zeolites.....	105
Table 5.2. Structural properties of DME versus MeCl.....	114
Table 5.3. Pure component empirical fitting parameters for DME and MeCl adsorption on 4A and 5A	121
Table 5.4. Pure component empirical fitting parameters for DME and MeCl on 4A and 5A..	123
Table 5.5. Adsorption kinetic model parameters for pure component DME and MeCl on 4A	127
Table 5.6. Adsorption kinetic model parameters for pure component DME and MeCl on 5A	128
Table 5.7. Freundlich empirical adsorption model parameters for pure component DME and MeCl on Si35-70, SiAmor and Si35-60	138
Table 5.8. Adsorption kinetic model parameters for pure component DME and MeCl on Si35-70	141
Table 5.9. Adsorption kinetic model parameters for pure component DME and MeCl on SiAmor	142
Table 5.10. Adsorption kinetic model parameters for pure component DME and MeCl on Si35-60.....	143
Table 5.11. Freundlich empirical adsorption model parameters for pure component DME and MeCl on AC8-12.....	150
Table 5.12. Adsorption kinetic model parameters for pure component DME and MeCl on AC8-12.....	153
Table 6.1. Empirical fitting parameters for pure component DME and MeCl adsorption isotherms on Pret-4A and Pret-5A.....	168

Table 6.2. Adsorption kinetic model parameters for pure component DME and MeCl on Pret-4A-5.....	170
Table 6.3. Adsorption kinetic model parameters for pure component DME and MeCl on Pret-5A-5.....	171
Table 6.4. Adsorption kinetic model parameters for pure component DME and MeCl on Pret-4A-15.....	172
Table 6.5. Adsorption kinetic model parameters for pure component DME and MeCl on Pret-5A-15.....	173
Table 7.1. Conditions for batch fixed bed adsorption of binary mixtures on Pret-4A	198
Table 7.2. Conditions and data for batch fixed bed adsorption of binary mixtures on Pret-5A203	
Table 7.3. Conditions and data for batch binary gas analysis on Pret-Si35-70	203
Table 7.4. Conditions for continuous flow adsorption of binary mixtures on Pret-4A	205
Table 7.5. Conditions for continuous flow adsorption of binary mixture on Pret-5A.....	210
Table 7.6. Conditions for continuous flow adsorption of a binary mixture on Pret-Si35-70 ...	213
Table 7.7. Conditions for continuous flow adsorption of binary mixture on Pret-SiAmor	215

CHAPTER I: INTRODUCTION, AIM AND OBJECTIVES

The main objective of the project was to investigate MeCl purification for the silicone industry. The project was funded by The Engineering and Physical Sciences Research Council (EPSRC) and the UK's main research funding agency, as part of a case award joint with the industrial partner Dow Corning, UK. The project proposal was developed as a possible solution for the challenging gas purification problem. In order to tackle the industrial problem the project objectives were divided into two key sections: objectives to fulfil the requirements of a PhD research and secondly to obtain a practical solution by solving a challenging problem for the industrial partner by providing rigours and a scientific approach, thus adding to the scientific knowledge in the research subject concerned. A detailed explanation of the problem and objectives are provided in the next sections.

1.1 Problem at hand

MeCl is an essential raw material used in the manufacture of silicone. However all technical grades of MeCl contain variable levels of DME, which poison the process. The current technology removes at least 99 % DME from the raw MeCl feedstock, which varies in concentration between 0.2 – 1.0 %. The current process involves contacting gaseous MeCl with liquid sulphuric acid (H_2SO_4). This converts the DME into dimethyl sulphate and methyl hydrogen sulphates, which reside in the liquid acid phase. Once the H_2SO_4 becomes saturated with sulphates (~30 – 35 % wt) it is regenerated via a combustion process and acid losses are replenished with fresh material. The one advantage of using H_2SO_4 is that it can also absorb water and methanol ($\text{MeOH}/\text{CH}_3\text{OH}$) from the MeCl, which are both occasionally present due to process setbacks. Major drawbacks with the current technology include a high capital cost, toxic nature of sulphate by-products and the costs associated to the replenishment of the H_2SO_4 . For the problem at hand several methods had been tried and tested by the industrial partner, such as distillation, alternative acids and solvents, absorptive and adsorptive materials. For various reasons, none of these methods have been found to provide a satisfactory solution. An example of this is shown through Fig. 1.1 which demonstrates that both MeCl and DME have very close boiling points, $-24.2\text{ }^\circ\text{C}$ and $-23.6\text{ }^\circ\text{C}$, respectively therefore making separation through distillation very hard.

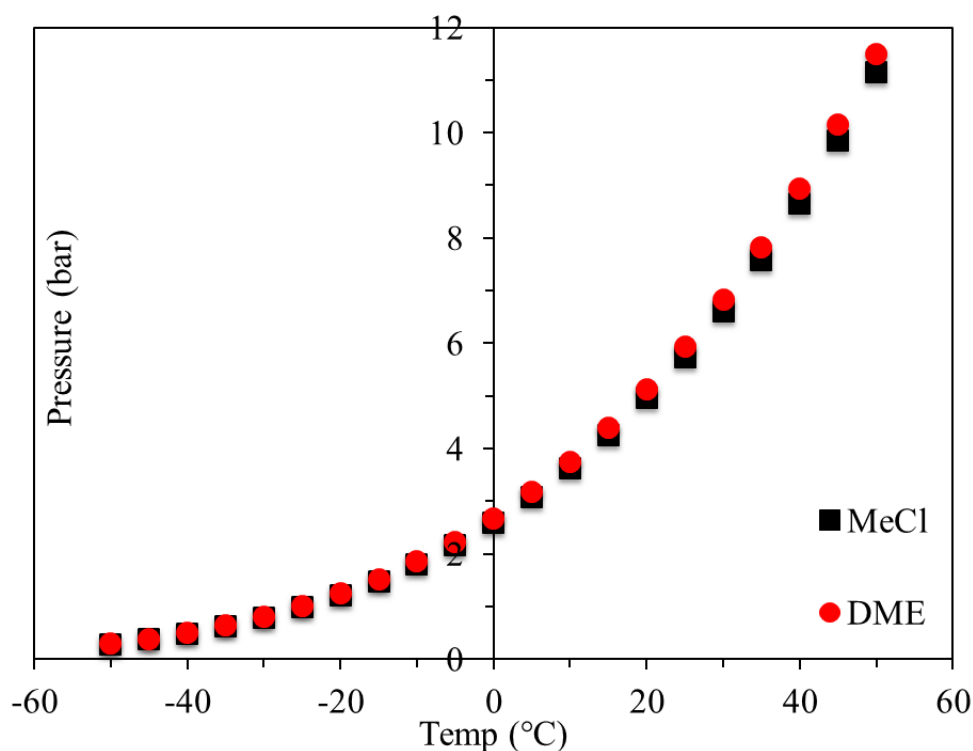


Fig. 1.1. Vapour liquid equilibrium curve for MeCl and DME

1.2 Company expectation

In order for the solution to be practically viable for commercial application Dow Corning has the following expectation for the solution:

A solution to purify MeCl streams containing DME and capable of processing at least 200,000 tonnes/year of MeCl with processing and capital costs (assuming 8 % annual cost of capital) with no more than 3 USD/tonne of MeCl treated. In addition no more than 2 tonnes CO₂/tonne DME removed and any solutions for recovering and re-using DME would be looked upon as favourable.

1.3 Proposed problem solution

The overall proposed concept involved two processes for separating the DME impurity from a gaseous MeCl stream and the utilisation of the separated DME impurity into a hydrogen rich product gas through steam reforming. It was proposed that separation and steam reforming could be carried out in a dual fluidised bed (DFB) system, such that the DME would be adsorbed and separated in one fluidised bed reactor, while the steam reforming took place in the second reactor as shown by Fig. 1.2. The original proposal was based on using a silica gel adsorbent. This was based on the assumption that the ether functional group in DME would bond strongly to the hydroxyl groups on the silica surface. Then the DME saturated adsorbent would be regenerated via combustion at high temperature in steam and air with a nitrogen (N₂) purge to produce a

hydrogen (H_2) rich syngas, carbon dioxide (CO_2) and N_2 . Furthermore, in between the two reactors, it was proposed that two cyclones and a particle cooling system would be used.

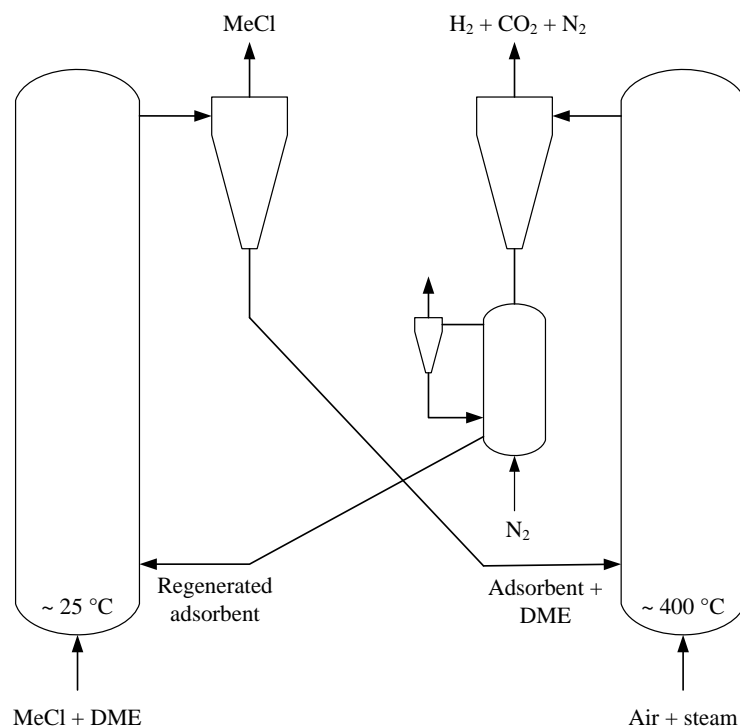


Fig. 1.2. Proposed MeCl purification using a DFB adsorption process

An alternative solution was to use a rhodium/cerium oxide (Rh/CeO_2) catalyst. Similar to the first approach using the DFB system as it was postulated that DME would dissociatively adsorb with on the catalyst in the first reactor at room temperature and steam reforming could be carried out in the second reactor producing high yield streams of H_2 rich syngas at elevated temperatures. Both processes provide a novel yet practical solution for the purification of MeCl on an industrial scale whilst having advantages within the limits of the solution problem.

With that being said following some in depth investigation of the components and methods available it was confirmed that adsorption/desorption of the DME and MeCl on various sorbents is an attractive yet feasible approach to obtain a project solution. Each adsorbent was selected based on their respective functionalities and following the recommendations and conclusions of the literature review. Following the purpose design, build, and commissioning of the experimental rig and the results of initial investigations and findings, the directions of the experimental work were modified and progressed accordingly. Most importantly, a decision was made to focus only on the adsorption process since desorption is irrelevant without a good understanding of the former. Substantial work was carried out on single component adsorption studies for the two components on the various adsorbents following different sorbent pre-treatment conditions. This

was followed by novel binary mixture adsorption investigations under varying conditions of pressure, temperature and impurities concentrations. As a result the sorbent regeneration and steam reforming of the DME were not considered and these are currently being investigated as part of another PhD project.

1.4 Objectives

The following objectives were defined as the core subject of the research to identify a suitable sorbent for MeCl purification and provide “a proof of concept” to satisfy the overall project objective through implementation of the proposed novel separation process:

- To study purification techniques for the separation of DME from MeCl mixtures including a detailed subject background and literature review.
- To design, construct and commission an experimental set-up to satisfy adsorption and desorption analysis.
- To characterise the different adsorbents using different analytical methods:
 - Brunner Emmett Teller (BET): to determine surface area and pore volume analysis.
 - Thermogravimetric analysis (TGA): for moisture content analysis and to determine the thermal stability of solids.
 - Scanning electron microscopy (SEM): to study the surface morphology of the adsorbent material.
 - Energy dispersive x-ray analysis (EDXA): to obtain surface elementary compositional analysis.
- To perform single pure component gas adsorption on different adsorbents at various conditions of temperature and pressure to optimise the adsorption/desorption of DME and MeCl, respectively.
- To perform binary gas adsorption on the different adsorbents and analyse mixtures using analytical methods i.e. GC-MS analysis for determination of purification behaviour.
- Complete analysis of results including isotherm measurements, empirical models, adsorption kinetics and heats of adsorption with a comprehensive discussion and conclusions.
- Suggest future potentials and recommendations for further process improvements and industrial applications.

The following define the company objectives:

- Must avoid large volumes of material requiring transportation over long distances,
- No toxic side products,
- Removal of > 99 % DME from the feedstock,
- Low cost technology,
- Less than 2 tonne CO₂/tonne DME removed,
- Must be suitable for a large industrial scale process.

1.5 Description of thesis chapters

The following briefly summarises the content of each chapter of the thesis:

Chapter I: Introduction, aim and objectives

This chapter introduces in detail the problem at hand and the original proposal for the research. The objectives of the research are divided as overall project objectives to satisfy a PhD criterion and the fundamental company objectives.

Chapter II: Literature review

Provides a comprehensive introduction, theory, background and general literature regarding the adsorption/desorption phenomena. This section highlights the fundamentals of adsorption, mechanisms, mathematic models (empirical and kinetic) and analysis of the interactions between adsorbates and adsorbents (heat of adsorption).

Chapter III: Experimental

Presents detailed information about the equipment used, set-up and materials used. The chapter has a short review on the experimental methods available to carry out adsorption/desorption, information about experimental adsorption systems, volumetric adsorption: system and the different adsorbent particle void volumes. This is followed by the equations used and descriptions of the procedures used for the estimation of the empty manifold and AC volumes, He expansion method, estimation of the different adsorbent void volumes, and overall isotherm measurements. This is followed by the calorimetric heat of adsorption method used, the results, discussion and overall chapter summary.

Chapter IV: Characterisation of adsorbents

Entails a short review on the different characterisation techniques available and used to obtain useful data in terms of physical and chemical information about the adsorbents to aid

adsorption/desorption separation. This is followed by the results and discussion for BET, SEM, EDXA and TGA analyses.

Chapter V: Pure component DME and MeCl adsorption/desorption on different adsorbents

This chapter provides a comprehensive literature review for DME and MeCl adsorption on various zeolites, silica gels, activated carbons and metal surfaces. This is followed by the single gas pure component adsorption/desorption analysis which compares pure component DME versus pure component MeCl data on each as received adsorbent following 1 h vacuum pre-treatment. The results and discussion details the empirical and kinetic models, heats of adsorption analysis which is followed by an overall chapter summary.

Chapter VI: Effect of pre-treatment and equilibrium time on adsorption isotherms

This chapter compares the effect of vacuum and thermal pre-treatment for the pure component DME versus pure component MeCl adsorption isotherms and the effect coupled with an increased equilibrium time on zeolites 4A and 5A, respectively. Analysis includes adsorption/desorption isotherms, empirical and kinetic models, heats of adsorption analysis and an overall chapter summary.

Chapter VII: Binary adsorption of MeCl: DME mixtures on different adsorbents

This chapter provides a brief literature review and background of binary adsorption for similar adsorbents used. Includes results and discussion for binary adsorption analysis of different MeCl: DME mixtures on thermally and vacuum pre-treated adsorbents. Quantitative analysis includes GC-MS calibration, qualitative and numerical quantification for gas separation behaviour of different concentration binary mixtures. The chapter is concluded with an overall summary.

Chapter VIII: Conclusions

This chapter concludes the work carried out in the research whilst linking the respective chapters to provide an overall summary. This is followed by the conclusions for the respective project and company objectives.

Chapter IX: Future work and recommendations

Highlights the achievements from the project, useful recommendations and potential future work which could be used to develop and enhance the quality of analysis. This is followed by a list of possible pathways for further research in and around the research topic.

CHAPTER II: LITERATURE REVIEW

Nowadays, there are numerous technologies for the separation of solid-liquid, liquid-liquid and solid-gas mixtures. A few technologies to mention are distillation, solvent extraction, absorption and adsorption. The adsorptive removal of undesirable impurities from gas or liquid streams can be classified as purification since the adsorbed species are generally only present in low concentrations and, in many cases, have little or no economic value. Generally the economic benefit of the process is derived from the increase in purity and hence the value of the stream containing the major component. With the continual rise of energy prices an economic incentive is more required now than ever. Due to its simplicity and near widespread applicability, distillation assumed a dominant role in separation technology for many years and is still the standard for which potential processes are measured. In recent times due to economical driving factors, alternative separation processes such as adsorption/desorption have attracted a lot of interest and attention. This rise has made distillation processes costly and uneconomic compared to adsorption processes. Generally for mixtures it is possible to find an adsorbent for which the adsorption separation factor is greater than the relative volatility, so that a more economic adsorptive separation is in principle possible.

The options for the gas purification and their potential applicability to the problem in hand are as follows:

- **Distillation:** Due to the close boiling points of MeCl ($\sim -23.6\text{ }^{\circ}\text{C}$) and DME ($\sim -24.2\text{ }^{\circ}\text{C}$) the process is not feasible for the separation of the two gases.
- **Absorption:** Although a proven method, its application is less attractive to due to the toxic by-products and high capital costs of replenishing the solvent.
- **Adsorption:** Widely used for selective adsorption of gases. However, there is a lack of published data on MeCl and DME and no sound scientific knowledge on their adsorption or desorption trends. As adsorption works on selectivity and the process required is purification it is believed that through investigation of this technique, the knowledge gap can be reduced and a solution can be obtained.

It is reported that the cost of an adsorption separation process is generally greater than that of distillation unit with an equivalent number of theoretical stages although higher separation factors can be attained in the adsorption system [1]. The break-even point depends on the system itself and the energy costs but as rough guide for bulk separation, if the relative volatility is lower than 1.25 then adsorption becomes a very competitive separation process [1, 2].

2.1 General background on dimethyl ether (DME) and methyl chloride (MeCl)

2.1.1 Dimethyl ether (DME)

DME is a relatively unexplored gas in adsorption applications. DME has numerous advantages including, but not limited to; high hydrogen to carbon ratio, high energy density, non-corrosive, non-carcinogenic, non-toxic nature and no carbon-carbon bonds. Consequently, it can be easily handled, stored, transported and burned with limited negative environmental impact. These factors make DME an attractive option for use as an alternative fuel for internal combustion engines. DME has an excellent combustion quality due to its high cetane number in the range of 55 - 60 compared to 40 - 55 for diesel [3]. DME is also seen a good alternative to liquefied petroleum gas (LPG) as it can be similarly condensed at -25 °C under atmospheric pressure or 5 - 6 atm at ambient temperature [4]. DME can be catalytically reformed to hydrogen at low temperatures compared to other competitive compounds such as ethanol and methane. Based on the advantages offered by the liquid phase dimethyl ether (LPDME) process DME has begun to attract considerable attention in the petrochemical industry for a variety of applications. The usage of DME as an alternative fuel is being tested in Europe, Asia and North America. DME can also be used as a starting material for the synthesis of hydrocarbons such as dimethyl sulphate or oxygenate products. With the search for new cleaner fuels the possibility of using DME for various energy use purposes has become more and more exciting. The potential suggests promising possibilities with limited downsides as decomposition and reforming of DME to hydrogen over various catalysts has led to good results [5-8]. Wang *et al.* [9] cite that due to its potential application in various sectors it was labelled 'A fuel for the 21st century'. Currently, the most common method for the commercial production of DME is by catalytic dehydration of MeOH [10]. DME is also produced as a by-product of MeOH synthesis [11] and from biomass driven syngas [9, 12]. The direct/one step synthesis from syngas to DME is still under development but reported to be thermodynamically and economically favourable. In any case DME synthesis is usually associated with undesirable by-products, which require further separation and purification steps, therefore its recovery/purification via adsorption can be of great importance for future applications and use.

2.1.2 Methyl chloride (MeCl)

MeCl is a colourless gas that compresses into a colourless liquid. It is a volatile organic compound which is a carcinogenic gas that is released to the atmosphere during its production and use. In almost all its commercial uses MeCl is used as a raw material and reacted to form other products. Exposure to high concentrations can be very harmful and cause serious health problems. Of all the alkyl halides MeCl is the largest contributor of organic chlorine to the atmosphere [13].

Processes such as biomass combustion, incineration of municipal and industrial waste, natural sources, marine algae and oceans through ocean hydrolysis are the most common sources of its emissions [13, 14]. MeCl is reported to be produced by marine microalgae and reactions involving chloride methyltransferase which has been found in the marine algae. It was estimated that around 5×10^6 tonnes per year is released of which $> 90\%$ is estimated to be from natural sources [14]. It has a very high vapour pressure and is soluble in water. Typically MeCl is representative of a technical grade close to 100 % with small impurities of water, MeOH, DME, acetone and hydrochloric acid (HCl); hence the objective of the project. Primarily MeCl is used for the production of silicones; other uses include quaternary ammonium compounds, butyl rubber and agricultural chemicals [14]. It is an important industrial product with an attractive global capacity. It is the fundamental starting material in the production of higher chlorinated products such as methylcellulose and silicones and in applications as a methylating agent. McInroy *et al.* [15] cite that the manufacture of MeCl can be achieved via two established routes: thermal chlorination/catalytic oxychlorination of methane or hydrochlorination of methane. It is via the hydrochlorination of methane that it is commercially most favourable in today's market. Wei *et al.* [16] report that the transformation of MeCl to higher hydrocarbons is one of the potential routes for natural gas utilisation especially with the continually increasing price of crude oil. This mainly arises as a result of the low cost of MeOH and the excess surplus of HCl via various chlorination processes. The process can be carried out in both liquid and gas phase. The liquid phase does not require a catalyst but a slight excess pressure of HCl, or catalytically in the presence of zinc chloride or iron chloride. The gas phase operates typically around $350\text{ }^{\circ}\text{C}$, over alumina or silica supported metal chloride catalysts.

2.2 Adsorption

Adsorption occurs when molecules diffusing in a fluid phase are held for a period of time by forces originating from an adjacent surface. The surface represents a gross discontinuity in the structure of the solid and atoms at the surface have a residue of molecular forces, which are not satisfied by surrounding atoms like those in a body of the structure. Adsorption is when the gas or vapour comes into contact with a solid and the solid uptakes some or part of it. The part that has disappeared either remains on the surface or enters inside the pores of the solid. Unlike absorption, whereby the fluid phase (gas or liquid) diffuses into the liquid or solid, during adsorption molecules form a distinct adsorbed phase rather than being consumed. Although both processes are different when they occur simultaneously it is termed sorption.

Only over the last 60 years or so that adsorption has developed to a stage where it is used on an industrial scale. For an adsorption process to be scaled up from a laboratory bench scale

experiment to a feasible yet economical commercial process many criteria have to be met and fundamentals understood. Adsorption separation can be ultimately achieved through one of three mechanisms [17]:

1. **Equilibrium effect:** occurs when there is a difference in the thermodynamic equilibria for each adsorbate-adsorbent (A-S) interaction.
2. **Kinetic effect:** occurs when there is a difference in the rate at which the adsorbate can travel into the internal structure of the adsorbent.
3. **Molecular sieving effect:** adsorbate molecules are separated based on their molecular size, therefore excluding larger particles with smaller pore openings.

2.3 Adsorption fundamentals

Adsorption is fundamentally dependent upon the interaction between the adsorbent surface and adsorbed species, however the four most important features involved during the investigation of adsorption analysis are [18]:

1. **Interface characteristics:** the surface characteristics of the adsorbate and adsorbent surface determine the nature of the bonding between the two. Knowledge of the main functional groups can be used to help manipulate and or target a particular type of interaction i.e. this could be done by modifying the adsorbent surface through impregnation with a catalyst.
2. **Adsorption isotherm:** through measuring the amount adsorbed in mol kg^{-1} or g g^{-1} this can be used to quantify the amounts adsorbed and determine the adsorption mechanism involved i.e. Type I-VI.
3. **Adsorption thermodynamics:** through evaluation of the thermodynamics a detailed insight of the mechanism involved, strength of interaction and kinetic analysis can be obtained to determine the feasibility of separation of binary mixtures.
4. **A-S interactions:** the A-S and adsorbate-adsorbate (A-A) interactions contribute to the overall adsorption behaviour. Therefore such information can give a greater understanding on types of bonding and information about co-operative and or competitive adsorption.

Adsorption itself seems a fairly simple concept but upon investigation it is evident that it is anything but. In order to understand the fundamentals in more detail it is important to appreciate how adsorbate molecules adsorb onto and into an adsorbent surface. Supported by Fig. 2.1 the process occurs as follows:

1. Adsorbate molecules move from the bulk gas phase to the external surface of the adsorbent.
2. The adsorbate molecules diffuse from the small external surface area into the micro, macro and mesopores of the adsorbent and adsorb onto the surface and in the pores.
3. As molecules diffuse to the different parts of the solid, physical and chemical bonding occurs. Initially this is due to concentration gradients of the molecules from the bulk phase.

Though this suggest that these three stages occur in series, in practice all three may be occurring simultaneously as conditions are not uniform across different parts of the adsorbent. Until equilibrium has been established the concentration is generally higher at the outer surface of an adsorbent pellet than in the centre.



Fig. 2.1. Adsorption steps: adsorbate molecules interacting with an adsorbent surface and pores, (Obtained from: [19])

2.3.1 Adsorbate-adsorbent (A-S) interactions

Adsorbate molecules can bond to the adsorbent surface physically (physisorption) or chemically (chemisorption) depending upon the nature of the molecules and surface. Table 2.1 demonstrates the main difference and similarities between the two. Ruthven [1] claims that there are many intermediate cases where it is not always possible to easily categorise a particular system. It is reported that almost all adsorption separation/purification processes depend on physical adsorption rather than chemisorption. Physisorption is a result of weak A-S interactions, which is a consequence of relatively weak non-specific VDW's forces that induce adsorption energies $\leq 80 \text{ kJ mol}^{-1}$. Generally the adsorbate diffuses along the adsorbent to non-specific locations on the adsorbent and therefore the process can be easily reversed. Weak VDW's forces however, cannot be applicable in cases where there is a dipole-dipole, induced dipole, donor-acceptor interactions or hydrogen bonding because the forces are specific to the respective chemicals with different functional groups. On the other hand, chemisorption results from highly specific but much stronger interactions and forms heats of adsorption $\leq 800 \text{ kJ mol}^{-1}$. Interactions can be a result of covalent (i.e. C-H), strong hydrogen (H-O) or ionic bonds (sharing of electrons) the adsorption process becomes in many cases irreversible due to the type of bond and its strength.

Table 2.1. Differences and similarities between physisorption and chemisorption

Physisorption	Chemisorption
<ul style="list-style-type: none"> • VDW's Forces • Non-specific • Rapid, non-activated and reversible • Only significant at low temperature • Monolayer or multilayer • Low heat of adsorption • No electron transfer, although polarisation of adsorbate can occur • No dissociation of adsorbed species • No activation energy required 	<ul style="list-style-type: none"> • Chemical forces: covalent, ionic • Highly specific • Activated, can be slow and irreversible • Possible over a wide temperature range • Multilayer formation only • High heat of adsorption • Electron transfer leading to bond formation between adsorbate and adsorbent surface • May involve dissociation • High activation energy required

Adsorption, which has resulted from the influence of VDW forces, is essentially physical in nature. The forces are weak and the energy released upon binding is of the same order of magnitude as the enthalpy of condensation ($\sim 20 \text{ kJ mol}^{-1}$). During physical adsorption the chemical identity of the adsorbate remains intact. The electrostatic effect that produces VDW's forces depends upon the polarity of the adsorbate and adsorbent, respectively. The chemical structure of a molecule determines whether it is a polar molecule or not. Polar molecules exhibit

a separation of positive and negative charges within the compound, referred to as a permanent dipole. Non-polar molecules have both positive and negative charges in the centre so they have no permanent dipole. Physical adsorption can result from one of three different effects:

1. **Orientation:** polar molecules attract because the negative charge of one molecule is attracted to the positive charge of the other.
2. **Dispersion:** when a non-polar molecule interacts with a non-polar surface it is due to the dispersion effect as they have fluctuating or oscillating dipoles as opposed to a permanent dipole. Fluctuating dipoles occur as a result of momentary changes in electron distribution around the nuclei. In non-polar substances when two fluctuating dipoles come together their total energy decreases and therefore fluctuates in the phase with one another i.e. dispersion effect.
3. **Induction:** when a polar molecule interacts with a non-polar molecule an induction effect is caused. The polar molecule induces polarity to the non-polar molecule when they are in close contact. The energy of this effect is determined by the polarizability of the nonpolar molecule; described by Miller [20] as the response of an electron cloud to an external field.

Generally the induction effect is very small compared to the other two effects and therefore adsorption systems typically use polar adsorbents to remove polar contaminants. This allows the intermolecular forces of attraction of the adsorbate to be stronger with the adsorbent than within molecules of itself in the same phase.

2.3.1.1 Total potential energies for adsorbate-adsorbent (A-S) interactions

The total potential energy of adsorption interactions can be subdivided into different parts representing contributions of different types of interactions between adsorbed molecules and the adsorbent. The total energy (ϕ_{total}) shown by Eq. (2-1) is the sum of all contributions resulting from the following:

- **Dispersion energy (ϕ_D):** Contributes regardless of the specific electric charge distributions in the adsorbate molecule, known as non-specific.
- **Close range repulsion (ϕ_R):** same as dispersion energy.
- **Polarisation energy (ϕ_P):** contributions are high for polar molecules with dipoles, or quadrupoles but for relatively non-polar surfaces the value is small.
- **Field dipole interaction ($\phi_{F-\mu}$):** has a significant contribution where adsorbate molecules have permanent dipoles and quadrupole moments. In the absence of these or the surface has no electric fields or is non-polar the value is zero.
- **Field gradient quadrupole interaction ($\phi_{\delta F-Q}$):** same as field dipole interaction.

- **Self-potential** (A-A interaction) (ϕ_{SP}): results from interactions between adsorbate molecules, the value increases at higher coverages where there is a heat of adsorption.

$$\phi_{total} = \phi_D + \phi_R + \phi_P + \phi_{F-\mu} + \phi_{\delta F-Q} + \phi_{SP} \quad (2-1)$$

Ertan [21] reports that often just the consideration of polarisation, dipole moment and quadrupole moments can allow for qualitative predictions to be made in terms of the relative strength of adsorption of the adsorbate onto a adsorbent or for a better understanding of the best type of adsorbent to use (polar or non-polar) for a particular separation.

2.3.2 Factors affecting adsorption

For adsorption/desorption to occur there are a number of factors that can affect the separation of molecules specifically in gas mixtures. A summary which is not limited to, highlights some key findings from literature which contribute towards gas purification of a gas mixture using adsorption/desorption phenomena [1, 21, 22]:

- The larger the adsorbent surface area the larger the adsorption capacity.
- The smaller the adsorbent particle size the lower the internal diffusional and mass transfer limitations to the penetration of the adsorbate molecule into the adsorbent i.e. adsorption equilibrium can be achieved more quickly and saturation capacity reached faster.
- Increased adsorption temperature decreases the amount adsorbed but increases the pressure of the adsorbate; this in turn raises the energy level of the adsorbed molecules. Molecules now have sufficient energy to overcome the VDW forces and migrate back to the gas phase. Molecules already in the gas phase now tend to remain in the gas phase due to the increased vapour pressure.
- Maintaining a partial pressure of the vapour proportional to the total pressure of the system allows for optimum adsorption. The increase in capacity is because there is a decrease in the mean free pathway of the vapour at higher pressures. As a result the molecules become more tightly packed together meaning molecules have a greater chance to fill the available adsorption sites.
- The gas velocity of the adsorbate is vital since the residence time affects the efficiency capture of adsorbate molecules. The lower the velocity the lower the contact time; the greater the velocity, the greater the probability of molecules reaching an available adsorption site.
- Humidity during adsorption can affect the capacity and efficiency of adsorption. At higher relative humidity more polar molecules can begin to compete with the non-polar ones.

- Contamination can obviously reduce adsorption and its capacity. Compounds with high boiling points and molecular weights have a high affinity for carbon.
- Specifically for gas purification there is a practical minimal and maximum limit to the bed depth; the minimum depth is based on the length of the mass transfer zone (MTZ) that is required which is effectively related to the rate of adsorption. A sufficient adsorbent bed depth is imperative for achieving efficient adsorbate removal.
- Non-polar adsorbents are more easily removed than polar especially for activated carbons as they have a higher affinity for non-polar molecules.

2.3.3 Adsorbent structure and functional groups

The structure of the adsorbent pores, which permeates the adsorbent and the equilibrium capacity of an adsorbent, affects the selectivity for different molecules. Typically molecular sieves are precise at uniquely separating on the basis of molecular size. Measuring the distribution of sizes and the associated surface area is near impossible. Only selected very expensive microscopes can help determine the surface of a species. There are two key elements of a surface which are paramount for adsorption: surface area and pore size. Both can be used to help determine whether adsorption can occur and if so how much. It is important to recognise that adsorbent surfaces are generally heterogeneous meaning they consist of a finite number of differing adsorption sites which can be determined using empirical adsorption models.

Since adsorbent surfaces consist of numerous surface functional groups. The adsorption of organic molecules is largely dependent on the amount and nature of surface oxide groups. According to Itodo and Itodo [23] functional groups such as carbon (C) and oxygen (O) are generally created during the activation process of the adsorbent. Other basic functional groups include: lactones, carboxylates and quinones. The presence of O containing basic groups leads towards irreversible adsorption, the less polar the adsorbate the higher the adsorption capacity. Moreover, higher molecular weights of adsorbates enhance adsorption until the size of the molecule becomes a limiting factor. Furthermore, solubility is too a key factor during adsorption, the lower the solubility of the adsorbate the higher the adsorption capacity since the interaction between the A-S would be greater than the forces between the A-A molecules [24].

There are four methods which can be experimentally conducted to modify the chemical nature of adsorbents to therefore target a particular type of interaction/separation [21]:

- **Cation exchange:** Changes the local electric fields and thus affect the polarization.
- **Decationization:** Removal of cations from a zeolite framework can alter the electric fields and reduce the interaction for molecules with permanent dipoles.
- **Pre-loading:** Adding small amounts of polar adsorbate (water) to the adsorbent thus hindering adsorption of less selective adsorbates as it cannot be displaced.
- **Purification:** Removal of impurities in the adsorbent through some type of pre-treatment.

2.4 Types of adsorbents

Adsorbents can be irregular, formed spheres and extruded pellets. In order to achieve optimum adsorption, the volume of the bed must be packed with as much surface area as possible, whilst trying to minimise the pressure drop through the bed. In order for adsorbents to be commercially attractive they must have:

- A large internal surface area.
- A pore diameter large enough to allow molecules to be adsorbed, whilst it is favourable if pores are small enough to exclude molecules.
- Be capable of regeneration whilst not ageing rapidly; thus not losing its adsorptive capacity through numerous regenerations/recycles.
- Be mechanically strong enough to withstand vibrations and bulk handling.

Since the number and types of adsorbents vary Table 2.2 shows the most common commercially active adsorbents used along with their respective physical properties.

Table 2.2. Typical physical properties of commercial adsorbents (Reproduced from: [17])



Whilst each adsorbent is capable of carrying out adsorption/desorption for separation/purification the correct choice of adsorbent is key, for the wrong choice and or incorrect operating conditions can lead to a lack of separation/purification. It is the surface characteristics of the adsorbate, which

determine the nature of the bonding between the A-S. Although adsorption has the benefit of selectivity any possible application has to be considered in collaboration with alternatives i.e. distillation, absorption, or selective desorption. Each separation process is able to exploit some difference between a property i.e. physical or chemical of the components to be separated. For distillation it is the volatility, for absorption it is the solubility and for extraction it is the distribution coefficient. Fundamentally, separation by adsorption/desorption depends on one component being more readily adsorbed or desorbed than another. Below we look at the four main commercially active adsorbents used in more detail.

2.4.1 Silica gel

Silica gel is a partially dehydrated polymeric form of colloidal silicic acid ($\text{SiO}_2 \cdot n\text{H}_2\text{O}$). The gel of polymeric colloidal silicic acid (salicylic acid), in the form of agglomerate of micro particles is formed when silicate solution is acidified. As the gel is heated, water is ousted leaving a hard, glassy structure with voids between the micro particles. Controlling the pH of the solution and presence of various cations in the solution allows for the gel to be precipitated and leads to different property gels. With careful control of the manufacture process different pore sized gels are produced. Most adsorbents have similar pore distributions however it is the respective surface functional groups which are largely responsible for different types of interactions. Silica gels have silanol groups on the surface, which are polarised and can form hydrogen bonds with molecules that are polar as shown by Fig. 2.2.

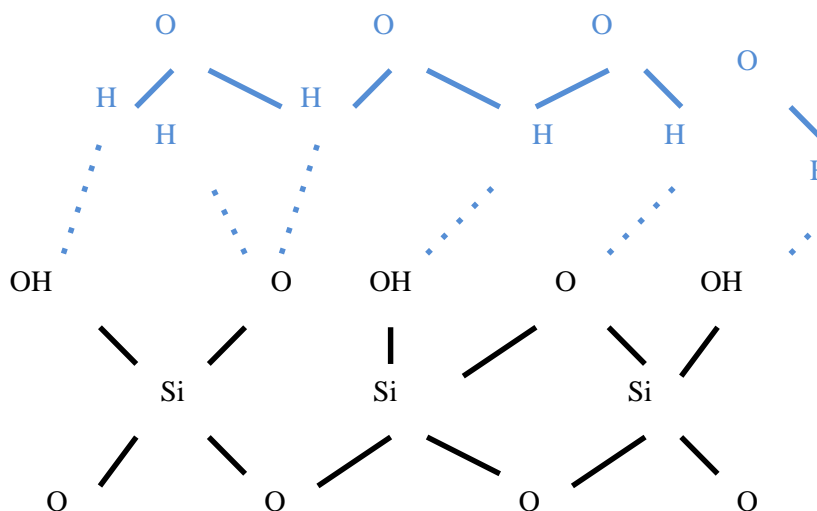


Fig. 2.2. Silica gel surface: silanol groups forming hydrogen bonds

The capacity of the adsorbent depends on the concentration of the silanols on the silica surface. Due to the hydrophilic and brittle nature of silica, if there is a rapid release of heat during

adsorption it can lead to shattering of the silica. However this can be countered by a stronger variety of gel with a reduced surface area. Thomas and Crittenden [25] add that at low temperatures the capacity of the gel for water is higher than alumina or zeolites. The presence of hydroxyls imparts the degree of polarity to the surface so that molecules such as water, phenols, alcohols and amines can form hydrogen bonds whilst unsaturated hydrocarbons form π -complexes and therefore these molecules are adsorbed in preference to non-polar molecules such as saturated hydrocarbons [1, 2].

2.4.2 Activated carbon

Activated carbon is usually made from thermal decomposition of carbonaceous material, which is then activated by reacting with steam or CO₂ at elevated temperatures. Activated carbons are made of small hydrophobic graphite layers with disordered, irregular and heterogeneous surface with hydrophilic functional groups. It has a non-polar surface although some polarity can arise from surface oxidation. Activated carbon contains heteroatoms on the surface with the main heteroatom being O thus allowing it to form different functional groups. Similarly it can form acidic and basic properties in aqueous solutions. Carbons with a high O content show acidic surface properties and cation exchange behaviour [26]. The ability for it to adsorb depends on the composition, mechanical strength and physiochemical properties [27]. Due to its highly porous nature there are numerous applications for the adsorbent ranging from solvent recovery to wastewater treatment; predominantly the latter. The total surface area available for adsorption is not significantly affected by the particle size and therefore small or large particles do not particularly affect the adsorption capacity, although the time to achieve equilibrium can vary due to diffusional effects. Characteristically activated carbons have a wide range of pores and the actual distributions of properties are sensitive to the preparation procedures as shown by Table 2.3.

Table 2.3. Physical properties of typical commercial activated carbons, (Reproduced from: [2])



An advantage of activated carbons is that it can be produced from low cost materials since it is a product of pyrolysis (char), which in the world today has a continually growing market. It also has the ease of activation, selectivity, regeneration and cost [27]. Particles > 1 mm are termed granular (GAC) and can be easily regenerated; smaller particles ($\geq 10 - \leq 74 \mu\text{m}$) are termed powdered (PAC) and can be only used for liquid adsorbates then separated by filtration. In order

to decrease mass transfer resistances small pores are preferred for gas phase adsorption whilst large pore diameters are recommended for liquids [1, 2, 28].

2.4.2.1 Carbon molecular sieves (CMS)

Most carbon molecular sieves (CMS) are prepared from anthracite or hard coal by controlled oxidation and thermal treatment. According to Do [28] activated carbons show little selectivity in the adsorption of molecules of different sizes. By further preparation more narrow pored distributions of micropore size can be prepared which behave as molecular sieves known as CMS. CMS's have a narrower pore distribution and therefore reduced adsorption capacity but their kinetic selectivity is said to be rather impressive. It is widely reported that it is difficult to reproduce between different batches of CMS for the same distribution of pore size [1, 28].

2.4.3 Zeolites

Comprising of SiO_4 and AlO_4 tetrahedra through the sharing of O atoms the porous crystalline aluminosilicates where formed from ancient volcanic ash flows, which settled in seas and lakes [25]. It is the world's only naturally occurring mineral that is negatively charged. It is such that it holds and locks many positively charged ions and great at adsorbing various environmental contaminants. Its crystalline lattice determines the micropore structure, which is precisely uniform with no distribution of pore size. Zeolite frameworks are an assembly of secondary polyhedral building units. In a framework each Al atom introduces one negative charge, which must be balanced by an exchangeable cation. These cations are located at preferred sites in the framework and play a huge role in determining the adsorptive properties. Through ion exchange, changes in the cation charge can provide useful and an exploitable means of modifying adsorptive properties i.e. replacing a Ca^+ cation with a Na^+ cation can reduce the pore apertures of the adsorbent.

An important aspect of zeolite is the Si/Al ratio which is never less than one but has no upper limit. The adsorptive properties show a systematic transition from aluminium rich sieves, which have high affinities for water and other polar molecules to microporous silicas such as silicate, which are essentially hydrophobic. The transition from hydrophilic to hydrophobic occurs at a Si/Al ratio from 8 – 10. When the Si/Al ratio is increased, which can only be modified by acid treatment the electrostatic field on the adsorbent surface is decreased [29]. De-alumination processes such as extraction, high temperature steam reforming and reactions with SiCl_4 can change the amount of Al in the frameworks. With increased de-alumination the electrostatic field inside the zeolite decreases and the surface becomes more hydrophobic. The adsorption equilibrium becomes more ideal and the surface becomes more homogeneous thus reducing A-S

interactions. As a result strong polar attractions between the surface and molecule are reduced and weaker dispersion forces become more dominant. Contrastingly, where the AI value is higher the nature of the interactions are always polar which leads to a steep slope at low relative pressures for isotherms [21].

Key qualities of zeolites include its high porosity and consistent matrix, which give it its high adsorptive qualities. Additional properties include high chemical and thermal stability, in turn increasing its capabilities for more precise and specific separation of gases such as water, CO₂ and light gaseous mixtures. Although the following is true for most adsorbents it is reported that in zeolites the following four factors can collectively contribute towards the separation/purification of mixtures: adsorption temperature, the rate at which molecules are adsorbed and/or diffuse to the structure, the relative size of adsorbate and pore opening size and the strength of adsorptive forces between A-S [22].

Unlike many other adsorbents a zeolite membrane can separate mixtures through all three viable adsorption mechanisms; thermodynamic equilibrium, diffusion differences and molecular sieving [30]. With the thermodynamic equilibrium position being a typical mode of separation for most adsorbents, the kinetic selectivity (intracrystalline diffusivity) and the molecular sieve properties of zeolites are determined by the free diameter of the windows in the intracrystalline channel structure. While the external surface area of a molecular sieve is available for molecules of all sizes, the internal area is only for molecules small enough to enter. Typically in adsorbents approximately, the external represents only 1 % of the total surface area. Zeolites preferentially adsorb molecules based on polarity and degree of unsaturation in organic molecules, in addition to selectivity and configuration. In a mixture, molecules small enough to enter the pores of the zeolite with a lower volatility, increased polarity and greater degree of unsaturation are more tightly held within the structure. For the mixture under consideration DME is more polarizable since it has a C-C bond unlike MeCl only having one C.

Each type of zeolite such as sodalite, chabazite, pentasil, mordenite and types X and Y are all structured differently and therefore allow for varying adsorptive properties. Do [28] and Ruthven [1] claim that due to the effects of vibration of both the diffusing molecule and crystal lattice during adsorption, molecules can penetrate the free diameter windows of the zeolite with a greater critical diameter than the free diameter itself. By blocking cations a dramatic reduction in the diffusivity of adsorbate molecules can be achieved. The extent of reduction depends upon the number and nature of cations since different cations show differing affinities to various molecules. Differing cationic forms of specifically zeolites can lead to significant differences in selective adsorption of a given gas. This is because the location and size of the interchangeable cations

affect the local electrostatic field and polarisation of adsorbate molecules. The capacity for adsorbates over the entire equilibrium pressure range can be related to two factors: number of cations per unit mass (cationic density) and the limiting volume of the micropores [21]. As an example Fig. 2.3 shows the different zeolites structures available for sorption.



Fig. 2.3. Line representations of zeolite structures: a) sodalite cage or β -cage or truncated octahedron; b) type A zeolite “unit cell”; c) types X and Y, or faujasite; d) cation sites in type A (8 in I, 3 in II and 12 III sites per unit cell; e) cation sites in types X and Y (16 I, 32 I', 32 II, 32 II', 48 III and 32 III sites per unit cell) (Obtained from: Yang, [2])

2.4.4 Activated alumina

A highly porous form of aluminium oxide with the formula $\text{Al}_2\text{O}_3 \cdot n\text{H}_2\text{O}$, has both acidic and basic characteristics yet more polar than a silica gel surface [25]. Ruthven [1] cites that it can be prepared either directly from bauxite or from the monohydrate by dehydration and re-crystallisation at high temperatures. The adsorbent is generally resistant to attrition and retains more of its adsorptive capacity at elevated temperatures, and controlled heating of the hydrated alumina can lead to its activation. Typically activated aluminas have a high affinity for especially water and hydroxyl (OH) groups whilst having an impressive mechanical strength but they cannot compete in terms of selectivity or capacity of molecular sieves. Generally activated aluminas have a similar affinity to water as silica gel but the latter has the greater capacity.

2.5 Adsorption equilibria and isotherms

Adsorption equilibria, is a dynamic concept which is achieved when the rate at which molecules adsorb on to a surface is equivalent to the rate they desorb. The capacity of an adsorbent for a particular adsorbate involves the interaction of three properties:

- Concentration C of the adsorbate in the fluid phase,
- Concentration C_s of the adsorbate in the solid phase,
- Temperature (T) of the system.

If one of the properties is kept constant then the other can be graphed to represent the equilibrium. Generally a plot of C vs C_s gives an adsorption isotherm if temperature is kept constant. An adsorption isostere is obtained by plotting C vs T when C_s is kept constant. In gas-solid systems, by expressing C as a pressure of adsorbate, then plotting C_s vs T gives adsorption isobars. If a vapour quantity, q , adsorbed by a solid at constant temperature and the steady state equilibrium partial pressure is, p , or concentration, c , then the adsorption isotherm is $q(p)$ or $q(c)$. Adsorption isotherms, which are paramount to adsorption, can exhibit different trends and thus demonstrate the mode of adsorption. The different forms, known as Types I, II, III, IV and V are explained in more detail below and illustrated in Fig. 2.4 [25, 31].

Type I: Adsorption is limited to the completion of a single monolayer of adsorbate molecules on the adsorbent surface. Generally observed for the adsorption of gases on microporous solids whose pore sizes are not much larger than the molecular diameter of the adsorbate; complete filling of these narrow pores then corresponds to the completion of a monolayer.

Type II: Here the isotherm does not exhibit a saturation limit. Once the monolayer is complete following successive layers proceed. Generally adsorbents with a wide distribution of pore sizes form this type of isotherm. Condensation of vapours can occur in larger pores of this type. The adsorbent also shows a high capacity for adsorption as the adsorbate saturated vapour pressure is reached.

Type III: Similar to Type II, Type III has a continuous convex with respect to partial pressure. This shows a steady increase in adsorption capacity with increasing relative pressure (P/P_0). The BET theory is not applicable to Type III. Generally, the model applies when an adsorbate molecule has a very weak interaction with the adsorbent or the interaction between the adsorbates is very strong. This type is observed in practise but less common to the above two.

Type IV: Again similar to Type II, however this isotherm terminates near to a P/P_0 of unity. Isotherms here are involved in capillary condensation of the adsorbate in their mesopores.

Type V: Similar to Type III at low P/P_0 , however a point of saturation is reached as P/P_0 is further increased. These isotherms are also observed in practise but again less common.

Type VI: When the adsorbent has a high uniform surface the adsorption of gas molecules occur in layer by layer formation thus the isotherm exhibits incremental step rise adsorption behaviour.



Fig. 2.4. Types of adsorption isotherms according to the International Union of Pure and Applied Chemistry (IUPAC), (Reproduced from: [31])

In practise the performance of an adsorbent is typically quantified at constant temperature by an adsorption isotherm. The resulting adsorption equilibria data provides essential physicochemical information for evaluating the applicability of an adsorption process as an operational unit.

Ho *et al.* [32] report that an accurate mathematical description of the isotherm based on a correct mechanism is essential for an effective adsorption process design. Adsorption isotherms which can be measured theoretically or experimental provide not only a clear indication of the suitability for a particular separation for each species but also the thermodynamics can be applied to obtain further key information. Subsequently, where the reverse of adsorption, desorption does not coincide with the isotherm the mismatch is known as a hysteresis has a key role in separation. The purpose of constant temperature measurements is to determine adsorption data at any specified temperature either by interpolation or extrapolation, only then through this can this knowledge be applied to predict multicomponent adsorption based on single pure component data [33]. In order to select the appropriate and most practical adsorbent, equilibrium data for different temperatures and pressures must be determined. If the equilibria data indicates a suitable choice then the kinetics properties need to be evaluated.

Empirical isotherm models can be used to describe experimental adsorption data where each model has various assumptions which can help give an insight into the type of mechanism involved, surface properties and the affinity of the adsorbent. On the contrary, chemical models provide a molecular description of the adsorption process using an equilibrium approach. In order to use and calculate parameters from these models, it is important to identify the available techniques that can be applied to determine the parameter values. Where there are two-parameter isotherms linear regression analysis is applicable and can be used. However where there are two or more parameters, non-linear optimisation methods or use of the solver add-in function within Microsoft Excel are best suited. According to Ho *et al.* [32] and Itodo *et al.* [23] linear regression methods are deemed not appropriate for calculating the coefficient of determination (R^2) for best fitting isotherm parameters with the former claiming a non-linear optimisation method (trial and error procedure using computer operation) provides a better way to obtain isotherm parameters as a higher R^2 can be achieved thus resulting in a lower error between the isotherm fitting model and the experimental data. Non-linear optimisation provides a more complex yet mathematically thorough method for determining isotherm parameter values therefore recommended over linear where possible.

According to the IUPAC pores in solids are divided according to their size in 3 main groups: micropores < 2 nm, mesopores $2 - 50$ nm, and macropores > 50 nm. Adsorption occurs into various pores at different relative pressures therefore various calculation models can be applied to determine the respective adsorption mechanisms. Ever since the initial isotherm equation by Langmuir for simple kinetic behaviour and statistical thermodynamics, various researchers have developed countless other isotherms for these two phase interactions. Although numerous adsorption models exist the choice of model can greatly influence the prediction of the adsorbate

transfer and potential process design. Limousin *et al.* [33] advise that an ideal model must be effective, comprehensive, realistic and predictive especially if it is to be implemented industrially. Table 2.4 shows some of the most commonly used adsorption mechanisms and models and the respective relative pressure ranges for which they are applicable.

Table 2.4. Gas sorption calculation mechanisms and models, (Reproduced from: [25, 31])



Goldberg and Criscenti [34] advise that applying the models must be treated with caution since they are simply numerical relationships used to fit data. Therefore some independent experimental evidence of an adsorption process must be present before any chemical meaning can be assigned to the isotherms. Since isotherms consist of curve fitting, the parameters are only valid for the conditions of the experiment and therefore predictions of adsorption behaviour under changing conditions can be difficult. The following sub-sections look at the most commonly applied empirical adsorption models in more detail.

2.5.1 Langmuir model

The model is based on dynamic equilibrium between adsorption and desorption. At higher concentrations the number of molecules adsorbed increases to the point of saturation. The rate of adsorption becomes proportional to the empty surface available as well as the fluid concentration. Molecules desorb at the same rate as they adsorb if they have sufficient activation energy. Though the isotherm generally applies for chemisorption it can be described for some moderately low coverage binary systems. The surface is considered to be homogenous and adsorption is limited to a single monolayer. The adsorption is localised to fixed sites and molecules do not migrate until desorbed. It is assumed the heat of adsorption is constant and independent of coverage. When the rate of adsorption and desorption are equal the rate constants are expressed as follows [25]:

$$k_{ads}P(1 - \theta) = k_{des}\theta \quad (2-2)$$

where k_{ads} and k_{des} represent the rate of adsorption and desorption, respectively. The more usual form of the Langmuir isotherm is written as:

$$\theta = \frac{n}{n_s} = \frac{bP}{(1 + bP)} \quad (2-3)$$

where θ is the surface coverage, n is the quantity adsorbed (mol kg⁻¹), n_s is the number of adsorption sites available in a single monolayer, b is the empirical parameter (affinity constant: a measure of how strong the adsorbate molecule is attracted to the surface) and P is the adsorbate pressure. Eq. (2-3) can be expressed in a linear form by Eq. (2-4) and therefore a plot of n/P vs P can allow for b and n_s to be determined graphically.

$$\frac{P}{n} = \frac{1}{n_s} P + \frac{1}{bn_s} \quad (2-4)$$

2.5.2 Freundlich model

According to Toreci *et al.* [35] the model shown by Eq. (2-5) can be used explain the adsorption behaviour of organic compounds from liquid systems onto activated carbon or gas adsorption onto heterogeneous surfaces. The parameter t is usually larger than one but depends on the heterogeneity of the adsorbent surface, the greater the value the greater the heterogeneity.

$$\theta = \frac{n}{n_s} = KP^{\frac{1}{t}} \quad (2-5)$$

The application of the model can be expressed in a linear form shown by Eq. (2-6) to determine values for K and t from a plot of $\log(n)$ vs $\log(P)$. Do [28] claims that the isotherm is best suited for moderate pressures as the isotherm equation does have a proper Henry's law behaviour at low pressure and the finite limit when the pressure is high ($P \rightarrow \infty$).

$$\log n = \log K + \frac{1}{t} \log P \quad (2-6)$$

2.5.3 Sips model

The following model shown by Eq. (2-7) is a combination of the Langmuir and Freundlich models for non-uniform surfaces. Since the Langmuir and Freundlich models do not apply for high pressure the following model has a finite limit for when the pressure is sufficiently high [28]. The Sips model can be reduced to the Langmuir model if t is unity which could then be applied for ideal surfaces. Similar to Freundlich the parameter is regarded as the parameter which characterises the system heterogeneity [21, 35]. The model is only really valid for sufficiently high pressures as it shares the same disadvantage as the Freundlich model at low pressures. Both Toreci *et al.* [36] and Do [28] have reported t to decrease as the temperature increases.

$$\theta = \frac{n}{n_s} = \frac{(bP)^{\frac{1}{t}}}{1 + (bP)^{\frac{1}{t}}} \quad (2-7)$$

2.5.4 Tóth model

This is another empirical model which obeys Henry's law at low pressure and reaches maximum adsorption at high pressures. Ertan [21] claims that the model gives a more extensive range of fit when applied to Type I isotherms as it has the advantage of giving correct limits for $P \rightarrow 0$ and $P \rightarrow \infty$. The equation gives a good description for many systems with sub-monolayer coverage.

$$\theta = \frac{n}{n_s} = \frac{bP}{[1 + (bP)^t]^{\frac{1}{t}}} \quad (2-8)$$

2.5.5 Brunauer Emmett Teller (BET) model

This isotherm applies to all models except Type I isotherms due to its monolayer assumption. The following theory is based on the concept of an adsorbed molecule which is not free to move over the surface, and exerts no lateral forces on adjacent adsorbate molecules. The theory allows different number of adsorbed layers to build on different parts of the surface. But it assumes the net amount of surface, which is associated with the monolayer or empty, is constant for any particular equilibrium condition. For the BET theory to be applicable the two main assumptions are there is no interaction between neighbouring adsorbed molecules and any heat evolved during the filling of the second or subsequent layers of molecules is equal to the heat of liquefaction. The most common form of the BET equation is shown by Eq. (2-9) [31]:

$$\frac{P}{q(P_s - P)} = \frac{1}{q_m C_{BET}} + \frac{(C_{BET} - 1) P}{q_m C_{BET} P_s} \quad (2-9)$$

where C_{BET} is the BET constant, q_m is the quantity in one monolayer and P_s is the saturated pressure.

2.5.6 Adsorption potential

The adsorption potential (ϵ) of a substance on a particular adsorbent can be predicted at a selected temperature and pressure. The theory can be applied for both mono and multilayer adsorption of gases and vapours on porous and non-porous adsorbents. Potential functions are used to determine detailed models for atom–atom interactions and a distribution of point charges is used to reproduce the polarity of the adsorbent and adsorbate molecules [22]. The adsorption potential shown by Eq. (2-10) is fundamentally, the chemical potential for the adsorbate to adsorb on to the

surface of the adsorbent. Generally, with time the adsorption potential is expected to decrease due to the formations of mono and multilayers on the surface of the adsorbent. The theory considers the potential of a point in adsorption space as a measure of the work done by surface forces. As a result this exerts a lower potential field as the distance from the adsorbent increases.

$$\varepsilon = RT \ln\left(\frac{P_s}{P}\right) \quad (2-10)$$

where R is the universal gas constant.

2.5.7 Dubinin equations

The characterisation of microporous solids and evaluation of the parameters that characterise the solid structure are important. Dubinin did extensive work to develop models to help understand the adsorption of gases on microporous solids as demonstrated in the following sub-sections.

2.5.7.1 Dubinin Radushkevich (DR) equation

Adsorption of molecules on surfaces having a constant energy of interaction is very rare as most solids are heterogeneous. As a result the heterogeneity can be determined by assuming that the energy of interaction between the surface and adsorbate is governed by some distribution [28]. The following form of the DR equation was proposed for adsorption following a pore filling mechanism and valid for describing the physical adsorption of gases/vapours on microporous solids such as activated carbon and zeolites.

$$q_e = q_s \exp\left[-\left(\frac{\varepsilon}{\beta E}\right)^2\right] \quad (2-11)$$

where q_e is the amount adsorbed at equilibrium, q_s is the theoretical isotherm saturation capacity, E is the characteristic adsorption energy and β is the affinity coefficient which is related to the A-S interactions. The DR model is a temperature dependant model unlike others therefore a plot of $\ln(q_e)$ versus ε^2 yields an energy characteristic curve.

2.5.7.2 Dubinin Astokhov (DA) equation

The DA equation is a more generalised relationship for the determination of micropore volume particularly for carbonaceous solids and zeolites. It takes into consideration interactions between the adsorbate molecules and any intracrystalline action if any. The relationship is similar to the DR equation but contains an empirical exponent (n) which describes the surface heterogeneity [28]. Notably, the DA equation reduces to the DR equation if $n=2$.

$$q_e = q_s \exp\left[-\left(\frac{\varepsilon}{\beta E}\right)^n\right] \quad (2-12)$$

2.6 Adsorption kinetics and models

It is imperative to know the adsorption and desorption rates in order to design and evaluate an adsorbent for a particular adsorption separation. It is therefore of interest to determine the respective coefficients characterising adsorbate transport within adsorbents. Although various kinetic models have been suggested for adsorption, the most common yet simplest is the Langmuir kinetics. According to Yao and Chen [37] adsorption kinetics are often treated in one of two ways: the reaction method and the diffusion (mass transfer) method. The importance of the two is shown by Fig. 2.5, which shows the individual steps of sorption on an adsorbent.



Fig. 2.5. Individual steps of a simple heterogeneous A-S interaction (A_1 - A_2) carried out on a porous adsorbent, (Reproduced from: [38])

Clearly the rate at which the adsorbates diffuse through the boundary, film and pore to the adsorption/active site contributes to the overall kinetic rate. The first reaction method step involves application of the pseudo first order, pseudo second order and Langmuir kinetic models; although others exist. These models are particularly popular due to their simplicity and because the respective model parameters can be obtained through linear and/or non-linear regression analysis of batch adsorption kinetic data. The downside is that the approach takes no consideration of the diffusion steps which are un-neglectably fundamental to most adsorption processes such as fixed, agitated batch and fluidised bed processes.

Diffusion methods include the film-pore, film-surface (film-solid or homogenous solid diffusion), film-parallel and or surface diffusion models are generally used less since they consist of complicated partial differential equations however since adsorption processes are so complex, mathematic models are best utilised for understanding the respective controlling mechanisms. The diffusion mechanisms mentioned are rate controlling and therefore the diffusion or mass transfer parameters (such as film mass transfer coefficient and surface diffusion coefficients) are fundamental parameters which at some point are necessary for the design of any adsorption process. The usual method of obtaining diffusion parameters is to match the solution to the film intraparticle diffusion model (IPD) equations to experimental kinetic data [37-39].

2.6.1 Pseudo first order model

For a batch contact time process the pseudo first order model based on the sorption capacity of an adsorbent is typically expressed as:

$$\frac{dq}{dt} = k'_{ads}(q_e - q) \quad (2-13)$$

where k'_{ads} is the rate constant (min^{-1}), q_e is the amount adsorbed at equilibrium, q is the amount adsorbed at the respective time (t) in mol kg^{-1} . If Eq. (2-13) is integrated for the boundary conditions of $t=0$ to $t>0$ and $Q=0$ to $Q>0$ then the following time dependence function is obtained:

$$\ln(q_e - q) = \ln q_e - \frac{k'_{ads}}{2.303} t \quad (2-14)$$

Therefore through a plot of $\ln(q_e - q)$ versus t , a straight line with a high R^2 demonstrates pseudo first order kinetics. An exponential function of the slope yields Q_{eq} and k'_{ads} is obtained from the intercept [40, 41]. The pseudo first order equation differs from the standard first order equation in two ways: $k'_{ads}(q_e - q)$ does not represent the number of available adsorption sites and the parameter $\ln(q_e)$ is an adjustable parameter which is often not equal to the intercept of a plot of $\ln(q_e - q)$ versus t , whereas for a typical first order process $\ln(q_e)$ should be the equal of the intercept for the above plot [42].

2.6.2 Pseudo second order model

The pseudo second order reaction is also based on the sorption capacity of an adsorbent but expressed as a chemisorption rate equation given by:

$$\frac{dq}{dt} = k''_{ads}(q_e - q)^2 \quad (2-15)$$

where k''_{ads} is the rate constant of the second order sorption ($\text{kg mol}^{-1} \text{min}^{-1}$). Upon integration of the same limits from the pseudo first order model for Eq. (2-15) the following linear time dependence function is obtained:

$$\frac{t}{q} = \frac{t}{q_e} + \frac{1}{k''_{\text{ads}} q_e^2} \quad (2-16)$$

where q_e and k''_{ads} are determined from the slope and intercept, respectively from a plot of t/q versus t [43].

2.6.3 Elovich model

Sorption data can be analysed using the Elovich model which is typically expressed as:

$$q = \frac{1}{\beta_E} \ln(\alpha\beta) + \frac{1}{\beta_E} \ln(t) \quad (2-17)$$

where α is the initial adsorption rate constant ($\text{mol kg}^{-1} \text{min}^{-1}$) and β_E is related to the extent of surface coverage and activation energy (kg mol^{-1}). To simplify the equation it is assumed $\alpha\beta_E \gg t$ and applying the same boundary conditions as with the pseudo first order equation. Through a plot of Q versus $\ln(t)$, β_E is obtained from the intercept then subsequently used to determine α [44].

2.6.4 Intraparticle diffusion (IPD) model

When mass transfer is the controlling step it is imperative to identify the diffusion mechanism therefore the following model is applied which is expressed as:

$$q = k_{\text{int}} \sqrt{t} \quad (2-18)$$

where k_{int} is the IPD rate constant ($\text{mol kg}^{-1} \text{min}^{-1/2}$). Through a plot of q versus $t^{1/2}$, k_{int} is obtained from the slope of linear fit. Pandey *et al.* [41] report that if the plot exhibits an initial straight line followed by a plateau then the latter represents equilibrium. Such plots can represent multi-linearity indicating that two or more adsorption steps take place [45]. The first shaper portion of the plot can represent the external surface adsorption or instantaneous adsorption stage. Whereas the second portion typically represents the gradual adsorption stage where IPD is rate controlled. The third portion is usually the final equilibrium stage where IPD starts to slow down due to extremely low adsorbate concentrations in the bulk.

2.6.5 Intraparticle diffusion (IPD) versus surface resistance layering

Understanding the adsorption kinetics in terms of uptake versus time scale is critically important for the design of an adsorption/desorption process. For example, a separation process based on pressure swing adsorption (PSA) or vacuum swing adsorption (VSA) requires precise knowledge of the adsorption time scale. Adsorption on different solids exhibit different modes of adsorption therefore it can be difficult to determine the actual kinetics in terms of mechanism involved. Ruthven [39] reports that the structural simplicity of a type A zeolite framework coupled with the well-defined pore channel systems make the adsorption mechanism quite difficult to differentiate. Similarly Cheung *et al.* [46] report that the numerous studies on adsorption kinetics has led to diverse views on the uptake and diffusion of adsorbates. It is reported that the crystal size, quality and extent of dehydration (pre-treatment) among other factors govern the mechanism of diffusion or uptake. Furthermore, adsorbate molecules can be adsorbed on zeolites via intracrystalline diffusion or surface layering. Each adsorption mechanism can be characterised by distinct linear relations expressed in terms of the fractional coverage n/n_{\max} and adsorption time, t_{ads} , as follows [39, 46]:

IPD controlled:

$$\frac{n}{n_{\max}} = A\sqrt{t_{\text{ads}}} \quad (2-19)$$

Surface resistance controlled:

$$\ln \left[1 - \left(\frac{n}{n_{\max}} \right) \right] = -Bt_{\text{ads}} \quad (2-20)$$

where A and B are constants and $\sqrt{t_{\text{ads}}}$ and t_{ads} is square root of and time of adsorption in seconds.

2.7 Heat of adsorption

The heat of adsorption is an important measure which gives information regarding the nature of the A-S and A-A interactions, strength of bonding, surface morphology and the pore structure of the adsorbent [47]. The magnitude of the heat released is strongly influenced by the surface coverage because this can alter the energetics of adsorption. Through the knowledge of the heat of adsorption, one can distinguish between physisorption and chemisorption. Adsorption is accompanied by changes of energy, specifically during the adsorption and desorption of the adsorbate. The heterogeneity of an adsorbent usually comes about due to the differences in adsorption strength at the sites. Deviations in heterogeneity can be detected from the shape of the adsorption isotherm and is usually evaluated by comparing the isosteric heat of adsorption at

different loadings. As adsorption proceeds, most of the more active sites get filled and the remaining less active sites release less heat. When the monolayer coverage is near complete heats of adsorption remain near constant. Kuo and Hines [48] cite that decreasing heats in adsorption indicate that the adsorbent surface is non-homogeneous. The temperature dependency of the equilibrium capacity is directly related to the heat of adsorption. It is beneficial to know both the equilibrium adsorption capacities and isosteric heats of adsorption (ΔH_s) for process design and analysis for the specific A-S system [49, 50]. The Clausius-Clapeyron equation also known as the van't Hoff equation to calculate the heat of adsorption [49] is shown by Eq. (2-21).

$$\Delta H_s = -R \left(\frac{\delta(\ln P)}{\delta \left(\frac{1}{T} \right)} \right)_\theta \quad (2-21)$$

which on integration gives:

$$\left(\ln \frac{P_1}{P_2} \right)_n = -\frac{\Delta H_s}{R} \left(\frac{T_2 - T_1}{T_1 T_2} \right) \quad (2-22)$$

Equally, the heat of adsorption can be determined from a more direct calorimetric method. Depending upon the type of set-up and equipment used an overall heat balance can be used to determine the subsequent heat of adsorption at different loadings [51]. Kobayashi *et al.* [52] report that drops in the differential heat of adsorption (Q_{diff}) at different loadings to be associated with adsorption at different adsorption sites. Garbacz *et al.* [53] compared the differential heats of adsorption using a calorimetric approach with the isosteric method. They demonstrated considerable differences between the methods and described the differences to be because the fundamental conditions for chemical equilibrium were not fulfilled. Due to molecular sieving effects and existence of narrow pores this strongly restricts the diffusion of the adsorbed molecules meaning the equilibrium distribution is not achieved. As a result they cited that the heat balance approach cannot be used as a substitute for measurements of adsorption isotherms at different temperatures particularly for microporous adsorbents. Meaning the heat balance approach which is theoretically correct is not recommended for the characterisation of adsorption systems hence why the thermodynamic approach is the preferred method.

2.8 Industrial applications of adsorption/desorption separation

Industrial adsorption processes have been largely employed in the last few decades as a result of their selective adsorption capabilities. Key adsorption processes have been applied for the separation of the following but not limited to: aromatics, air pollutants, N_2/O_2 , solvent recovery, ultra-purifications, bio-separations, hazardous chemicals and olefins/paraffin [54]. Without going into too much detail the implementation of adsorption on a commercial scale is the given by the following classification [1]:

1. PSA,
2. TSA,
3. Variations on PSA and TSA:
 - a. Temperature-pressure swing adsorption (TPSA),
 - b. VSA,
 - c. Stimulated moving bed (SMB).

According to Cavalcante Jr, [54] industrial adsorption processes can be classified in three ways:

1. **Sorbate concentrations:** adsorption processes can be classified as purification and bulk separation. In a mixture one component is removed from a mixture of high concentration.
2. **Mode of operation:** these can be classified further as:
 - a. Cyclic batch,
 - b. Continuous counter-current,
 - c. Chromatographic.
3. **Regeneration methods:** following adsorption through the addition of an agent (physical or chemical) to the equilibrium conditions, subsequent clean desorption can be carried out as follows:
 - a. TSA,
 - b. PSA,
 - c. Desorbent displacement,
 - d. Purge with inert.

Rezaei and Webley [55] cite that improvements in performance and cost effectiveness of cyclic swing adsorption processes are dependent on parameters which are dictated by the adsorbent loading per unit volume, pressure drop, mass transfer properties and thermal management. These factors contribute to the sizing of equipment, the product recovery and the energy consumption.

CHAPTER III: EXPERIMENTAL

This chapter presents detailed information about the equipment used, set-up and materials used for the designed, built and commissioned experimental adsorption/desorption rig. The short literature review gives a brief overview of the analytical techniques available for aiding adsorption/desorption separation through collective physical and chemical adsorbent information. The literature also includes information about the different types of particle void spaces. This is followed by a short results and discussion section for validating the rig and determining the error in sorption measurements.

3.1 Literature review

3.1.1 Experimental adsorption analysis

In order to carry out adsorption analysis particularly on at a laboratory scale, the experiment set-up, technique and quantifying analysis methods used must be feasible and accurate for qualitative quantification. This is extremely important since sorption is highly sensitive to changes in pressure, temperature and volume therefore if certain parameters are not controlled and accurately determined this can lead to an accumulation of error which could ultimately result in serious design and scale up errors. Leofanti and co-workers [56] report that three techniques exist for quantitative determination of adsorbed molecules onto adsorbents:

1. **Static volumetric techniques:** where an outgassed solid is contacted with a known volume of gas and the adsorbed quantity is determined through pressure decrease.
2. **Static gravimetric techniques:** similar to the above technique but instead adsorption is determined through weight increase by the solid.
3. **Dynamic techniques:** involve probe molecules being passed through the solid continuously or by pulse then analysed by GC analysis.

Static techniques give more precise data but are naturally slow and very delicate due the difficulty in recognising the equilibrium conditions and of distinguishing between chemisorbed and or physisorbed molecules. Notably the techniques provide better tools for qualitative analysis than dynamic ones. Many technological processes involved are driven by adsorption equilibrium. Gas equilibrium can be measured in several ways with the recording of the temperature and pressure being paramount to the technique. Volumetric methods are mainly based on a mass balance of the amount of gas adsorbed onto the adsorbent assuming Ideal gas laws apply. Gravimetric analysis relies on a highly sensitive microbalance for measuring the amounts of gas adsorbed as opposed to Ideal gas laws. It was reported that in some cases both techniques; volumetric and gravimetric measurements can be performed simultaneously but the costs associated are very high [57]. Webb [58] reports that the volumetric technique is convenient for obtaining high-resolution

measurements for isotherms at specifically low to atmospheric pressure whilst any commercial designs of the technique are totally automated. To obtain high resolution isotherms, precise dosing steps are required in the process of reaching equilibrium. Consequently automation is vital which is attainable using the dynamic chemisorption technique, The latter applied by Mulgundmath *et al.* [59] through use of a thermal conductivity detector (TCD) reported that the quantity that is not adsorbed can be measured from each dose. Other techniques such as temperature programmed desorption (TPD) and temperature programmed oxidation (TPO) are particularly suited for performing temperature program analysis.

3.1.2 Volumetric adsorption: system and void volumes (V_0)

Volumetry also known as manometry is the oldest method to investigate the sorption of gases in solids. The concept is simple: a given amount of adsorbate gas is expanded from one cell to another which has been initially vacuumed. Upon expansion the adsorbate gas adsorbs internally and externally in and on the surface of the adsorbent, whilst the rest of the gas remains around the adsorbent. Although the amount adsorbed can be calculated by a simple mass balance the void volume must be known, defined as the volume which cannot be penetrated by the adsorbate [60, 61]. Since solid materials contain cavities, channels, pores or interstices they are regarded as porous. Using the British standards institute (BSI) definitions for various types of volumes when solids come into contact with an external fluid. Supported by Fig. 3.1 Webb [61] reports the respective definitions as: voids that connect the surface are referred to as open pores and interior voids which are in accessible from the surface are called closed/blind pores.



Fig. 3.1. The different types of volumes associated with solid particles (Obtained from: [61]) If we consider a porous spherical particle to have a film (envelope) around it containing the open and closed pores this is called the external void volume. Therefore the volume between particles

is known as the interparticle void volume which excludes any pores and penetration into the particle. In addition, pores can be further classified according to their pore shape: cylindrical, ink, funnel or slit shaped [62].

The He expansion method can be used to estimate the void volume within an AC prior to carrying out adsorption. According to Malbrunot *et al.* [63] and Ozdemir [64] He adsorption in and on the solid was assumed to be negligible therefore its expansion from one volume to the other was successfully used to determine the void volume. Since He has the smallest molecular size (2.2 Å) of the inert gases and typically adsorbent surfaces with pores are wider than its molecule size, it is very unlikely that the He molecules would not enter these pores especially with increasing pressure [65]. Webb [61] supports the argument that He will penetrate readily into very fine pores. Whilst Keller and Staudt [60] cite that He would actually penetrate porous adsorbents materials for ever if given the time. It was concluded that He is sorbed in all porous materials at even low pressure and high temperatures although other gases such as N₂, Ar, CO₂ at high purity have been reported to be used to characterise the pore system of porous materials [60, 63, 66].

Once a gas stream at any given pressure is released into another cell volume a sudden drop in pressure is to be expected due to the increase in volume for the gas and the equilibration between the two regions. Consequently, when the same procedure is carried out with an outgassed adsorbent contained within the AC and the adsorbed quantity is determined it is necessary to rule out any adsorption that is accounted for due to the filling of empty space and/or deposition to the surface of the pipework, which may be a monolayer or several multilayers of adsorbate, depending upon the pressure. Deposition is reasonably postulated since no surface is completely smooth without the presence of cracks and or microscopic pores. Although these cause uncertainties in measurement this can be reduced by performing further experiments with the same gas to an empty AC. Depending upon the quantification method used empty AC runs are defined as system volume, adsorption correction values.

Semelsberger [67] carried out a blank experimental run whilst using a tapered element oscillating micro-balance (TEOM) for the uptake of DME on various supports and catalysts. An empty run was described to account for apparent mass change during the experiment. Resulting mass readings of blank runs can be subtracted from actual runs to provide the corrected mass. Similarly, Purewal [68] claims a useful way to determine the accuracy of Sieverts instrument is to collect an adsorption isotherm with an empty outgassed AC. If a constant temperature is maintained then no real adsorption should occur. Changes in temperature result in small amounts of adsorption on the AC walls, whilst substantial adsorption is indicative of cumulative experimental error. According to results obtained by Purewal [68] empty run experiments exhibited a linear trend as

shown by Fig. 3.2 for his Sieverts experiment. With this in mind it is important to recognise that the correction factor only applies for the Sieverts method which is repeated at each incremental pressure to construct an isotherm and not the differential pressure method equations as shown in section 3.5.



Fig. 3.2. The reported adsorption correction factor for experimental hydrogen adsorption on activated carbon using the Sieverts method, (Obtained from: [68])

3.2 Experimental

3.2.1 Apparatus for adsorption

Adsorption and desorption analysis was carried out using a purpose designed, built and commissioned volumetric experimental rig for pure and binary gas analysis. Fig. 3.3 shows a simplified drawing of the volume regions.

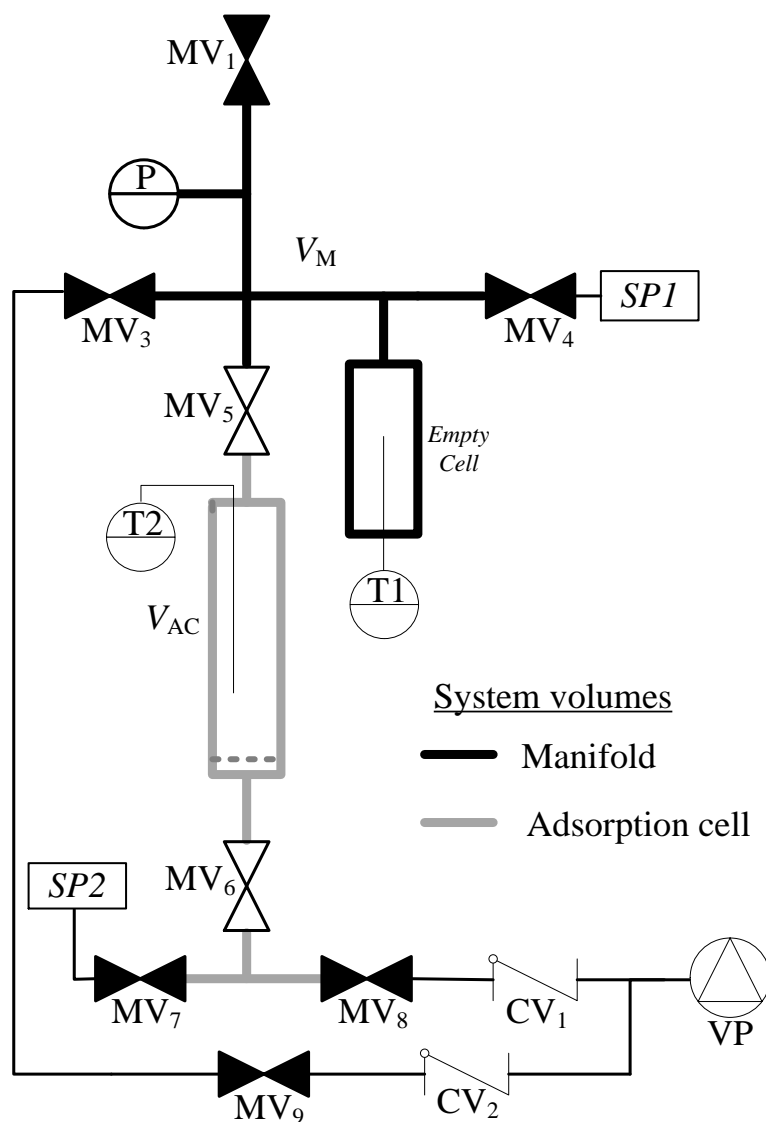


Fig. 3.3. Simplified process flow diagram for adsorption/desorption system volumes

The set-up was constructed in-house using Swagelok fixtures and fittings and mainly consists of five parts: (i) gas flow meter (ii) manifold region (iii) digital pressure gauge (iv) AC (v) vacuum pump (VP). The AC used was a custom-built vertical stainless steel cell commercially known as a FlowCat reactor (6 mm I.D. x 151 mm) supplied by HEL Group Ltd, UK. This was equipped with a very fine mesh (50 μ) at the bottom to support the adsorbent and a top removable screw on/off nut with two potential inlets and capability for loading and unloading the adsorbent.

Fig. 3.4 shows the AC assembly details including dimensions and details on fitting connections provided by the supplier.



Fig. 3.4. AC assembly and dimension drawing (Obtained and supplied: HEL group Ltd, UK)

A pre-calibrated flow meter (type: Variable-Area; Brooks Instruments, UK) was positioned prior to the manifold region to control and measure the gas supplied to it. A high precision digital pressure gauge (model: DPG409; Omega Engineering, UK) in the range of 0 - 500 psiA (max of 34.02 atm) and gauge error ± 0.02 psiA ($\pm 1.36 \times 10^{-3}$ atm) was positioned in the manifold line. The pressure gauge was connected to a data acquisition module (type: OM-USB1208FS) to record the pressure every one second. Two K-type thermocouples were connected to a data logger (model: HH806AWE; Omega Engineering, UK) to record the temperature in the manifold and inside the AC every one second. A heating tape (model; HT9; Fisher Scientific, UK Ltd) was wrapped around the AC and connected to a power controller for heat supply during high

temperature analysis. A hybrid vacuum pump; combination of a two-stage rotary vane pump and a two-stage chemistry diaphragm pump for optimized corrosion resistance (model: Vacuubrand RC6 Chemistry Hybrid, Radleys, UK) was used to create an ultimate vacuum of 2×10^{-6} atm prior to adsorption. The whole set-up was mounted inside a metal framework as shown in Fig. 3.5. All experiments were conducted inside a fume-cupboard due to the nature of the adsorbate gases. Moreover, since the adsorption/desorption bench scale rigs are very sensitive to changes in operating conditions to ensure all results obtained were accurate, the system was regularly tested for leaks. The system was filled with He to a pressure of 10 atm and enclosed within the system overnight to record any changes in pressure.

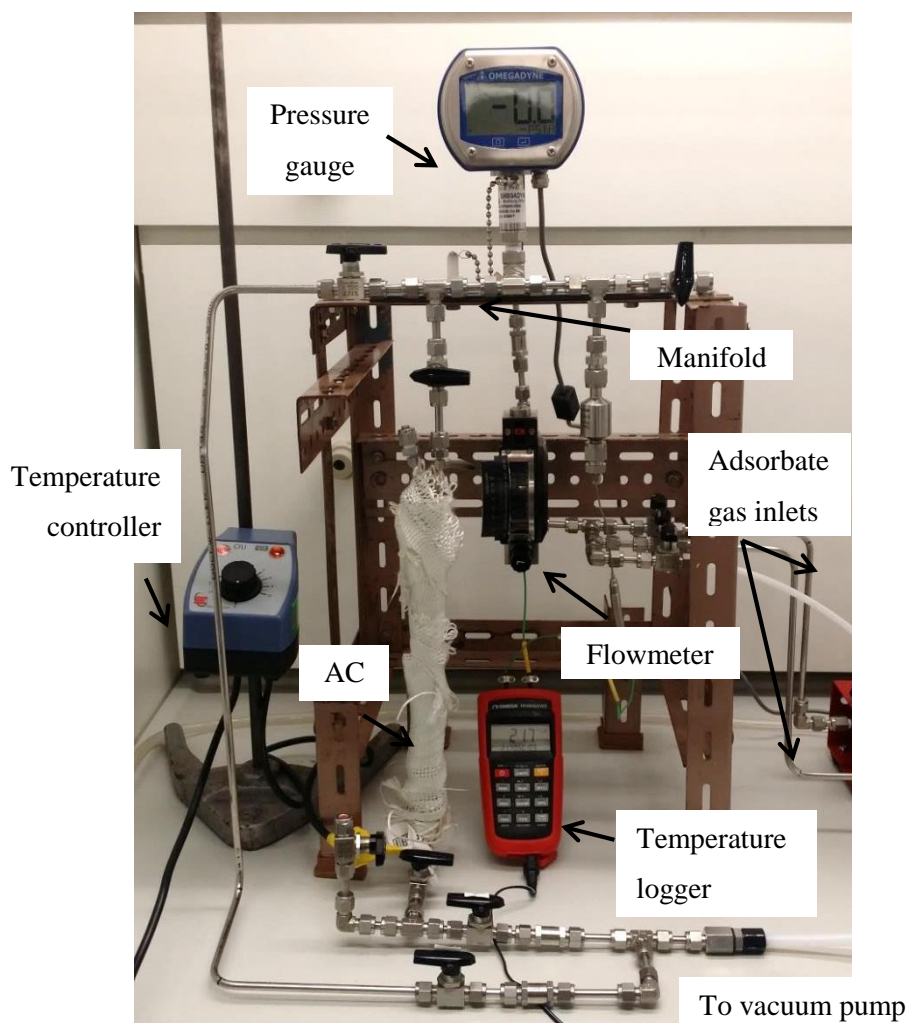


Fig. 3.5. Image of experimental adsorption/desorption rig

3.2.2 Adsorbate gases

Since the objective of this work was to remove DME from MeCl mixtures only these gases were used at the following concentrations:

- DME: $\geq 99.0\%$
- MeCl $\geq 99.5\%$

The gases were contained in 400 g gas cylinders and fitted in Aldrich Sure/Pac gas stations equipped with pressure control valves to dose into the system as shown by Fig. 3.6.

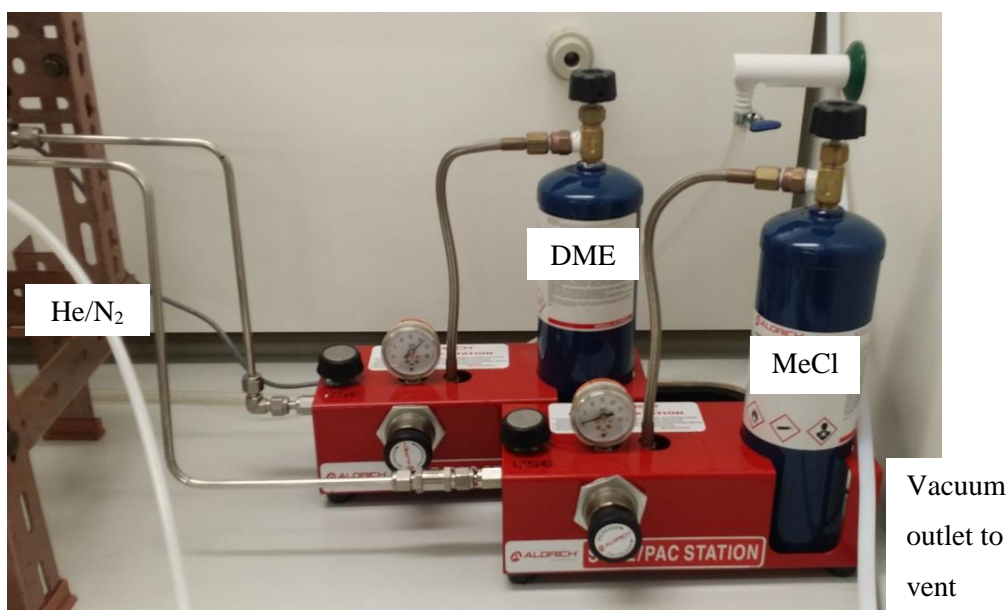
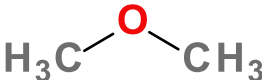
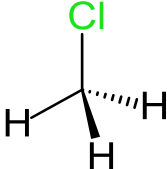


Fig. 3.6. Gas stations used to dose gaseous DME and MeCl to the adsorption/desorption rig

Both, gases and gas stations were provided by Sigma Aldrich, UK. Following an assessment of the material safety data sheets (MSDS) for all chemicals it was recognised that a risk assessment was required prior to experimentation. In addition to the above chemicals, N₂ and He were acquired. Both inert gases were obtained in-house from BOC, UK and Air Products and Chemicals, UK, respectively. The respective MSDS's for all gases have not been included in this work due to their wide availability in literature and/or electronically.

In order to select a suitable adsorbent for separation it was important to analyse physical and chemical properties of the two components in more detail therefore Table 3.1 highlights and compares key physical and chemical properties of DME and MeCl. Interestingly it can be seen that DME has solubility in water that is more than sixty times greater whereas MeCl is a smaller molecule with a higher polarity.

Table 3.1. Physical and chemical properties comparison table for DME and MeCl

Parameter	DME	MeCl	Ref.
Empirical formula	(CH ₃) ₂ O	CH ₃ Cl	
Molecular structure			
Molecular weight, $g\ mol^{-1}$	46.07	50.49	MSDS's
Melting point, °C	-141	-98	
Boiling point, °C	-24.8	-24.2	
Critical temperature, °C	127	143	
Auto ignition temperature, °C	226	632	
Vapour pressure at 20 °C, atm	5.03	4.99	
Relative density at 25 °C, $g\ cm^3$	0.73	0.92	
Gas density, $kg\ m^{-3}$	1.59	2.13	
Solubility at 25 °C, $g\ L^{-1}$	353	5.32	
Dipole moment, D	1.30	1.89	[22]
Molecular dimensions, Å	~ 4.3-5.0	3.7x3.7x4.6,	[69]
Polarizability, $10^{-24}\ cm^3$	4.72, 5.35	4.18	[70]
Magnetic susceptibility, $10^{-29}\ cm^3$	-	4.42, 5.16, 5.29	[20]
Molecular surface area, nm^2	-	5.30	[70]
Accessible surface area, nm^2	-	0.846	[71]
Polar surface area, nm^2	-	0.725	
Polar surface area, nm^2	-	0.092	
Molecular volume, nm^3	-	0.063	

3.2.3 Adsorbents

In order to investigate the potential of adsorption and desorption of the above gases, the following adsorbents were selected and used for pure and binary adsorption analysis:

- Zeolite molecular sieve 4 Å, 8 – 12 mesh (4A),
- Zeolite molecular sieve 5 Å, 30/40 mesh (5A),
- Silica gel, grade 10181, 35-70 mesh (Si35-70),
- Silica amorphous, precipitated (SiAmor),
- Silica gel, grade 646, 35-60 mesh (Si35-60),
- Activated carbon 8-12 mesh (AC8-12).

All adsorption/desorption analysis on the adsorbents was carried out on as received particles and following the specified pre-treatment. The various adsorption/desorption conditions for the different experiments are defined in each subsequent results chapter. Fig. 3.7 shows the physical appearance of each adsorbent. As can be seen zeolites 4A and 5A have similar tanned colour appearances but are different in shape. The silica gels are typically white in appearance but show no real visible differences in appearance and the activated carbon is granular and black in colour. All particles were used as shown in Fig. 3.7 without any crushing and or sieving of particles. The actual size of particles is further demonstrated from the SEM analysis which is shown in section 4.2.2.



Fig. 3.7. Physical appearance of the different adsorbents used

Additionally Table 3.2 shows the physical properties of the adsorbents used above as provided by the supplier. All adsorbents were supplied by Sigma Aldrich, UK.

Table 3.2. The physical properties of the adsorbents, as received from the supplier

Adsorbent properties	Zeolites	
	4A	5A
Appearance	Spherical with tan colour	Non-spherical particles
Mean particle size, μm and mesh	2464 - 1533 μm (8 - 12 mesh)	510 - 380 μm (30 - 40 mesh)
Mean pore diameter, \AA	4	5
Bulk density, $kg\ m^{-3}$	578	720
Regeneration temperature, $^{\circ}C$	200 – 315	200 – 315
Specific heat capacity, $kJ\ kg^{-1}\ K^{-1}$	0.96	0.96
Chemical composition	1 Na ₂ O: 1 Al ₂ O ₃ : 2.0 \pm 0.1 SiO ₂ : x H ₂ O	0.8 CaO: 0.2 Na ₂ O: 1 Al ₂ O ₃ : 2.0 \pm 0.1 SiO ₂ : x H ₂ O

Adsorbent properties					
Adsorbent	Pore size	Pore volume	Bulk density	Surface area	Microns
	\AA	$cm^3\ g^{-1}$	$kg\ m^3$	$m^2\ g^{-1}$	μm
Si35-70	40	0.68	500	675	200 – 500
SiAmor	60	0.75	530	480	250 – 500
Si35-60	150	1.15	350	300	250 - 500
AC8-12	-	-	250-550	-	1680 - 4760

3.3 Estimation of empty manifold (V_M) and adsorption cell (AC) volumes

For quantifiable volumetric adsorption and desorption measurements it was essential to accurately determine the empty manifold, (V_M); empty AC, (V_{AC}) and void volumes of each respective adsorbent, (V_0) when loaded into the AC. Therefore in order to determine the volumes the He expansion method was implemented.

3.3.1 Helium (He) expansion method

The empty manifold and AC volumes were determined as follows:

1. Consider the initial conditions of the manifold and AC to have moles of gas (n_{M1} and n_{AC1}) at pressures and temperatures of P_{M1} , T_{M1} and P_{AC1} , T_{AC1} .
2. The manifold region is then charged with n moles of new gas at a pressure and temperature of P_{M2} , T_{M2} . Here the moles of gas at this point become ($n_{M1} + n$).
3. The two regions are then allowed to equilibrate and therefore the moles of gas in both regions are at pressures and temperatures of P_{M3} , T_{M3} and P_{AC3} , T_{AC3} . At equilibrium the manifold and AC contains ($n_{M1} + n - \Delta n_M$) at P_{M3} , T_{M3} and ($n_{AC1} + \Delta n_{AC}$) at P_{AC3} , T_{AC3} respectively.
4. In turn the final conditions of P_{M3} , T_{M3} and P_{AC3} , T_{AC3} become the new initial conditions P_{M1} , T_{M1} and P_{AC1} , T_{AC1} for the next subsequent experiment.

Where Δn represents the adsorption uptake into the adsorbent, Δn_M represents the volume of gas released from the manifold to the AC and Δn_{AC} represents the amount of gas remained free in the AC after the end of the run (i.e. at equilibrium). Subscripts 1-3 represent the different stages of the procedure. Since no adsorption occurs with empty volumes $\Delta n_M = \Delta n_{AC}$ this leads to:

$$(n_{M1} + n) - (n_{M1} + n - \Delta n_M) = (n_{AC1} + \Delta n_{AC}) - (n_{AC1}) \quad (3-1)$$

The equation can be written in measurable quantities by substituting n , for the Ideal gas equation including the compressibility factor, z .

$$\begin{aligned} \left(\frac{P_{M2}}{z_{M2} T_{M2}} \frac{V_M}{R} \right) - \left(\frac{P_{M3}}{z_{M3} T_{M3}} \frac{V_M}{R} \right) \\ = \left(\frac{P_{AC3}}{z_{AC3} T_{AC3}} \frac{V_{AC}}{R} \right) - \left(\frac{P_{AC1}}{z_{AC1} T_{AC1}} \frac{V_{AC}}{R} \right) \end{aligned} \quad (3-2)$$

The basic principle here is that assuming no adsorption takes place when the He expands from the manifold to the empty AC volume, then the left hand side of the volumetric balance equation

given in Eq. (3-2) reduces to zero (i.e. $\Delta n = 0$) and the equation can then be rearranged to give the ratio of the manifold volume to AC volume as follows:

$$\frac{V_M}{V_{AC}} = \frac{\left(\frac{P_{AC3}}{z_{AC3}T_{AC3}} - \frac{P_{AC1}}{z_{AC1}T_{AC1}}\right)}{\left(\frac{P_{M2}}{z_{M2}T_{M2}} - \frac{P_{M3}}{z_{M3}T_{M3}}\right)} = x_1 \quad (3-3)$$

To obtain the second equation for the unknown parameters V_M and V_{AC} another expansion experiment was carried out by filling the AC with a given volume of non-porous glass beads (GB). The use of the non-porous glass beads allows for calibration of the manifold and the AC volumes. Using this procedure the second equation for the ratio of the manifold volume to the void volume in the adsorption was given by:

$$\frac{V_M}{V_{AC} - V_{GB}} = \frac{\left(\frac{P_{AC3}}{z_{AC3}T_{AC3}} - \frac{P_{AC1}}{z_{AC1}T_{AC1}}\right)}{\left(\frac{P_{M2}}{z_{M2}T_{M2}} - \frac{P_{M3}}{z_{M3}T_{M3}}\right)} = x_2 \quad (3-4)$$

With the average values of x_1 and x_2 available, the empty volumes of V_M and V_{AC} , respectively were determined from:

$$V_M = aV_{AC} = \left(\frac{x_1x_2}{x_2 - x_1}\right)V_{GB} \quad (3-5)$$

$$V_{AC} = \left(\frac{x_2}{x_2 - x_1}\right)V_{GB} \quad (3-6)$$

3.3.1.1 Compressibility factors (z)

The compressibility factors of DME and MeCl were calculated using the generalised Pitzer correlations for the 2nd virial coefficient. The correlation was chosen for the validity for low to moderate pressures and deemed by Smith *et al.* [72] as most accurate for non-and slightly polar molecules. The overall correlation for z was calculated using Eq. (3-7) with the expanded version shown by Eq. (3-8):

$$Z = Z^0 + \omega Z^1 \quad (3-7)$$

where the coefficients Z^0 and Z^1 are functions of temperature only and the acentric factor, ω , is determined by Eq. (3-9). The acentric factor is applied to the correlation to correct for systematic

deviations of the fluid thermodynamic properties specifically for non-spherical molecules or with molecules with polar groups.

$$Z = 1 + \frac{BP}{RT} = 1 + B^0 \frac{P_r}{T_r} + \omega B^1 \frac{P_r}{T_r} \quad (3-8)$$

$$\omega = -1.0 - \log(P_r^{sat})_{T_r=0.7} \quad (3-9)$$

where P_r and T_r is the reduced pressure and temperature of the gas. The coefficients for Eq. (3-8) were calculated using Eq. (3-10) - (3-13):

$$Z^0 = 1 + B^0 \frac{P_r}{T_r} \quad (3-10)$$

$$Z^1 = B^1 \frac{P_r}{T_r} \quad (3-11)$$

$$B^0 = 0.083 - \frac{0.422}{T_r^{1.6}} \quad (3-12)$$

$$B^1 = 0.139 - \frac{0.172}{T_r^{4.2}} \quad (3-13)$$

where B^0 and B^1 are functions of reduced temperature, T_r only. The compressibility factor for He was determined [73, 74] using Eq. (3-14):

$$z_{He} = 1 + \frac{(0.00147 - 0.000004779T + 0.0000000492T^2)}{P} \quad (3-14)$$

3.3.2 Determination of particle (glass beads) density

A standard water displacement method was carried out experimentally to determine the particle density of glass beads. A graduated test tube was filled with water then a measured quantity of solid particles was added and the quantity of water displaced measured. The overall particle density of the glass beads were calculated by Eq. (3-15):

$$\rho = \frac{\text{mass of solid particles added}}{\text{volume of water displaced}} \quad (3-15)$$

3.4 Estimation of the void volume (V_0) in the adsorption cell (AC)

The void volumes for the different adsorbents contained within the AC for known amounts of adsorbent were estimated experimentally using the He expansion method as reported in open literature [64]. The data produced was further confirmed by using a simple theoretical method based on the Geldart correlation [75]. The void volume is the available volume to the gas-phase in the AC, which is not occupied by the volume of the skeleton volume of the solid adsorbent. It can debatably be assumed that He has the smallest molecular size and is a non-adsorbing gas; therefore it can be used to determine the actual available void volume in the AC. Prior to using different adsorbents a series of He expansion experiments were conducted from the manifold into the AC region over the operating pressure range. For quantification two major assumptions were made a) the He does not penetrate into the regions that are inaccessible for the MeCl and DME and b) the He is not absorbed or adsorbed by the adsorbents. The respective void volume for each adsorbent was carried out in the same way as with the glass beads but the following equations were used:

$$\frac{V_M}{V_0} = \left(\frac{V_M}{V_{AC} - V_s} \right) = \frac{\left(\frac{P_{AC3}}{z_{AC3}T_{AC3}} - \frac{P_{AC1}}{z_{AC1}T_{AC1}} \right)}{\left(\frac{P_{M2}}{z_{M2}T_{M2}} - \frac{P_{M3}}{z_{M3}T_{M3}} \right)} = x_3 \quad (3-16)$$

$$V_0 = \frac{V_M}{x_3} \quad (3-17)$$

The theoretical method is based on the reputed data by Geldart [75] which correlates the void fraction for packed beds against the particle diameter as shown in Fig. 3.8. The void in the AC was obtained by multiplying the AC volume with the void fraction for the corresponding particle size.

$$V_0 = V_{AC} \times \text{void fraction} \quad (3-18)$$



Fig. 3.8. Reported static-bed void fraction as function of particle size, (Reproduced from: [75])

3.5 Pure component adsorption/desorption

For the adsorption and desorption of DME and MeCl all adsorbents were chosen with a purpose. The two different types of synthetic zeolites, namely types 4A (4 Å) and 5A (5 Å), were selected for this study due to their pore size distributions being close to the molecular dimension of DME and MeCl, respectively and other reasons reported earlier. Walker *et al.* [76] reported the average free aperture pores sizes of 4A and 5A to be 3.5 Å and 4.2 Å respectively, whereas Triebe *et al.* [77] reports these to be 3.8 Å and 4.4 Å, respectively. It is important to recognise that these are the mean apertures and the actual pore size distribution may vary slightly depending on the manufacturing procedure. The physical and chemical properties of the zeolites used as provided by the supplier, are given in Table 3.2. The silica gels were selected due to the findings from the literature review whereby the different authors carried out respective pure component adsorption on comparable silica gels with similar properties therefore it was logical to the confirm behaviour and compare the adsorption trends with the other adsorbate. Furthermore, it was important to compare the effect of pore size, surface composition and surface area of the adsorbents to gain insights into how each property can affect adsorption for the respective adsorbates i.e. surface area, pore size and volume. The activated carbon was selected for its substantially high surface area and reports regarding MeCl having a high affinity for the solid [70]. Ultimately it was equally important to compare its behaviour with DME under similar conditions.

The two similar volumetric adsorption/desorption quantification methods using a) the Sievert method and b) differential pressure method were operated in batch mode. Although they are theoretically similar; the Sievert method uses a mass balance through gas densities and volume to measure the excess adsorption that occurs on/in the adsorbent with a single dose of adsorbate gas. Whereas the displacement pressure method uses a volumetric balance in terms of moles and volume and allows for incremental adsorption to be carried out on the same sample. Purewal [68] reports that the Sievert method is simple but requires the procedure to be repeated at incremental pressures to obtain a complete isotherm. In terms of procedure the Sieverts method considers adsorption as two stages; initial and final whilst the displacement method uses three stages: initial equilibrium conditions between the manifold and AC region, the dosed manifold and then final equilibrium stage. In order to maintain consistency within the work and use the most accurate method, the differential pressure method was used throughout. The experimental procedures for a single experiment using each technique are described below in order of occurrence. Adsorption/desorption analysis shown in section 5.3 was carried out on as received adsorbents subjected to 1 h vacuum only with a 5 min equilibrium time per increment. The subsequent analysis in section 6.2 was carried out on thermally pre-treated zeolites in vacuum for 15 h at 150 °C with an equilibrium time of 15 min per increment. For the respective experimental methodologies Fig. 3.3 is referred to for the positioning of valves and pressure and temperature readings:

3.5.1 Sievert method

1. The AC was filled approximately 90 % full with an adsorbent of choice then the AC was gently tapped down to ensure good packing.
2. The entire system was vacuumed for 1 h to achieve ultimate vacuum.
3. The AC and manifold regions were then isolated using valves MV_{1-6} . The manifold was filled slowly to the desired pressure. Once the desired manifold pressure was achieved the pressure and temperature (P_1 , T_1) were recorded. Each respective manifold pressure was maintained in the region for 2 min to settle prior to allowing for equilibrium to be reached with the AC.
4. Valve MV_5 was then opened and allowed for equilibrium to be reached between the two regions. The pressure and temperature (P_2 , T_2) were then recorded once the equilibrium time was reached.
5. For desorption the procedure was reversed, by isolating the two regions, then removing a portion of gas from the manifold through the vacuum line to a desired pressure then the two regions were allowed to equilibrate.
6. Following each experiment the AC was removed from the system and the adsorbent was un-loaded then re-loaded for a subsequent experiment.

7. In turn adsorption was carried out at incremental pressures of 0.50 atm up to the respective adsorbate gas saturation vapour pressures.

3.5.2 Differential pressure method

1. The AC was filled approximately 90 % full with an adsorbent of choice then the AC was gently tapped down to ensure good packing.
2. For adsorption on the as received adsorbents the entire system was vacuumed for 1 h to achieve the ultimate vacuum. Similarly, experiments on thermally pre-treated adsorbents were carried out following thermal pre-treatment to the adsorbent within the AC at 150 °C in vacuum for 15 h.
3. The AC and manifold regions were then isolated using valves MV₁₋₆, whilst the initial pressure and temperature were recorded (P_{M1} , T_{M1} and P_{AC1} , T_{AC1}).
4. With the AC isolated the manifold region was then gradually filled by opening valve MV₁ with the adsorbate gas being controlled by the flow meter to reach the desired incremental pressure. The manifold temperature and pressure (P_{M2} , T_{M2}) were then recorded after reaching constant values (2 min).
5. Then MV₅ between the manifold and the AC was opened and the two regions were allowed to equilibrate before recording the final pressures and temperatures in the two regions (P_{M3} , T_{M3} and P_{AC3} , T_{AC3}). Equilibrium times of 5 min and 15 min were investigated for isotherms of both adsorbates on the various adsorbents.
6. Adsorption was then carried out at incremental pressures of ~ 0.50 atm up to the respective adsorbate gas saturation vapour pressures.
7. In terms of pressure swing desorption (PSD) the process was reversed whereby the regions were isolated then a portion of the manifold was released to vacuum then the regions allowed to equilibrate for the same adsorption equilibrium time then step wise down in pressure increments. Temperature swing desorption (TSD) analysis was carried out by heating the AC then subsequent gas samples were taken from the respective manifold and AC regions. Desorption methods particularly TSD were carried out slightly differently due to experimental limitations of the system and are explained in Chapter VII.

3.5.3 Determination of adsorption and desorption isotherms

Both the Sieverts and differential pressure methods were quantified in terms of surface excess adsorption Δn^{ex} in terms of g g^{-1} and mol kg^{-1} , respectively:

3.5.3.1 Sieverts method

Where the overall mass balance is given by:

$$m^{ex} = \frac{1}{m_s} \times (m_i - m_f) \quad (3-19)$$

where the amount adsorbed at the initial and final stage was determined by:

$$m_i = \rho(P_1, T_1)V_M \quad (3-20)$$

$$m_f = \rho(P_2, T_1)V_M + \rho(P_2, T_2)(V_{AC} - V_{adsorbent}) \quad (3-21)$$

3.5.3.2 Differential pressure method

Where the overall mass balance is given by:

$$\Delta n^{ex} = \frac{1}{m_s} (\Delta n_M - \Delta n_{AC}) \quad (3-22)$$

by expanding Eq. (3-22) using the Ideal gas equation the differential uptake at each pressure increment was determined by:

$$\Delta n^{ex} = \frac{1}{m_s} \left[\left(\frac{P_{M2}}{z_{M2}T_{M2}} - \frac{P_{M3}}{z_{M3}T_{M3}} \right) \frac{V_M}{R} - \left(\frac{P_{AC3}}{z_{AC3}T_{AC3}} - \frac{P_{AC1}}{z_{AC1}T_{AC1}} \right) \frac{V_0}{R} \right] \quad (3-23)$$

Since adsorption was carried out in succession with incremental pressure on the same adsorbent, the final conditions of the first set of tests (P_{M3} , T_{M3} and P_{AC3} , T_{AC3}) became the new initial conditions (P_{M1} , T_{M1} and P_{AC1} , T_{AC1}) for the next subsequent pressure until the maximum saturation vapour pressure of the respective adsorbate gas was reached. In order to construct the adsorption isotherm and determine the cumulative amount adsorbed at any i^{th} step, the uptake at each incremental pressure was summated as follows:

$$[n_{total}]_i = \sum_{i=1}^i \Delta n_i \quad i = 1, 2, 3 \dots \quad (3-24)$$

3.5.4 Calorimetric heat of adsorption

In this work the heat of adsorption at different loadings was determined using a new calorimetric method based on direct temperature measurements. The calorimetric method was derived from the heat balance around the AC during adsorption as follows:

$$dQ_{ads} = dQ_s + dQ_{g_{free}} + dQ_{g_{ads}} + dQ_{th} + dQ_{loss} \quad (3-25)$$

where Q_{ads} is the total heat released during adsorption and the terms in the right side represent the heat gained by the solid adsorbent (Q_s), the heat gained by the free gas $Q_{g_{free}}$ surrounding the adsorbent (non-adsorbed gas), the heat gained by the adsorbed gas ($Q_{g_{ads}}$), the heat gained by the thermocouple rod Q_{th} and the heat loss to the surrounding through the AC walls (Q_{loss}), respectively. For each experiment both the temperature and pressure changes were recorded simultaneously. Fig. 3.9 illustrates an example of the typical recorded data during an adsorption experiment for DME adsorption on to zeolite 5A which was subjected to 1 h vacuum pre-treatment. Typically for all experiments it was observed that the pressure decreased quickly due to rapid adsorption on and into the vacant adsorption sites coupled with a high initial heat spike due to the interaction of the respective adsorbate molecules with the various different strength adsorption sites.

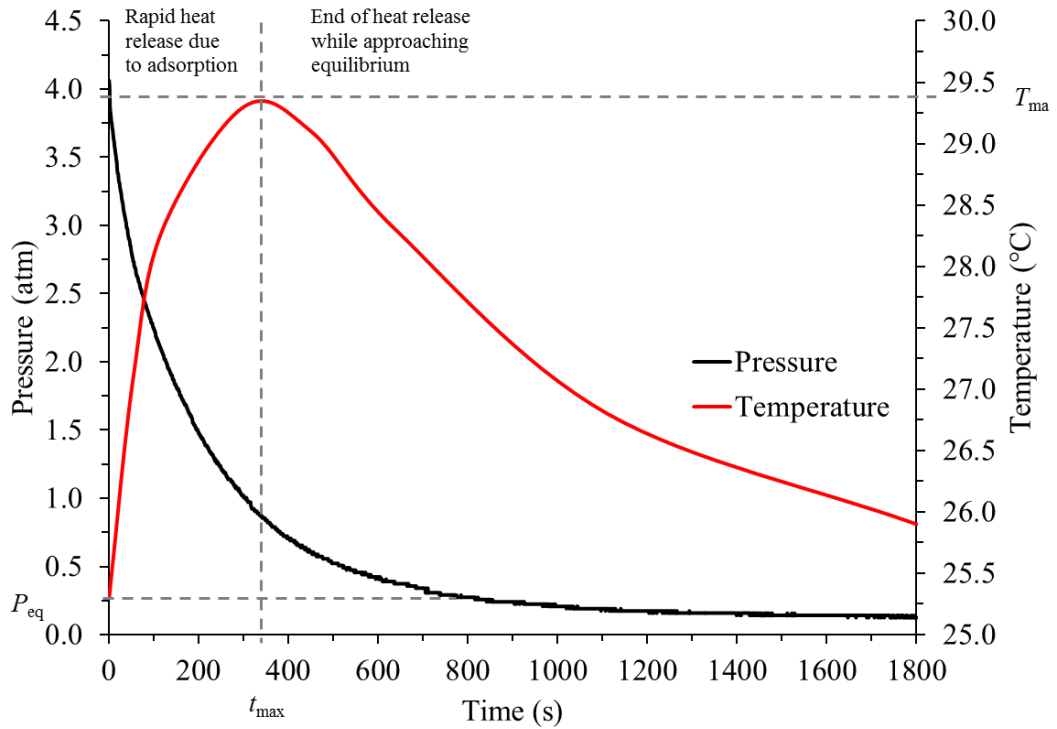


Fig. 3.9. An example of the variation in temperature and pressure inside the AC during experimental DME adsorption on as received zeolite 5A subjected to 1 h vacuum pre-treatment

In deriving Eq. (3-25) a number of assumptions were made as follows:

1. Negligible thermal resistance at the solid-gas interphase, hence both phases inside the AC are assumed to be at instantaneous thermal equilibrium. The quantities adsorbed and temperature changes due to resistances are so small they are reasonably assumed to be negligible.
2. The recorded temperature during the adsorption represents the temperature of the solid and gas phases ($=T_b$). This is a reasonable assumption since the quantities adsorbed are small, all temperatures are recorded to one decimal place and the temperature change due to adsorption occurs at a greater magnitude i.e. difference of 1 - 10 °C opposed to $< 0.1^\circ\text{C}$.
3. The internal wall in the AC is at thermal equilibrium with the gas/solid phase inside the cell ($T_{w \text{ inside}} = T_b$). As mentioned above the temperature difference between the wall and the gas/solid phase is relatively insignificant to the heat released due to adsorption on the solid.

According to these assumptions and the recorded temperature and pressure during adsorption, the equation can be written to calculate the amount of heat released at any time during the adsorption as follows:

$$\begin{aligned} Q_{ads}(t) = & m_s C_{p_s} \int_{T_o}^{T_b(t)} dT_b \\ & + (m_{g \text{ free}} + m_{g \text{ ads}}) C_{p_g} \int_{T_o}^{T_b(t)} dT_b \\ & + m_{th} C_{p_{th}} \int_{T_o}^{T_b(t)} dT_b \\ & + hA \int_{t_o}^t [T_b(t) - T_{amb}] dt \end{aligned} \quad (3-26)$$

where m_s , $m_{g \text{ free}}$, $m_{g \text{ ads}}$ and m_{th} are the masses of the adsorbent, free adsorbate gas, adsorbed gas and thermocouple, respectively. C_{p_s} , C_{p_g} and $C_{p_{th}}$ are the specific heat capacities of each adsorbents, the adsorbate gas and thermocouple rod respectively. T_b is the bulk temperature, t is the time, h is the heat transfer coefficient and A is the heat transfer area. The cumulative calorimetric heat of adsorption (H_c) in units of kJ mol^{-1} is then given by adding the heat released at incremental pressure divided by the cumulative moles of adsorbate adsorbed (n_{ads}) such that:

$$[H_c]_i = \frac{\sum_{i=1}^i [Q_{ads}(t_{\max})]_i}{[n_{ads}]_i} \quad (3-27)$$

In estimating the heat transfer coefficient used in Eq. (3-27), the equation for natural convection from a vertical heated plate was used as follows:

$$h = \frac{Nuk}{L} = C_b Ra^\gamma \quad (3-28)$$

where the constants, C_h and γ are taken as 0.10 and 0.33. The Rayleigh (Ra) number is expressed in terms of Grashof (Gr) and Prandtl (Pr) numbers as follows:

$$Ra = Gr Pr = \frac{g\rho^2\beta_{Ra}C_p(T_w - T_{amb})L^3}{\mu k} \quad (3-29)$$

where g is the acceleration due to gravity, β_{Ra} is the thermal expansion coefficient, μ is the viscosity and k is the thermal conductivity. Fig. 3.10 shows example of the calculated heat transfer quantities given in the right hand side of the theoretical Eq. (3-26) for a selected experimental DME adsorption test on as received zeolite 5A subjected to 1 h vacuum pre-treatment. The figure demonstrates that the majority of heat released from adsorption is due to the interaction between the adsorbing adsorbate and the active sites of the adsorbent owing to the greater heat capacity of the solid. As can be seen the heat released to the thermocouple, surroundings and free and adsorbed gas in the AC is relatively insignificant compared to the heat from the adsorbent. To quantify in terms of unit mass the calorimetric heats of adsorption for each component in the graph from left to right was calculated to be 0.14, 0.28, 4.26, 0.10 and 0.06 kJ mol⁻¹, respectively with total calorimetric heat of adsorption value of 4.83 kJ mol⁻¹ at a surface coverage of 0.75.

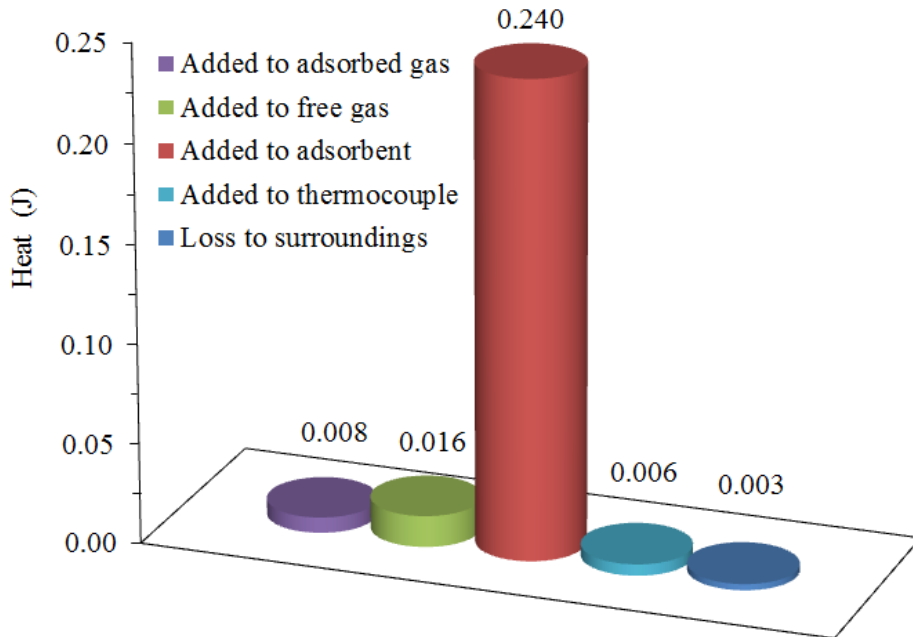


Fig. 3.10. An example of the experimentally calculated heat transfer for the adsorption of DME on as received zeolite 5A subjected to 1 h vacuum pre-treatment when $\theta = 0.75$

3.6 Results and discussion

3.6.1 Experimental determination of the empty manifold and adsorption cell (AC) volumes

The empty manifold and AC volumes were estimated to be 20.22 cm³ and 9.02 cm³, respectively. Fig. 3.11 shows the values of constants x_1 and x_2 , given by Eq. (3-3) and (3-4), respectively at incremental pressures within the range of 0-10 atm. For each working pressure the experiments were triplicated to ensure reproducibility. The overall maximum error for x_1 and x_2 were 2.72 % and 4.46 % and the standard deviations were 1.60 % and 2.97 %, respectively. These results confirm good accuracy and reproducibility of the measurements. It can be seen that the ratio for empty cell volume remained near constant for each incremental pressure. Once the particles were introduced into the AC the error increased only slightly for the glass beads. Ozdemir [64] and Kumar [74] both claim that He adsorption during gas expansion between two regions can be deemed negligible. On evidence of the experimental results obtained in Fig. 3.11 it can be seen that there is a larger deviation with the glass beads experiment therefore supporting evidence of possible adsorption and or deposition to the surface walls which is further supported in section 3.6.3. Since no surface is uniformly perfect without pores, crack and cavities it can be assumed that some He molecules weakly adhere to the surface of the walls and therefore causes a slight deviation over the pressure range.

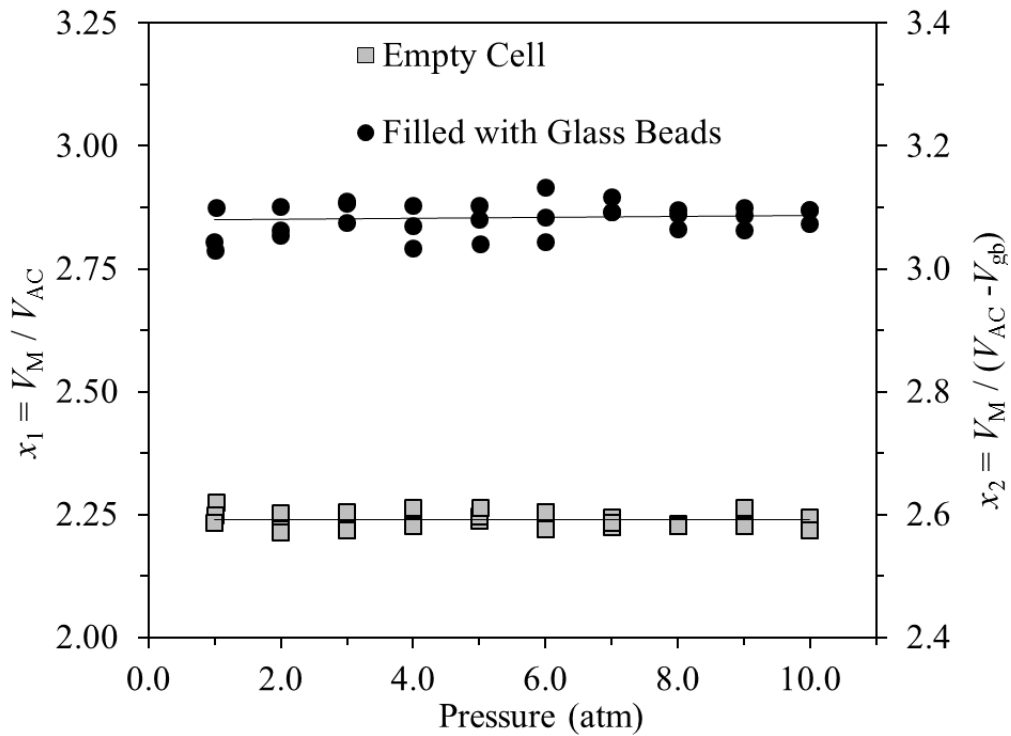


Fig. 3.11. The volume ratios for empty manifold and AC volumes, $x_1 = V_M / V_{AC}$

3.6.2 Empty adsorption cell (AC) validation for pure component dimethyl ether (DME) and methyl chloride (MeCl) adsorption

Before sorption analysis was conducted it was important to test and confirm the behaviour of both DME and MeCl adsorbate gases within an empty AC using the differential pressure method to confirm a correction factor was not needed for the implemented quantification method as reportedly needed for the Sieverts method shown in section 3.1.2. Subsequently, Fig. 3.12 shows the empty AC isotherms for DME (black squares) and MeCl (red circles), respectively at 20 °C. As can be seen by the numerical quantities ($\pm 10^{-5}$) and negligible adsorption observed for empty AC. An isotherm could not be constructed due to the negative sign of the values. This negative behaviour is a result of negligible surface deposition as reported earlier. Higher pressures were not tested due to the maximum vapour pressure of the gases used.

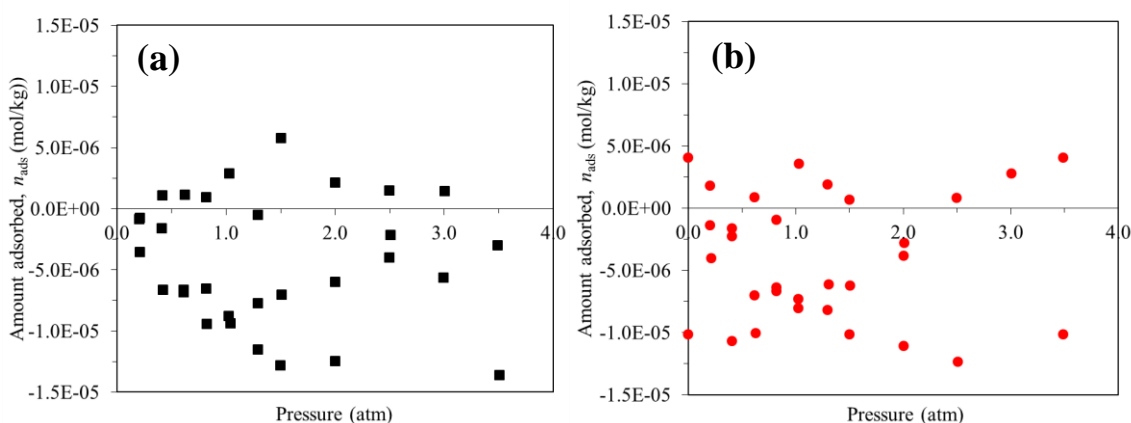


Fig. 3.12. Empty AC isotherms at 20 °C for pure component a) DME and (b) MeCl

3.6.3 Experimental void volume (V_0) determination

3.6.3.1 He versus N₂ versus Ar

Following the comments from Keller and Staudt [60] regarding the use of N₂ and Ar for particle void volumes and knowing how important the void volume is to the determination of the adsorption isotherms. It was particularly essential to confirm its non-adsorbing behaviour to determine the different void volumes for each adsorbent. As a result He adsorption was compared under the same conditions with N₂ and Ar to primarily prove the eligibility of He over N₂ and Ar to use for void volume determination under the conditions considered. Fig. 3.13a shows the value of parameter x_3 from Eq. (3-16) and Fig. 3.13b shows the adsorption isotherms at 20 °C for He, N₂ and Ar on 1 h vacuumed zeolite 5A. It is shown that while N₂ and Ar adsorb in reasonably quantities respective to their molecular size, He shows no adsorption at low pressure and a very limited negative amount adsorbed as the pressure increases which is indicative of surface depositions. These results strongly confirm the applicability of the He expansion technique in determining void volumes.

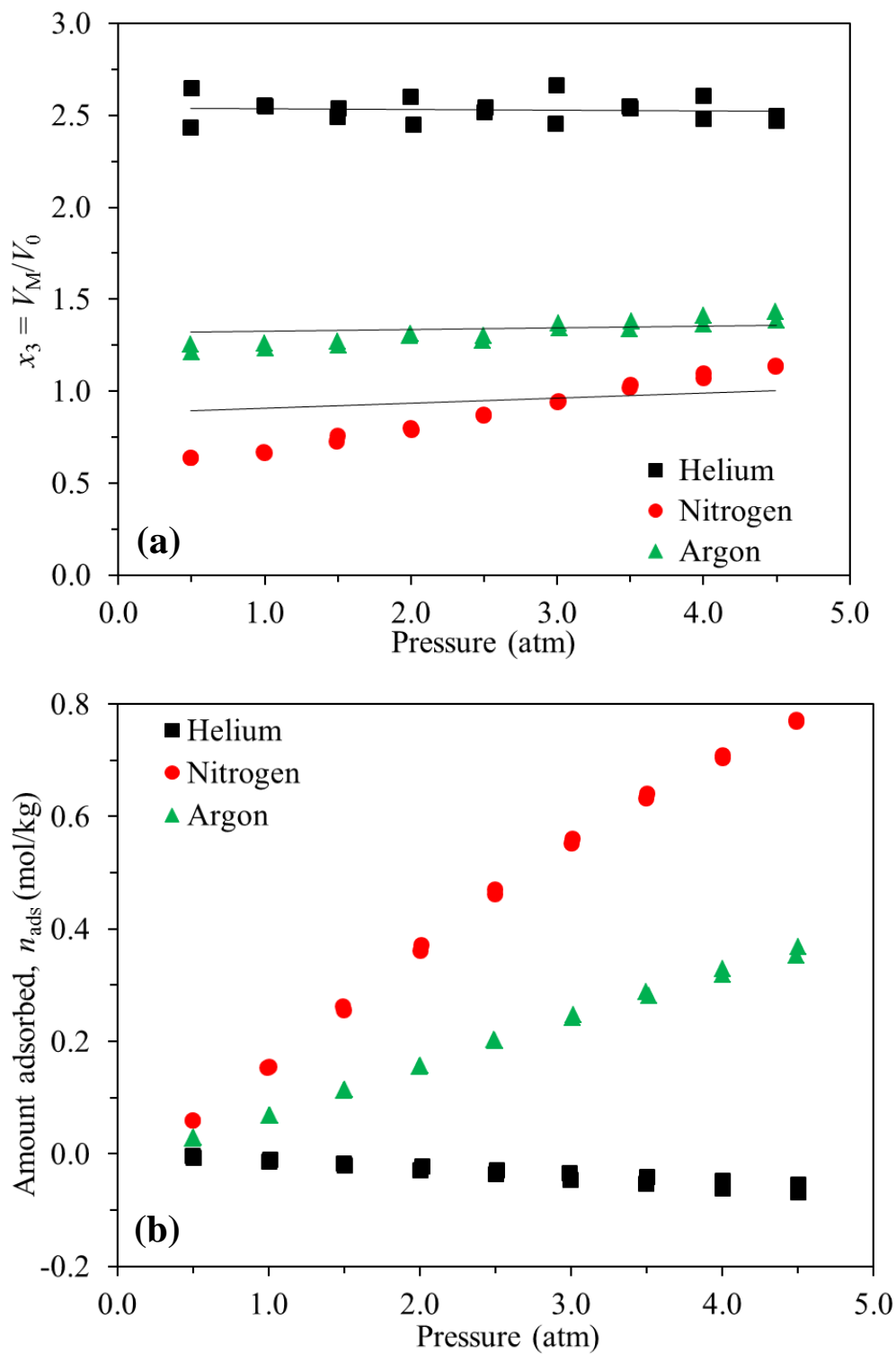


Fig. 3.13. a) The ratio of manifold volume to adsorbent void volume versus gas expansion pressure and b) adsorption isotherms at 20 °C for He, N₂, and Ar on zeolite 5A

3.6.3.2 Adsorbent void volumes (V_s)

Since six different adsorbents were used in this work each solid was characterised for the void volume using the experimental He expansion method from the manifold region to the loaded AC. For each case the quantity to fill ~ 90 % of the AC was determined then the respective estimated void volume was used for the isotherm measurements. Table 3.3 shows the fitting parameter (x_3) used to determine the respective void volumes for each adsorbent. As can be seen all adsorbents demonstrated good consistency through the 0.5 - 4.5 atm pressure range. The standard deviations for the different adsorbents ranged from 2.19 - 3.86 % thus demonstrating acceptable reproducibility of the respective void volumes at different incremental pressures.

Table 3.3. The experimentally obtained ratio of manifold volume to the respective adsorbent void volume (x_3)

Pressure (atm)	4A	5A	Si35-70	SiAmor	Si35-60	AC8-12
$x_3 = V_M/V_0$						
0.5	2.53	2.54	2.62	2.48	2.50	2.32
1.0	2.50	2.58	2.65	2.55	2.45	2.30
1.5	2.53	2.56	2.58	2.53	2.45	2.37
2.0	2.53	2.55	2.59	2.44	2.53	2.37
2.5	2.49	2.54	2.66	2.49	2.50	2.33
3.0	2.56	2.54	2.65	2.50	2.51	2.34
3.5	2.49	2.55	2.62	2.45	2.49	2.38
4.0	2.45	2.54	2.62	2.46	2.56	2.40
4.5	2.45	2.50	2.61	2.49	2.55	2.29
Average	2.50	2.55	2.62	2.49	2.50	2.34
Error (%)	4.43	3.36	3.01	4.58	4.51	4.77
Stan. Dev. (%)	3.76	2.19	2.79	3.65	3.86	3.72

CHAPTER IV: CHARACTERISATION OF ADSORBENTS

4.1 Background and literature review

4.1.1 Adsorbent characterisation techniques

For an interaction between an adsorbate molecule and an adsorbent surface to occur it is dependent upon the physical and chemical properties of both the adsorbate and adsorbent, respectively. The surface behaviour of the adsorbent is vital since it is the only parameter that can be modified in terms of functionality. Surfaces can be created, modified, damaged and even destroyed. But to fully understand the reactivity and properties of a surface the following must be determined: physical topography, chemical composition and structure, atomic structure and adsorbate bonding. Understandably, no single technique can provide all this information. Consequently several techniques must be used in collaboration for a detailed physical and chemical background to be gathered. Table 4.1 highlights some analytical techniques that can be applied to determine certain properties of a surface and those which have the largest impact to both fundamental and applied surface analysis. It is characteristic for most surface analysis techniques to be carried out in vacuum to avoid contamination namely between a surface and any air within a system. In terms of adsorption this is also true since all observed literature has reports of some type of adsorbent pre-treatment: at least vacuum to avoid contamination with other gaseous components such as air and moisture. Although others techniques exist, below we look at some different adsorbent characterisation techniques in more detail.

Table 4.1. Surface analysis techniques and obtainable information, (Reproduced from: [78])



4.1.2 Determination of porosity: mercury intrusion porosimetry (MIP) and Brunauer Emmett Teller (BET) analysis

There are a wide range of techniques and adsorption models available that allow us to calculate the volume of particles when in contact with an external fluid. Since there are various types of pore volume distributions the actual volume of each type is extremely challenging to determine. According to several reports mercury a non-wetting fluid can be used in a technique known as mercury intrusion porosimetry (MIP) to determine the envelope, bulk and skeletal volumes of solid particles [58, 61]. At low pressure the mercury adsorbs on/into the solid giving the bulk

density, then at high pressure (60,000 psi) the fluid is forced down to 0.003 μm pores. High pressure analysis is required since non-wetting fluids require strong hydrostatic pressures to enter pores. Then through manipulation of the data the respective pore volume distributions can be successfully determined. Although the method can calculate the surface area of a solid it is reported that N_2 adsorption at 77 K is better suited since the N_2 is independent from the sample nature, pore shape and sensitive to the surface roughness.

N_2 multilayer adsorption at 77 K through BET analysis provides a precise specific surface area evaluation of various materials as a function of relative pressure. The technique is widely used for external surface area and pore area evaluations to determine properties such as the total specific surface area, pore volume and pore size distribution of solid materials [66, 79]. Prior to adsorption the sample must be outgassed and thermally treated depending upon the nature of the material to eliminate contamination. The specific surface area is determined by physical adsorption of the adsorbate molecules on the solid surface by calculating the amount adsorbed corresponding to a monolayer on the surface as a result of physical adsorption between the adsorbate and adsorbent surface. Adsorption mechanisms such as the Barrett-Joyner-Halenda (BJH) and de Boer (t-plot method) can be applied to determine the pore area and volume. Unfortunately, although the technique provides good surface properties the technique is rarely used for data analysis of low relative pressure adsorption due to the level of accuracy required. The technique has also been reported to be used to investigate the chemical modifications of the silica surfaces with silanes as it causes a distinct change in the surface properties due to the attachment of a different functional group [80].

4.1.3 Scanning electron microscopy (SEM) and energy dispersive x-ray analysis (EDXA)

SEM analysis provides images of samples through a focused beam of electrons in a raster pattern; a raster scan being a rectangular pattern of image capture and reconstruction by television. As the electrons interact with the atoms in the sample they produce various signals which are detected and contain information about the surface topography and chemical composition. The SEM measures the surface morphology of conducting and non-conducting materials by analysing back-scattered electrons (BSE) and secondary electrons (SE). With the provision of vacuum, samples are prepared on button sized discs and coated with a surface coat i.e. gold to provide a path for the incident electrons to flow to ground. For chemical analysis the system makes use of the x-rays emitted by the solid sample. All atomic numbers from 4 (Be) to 92 (U) can be detected in principle, but not all instruments are equipped for light elements (< 10). The simplicity of x-rays quantitative analysis only involves measuring peak intensities for each element in relative atomic

percentages [81]. Whilst the above techniques can be applied to various scientific applications for different purposes the objective of utilising the techniques for adsorption studies is to characterise the adsorbents and obtain useful information for adsorption/desorption behaviour to occur as demonstrated by [67, 82].

4.1.4 Thermogravimetric analysis (TGA)

Thermogravimetric analysis is a method for thermal analysis to a sample in which it undergoes physical and chemical change in specified conditions. Samples are measured as a function of increasing temperature (with a constant heating rate) or time (with constant temperature and or constant mass loss). The analysis can be used to provide details about physical phenomena such as phase transitions, vapourisation, sublimation and sorption. Details on chemical phenomena include oxidation, reduction, decomposition, dehydration and chemisorption. Typically TGA is used to determine characteristics of materials that exhibit mass loss or gain due to the environment they are heated in i.e. N_2 or O_2 . In terms of adsorbents TGA can be particularly useful to determine the relative moisture content of the sample. Since adsorbents are typically thermally stable at high temperature, the analysis can be used to determine the maximum temperature before the sample exhibits degradation. If the technique is used along with infra-red spectroscopy (IR) the technique could be used to determine the relative portion of functional groups on the solid. Since silica gels contain various functional groups on the surface responsible for adsorption. Through thermal treatment in inert conditions the surface functional groups undergo chemical change therefore depending upon the ramping rate and IR analysis TGA could be used to determine the different percentage of functional groups based on the thermal stability of the respective functional groups.

TGA is a widely used tool for the characterisation of solids, as shown by [83, 84] the technique can be used to determine the moisture content and thermal stability of an adsorbent, which can be then used to define the optimum adsorbent thermal pre-treatment conditions and/or upper limit operating conditions. Tabrizy *et al.* [85] cite that TGA can provide a quantification of an adsorbed material and a measure of the adsorption enthalpy. The method has the advantage that it can be applied to all organic adsorbates and does not require aromaticity or functional groups for detection. The uptake characteristics of A-S bonding can be studied by thermogravimetric, volumetric and dynamic column breakthrough methods. Wang *et al.* [84] developed a TGA system for condensable gas adsorption on solid adsorbents under sub-atmospheric conditions by modifying the standard Cahn TG 2121 TGA. They performed isotherm measurements of water vapour adsorption on the Fuji Davison type RD silica gel and ethanol vapour adsorption on the Maxsorp II activated carbon. They claim through their research, the thermogravimetric systems mentioned above are either inaccurate and or very expensive, whilst it was estimated that a Rubotherm gravimetric analyser for measuring adsorption costs around US\$150,000 - 200,000.

4.1.4.1 Thermal pre-treatment of silica gels for adsorption

Since silica gels have various functional groups on the surface this can result in heterogeneous adsorption. Fig. 4.1 illustrates the four different functional groups on the surface. Each group can result in a different mode of adsorption through rate or strength of interaction. As demonstrated by the TGA analysis high temperature thermal treatment can lead to solid degradation and or modifications to namely surface functional groups. Under different conditions i.e. in presence of heat (in N_2 or O_2) and vacuum these can have different impacts to the solid properties and functionality. There are various techniques that exist to remove/destroy certain functional groups which can then be used to selectively adsorb different adsorbates. Below we look at the effect on the surface functional groups of silica gel following thermal pre-treatment ($> 1200\text{ }^\circ\text{C}$) in an inert atmosphere with vacuum. Although the above has not been implemented it was important to demonstrate its effect and show the potential this could have to concentrate a particular type of A-S interaction. It is proposed that the technique could be used to determine the affinity of adsorbates for certain functional groups by measuring the amounts adsorbed following different temperature adsorbent pre-treatment particularly at temperatures in the range of $400 - 900\text{ }^\circ\text{C}$.

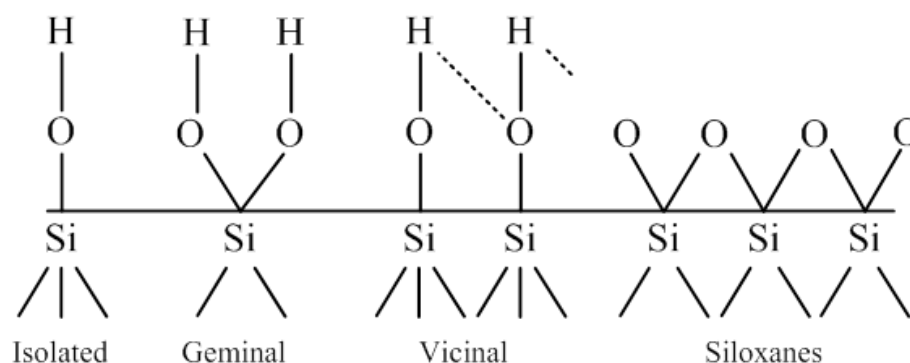


Fig. 4.1. The different functional groups on silicas

Below we look at the physicochemical changes of silica surfaces when exposed to vacuum and high temperature in stages:

1. **Stage 1:** initially all different types of silanol groups are present and the surface is typically covered with physically adsorbed water including multiple layers. OH groups are present inside the silica skeleton whilst the surface OH groups and adsorbed water are saturated with a hydrogen bonded network.
 - a. Transition from 1-2 ($25\text{ }^\circ\text{C}$ in vacuum): complete removal of multiple layers of physically adsorbed water and the process can be reversed with the presence of water.
2. **Stage 2:** ($25\text{--}190\text{ }^\circ\text{C}$ in vacuum) all the silanol groups are present and the surface is covered with a single or less layer of physisorbed water with complete removal towards the upper temperature. Internal OH groups are still present inside the skeleton.

- a. Transition from 2-3: by 190 °C all the physisorbed monolayer is removed but can be readily reversed upon the introduction of excess water.
3. **Stage 3:** (190 – 400 °C in vacuum) the degree of hydroxylation decreases significantly by just under half. All the silanol groups are still present but the concentration of single OH groups increases due to the loss of H-bonds particularly when the temperature reaches the upper limit. The vicinal bridged OH groups decreases with temperature and disappear at the upper limit. The internal OH gradually disappears with temperature.
 - a. Transition from 3-4: gradually the vicinal OH groups are removed whilst the free single and geminal OH groups remain. The process is still reversible and re-hydroxylation can take place upon the introduction of excess water.
4. **Stage 4:** (400 – 900 °C in vacuo) with temperature the amount of surface hydroxyls decrease as do the free and geminal OH groups on the surface. When the temperature is 800–900 °C all geminal and internal OH groups are removed. The concentration of the siloxanes bridge increases and the whole surface becomes covered by SiOSi groups. Consequently, there is expected shrinkage and sintering of the SiO₂ matrix.
 - a. Transition from 4-5: whilst there is complete removal of geminal and free OH groups inside the silica the single silanols remain on the surface. Now the process is barely reversible at room temperature and would take a very long time to be reversed.
5. **Stage 5:** (900 – 1200 °C) the concentration of free OH groups continues to decrease until they are completely diminished whilst the concentration of siloxanes bridges increases. At this point the shrinkage and sintering of the silica continues.
 - a. Transition from 5-6: there is complete removal of all OH groups from the silica surface and complete coverage of the surface with SiOSi groups.
6. **Stage 6:** (> 1200 °C) the silica surface now only consists of only siloxane bridges.

4.1.5 Fourier transform infra-red (FTIR)

Fourier transform infrared (FTIR) spectroscopy is a chemically specific analysis technique used to identify chemical and functional groups in a sample. The technique is used to obtain a spectrum of absorption and transmission thus creating a molecular fingerprint of the sample. The absorption peaks for the sample correspond to frequencies of vibrations between the bonds of atoms making up the material. Since no two compounds can produce the exact same spectrum the technique can be successful used to qualitatively analyse a sample. Further quantitative analyse can be conducted since the peaks in the spectrums are relative to the amount within the sample. Whilst FTIR has been successfully used for various applications [16, 86-89] a related study by Anderson and Rochester used the technique to determine the adsorptive bonds between DME and the

different surface functional groups [90]. The adsorbent was analysed prior and post adsorption to determine and quantify the different A-S interactions.

4.1.6 Gas chromatography and mass spectrometry (GC-MS) analysis

GC-MS is an analytical tool which combines gas or liquid chromatography with mass spectrometry to identify the respective component within a sample. When a sample is injected in to a GC-MS system the GC separates the mixture into pulses and the MS identifies the quantities of the chemicals. Once the sample is injected it is carried through the column by the inert carrier gas (He) to the MS. Depending upon the type of column used and settings of the method for analysis, the GC can separate molecules from the mixture based on particular physical properties i.e. volatility or polarity as they pass through the column with time. After passing through the GC the chemical pulses continue to the MS and the molecules are bombarded with electrons which causes the molecules to fragment and turn into ions. Following ionisation they pass through an electromagnetic field which filters ions based on mass to charge (m/z) and then become detected and quantified during the detection stage. Fig. 4.2 illustrates a typical GC-MS system.

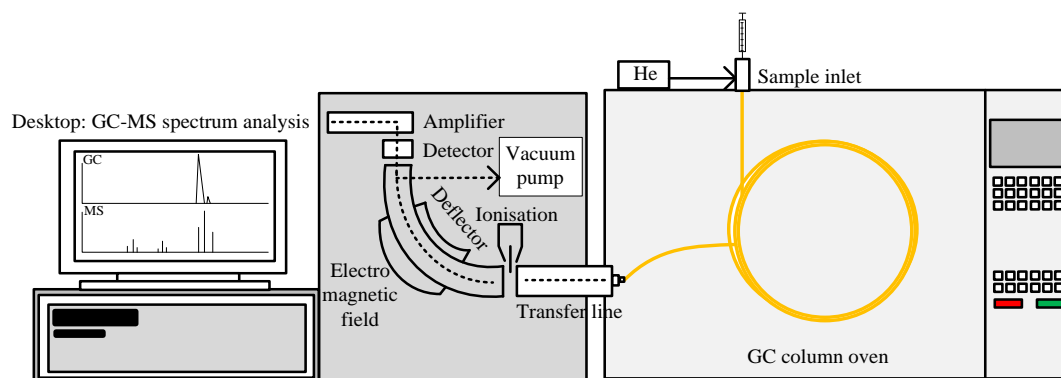


Fig. 4.2. GC-MS illustration

In order to quantify qualitatively using any analytical system there has to generally be some type of calibration to the system for the type of analysis required. For the above there are several approaches to calibration. The choice selection depends on the nature of the detected response, system configuration, analysis goals, sample type, its preparation and protocol. The three types commonly used are:

1. **External calibration:** uses a response (abundance) vs quantity (concentration), a function that is then used to estimate the concentration of an analyte in a separately analysed sample.
2. **Internal calibration:** uses a relative response function of the target analyte to another reference compound that is added pre-analysis.

3. **Standard addition:** uses a response function based on addition of incremental known amounts of the analyte of interest to a sample to determine the original analyte concentration.

A calibration curve can be used to estimate the amount of the analyte in a sample of unknown concentration. For reliability of analysis the overall results from the data must be stable and consistent and therefore consistency of all the factors relating to analysing the sample are imperative such as injection size, split ratio, temperature, flow rate, pressures and detector set points. During the injection procedure it is important to ensure that the time from injecting the sample and starting analysis is consistent. Time delays between injecting the sample and initiating the analysis can lead to drifts or changes in the retention times of the analytes. Since each analyte gets retained at a particular retention time drifts in retention times can lead to inaccurate quantification. This can be particularly detrimental to an analysis if two components retain around similar retention times. If two components become conjoined in the GC spectrum then the respective retention times become vital. By ensuring consistency and through knowledge of the retention times quantification through the MS is possible for each component.

4.2 Results and discussion

4.2.1 Brunauer Emmett Teller (BET) analysis

BET analysis was carried out to analyse the physical properties of the adsorbents. The analysis was carried out using an advanced Nova system (model: Quantachrome Nova 4000e) with liquid N₂ at 196 °C. Each sample was degassed at 150 °C for 12 h to remove any moisture, impurities and open pores, then samples were weighed (dry basis) before being subjected to full isotherm BET analysis. It has been often reported that Ar should be used over N₂ for the analysis of microporous materials particularly zeolites because of the validity of the monolayer capacity. However Bae *et al.* [66] used both gases to determine the surface areas for ultramicroporous materials and found results to be in good agreement. Although there are reservations on the use of N₂ for zeolites it is still considered the standard method and particularly useful for comparing surface areas and pore volumes particularly for zeolites.

Table 4.2 shows the surface area and pore distribution data from the results of the BET analysis of the surface area and pore volume for the zeolites, silica gels and activated carbon used. On comparison of the zeolites it can be seen that 5A has a substantially larger total surface area, which consists mainly of micropores than 4A. This is no surprise since 4A has a smaller surface to volume ratio as seen by its physical appearance from Fig. 3.7. The pore diameters could not be reported accurately using the BET since the pores are smaller than the detectable range for this type of analysis.

Table 4.2. BET surface area and pore distribution analysis for the adsorbents used

Adsorbent	Surface area (m ² g ⁻¹)	Pore volume (ml g ⁻¹)	Micropore area (m ² g ⁻¹)	Ex. surface area (m ² g ⁻¹)	Pore diameter (Å)
<i>Zeolites</i>					
4A	25.44	-	-	25.44	-
5A	436.03	0.11	395.05	40.98	-
<i>Silica gels</i>					
Si35-70	558.34	0.68	-	-	38.79
SiAmor	489.57	0.92	-	-	58.52
Si35-60	288.12	1.15	-	-	98.70
<i>Ac. Carbon</i>					
AC8-12	633.90	0.37	385.20	248.70	38.96

Of the silica gels the data obtained concurred quite well with the suppliers data. Si35-70 was reported to have surface area of 675.0 m² g⁻¹ but experimental analyse gave a value of 558.3 m² g⁻¹ while the other two gels gave closer surface areas to the supplier data with expected areas of 480.0 and 300.0 m² g⁻¹ for SiAmor and Si35-60, respectively. Of the pore volumes the BET data over estimated the expected 0.75 ml g⁻¹ for SiAmor, but resulted in the expected pore

volumes for the other two gels. The BET also under estimated the pore diameter for Si35-60, whereas the estimations were accurate for Si35-70 and SiAmor, respectively. The differences particularly with the gels are attributed to the respective manufacturing process and that no batch is the same as the next. AC8-12 was analysed to be the most microporous solid of the selected range. It gave the largest surface area and a lower pore volume than any of the silica gels.

4.2.2 Scanning electron microscopy (SEM) and energy dispersive x-ray analysis (EDXA)

For SEM analysis the samples were coated with gold to improve the conductivity of the electron beams, and then subjected to a vacuum condition in a chamber prior to analysis. The SEM analysis was carried out using energy dispersive x-ray analysis (EDXA) technique (model: Link System 1000 analyser) and a scanner (model: Cambridge Stereoscan 90). For the EDXA triplicate analyses for the same batch were taken and the average compositions used.

Fig. 4.3 shows the SEM images for both zeolites; 4A and 5A, a selected silica gel (Si35-60) and the activated carbon used at low and high magnification. It can be seen that 4A is a relatively spherical with what appears to be a smooth surface, whereas 5A has an irregular shape with sharp edges. The 4A beads are larger in size $\sim 2000\ \mu\text{m}$ while 5A particles are in the range of $350 - 500\ \mu\text{m}$. As can be seen 4A displays limited porosity unlike 5A, which is highly porous solid with visible cracks and cavities present. Since the silica gels appeared very similar in size and shape, images of Si35-60 have been shown in Fig. 4.3e and Fig. 4.3f as an example. It can be seen that although the silica gel contains a high surface area, the surface appear very smooth due to it being a gel. Compared to the 5A, Si35-60 has a less visible porosity but has more definitive edges. AC8-12 appears very porous from with what appears to be strings of fibre at low and high magnification as shown by Fig. 4.3g and Fig. 4.3h. This is no surprise since it is a highly microporous with a substantially large surface area.

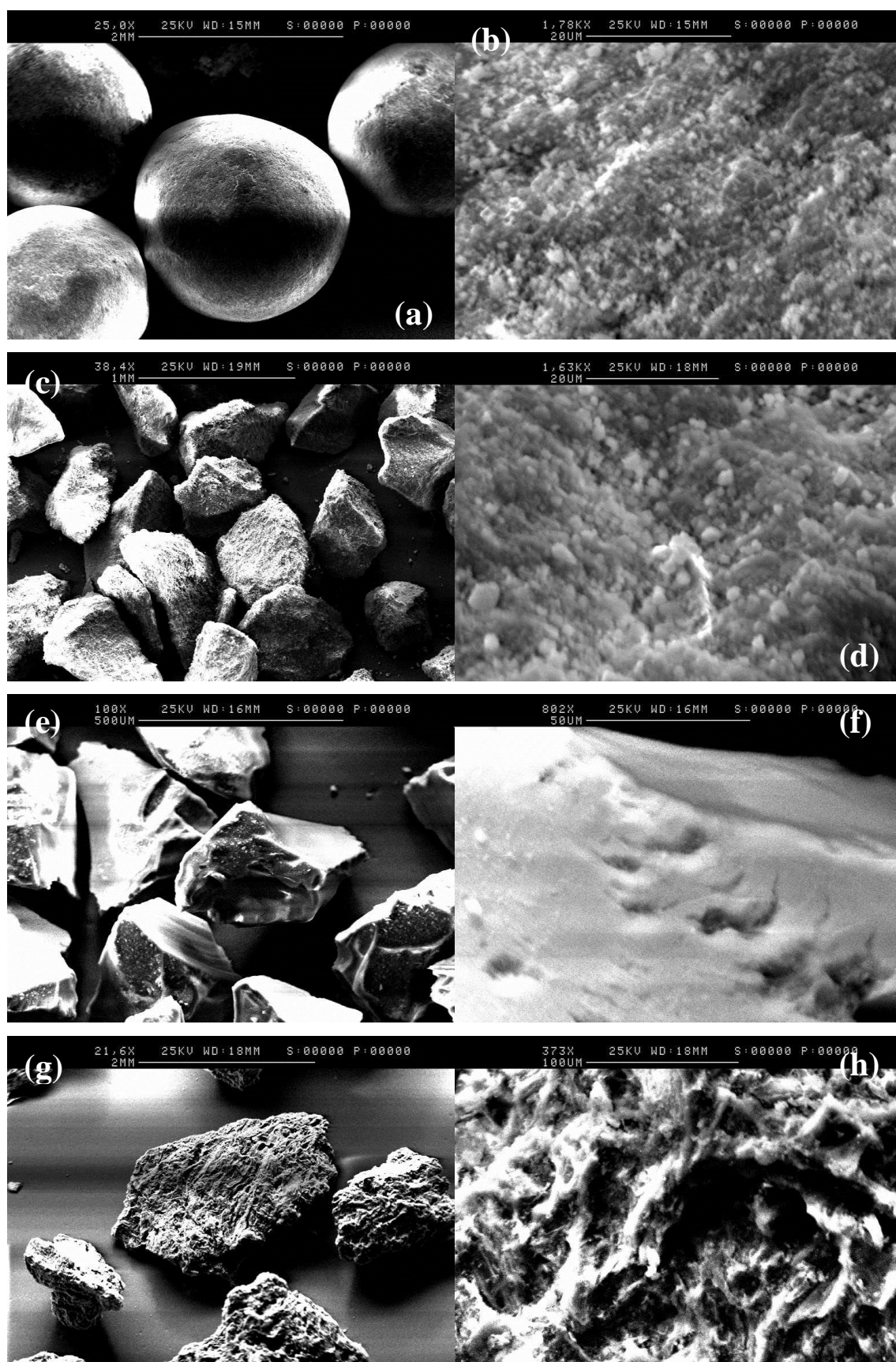


Fig. 4.3. SEM images at low and high magnification for: a, b) 4A; c, d) 5A; e, f) Si35-60 and g, h) AC

The EDXA analysis shown in Table 4.3 compares the elementary compositions of all adsorbents. With the zeolites O is a major element in both, but 4A contains less Ca and more Na as opposed to 5A, which supports the chemical composition formula given in Table 3.2. At low temperature $\leq 27\text{ }^{\circ}\text{C}$, the high O content is desirable as it allows for the adsorption and dissociation of DME into methoxy species on the surface of the particles [65]. Both zeolites have a low Si/Al ratio, which according to Semelsberger [67] and Jiang [88] is a desirable chemical property for high DME uptake. The zeolites appear to have more trace quantities of other adsorbents because they are the world's only naturally occurring adsorbent.

The EDXA for the silica gels show that O and silica are the two main components. As can be seen the larger the pores the larger the O content, whilst the smaller the size the larger the silica content. Although trace amounts of other components are likely present the analysis gives the surface composition for the selected surface area and is therefore not entirely representative of each sample. Nevertheless, the composition analysis can be used later to help understand the adsorption behaviour during the pure and binary analysis. AC8-12 on the other hand has a near 100 % carbon content with negligible amounts of Ca and O.

Table 4.3. EDXA data analysis for all adsorbents used

Adsorbent	Percentage composition (%)								
	C	O	Na	Si	K	Ca	Ti	Fe	Al
<i>Zeolites</i>									
4A	Trace	< 67	< 10	< 6	< 7	Trace	Trace	< 6	< 5
5A	< 4	43	< 2	< 2	< 5	39	< 3	Trace	Trace
<i>Silica gels</i>									
Si35-70	-	< 88	-	< 12	-	-	-	-	-
SiAmor	-	< 80	-	< 20	-	-	-	-	-
Si35-60	-	< 71	-	< 29	-	-	-	-	-
<i>Ac. carbon</i>									
AC8-12	< 97	< 2	-	-	-	< 2	-	-	-

4.2.3 Thermogravimetric (TGA) analysis

TGA was carried out on all adsorbents using the PerkinElmer Pyris 1 thermogravimetric analyser. Since the TGA analysis method is useful to determine the moisture content and the thermal stability of the adsorbent. The samples were heated in the presence of N₂ at a constant flow of 60 ml min⁻¹. The heating was carried out in the following sequence:

1. Heating from 50 to 105 °C at the rate of 5 °C min⁻¹.
2. Hold for 5 min at 105 °C.
3. Heating from 105 to 900 °C at the rate of 5 °C min⁻¹.
4. Hold at the final temperature for 15 min.
5. Cool back down to 50 °C at a rate of 20 °C min⁻¹.

4.2.3.1 Zeolites: 4A and 5A

Fig. 4.4 shows the mass loss and percentage derivative mass loss for zeolites 4A and 5A, respectively, after heating up to 900 °C in N₂. The mass loss curves for both zeolites exhibit similar trends with the rapid mass loss taking place within the temperature range of < 200 °C. At 100 °C the adsorbents lost around 5 % of their original masses, which can mainly be attributed to the evaporation of surface free moisture. This corresponds to the first peak in the differential weight loss curve. From 100 - 200 °C both adsorbents show additional weight loss of ~ 10 %, most probably due to desorption of occluded moisture and other gases, however, the differential loss is slightly different with 4A showing a second peak occurring at a lower temperature of ~ 150 °C. In the temperature range of > 200 °C, both adsorbents show negligible mass losses, thus indicating reasonable thermal stability at elevated temperatures. This is in agreement with the results of Knowlton and White [91] where it was reported that there are at least three types of water present in zeolites: crystal water, loosely bound water and tightly held water. The first two were reported to be easily removed within the temperature range of 50 – 200 °C.

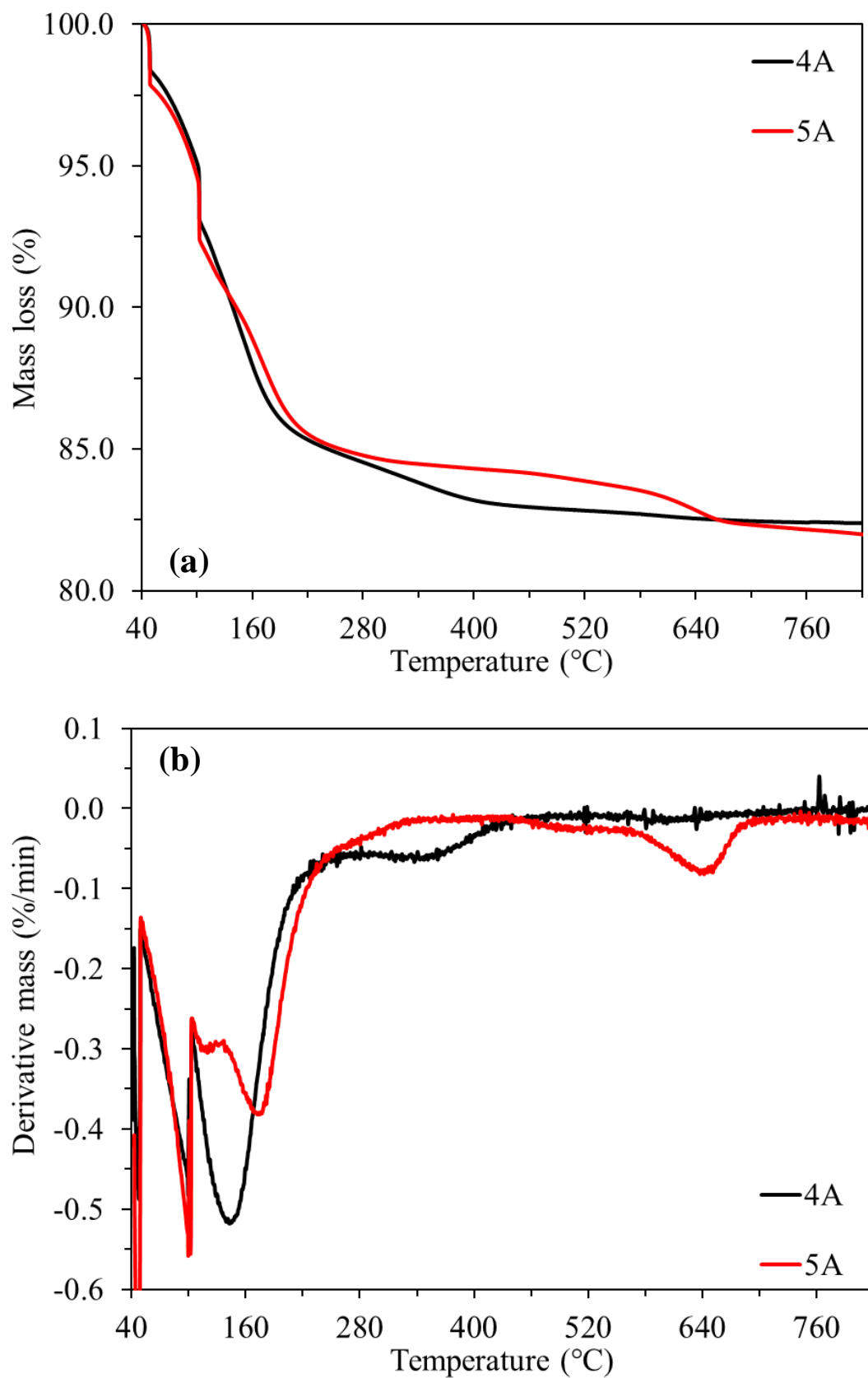


Fig. 4.4. TGA for a) mass and b) derivative weight loss versus temperature for zeolites 4A and 5A

4.2.3.2 Silica gels: Si35-70, SiAmor and Si35-60

Fig. 4.5 shows the mass and percentage derivative mass loss for the different silica gels used. It can be observed that all three silica gels exhibited similar mass loss trends following thermal treatment since they all consist of similar properties; high Si and O content. With that being said it was particularly important to distinguish the difference between the three gels since one is precipitated amorphous silica and the other two are standard high grade silica gels. The high grade silica gels: 35-60 and 35-70 mesh differ in pore volume, size and surface area. The impact of this is demonstrated in the figures as Si35-60 exhibited the least mass loss trend with temperature since it has the lowest surface area and pore volume. On the other hand, SiAmor showed a larger mass loss trend compared to Si35-70 because the former has a larger accessible pore diameter and volume even though it has a smaller surface area. If SiAmor were high purity and not precipitated amorphous the mass loss curve may would have followed the trend in between the Si 35-60 and Si 35-75 curves, respectively. But the increased mass loss behaviour is attributed to the adsorbent preparation procedure which involves acid treatment, washing and dehydration thus affecting the type and quantity of functional groups on the surface.

Overall all silica gels showed excellent thermal stability with the maximum mass loss of ~ 5-7 % for temperatures up to 800 °C. All three gels exhibited rapid mass owing to surface moisture and impurities on the surface of ~ 2 - 5 % up to 100 °C with negligible amounts thereafter up to 300 °C. Similarly, the derivative percentage mass loss curves shows two peaks for the different stages of the removal for surface and occluded moisture. As the temperature increases more strongly bound surface moisture is removed, then as the temperature increases further the occluded moisture within pores is driven out. The slight drop in mass loss which is supported by the slight derivate mass peak at 400 °C can be attributed to the removal of vicinal silanol groups [92]. Zhuravlev [92] reports that when silica is vacuumed at room temperature or heated to 150 °C this removes hydrogen bound water on the silica. It is reported that low temperature vacuum is the only way to remove the water without disturbing the OH groups. In order to remove all physically adsorbed water, 120 °C is the minimum temperature and if exposed to air moisture would become adsorbed. Since silica is microporous water can be retained within the pores at temperatures up to 180 °C even though the surface wide pores begin to free off OH groups. It is widely reported that dextroxylation of OH groups occurs above 180 °C. However the boundary temperature of the surface which causes the removal physisorbed water varies in literature with temperatures reported to be 120-300 °C for the removal of physisorbed water [92]. Such variations can be attributed to the manufacture and treatment of the gels.

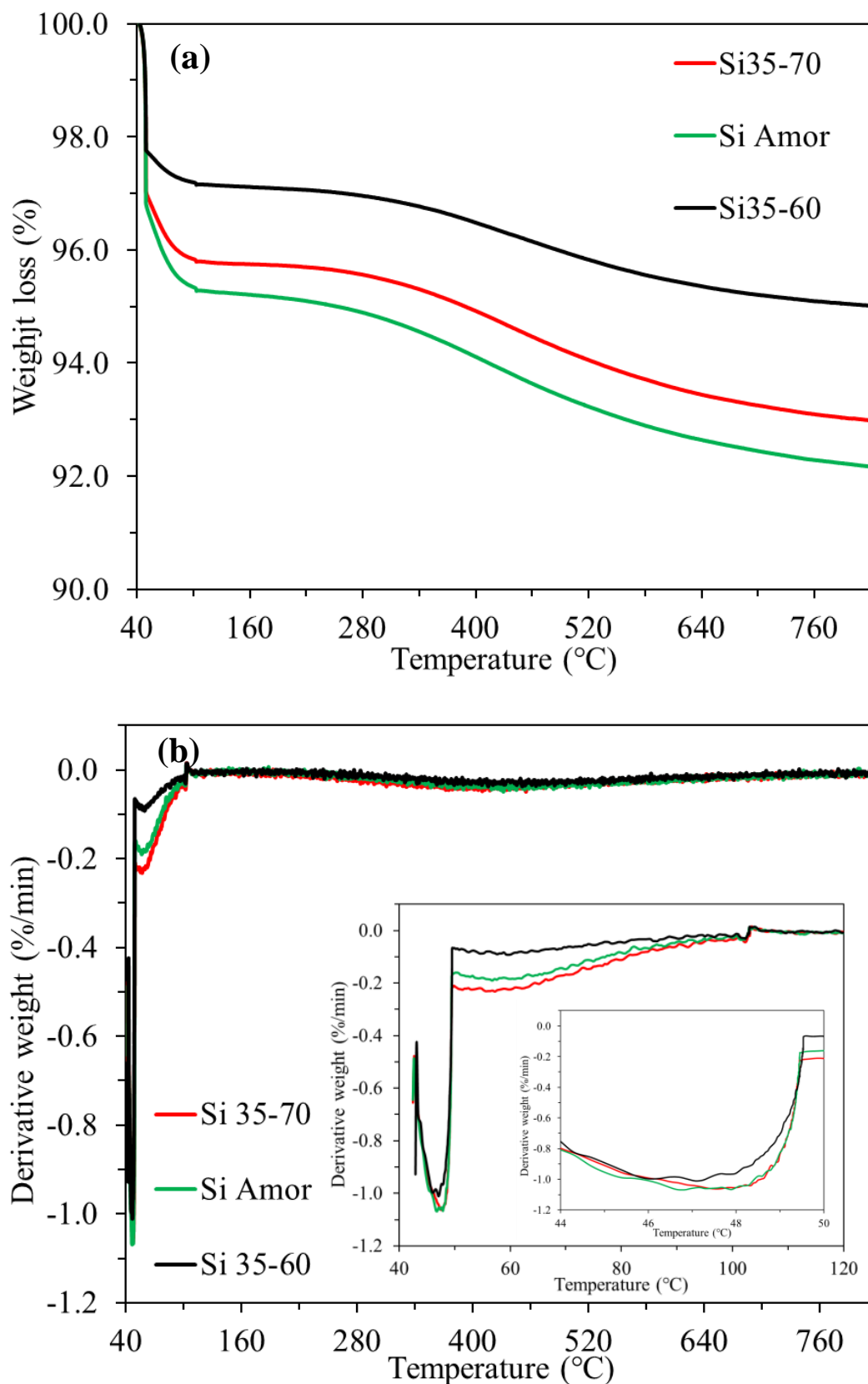


Fig. 4.5. TGA for a) mass and b) derivative weight loss versus temperature for Si35-70, SiAmor and Si35-60

4.2.3.3 Activated carbon: AC8-12

Fig. 4.6 shows the mass and the percentage derivative mass loss for a selected activated carbon type 8-12 mesh. Similar to the silica gels analysed the adsorbent exhibited a mass loss of $\sim 4\%$ below $100\text{ }^{\circ}\text{C}$ owing to physically adsorbed moisture. Up to $800\text{ }^{\circ}\text{C}$ the adsorbent exhibited a maximum of $\sim 8\%$ mass loss thus demonstrating high temperature thermal stability. The behaviour is reported to be similar to that of coal whereby moisture is removed below $100\text{ }^{\circ}\text{C}$ and no real mass loss until $400\text{ }^{\circ}\text{C}$. In terms of the sample mass loss this occurred around $550\text{ }^{\circ}\text{C}$ which was due to removal of volatiles [26].

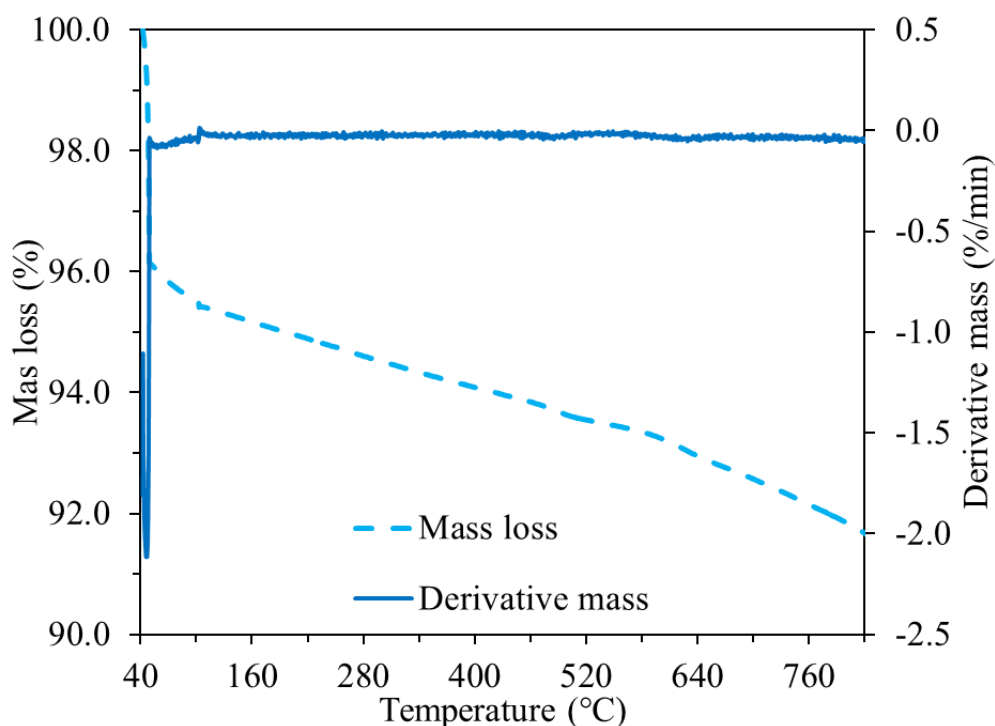


Fig. 4.6. TGA for mass and derivative weight loss versus temperature for AC8-12

4.2.4 Gas chromatography and mass spectrometry (GC-MS) analysis

GC-MS analysis was used for binary gas adsorption analysis and is detailed in Chapter VII.

4.3 Summary

The following summarises the key findings from the chapter:

- The BET surface area results for the adsorbents, with the largest surface area was AC8-12 followed by Si35-70, SiAmor, zeolite 5A, Si35-60 and zeolite 4A.
- The EDXA showed that the zeolites had trace quantities of other metal ions unlike any other adsorbents. Moreover, zeolites 4A and 5A consisted of Na and Ca respectively with O as a major component in both.
- The EDXA for the silica gels demonstrated that the greater the surface area the greater the O composition and lesser Si composition.
- The EDXA for AC8-12 showed that the adsorbent contains < 97 % of C.
- From TGA both zeolites demonstrated approximately 5 % mass loss up to 100 °C and up to 10 % mass loss up to 150 °C.
- From TGA the silica gels demonstrated approximately 4.5 % mass loss up to 150 °C and between 5 - 7 % mass losses up to 800 °C.
- From TGA.AC8-12 demonstrated around 4.5 % mass loss up to 150 °C and approximately 8 % mass loss up to 800 °C

CHAPTER V: PURE COMPONENT DME AND MECL ADSORPTION/DESORPTION ON DIFFERENT ADSORBENTS

5.1 Introduction

Gas separation and purification by adsorption/desorption has been widely reported for a wide range of different adsorbates such as methane, ethane, butane, propane, aromatics and air pollutants on various types of adsorbents [77, 93]. However there have been no reported applications or literature to suggest utilising adsorption/desorption for the removal of DME from MeCl streams or vice versa. As mentioned in Chapter II there are various types of adsorbents from zeolites, silica gels to activated carbons with each capable of gas separation/purification through adsorption (equilibrium), diffusion differences (kinetic) and/or molecular sieving effects. Ultimately, to exploit equilibrium adsorption properties one or more components are selectively adsorbed in and on the adsorbent. The materials rely on equilibrium properties for separation therefore the diffusion rates do not influence selectivity. Usually adsorbent pore apertures are substantially larger compared to the molecular dimensions of the adsorbate which leads to faster diffusion rates. Therefore the time allocated is controlled by the time taken to reach thermodynamic equilibrium. Generally, activated carbons and zeolites are capable of improving the separation effectiveness by controlling the rate at which molecules diffuse in and out the material. Diffusional effects which are exploitable and advantageous are a result of small pore size and high surface areas. The kinetic selectivity and molecular sieve properties are typically determined by the nominal diameter of the windows in the channel structure. Two limiting cases of this type of adsorption can be: size exclusion which can lead to high separation selectivity or sufficiently large diffusion rates that allow preferential uptake of one component over another in the adsorption time, known as a kinetic based separation and through chemical compositions which are primarily used for controlling adsorption affinity whereby the structural properties of adsorbent are used for controlling diffusion rates. With the above in mind it was important test both adsorbates with at least one of the respective types of adsorbents. The following details the reported literature for DME and MeCl respectively, on the different types of adsorbents followed by a detailed comparison of DME versus MeCl (pure components) for the adsorption and desorption on the different adsorbents as received following 1 h vacuum pre-treatment only.

5.2 Literature review

5.2.1 Reported studies on dimethyl ether (DME) and methyl chloride (MeCl) adsorption/desorption separation

For the removal of DME from MeCl streams currently two methods exist. The existing method in operation by Dow Corning Limited implements the invention by Post *et al.* [94] that removes at least 99 % of the DME from the raw MeCl feedstock, which varies in concentration between 0.2 – 1.0 %. The invention uses a process known as catalytic cleavage by means of HCl of DME from crude MeCl, which is produced by catalytic esterification of MeOH. The molar ratio of HCl/DME must be at least 2:1, the higher the ratio (up to 10:1) the lower the attainable residual content of DME. The preparation of MeCl based on its esterification of MeOH with HCl in the temperature range 350 - 400°C; over an aluminium oxide catalyst. Due to various amounts of DME being formed as by-products they are removed from the reaction zone together with the MeCl. Post cooling to room temperature and once the water has been condensed the residual MeCl still contains traces of: MeOH, < 0.03 %; DME, 0.3 - 2.0 %; HCl, < 2.0 % and water, ~ 0.1 %. The crude MeCl is then washed and dried with H₂SO₄ (80 - 90 % wt, preferably at the higher limit). Subsequently, the H₂SO₄ fixes to the residual water, traces of MeOH and near enough all DME. The acid converts the DME into dimethyl sulphate (CH₃O)₂SO₂ and methyl hydrogen sulphates (CH₃HSO₄), which reside in the liquid acid phase. Once the H₂SO₄ becomes saturated with sulphates (~ 30 – 35 % wt) it is regenerated via a combustion process. While the process removes nearly all DME and other impurities from crude MeCl, the key issue is the economic and environmental issues using H₂SO₄.

Since both MeCl and DME have very close boiling points, ordinary distillation has proved to be a non-effective method for separating both components. However according to Roth *et al.* [95] a two-stage distillation process in which an extractant is used in one stage can be utilised to achieve the above. Although there are no reported applications the theoretical stages are detailed below:

1. Feed the MeCl/DME mixture into a packed extractive distillation column.
2. Adding an organic liquid, (ideally organic liquids with a boiling point under atmospheric pressure which is at least 80 K higher than the boiling point of DME under atmospheric pressure), aqueous salt solution or water as an extractant in the top of the column. The extractant is preferred to be cooled (5 - 50 °C) with distillation occurring in the range of 1 - 25 bar.
3. MeCl vapours are removed from the top of the column.
4. The mixture of DME and the extractant are removed from the bottom of the column.
5. Ideally, the DME extractant mixture is sent to a heat exchanger where it is heated.

6. Introducing the DME/extraction mixture into a distillation column and removing the DME vapours from the top of the second column.
7. Finally, the extractant can be removed from the bottom of the second column and recycled.

5.2.2 Adsorption/desorption using zeolites

There have been limited studies involving pure component DME and MeCl adsorption and/or purification/separation from binary mixtures using zeolite and or molecular sieves. The following details the reported literature for each component on the above.

5.2.2.1 Dimethyl ether (DME) adsorption/desorption and removal from other streams

Table 5.1 reviews four reported studies for the pure component sorption of DME on zeolites. As can be seen only the study by Kobayashi *et al.* [52] carried out an actual volumetric experiment in terms of amount adsorbed and binary adsorption analysis with mixtures of MeOH reporting different temperature isotherms, empirical models and details on the heat of adsorption. In a later study they also empirically modelled the binary behaviour of DME and ethane mixtures but on the same adsorbent [96]. The reported studies involving TEOM and *in-situ* FTIR analysis are not so relevant since they focused largely on different adsorption aspects such as the A-S bonding. Unfortunately, none of the studies demonstrated any relation to molecular sieving or details on kinetics.

Two inventions related to sorption and zeolites are reported for the removal of DME impurities from mixtures containing hydrocarbon mixtures [97] and liquid olefin C₃-C₅ feeds [98]. The patent invention by Reyes *et al.* [97] utilizes both TSA and PSA to separate DME from hydrocarbon mixtures using eight membered ring zeolites due to their pore window sizes being comparable to molecular dimensions of DME, consequently increasing the adsorption capacity. Other reported adsorbents include ion exchange resins, mesoporous solids and activated carbons. The upper adsorption temperature limit for PSA is recommended to be in the range 323 – 523 K for the pressure range of 5 – 200 kPa to avoid unwanted side reactions and polymerisation during desorption. The zeolite is reported to adsorb the DME in less than 120 s and regeneration is carried out in the partial pressure range of 0.2 – 5.0 kPa. During TSA adsorption is carried out firstly at the lower temperature then subsequent desorption at higher temperatures. The recommended operating temperature is in the range of 323 – 423 K for the pressure range of 20 – 200 kPa.

Table 5.1. Reported studies on DME adsorption on various zeolites

Adsorbent <i>Type, properties, method</i>	Conditions <i>Temperature, pre-treatment</i>	Amount adsorbed <i>Max ads.</i>	Comments	Ref.
Zeolite SAPO-34 (Surface area: 1247.0 m ² g ⁻¹ ; Pore size: 5.5 Å) <i>Volumetric ads.</i>	Ads. at 298, 333, 373 K Heated at 673 K and outgassed for 5 h	2.20, 1.84, 1.25 mmol g ⁻¹	Adsorbed by more than one DME molecule per acid site; Further adsorption sites at high pressure to increasing adsorption with coverage; Differential heat ~60-70 initially then constant ~45 kJ mol ⁻¹ ; Irreversible adsorption quantities calculated at all temperatures.	[52]
Zeolites Various zeolite and copper zinc composite catalysts Zeolites such as: Y(2.5) Si/Al - 15 ZSM-5 Si/Al - 15 <i>TEOM</i>	358 K 0.78 atm	659-309 μmol g ⁻¹ 575-197 μmol g ⁻¹	DME uptake favoured by a lower Si/Al ratio; Higher DME affinity for type Y zeolites over ZSM-5; Desorption was carried out using residual gas analysis (RGA); Desorption temperatures of DME increased with increasing Si/Al ratio for type Y zeolites.	[67]
Zeolite H-ZSM-5 Si/Al - 12.0 (HZ-12) Si/Al - 27.0 (HZ-27) <i>In-situ FTIR</i>	Ads. at 423, 473 and 523 K Purged with N ₂ (330 mL min ⁻¹) at 673 K for 4 h	-	At 423 K strongly adsorbed on Brønsted acid sites; At 473 K partial dissociative adsorption on HZ-12, not with HZ-27; At 523 K showed dissociative adsorption.	[88]
Zeolite ZSM-5 H-ZSM-5 (Si/Al - 15.0) Na-ZSM-5 (Si/Al - 26.0) <i>In-situ FTIR</i>	Ads. at 293, 373 and 473 K Purged with N ₂ (400 mL min ⁻¹) at 673 K	-	At room temp hydrogen bonding, occurs mainly internally (pores); At 373 K only interactions with internal hydroxyl groups occur; Dissociative adsorption/chemisorption at higher temperatures.	[89]

Nagji and Corvini [98] recommend zeolite types *X* and *Y* namely: faujasite, for the selective removal of DME from liquid olefin mixtures. They report that selective adsorption of DME occurs within the adsorbent bed in the temperature range of 0 - 50 °C and pressure range of 15 - 500 psiA thus allowing the purified liquid olefins stream to pass in the effluent. Subsequent regeneration occurs in the temperature range of 150 - 300 °C and a non-adsorbing purge gas can be used for desorption.

Smith Jr *et al.* [99] designed a process to remove DME and MeOH from C₄ hydrocarbon streams which exploited the difference in solubility of the components with water. The process fractionates a mixture of the aforementioned components at 200 - 300 psig. The top fraction containing the mixture is condensed with water. The low temperature is important since it is favourable for the solubility of DME in water. The water and hydrocarbon phases are separated in the decanter whilst being continuously removed. The water is enriched containing DME, MeOH and hydrocarbons to the limit of their solubility. Since hydrocarbons are largely insoluble in water, it is returned to the distillation column. Then the water enriched with DME, MeOH and any soluble hydrocarbons is heated and passed to the flash drum at ideally atmospheric pressure and 20 – 50 °C. Finally the DME and solubilised hydrocarbons become vapourised and removed which can be burnt off since it is a small stream.

5.2.2.2 Methyl chloride (MeCl) adsorption/desorption and removal from other streams using zeolites

Similar to DME, very few relevant articles have been published for MeCl adsorption on zeolites and or molecular sieves. Of these two relevant literature articles have been summarised: one reported study by Toreci *et al.* [35] and a patent invention by Zarchy *et al.* [69]. The former reported the adsorption separation of MeCl from N₂ using ZSM-5 and mesoporous SBA-15. They used and modelled the isotherms using empirical models and used the data to predict for binary mixtures. They also demonstrated MeCl isosteres, heats of adsorption and determined separation factors for mixtures.

According to Jaumain and Su [79] MeCl interacts by its negatively charged chlorine atom with the polarised hydrogen atoms of hydroxyls in zeolites through hydrogen bonding. For their investigation of monitoring the Brønsted acidity of zeolites by means of *in situ* FTIR and catalytic testing using MeCl as the probe molecule they studied the acid activity for temperatures in the range -140 - 100 °C. They cite that the interaction between the MeCl molecule and the surface hydroxyls was dependent upon the temperature and heterogeneity of the acidic hydroxyls. Contingent upon the zeolite used, generally at temperatures below -130 °C the Si-OH-Al located in the large cages were observed to be occupied. Above and around room temperature the

hydroxyls located in the large cages increased in intensity due to regeneration, with a higher temperature required for zeolites with a greater Si/Al ratio. For the temperature range studied no peaks related the hydroxyls located in the small cages were detected suggesting that these hydroxyls were not accessible for MeCl. The regeneration of the hydroxyls at higher temperatures is due to the increase in kinetic energy of the molecule with increasing temperature thus meaning the interaction between the hydroxyl and MeCl molecule was weakened. The study demonstrated that depending upon the heterogeneity and acid strength of hydroxyls the MeCl molecule was retained at high temperatures at the very strong active sites. Upon adsorption of MeCl with the different zeolites they observed that some hydroxyl peaks were unaffected by adsorption indicating inaccessibility of these OH groups to MeCl. However they stressed that no interaction between these OH groups and MeCl shows that MeCl cannot penetrate into these small cages. Moreover MeCl interacted with the silanol groups; however the interaction was reported to be progressively restored towards higher temperatures suggesting weak interactions between the two.

A much-related invention by Zarchy *et al.* [69] patented the process for separation and recovery of MeCl from vent streams containing isobutene. With use of the conventional PSA process, they added two more steps to the basic cycle thus allowing them separate MeCl from isobutene using crystalline molecular sieves such as silicoaluminophosphates and aluminophosphates. The invention accomplishes separation by selecting adsorbents with pore opening in the range $3.7 \times 3.7 - 4.9 \times 5.7 \text{ \AA}$ thus excluding the larger isobutene ($4.9 \times 5.7 \times 6.2 \text{ \AA}$) molecules and allowing the more adsorbable component (MeCl) to adsorb. The following points were cited as important factors for the separation:

1. Increasing the temperature slightly increases the pore size of the adsorbent to some extent.
2. The adsorption strength for the adsorbed species, i.e. MeCl, boiling point ($-24.2 \text{ }^{\circ}\text{C}$) has a larger dipole moment resulting in a stronger interaction with cations in the adsorbent.
3. For economical operation the adsorbent should preferably have a linear adsorption isotherm with respect to the adsorbed components partial pressure.
4. No or minimum cations present on the surface of the adsorbent are favoured thus increasing adsorption capabilities. A zeolite with minimum cations and high Si/Al ratio was used to limit the interaction between alumina and HCl a consequent of HCl production during adsorption.
5. Agglomerating any crystalline molecular sieve with a binder ensures the adsorbent has sufficient physical properties, e.g. silicas, aluminas, metal oxides and clays.

The complex invention is shown by Fig. 5.1 and detailed below:

1. A vapour effluent stream enters a purification zone comprising of MeCl, N₂ and C₁-C₅ hydrocarbons.
2. Some MeCl is recycled, whilst the remaining MeCl and other two components go to the pressure swing adsorption zone (stream 2);
3. Three adsorption beds are preferred though two beds are acceptable (at least one solid adsorbent bed), with the following adsorption conditions: temperature 20 – 120 °C and pressure ~ 0.98 - 16.8 atm;
4. As a result of the size selective adsorbent the C₁-C₅ hydrocarbons and preferably enriched isobutene leave the adsorber via vent (stream 4) during an adsorption step at the respective conditions.
5. The first effluent from the adsorber passes to an incinerator containing < 10 % wt chlorinated hydrocarbons including some MeCl.
6. To increase recovery of a high purity MeCl stream an external co-purge step or co-current displacement step is introduced to rinse the adsorption bed prior to any de-pressurisation step.
7. Following co-purging, the bed is de-pressurised and purged to provide a high purity MeCl desorbed effluent (stream 5) at pressures of 0.0069 – 0.98 atm.
8. The adsorption bed is advised to be purged with a portion of the product gas then withdrawn during the concurrent displacement step or during the adsorption step.
9. The desorbed effluent stream (stream 5) passes the MeCl to a liquefaction zone which becomes compressed at ≥ 11.8 atm, cooled to ≤ 35 °C then flashed to separate non-condensable gases including N₂.
10. Stream 7 going into stream 3, indicates the displacement gases used for co-purge.



Fig. 5.1. Flow Diagram for separation & recovery of MeCl from vent streams of isobutane, (Reproduced from: [69])

5.2.3 Adsorption/desorption using silica gels

Compared to zeolites there have been more reported studies for the pure component adsorption of DME and MeCl, respectively on silica gels as shown below.

5.2.3.1 Dimethyl ether (DME)

Two studies have been reported for the sorption of DME on silica gels, first a pioneering study by Robinson and Ross [100] and then another by Anderson and Rochester [90]. Both studies concordantly reported DME adsorption on silica gel as a result of hydrogen bonding. Robinson and Ross [100] investigated the adsorption of DME at its boiling point on a range of silica gels through adsorption/desorption isotherms and isothermal calorimetric heats of adsorption. Through their research they found that moderately strong hydrogen bonds were formed between the O atom on the ether and the surface hydroxyls. Using an all glass quartz spring vacuum the silica gel of particle size 75 - 150 μ was used for gels heat-treated at 240, 500, 700 and 900 °C.

Additional tests included impregnating the silica gel with 0.274 % w/w aluminium in a solution of aluminium nitrate. Their results showed that adsorption of DME when $\theta = 0.01 - 0.10$ gives a high heat of adsorption in the range of 20 and 16 kcal mol⁻¹. For the specific model it was believed that a strong hydrogen bond formed at low coverages. It was claimed that this was due to surface heterogeneity, where the most vulnerable to change silanol groups interacted with the adsorbed molecules first. The formation of hydrogen bonding with silanol groups was attributed to the following: the angle of C-O-C bond in DME is $111 \pm 4^\circ$ thus indicating that the O₂ atom uses sp³ hybrid orbitals, two half-filled sp³ orbitals overlapping with those of the carbon atoms and two occupied by electron pairs. It is therefore these two electron pairs, which are available for hydrogen bond formation. Similarly, Anderson and Rochester [90] reported that for weakly adsorbed DME only one methoxy group in each molecule was bonded to each silanol group. The stronger mode of adsorption involved both methoxy groups in each DME molecule bonded to the adsorbent and therefore formed a dominant mode of adsorption at low coverages. It was cited that because of the strong hydrogen bonds, subsequent desorption showed evidence of resistance even after prolonged vacuum. According to Robinson and Ross [100] gels treated at lower temperatures showed increased sorption as shown by Fig. 5.2.



Fig. 5.2. Adsorption/desorption isotherms for DME at 248.2 K on A, 240; B, 500; C, 700 & D, 900 °C, (Obtained from: [100])

It was suggested this was mainly due to dual site adsorption occurring with some single site adsorption, with the latter likely of being more dominant with increasing coverage. Following impregnation with aluminium they found adsorption increased with temperature to the formation of Brønsted and Lewis acid sites. It was thought to be a result of adsorption or condensation of a basic form of aluminium on a surface hydroxyl group and the aluminium complex is subsequently able to interact with an adjacent hydroxyl group instigating a proton dissociation yielding a Brønsted acid site. Similarly, at higher temperature the DME molecules, which were initially adsorbed, accepted the dissociated proton forming a charged species resulting in molecules adsorbing in clusters thus increasing DME adsorption. It is only with the dehydration of Brønsted centres which resulted to the formation of Lewis sites where the aluminium atom bonds to three O atoms, thus leaving an electron pair vacancy in its valence shell.

5.2.3.2 Methyl chloride (MeCl)

Similar to DME there are two reported studies of MeCl adsorption on silica gels of particular relevance; Kuo and Hines [48] and Kuo *et al.* [50]. In both papers it was reported that MeCl weakly adsorbs on to the silica gel, predominantly a result of weak VDW's forces. Kuo and Hines [48] used a 80-100 mesh gel and conducted adsorption gravimetrically using a Cahn R-2000 electro balance within a vacuumed bottle at 25 °C. They applied the Polanyi theory and claim that the adsorption potential decreases with time due to the filling of sites on the adsorbent and the distances between the adsorbate molecules and adsorbate lengthen. By implementing the Dubinin theory for pore filling of microporous solids they obtained a generalised equation as shown by Eq. (5-1). They reported the affinity coefficient (β_M) of MeCl to be 0.95 on silica gel which increases to 1.2 - 1.8 and 3.0 - 6.0 for zeolites and activated carbons, respectively.

$$W = 0.301 \exp \left[- \left(\frac{\varepsilon}{1.374 \beta_M} \right)^{1.42} \right] \quad (5-1)$$

The study by Kuo *et al.* [50] is an extension to the earlier work from Kuo and Hines [48]. They investigated the correlation of MeCl, methylene chloride, chloroform and carbon tetrachloride adsorption data on silica gel. Adsorption was carried out at three temperatures 288, 293 and 298 K from low pressure up to saturation. Regeneration of the adsorbent was carried out by evacuating the system and heating the adsorbent to 423 K overnight for 4 – 10 h. Adsorption data for all four chemicals exhibited Type I according to the Brunauer classification and showed no apparent hysteresis when desorbing. An absence of capillary condensation was observed which indicated a majority of micropore adsorption in the silica gel. For the homologous series, the amount of adsorbate removed increased as the molecular weight of the adsorbate increased. The maximum capacities for the homologous series fell on a single curve for each temperature suggesting that the curves may be used to predict maximum capacities of other compounds in the

series. Increasing temperature was observed to weakly influence the saturation capacity of the gel with saturation capacities of 6.93, 6.81 and 6.61 mmol g⁻¹, respectively. Silica gel was concluded to be effective for the adsorption of chlorinated hydrocarbons notably with increasing pressure. Other studies have been reported on silicon surfaces such as Si(100) and Si(100)2 x 1 by Brown and Ho [101], with further work carried out by Woelke *et al.* [102], however they were led to the conclusion that MeCl adsorbed on Si surfaces dissociatively.

5.2.4 Adsorption/desorption on other adsorbents

5.2.4.1 Dimethyl ether (DME)

Other studies involving the adsorption of DME on metal surfaces have been reported. Bugyi and Solymosi [103] claim that adsorption of DME on a clean Rh(111) surfaces has a positive outward dipole moment and the adsorption is characterised by the reduced work function of the Rh(111) surface. DME is reported to adsorb molecularly on clean Rh(111) at 100 K and desorb without any detectable dissociation. At higher temperatures (250-300 K) it is reported that partial dehydrogenation of DME proceeds and pre-adsorbed O atoms activate DME molecules even at (100-190 K) to produce methoxy species. Farkas *et al.* [104] claim that DME represents a challenging compound for it is a symmetrical molecule and its activation and dissociation on metal surfaces is extremely difficult. They supposed that the chemistry of DME on clean Mo₂C/Mo(100) displays a somewhat higher reactivity compared to metal surfaces. Kasahara and Koichi [105] using infrared reflection adsorption (IRA) spectra were able to conclude that DME adsorbed at 80 K on Cu(111) and Ag(111). The IRA indicated that the adsorbate takes on an orientation in which the C₂ axis bisects the COC angle which tilts away from the surface normal within the plane perpendicular to the substrates as shown by Fig. 5.3.



Fig. 5.3. Schematic representation of adsorption structures of DME on Cu(111) and Ag(111) surfaces, (Obtained from: [105])

5.2.4.2 Methyl chloride (MeCl)

There have been numerous reports of adsorption of MeCl onto various surfaces/adsorbents such as metal surfaces [13, 101, 106], charcoal [107, 108] and activated carbon fibres [109] due to its presence as an air and water pollutant. The earliest reported studies were on charcoal from $-32^{\circ}\text{C} - 237^{\circ}\text{C}$ [107, 108]. The latter discussed the role of the chlorine atom during the adsorption process and came to the conclusion that because the chlorine atoms have a large electronegativity it is strongly attracted to the carbon atoms. Mariwala and Foley [70] cite that the permanent dipole on MeCl contributes to electrostatic forces to the potential interaction with the carbon atom which as a result can complicate otherwise simple VDW's forces. In addition, adsorption at higher temperatures on carbogenic materials allows for increased effective diffusivities and thus resulting in shorter equilibrium times. Molecular and dissociative adsorption was observed by Ali *et al.* [110] on iron, nickel, palladium, lead, gold and copper surfaces. At temperatures $> 300\text{K}$ dissociative chemisorption occurred with the evolution of by-product gases such as methane, ethane and hydrogen due to the reactions between the adsorbate and surface. Wu *et al.* [109] reported that adsorption on activated carbon fibres gave a heat of adsorption value of 38.5 kJ mol^{-1} predominately associated with physisorption and that a more complete desorption isotherm is observed when the adsorbent has a more homogeneous pore structure. Wei *et al.* [86] report that MeCl can be transformed into longer chain hydrocarbons as a potential route for natural gas utilization. Although the process does not involve sorption, the catalysts used, HZSM-5 and SAPO-34 have been used for sorption studies as demonstrated earlier. It was reported that both catalysts give high selectivity's for conversion of MeCl to gasoline.

5.2.5 Theoretical comparison: dimethyl ether (DME) versus methyl chloride (MeCl)

Since the kinetic selectivity and molecular sieve properties are determined by the nominal diameter of the windows in the channel structure and for one component to have a greater affinity to the surface functional groups for equilibrium separation. In order to manipulate kinetic selectivity and/or molecular sieving effects it was important to determine the properties of the adsorbate gases namely the molecular dimensions since other physical and chemical properties between MeCl and DME have been exploited. According to Borgmann *et al.* [111] small molecular sieves in the range of $4.3 - 5.0 \text{ \AA}$ are more favourable for the adsorption of DME. Whereas Zarchy *et al.* [69] reports the molecular dimensions of MeCl to be approximately $3.7 \times 3.7 \times 4.6 \text{ \AA}$. Evidently, suggesting MeCl is the smaller of the two. Tamagawa *et al.* [112] and Preuss *et al.* [113] reported the structural properties of DME and MeCl, respectively as shown by Table 5.2. Subsequently it is these bond lengths and angles that determine the respective

molecular dimensions. On analysis it can be seen that both molecules are in the range of $\sim 4.0 - 5.0 \text{ \AA}$, as a result zeolite molecular sieves 4A and 5A were selected and tested.

Table 5.2. Structural properties of DME versus MeCl

Compound	Angstroms (\AA)					
	$r_g(\text{C-O})_{(\text{av})}$	$r_g(\text{C-H})_{(\text{av})}$	$\phi_{(\text{av})}(\text{C-O-C})$	$\phi_{(\text{av})}(\text{HCH})$	C-Cl	C-H-H-H
$(\text{CH}_3)_2\text{O}$	1.415	1.118	111.8	109.2	-	-
CH_3Cl	-	1.090	-	110.6	1.78	51.8

The following demonstrates a theoretical comparative analysis of DME versus MeCl adsorption on zeolites 4A and 5A, respectively; supported by literature. Apart from the differences discussed thus far, the surface chemistry of the adsorbents must also be considered. The surface functional groups of both zeolites 4A and 5A consist of Na^+ and Ca^+ cations (protons), respectively (Table 3.2). Both are therefore considered to be Lewis acids whereby they have an electron accepting tendency. Generally when a water molecule interacts with a proton it is through the lone pair of electrons on the O that donate electrons thus forming a bond; whereby the O behaves as a Lewis base. Following only 1 h vacuum of the zeolites only the weakly bound moisture/impurities is removed from the surface and pores meaning some strongly bound moisture/impurities are still molecularly adsorbed at strong adsorption sites thus reducing the adsorbent capacity as demonstrated from the TGA.

Let us consider the interaction between DME and MeCl with surface hydroxyls. Although other A-S interactions occurs i.e. A-Si or A-Al, Fig. 5.4 shows an aluminosilicate framework of a zeolite and the molecular interaction between a water, DME and MeCl molecule to adsorbent surface hydroxyls groups. The position of the Na^+ ion represents the cation responsible for the pore openings on the surface of the adsorbent, thus meaning more adsorption sites are available for molecules within the acceptable pore range in the micropores. If we recall according to Jaumain and Su [79] MeCl interacts by its negatively charged chlorine atom with the polarised hydrogen atoms in zeolites through hydrogen bonding. In this instance hydrogen bonding is actually a misnomer since it is not a true hydrogen bond but instead more of a strong dipole-dipole attraction. This is because true hydrogen bonding is the electrostatic attraction between polar molecules where the hydrogen interacts with an electronegative atom such as: N, O or fluorine (F). On the contrary, DME molecules interacts via genuine hydrogen bonding through the negatively charged O atom [100]. It is known that in terms of adsorption the order of bond strengths are as follows ionic > covalent > hydrogen > dipole > VDW's. In terms of relevance to the adsorbates theoretically hydrogen bonding is roughly 10 times stronger than dipole-dipole interactions [78]. Comparatively, DME behaves similarly to water in that adsorption is typically dominated through the O atom. The electrons in the outer shell are further away from the nucleus therefore more readily capable of donating electrons to the empty orbitals of the protons compared

to MeCl. In terms of MeCl the chlorine atoms outer electron shell is full and the molecule is more electronegative meaning electrons are more tightly held and its subsequent electron cloud is smaller compared to DME. In addition O has a greater base strength than chlorine therefore DME is capable of adsorbing faster.

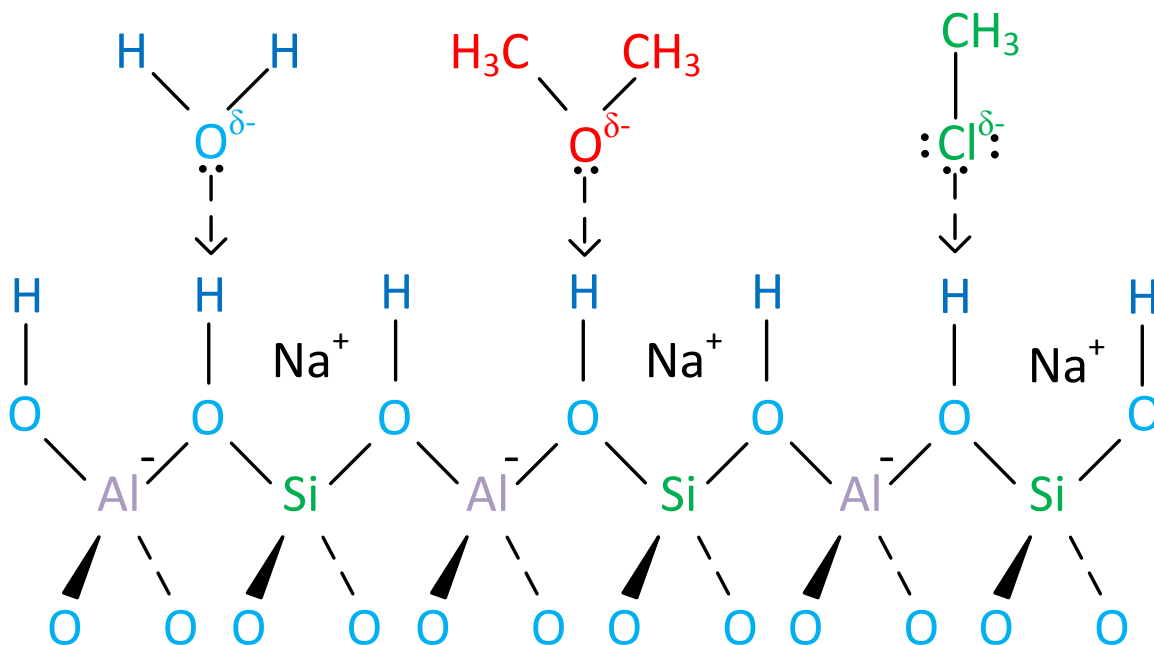


Fig. 5.4. Zeolite surface hydroxyls interacting molecularly with a water, DME and MeCl molecule

It is worth noting that pure component analysis of DME on the two zeolite molecular sieves has already been published [114] and therefore similar and extended analysis has been conducted for MeCl and compared. Apart from the aforementioned exploitable differences other useful points from the literature review are highlighted below:

- In a mixture, molecules small enough to enter the pores of the zeolite with a lower volatility, increased polarity and greater degree of unsaturation are more tightly held within the structure. DME is more polarizable since it has a C-C bond unlike MeCl only having one C, however the latter is smaller with a larger dipole.
- Physical affinity of the adsorbate for the adsorbent which is attributed to the functional groups on the respective adsorbent surfaces i.e. higher silanols on silica gel surface the higher the adsorption capacity for DME [67]. Similarly, this was also true for MeCl as shown by Toreci *et al.* [35, 79].
- MeCl has a higher dipole moment of 1.89D, whereas DME has a dipole of 1.30D. This may lead to stronger interactions between MeCl and certain functional groups on the different adsorbent surfaces.

- Since MeCl has a relatively permanent dipole it can contribute to electrostatic forces to the potential of interaction with carbon. As a result this can complicate otherwise simple VDW's forces [70].
- Displacement of a particular component within a mixture: in mixtures the more volatile components are susceptible to displacement. For the problem at hand MeCl is more volatile and larger relative molecular mass (RMM).
- Diffusion of the adsorbate into/onto the adsorbent due to mass and heat transfer resistances resulting from physical and chemical differences.
- Compounds with high boiling points and molecular weights have a high affinity for carbon.
- Adsorption of MeCl on carbogenic material at higher temperatures is reported to influence higher effective diffusivities which leads to substantially shorter equilibrium times [70].

5.3 Results and discussion

5.3.1 Pure component adsorption/desorption of dimethyl ether (DME) and methyl chloride (MeCl) on zeolites 4A and 5A

All adsorption and desorption isotherms figures are expressed in terms of pressure (atm) and/or relative pressure (-). It was particularly important to show the latter due to experimental limitation of not being able to reach pressures close to saturation due the maximum vapour pressure contained within the gas cylinders and the quantity's depletion with time. The following section entails a comprehensive comparative pure component adsorption/desorption analysis for both adsorbates on each zeolite. All adsorption isotherms are shown in terms of relative pressure for the pure component data for DME and MeCl, respectively and data compared.

5.3.1.1 Pure component adsorption

Fig. 5.5 and Fig. 5.6 show adsorption isotherms in terms of relative pressure for the pure component adsorption isotherms for DME and MeCl on 4A and 5A, respectively at constant room temperature (20 °C) following a 5 min equilibrium time at each incremental pressure.

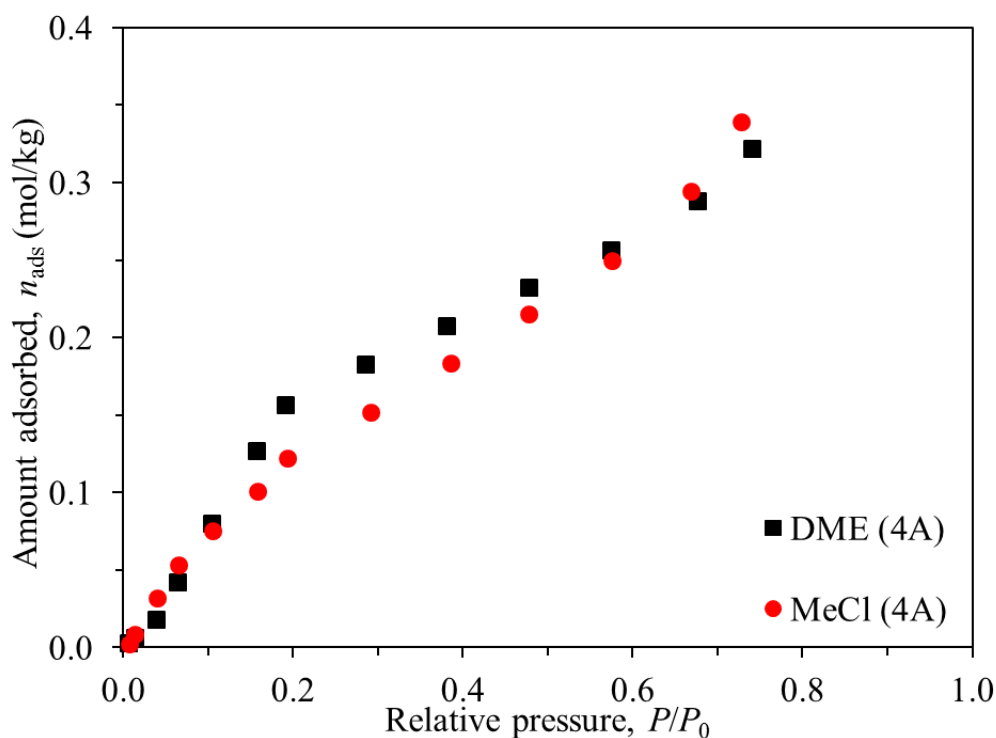


Fig. 5.5. Pure component DME and MeCl adsorption isotherms on 4A at 20 °C

Within the conditions considered DME and MeCl had adsorption capacities of 0.32 and 0.34 mol kg⁻¹, respectively. As can be seen in Fig. 5.5 on 4A both gases exhibit similar trends with MeCl adsorbing marginally more when the P/P_0 was < 0.1, then between 0.15 - 0.60 DME adsorbs more with MeCl adsorbing more again from 0.70 - 0.80. The adsorption in the < 0.15 region can be

explained by adsorption at the strong adsorption sites and in the pores since adsorption proceeds in terms of site strength and in the pores at low pressures. With increasing pressure the continual rise in adsorption could be attributed to dual site adsorption and or adsorption on different adsorption (weaker) sites as observed by Kobayashi *et al.* [115]. Moreover both gases demonstrated evidence of continually increasing adsorption uptake behaviour towards saturation.

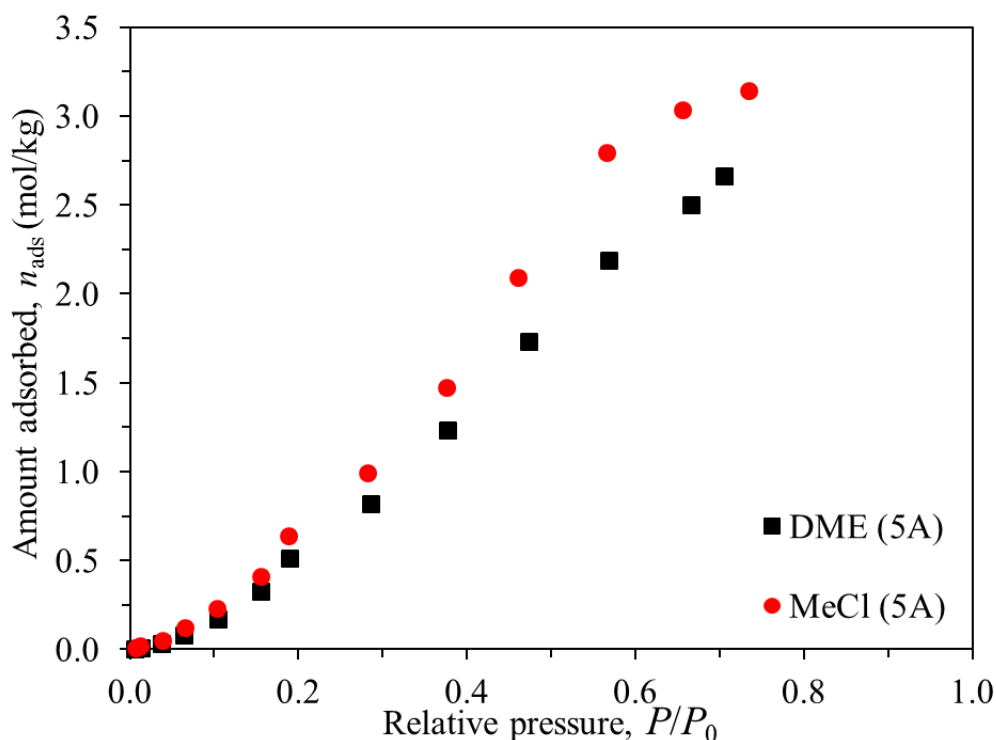


Fig. 5.6. Pure component DME and MeCl adsorption isotherms on 5A at 20 °C

Fig. 5.6 shows the adsorption isotherms for DME and MeCl on 5A in terms of relative pressure. Within the conditions considered DME and MeCl had adsorption capacities of 2.66 and 3.14 mol kg⁻¹, respectively. Both adsorbates exhibited similar trends especially with MeCl exhibiting the greater capacity at each incremental pressure when $P/P_0 < 0.2$. The effect of this was greater when $P/P_0 > 0.2$ up towards saturation. Both gases show linearity in the moderate pressure region with MeCl showing evidence of plateau at $P/P_0 \sim 0.75$. Although the DME isotherm did not show plateau this was evident from the uptake data which suggested a reducing trend at high pressure; at a lower adsorption capacity than MeCl. At very low pressure it was evident the equilibrium time was insufficient for true thermodynamic equilibrium to be reached. It is important to recognise that zeolite 5A has a substantially larger microporous surface area resulting in significantly more adsorption sites meaning generally a longer equilibrium time is required compared to the low surface area zeolite 4A. A further consideration is that some adsorption sites are occupied due to occluded moisture and impurities as shown earlier from the TGA analysis since the adsorbent was not thermally pre-treated. In terms of the pore size, the 5A adsorbent has pore openings within the acceptable range for both DME and MeCl molecules,

respectively. It is plausible that the greater adsorption capacity of MeCl compared to DME is because it is a smaller molecule therefore assuming complete monolayer coverage more molecules are adsorbed per unit area. The next section gives a greater insight into the isotherm types as the data is fitted to different empirical models followed by the kinetics and differential heat of adsorption. In terms of isotherms comparison for the conditions considered no immediate exploitable differences can be observed for DME and MeCl on 4A and 5A, respectively.

5.3.1.2 Pure component empirical adsorption models

Fig. 5.7 shows the applicable Langmuir, Freundlich Sips and Tóth empirical models applied to DME and MeCl adsorption on 4A and 5A, respectively in terms of pressure. In conjunction with Fig. 5.5 it can be seen that the adsorption of DME on 4A (Fig. 5.7a) appears to exhibit a Type II classification whereas MeCl (Fig. 5.7b) appears to adsorb exhibiting a Type I classification.

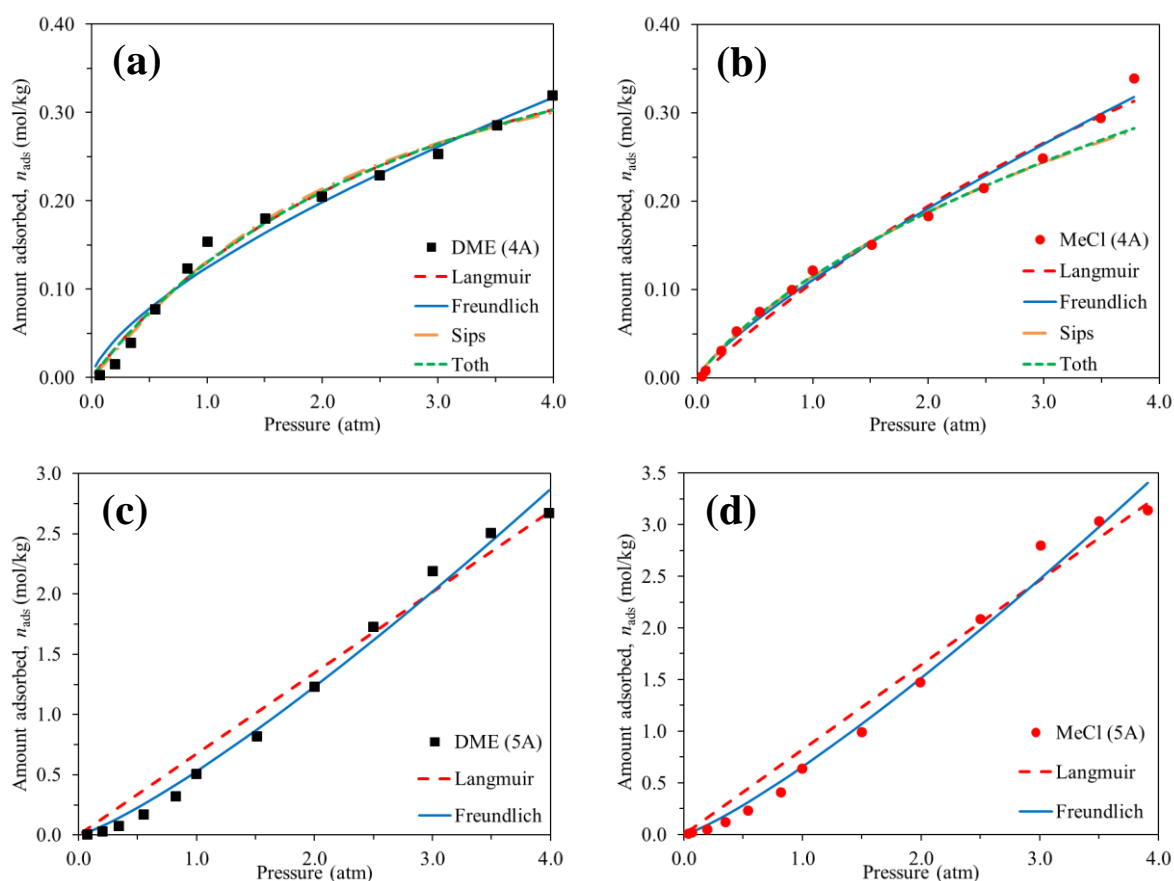


Fig. 5.7. Pure component empirical adsorption models for a) DME on 4A; b) MeCl on 4A; c) DME on 5A and d) MeCl on 5A

Type II isotherms (often referred to as sigmoid isotherm) are commonly observed with microporous solids or those exhibiting limited porosity; the latter in this case. Such curves are characterised by a steady increase in adsorption with increasing pressure. The observed inflection point at $P \sim 1$ atm and Fig. 5.5: $P/P_0 \sim 0.20$ represents the transition from complete monolayer to

multilayer adsorption. Type I isotherms is due to adsorption on a microporous solid. The interaction may be strong enough to bring about a complete filling of the pores at a low relative pressure. The difference in isotherm type clearly points towards the molecular dimensions of the molecules playing an important role. The adsorbent is microporous to the molecule capable of pore penetration whilst exhibiting limited porosity for DME due to its larger size. Although both adsorbates on 5A exhibit poor low-pressure adsorption behaviour, both isotherms can be interpreted at Type I isotherms (Fig. 5.6) as shown by, Fig. 5.7c and Fig. 5.7d for DME and MeCl, respectively. This is further supported by the respective pure component adsorption uptake trends shown in Fig. 5.8, which show the decreasing uptake points towards the respective saturation pressures. As mentioned earlier both demonstrate evidence of plateau towards saturation symptomatic of this isotherm type. Although there is evidence of a low solid-gas affinity at low pressure typical of Type III isotherms this is due to the molecules not having sufficient free energy to adsorb within the equilibrium time (i.e. taking longer to reach true equilibrium). Due to trends of the experimental data only the data on 4A could be fitted to all four models, whilst only the Langmuir and Freundlich models could be fitted to the data on 5A. The reason the data fitted well to the Freundlich model is due its validity at moderate pressure whereas the others were not applicable due to a) the concave shape of the plot at low pressure which is required for the Langmuir and Tóth models, respectively, and b) the continually increasing adsorption behaviour at high pressure which affects the Sips and Tóth models.

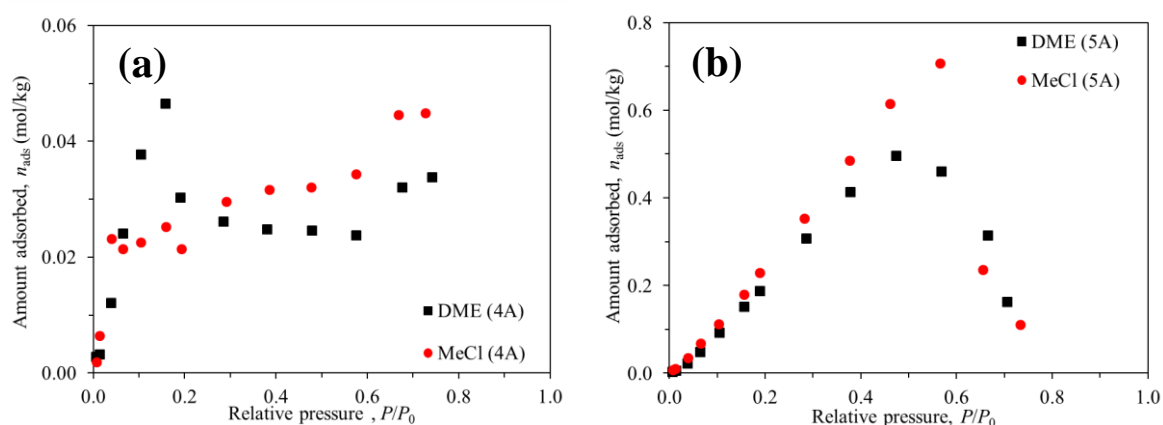


Fig. 5.8. Pure component adsorption uptake trends for DME and MeCl on a) 4A; b) 5A

Table 5.3 shows the fitting parameters for the adsorption of DME and MeCl on both zeolites. In terms of DME adsorption on 4A the adsorption data resulted in an experimental n_s value of 0.319 mol kg⁻¹. The predicted values from the fitting models for the Langmuir, Sips and Tóth were 0.544, 0.454 and 0.529 mol kg⁻¹, respectively. For MeCl on 4A the predicted values for n_s in the same order were 0.993, 0.861 and 2.491 mol kg⁻¹, respectively. Although the predicted n_s values appear to be larger than the experimental values it is important to recognise that the experimental isotherm is incomplete towards saturation meaning the true value of n_s is relatively unknown.

Customarily the empirical model with the highest R^2 is used to describe the behaviour of an adsorbate with an adsorbent. For DME on 4A all models fitted with the Langmuir, Sips and Tóth models all exhibiting an R^2 of 0.996 but varying n_s values. Limousin *et al.* [33] report that isotherms should be generally fitted to simple models such as Langmuir before using more complex models to describe A-S systems. MeCl on the other hand fitted best to the Sips and Tóth models with the latter appearing to result in a slightly overestimated value of n_s . In terms of comparing the different parameters DME exhibits a larger rate constant and greater heterogeneity according to the Freundlich model on 4A. In terms of both gases on 5A the Langmuir model was not applicable due to the lack of applicability for the conditions considered. According to the Freundlich model MeCl exhibited a larger rate constant and greater heterogeneity on 5A.

Table 5.3. Pure component empirical fitting parameters for DME and MeCl adsorption on 4A and 5A

Parameters		4A		5A	
		DME	MeCl	DME	MeCl
Langmuir	b	0.315	0.122	6.87×10^{-4}	3.85×10^{-4}
	n_s	0.544	0.993	980.77	1110.12
	R^2	0.996	0.995	0.991	0.988
Freundlich	K	0.124	0.111	0.528	0.656
	t	1.481	1.263	0.819	0.828
	R^2	0.993	0.997	0.995	0.994
Sips	b	0.451	0.113	-	-
	n_s	0.454	0.861	-	-
	c	0.886	1.166	-	-
	R^2	0.996	0.999	-	-
Tóth	b	0.320	0.095	-	-
	n_s	0.529	2.491	-	-
	c	1.030	0.431	-	-
	R^2	0.996	0.999	-	-

5.3.1.3 Different temperature isotherms with fitting model

In order to design an adsorption/desorption separation system it is important analyse the adsorption behaviour at different temperature conditions so that the thermodynamic heat of adsorption approach can be used. The work on differential heats of adsorption for DME on zeolites has already been published therefore the same procedure was repeated and compared to with the MeCl analysis. For the untreated zeolites with a 5 min equilibrium time the isotherms were determined at 20, 30 and 40 °C. Since adsorption was carried out within a moderate range of pressure it was appealing to fit the isotherms to the best fitting Freundlich model.

The model was modified to incorporate the equilibrium constant parameters, K and α as a function of temperature as follows:

$$K = k_1 \exp\left(\frac{-E_a}{RT}\right) \quad (5-2)$$

$$\alpha = k_2 \left(\frac{T}{T_{Ref}}\right)^m \quad (5-3)$$

Fig. 5.9 shows the adsorption isotherms for DME and MeCl at 20, 30 and 40 °C on zeolites 4A and 5A, respectively. Within the conditions considered in this study, the maximum adsorption capacity at 20 °C on 5A was found to be more than eight times higher than the capacity on 4A for both gases.

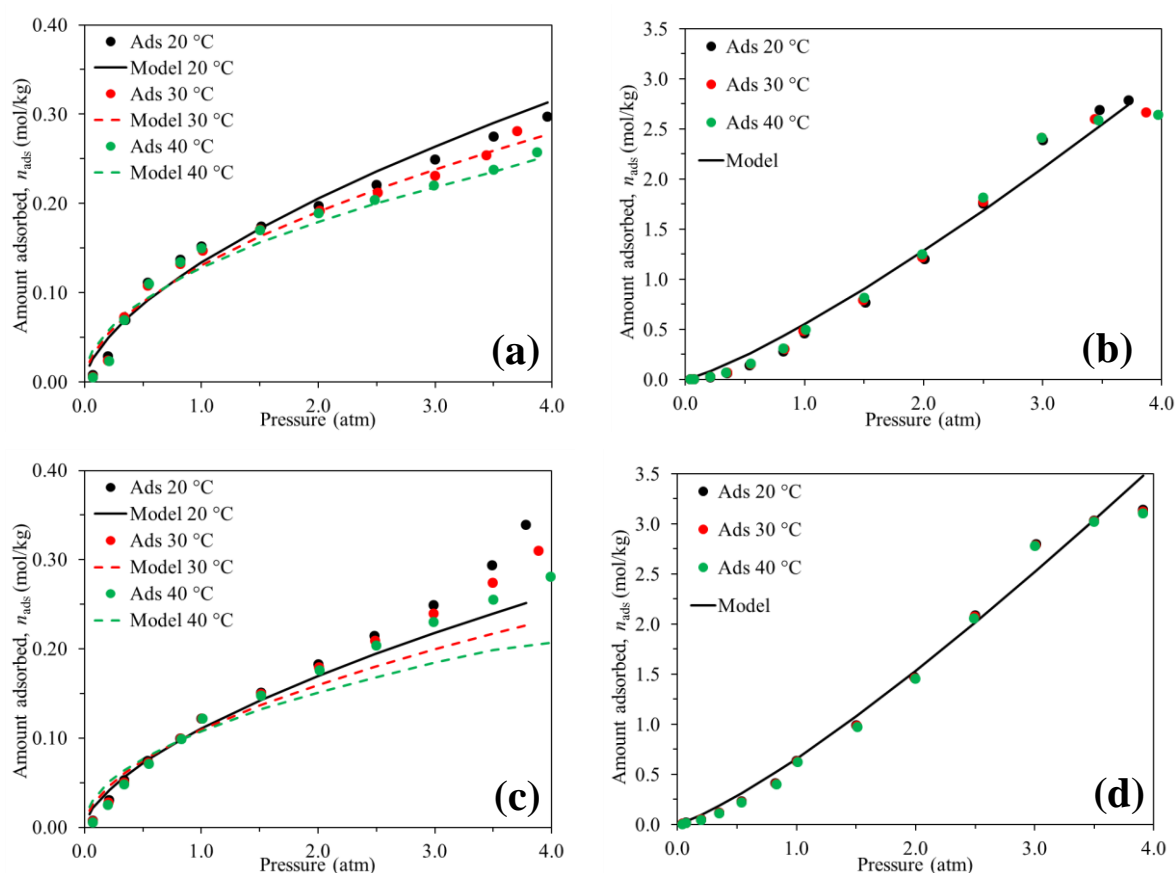


Fig. 5.9. Pure component adsorption isotherms fitted to Freundlich model at 20, 30 and 40 °C for DME on a) 4A and (b) 5A and MeCl on c) 4A and d) 5A

The significantly reduced capacity with the latter can be attributed to the differences in surface area, micropore volume and pore size. Adsorption on 4A showed that low temperatures were favoured for increased adsorption. This behaviour can be explained by the Le Chatelier's principle, meaning endothermic desorption is possible when temperature increases, hence less adsorption at higher temperatures. This is plausible since the homogenous and flat surface of 4A makes it much easier for molecules to desorb as its density changes with temperature. In contrast

adsorption on 5A is insensitive to temperature at least within the conditions considered. Hypothetically, this could be due to a) molecules being predominantly locked inside the pores b) the interaction of the adsorbate with the occluded moisture molecules thus forming stronger bonds and c) the effect of the short equilibrium time meaning molecules have less mobility.

Table 5.4 shows the fitting parameters for the model and additional parameters shown in Eq. (5-2) and (5-3). The activation energy used in Eq. (5-3) was obtained from the Arrhenius plot shown by Fig. 5.10. As can be seen by the values in the table DME requires greater activation energy than MeCl for both adsorbents thus supporting earlier reports of DME having a stronger interaction than MeCl. Since adsorption on 5A was independent of temperature for reasons discussed above it was fitted to constant parameters. As can be seen MeCl on 4A could not be fitted well to the model compared to the other combinations. This is believed to be a result of the isotherm fitting continually increasing at high pressures thus affecting the applicability of the models. The purpose of showing the R^2 is to demonstrate validation of the Freundlich model to the data.

Table 5.4. Pure component adsorption empirical fitting parameters for DME and MeCl on 4A and 5A

Adsorbate	T_{Ref} (K)	<u>4A</u>				<u>5A</u>			
		k_1 (atm^{-1})	k_2 (-)	m (-)	$-E_a$ (kJ mol^{-1})	k_1 (atm^{-1})	k_2 (-)	m (-)	$-E_a$ (kJ mol^{-1})
DME	293	0.065	1.713	1.360	17.29	0.127	0.715	2.244	35.16
MeCl	293	0.080	1.264	2.018	7.90	0.436	0.818	0.366	9.88

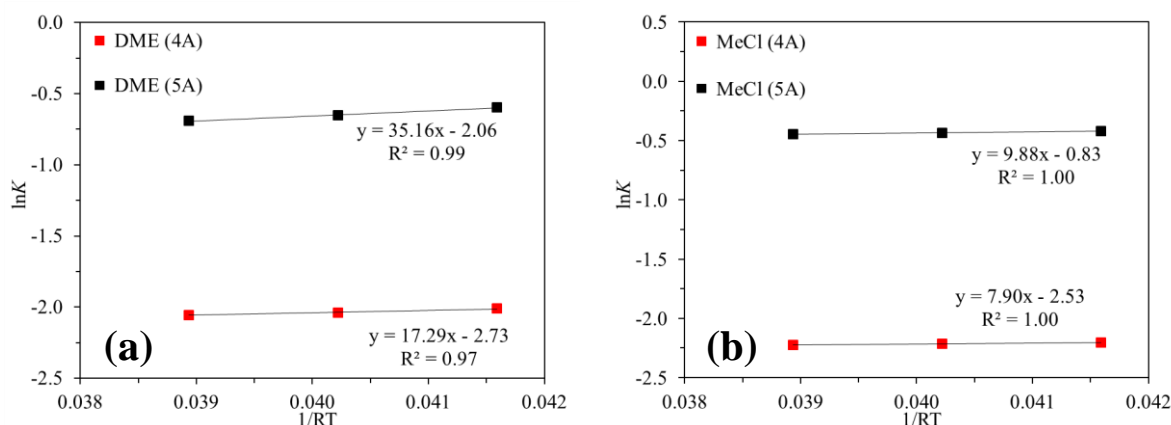


Fig. 5.10. Dependence of the Freundlich model parameter, K , on temperature for pure component adsorption of a) DME and b) MeCl on 4A and 5A

5.3.1.4 Pure component desorption isotherms

Fig. 5.11 and Fig. 5.12 show the adsorption and subsequent desorption isotherms for DME and MeCl on 4A and 5A, respectively at 20 °C. As the figure shows both gases exhibit similar hysteresis under the conditions considered on both adsorbents. In both cases in terms of hysteresis two factors are believed to be the cause of poor hysteresis: a) short equilibrium time (5 min) and b) the role of moisture within the samples due to lack of thermal pre-treatment.

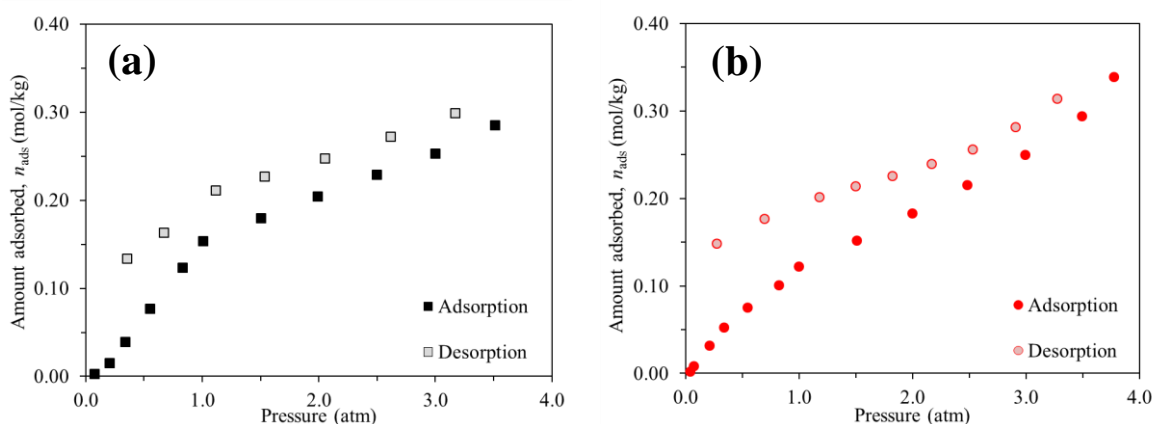


Fig. 5.11. Adsorption and desorption isotherms for pure component a) DME and b) MeCl on 4A at 20 °C

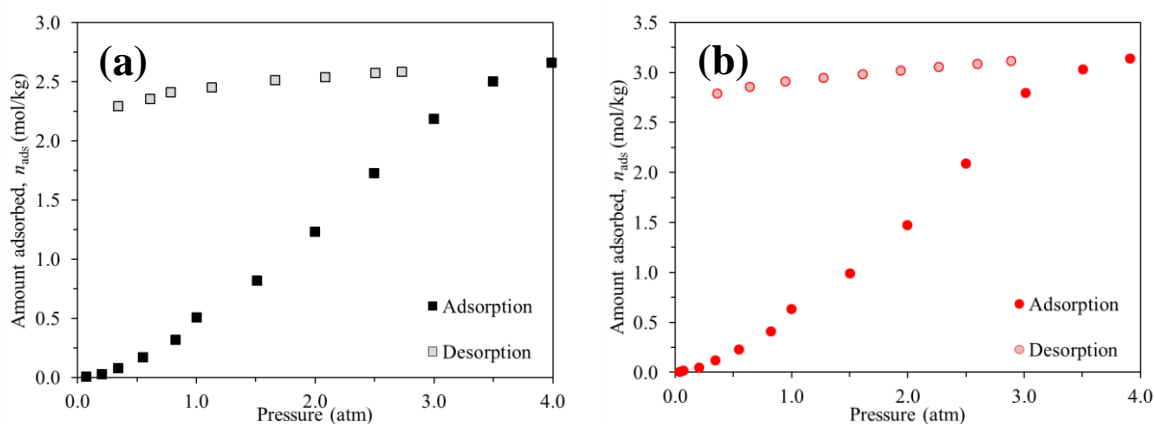


Fig. 5.12. Adsorption and desorption isotherms for pure component a) DME and b) MeCl on 5A at 20 °C

The short equilibrium time is especially responsible because desorption is generally a longer process than adsorption due to the greater energy required to overcome surface tension. The equilibrium time was evidently insufficient for adsorption especially at low pressure let alone desorption. Since the systems were not in true equilibrium especially for adsorption, molecules are likely to shift between adsorption and desorption leading to a larger hysteresis. Where adsorption occurs in the pores desorption takes longer because during the short equilibrium time first the surface molecules are desorbed before the adsorbed molecules within the pores become desorbed. In terms moisture, its presence can result in a) differences in the strength of interactions

between A-S and A-A and b) desorption of the moisture amongst the respective adsorbate gas molecules resulting in quantitative error. The effects of moisture are postulated but require further investigation for confirmation. Lower pressures could not be reached due to limitations of system whereby release of manifold quantities were manually released using a non-ideal manual valve.

5.3.1.5 Pure component adsorption kinetics

As reported by Yao and Chen [37] adsorption kinetics are often treated in one of two ways: determination of the reaction method and the diffusion method. These methods have been defined in some detail in Chapter II: Adsorption kinetics and models. In this section the adsorption rates were determined using the adsorption kinetic rate models (Eq. (2-13) - (2-18). The diffusion mechanisms were determined using the uptake data i.e. determining if adsorption is controlled by intracrystalline diffusion or surface resistance to find the rate limiting step [39] as shown earlier in Eq. (2-19) and (2-20). In order to understand the kinetics and determine the rate at different adsorption pressures (0.5 - 3.5 atm with increments of 0.5 atm) the different kinetic adsorption rate constant values were compared for each model at each pressure. This procedure allowed for the overall trends to be observed and supporting theories to be confirmed for the behaviour of the gases on the different adsorbents. For each adsorption pressure each kinetic model was applied and evaluated and compared with each model at that particular pressure and other pressures in the isotherm measurement. The model with highest R^2 was deemed the most applicable model with values closer to unity being more desirable. For each model which shows the best fitting, the R^2 value is underlined and has bold text to highlight the most applicable fitting model for the respective conditions.

Table 5.5 and Table 5.6 show the adsorption kinetic equation and fitting parameters at increasing pressure increments for the pure component data for DME versus MeCl on 4A and 5A, respectively. As can be seen of the four kinetic models the Elovich model fitted least for both gases (lowest R^2 value), with MeCl exhibiting the better fitting. The lack of fitting was no surprise since this model is generally applicable to chemisorption type interactions which were not anticipated for the interactions considered. The kinetic adsorption rate constants for the different adsorption pressures for both gases on 4A were applicable to the IPD model at 0.5 atm. The pseudo second order kinetics was found to be applicable for all other higher pressures (1.0 - 3.5 atm). Over the entire pressure range the overall R^2 values for DME and MeCl to the pseudo second order model were the highest of all models, with values of 0.991 and 0.987, respectively (average R^2 for the pseudo second order model isotherm data). With increasing pressure both gases exhibited constant pseudo second order kinetics thus demonstrating the same order of reaction kinetics throughout the entire isotherm measurement. The early IPD model applicability can be explained by the molecules adsorbing into the pores which is plausible since adsorption into pores

typically occurs at low pressure. With that being said the R^2 for the pseudo second order model was equally high demonstrating the order of reaction, since the model with the highest R^2 is deemed to be the most suitable fitting. It is believed that initially both gases exhibit some natural pore filling at low pressure (0.5 atm), assuming some pores are large enough for DME to enter but potentially block the pores as they go deeper.

Assuming pseudo second order kinetics DME adsorbs a little over 3.5 times faster at 1.0 atm than MeCl and generally more than twice as fast as MeCl in the 1.5 - 3.5 atm pressure range. Azizian [116] reported that pseudo second order kinetics occur because the concentration of the bulk gas phase is comparable to the fractional uptake divided by the coverage at equilibrium. For the case considered the pseudo second order kinetics is partially due to the unusually low adsorbent surface area which meant there were limited adsorption sites available for adsorption therefore the bulk adsorption at each pressure occurred rapidly then very slow thereafter. Moreover due to the short equilibrium time, the adsorbent capacity at each pressure was not achieved. In terms of the IPD plot, assuming IPD kinetics MeCl exhibited a fairly constant rate constant value from 0.5 - 3.0 atm then doubled at 3.5 atm. DME exhibited an overall increasing rate constant value trend with increasing pressure. The inconsistencies of the pseudo first order and IPD models are due to their lack of applicability to the data at the respective pressures.

Table 5.5. Adsorption kinetic model parameters for pure component DME and MeCl on 4A

<u>DME on 4A</u>										
Adsorption pressure <i>atm</i>	<u>Pseudo first order</u>		<u>Pseudo second order</u>		<u>Elovich</u>			<u>IPD</u>		
	k'_{ads} (s ⁻¹)	R^2	k''_{ads} (mol kg ⁻¹ s ⁻¹)	R^2	α (mol kg ⁻¹ min ⁻¹)	β (kg mol ⁻¹)	R^2	k_{IPD} (mol kg ⁻¹ -mol ^{-1/2})	C_{IPD} (constant)	R^2
0.5	0.025	0.957	0.232	0.961	0.112	29.48	0.695	0.043	0.004	<u>0.969</u>
1.0	0.027	0.792	1.033	<u>0.995</u>	0.252	52.18	0.333	0.032	0.019	0.805
1.5	0.032	0.785	0.967	<u>0.998</u>	0.488	36.50	0.285	0.048	0.033	0.757
2.0	0.061	0.927	0.682	<u>0.997</u>	0.507	23.92	0.344	0.068	0.040	0.791
2.5	0.015	0.579	0.736	<u>0.988</u>	0.706	35.29	0.241	0.053	0.039	0.725
3.0	0.020	0.510	0.816	<u>0.999</u>	1.125	20.61	0.250	0.088	0.066	0.717
3.5	0.066	0.924	1.454	<u>1.000</u>	1.015	30.89	0.218	0.062	0.050	0.688
<u>MeCl on 4A</u>										
Adsorption pressure <i>atm</i>	<u>Pseudo first order</u>		<u>Pseudo second order</u>		<u>Elovich</u>			<u>IPD</u>		
	k'_{ads} (s ⁻¹)	R^2	k''_{ads} (mol kg ⁻¹ s ⁻¹)	R^2	α (mol kg ⁻¹ min ⁻¹)	β (kg mol ⁻¹)	R^2	k_{IPD} (mol kg ⁻¹ -mol ^{-1/2})	C_{IPD} (constant)	R^2
0.5	0.023	0.950	0.255	0.952	0.093	34.11	0.707	0.037	0.003	<u>0.957</u>
1.0	0.024	0.976	0.281	<u>0.978</u>	0.157	27.92	0.602	0.049	0.011	0.956
1.5	0.029	0.982	0.086	<u>0.991</u>	0.128	18.98	0.846	0.045	0.025	0.926
2.0	0.055	0.924	0.128	<u>0.997</u>	0.176	17.95	0.764	0.048	0.040	0.860
2.5	0.027	0.875	0.170	<u>0.997</u>	0.237	18.99	0.658	0.047	0.053	0.787
3.0	0.027	0.857	0.212	<u>0.998</u>	0.255	20.77	0.612	0.043	0.055	0.753
3.5	0.059	0.891	0.816	<u>0.999</u>	1.125	20.61	0.250	0.088	0.066	0.717

^a R^2 values which are bold and underlined show that, that particular model is most applicable for the data analysis at that respective pressure/condition.

Table 5.6. Adsorption kinetic model parameters for pure component DME and MeCl on 5A

<u>DME on 5A</u>										
Adsorption pressure <i>atm</i>	<u>Pseudo first order</u>		<u>Pseudo second order</u>		<u>Elovich</u>			<u>IPD</u>		
	k'_{ads} (s ⁻¹)	R^2	k''_{ads} (mol kg ⁻¹ s ⁻¹)	R^2	α (mol kg ⁻¹ min ⁻¹)	β (kg mol ⁻¹)	R^2	k_{IPD} (mol kg ⁻¹ -mol ^{-1/2})	C_{IPD} (constant)	R^2
0.5	0.022	0.970	0.059	0.815	0.119	18.35	0.826	0.064	-0.009	<u>0.985</u>
1.0	0.024	0.992	0.048	0.909	0.260	9.82	0.789	0.123	-0.005	<u>0.994</u>
1.5	0.026	0.984	0.030	0.914	0.432	5.99	0.784	0.202	-0.006	<u>0.993</u>
2.0	0.027	0.982	0.021	0.901	0.558	4.45	0.800	0.269	-0.014	<u>0.990</u>
2.5	0.027	0.989	0.022	0.939	0.761	3.71	0.754	0.332	0.006	<u>0.991</u>
3.0	0.027	<u>0.998</u>	0.024	0.964	1.141	2.87	0.698	0.441	0.044	0.964
3.5	0.027	0.965	0.081	<u>0.991</u>	1.022	5.77	0.511	0.249	0.086	0.907
<u>MeCl on 5A</u>										
Adsorption pressure <i>atm</i>	<u>Pseudo first order</u>		<u>Pseudo second order</u>		<u>Elovich</u>			<u>IPD</u>		
	k'_{ads} (s ⁻¹)	R^2	k''_{ads} (mol kg ⁻¹ s ⁻¹)	R^2	α (mol kg ⁻¹ min ⁻¹)	β (kg mol ⁻¹)	R^2	k_{IPD} (mol kg ⁻¹ -mol ^{-1/2})	C_{IPD} (constant)	R^2
0.5	0.020	0.972	0.066	0.824	0.108	20.28	0.833	0.058	-0.008	<u>0.988</u>
1.0	0.021	0.996	0.048	0.906	0.254	10.07	0.786	0.120	-0.005	<u>0.997</u>
1.5	0.028	0.974	0.012	0.927	0.193	7.34	0.958	0.113	-0.003	<u>0.994</u>
2.0	0.027	0.986	0.009	0.937	0.286	5.14	0.955	0.161	0.003	<u>0.994</u>
2.5	0.027	<u>0.988</u>	0.011	0.963	0.441	4.21	0.906	0.201	0.050	0.983
3.0	0.029	<u>0.991</u>	0.007	0.955	0.454	3.47	0.946	0.239	0.024	0.989
3.5	0.040	<u>0.989</u>	0.024	0.964	1.141	2.87	0.964	0.441	0.044	0.964

^a R^2 values which are bold and underlined show that, that particular model is most applicable for the data analysis at that respective pressure/condition.

Table 5.6 shows the fitting parameters for the kinetic models when the DME and MeCl data was fitted for 5A. Similar to 4A the Elovich model did not apply; with MeCl demonstrating the better fitting for the model when compared to DME. According to the data both gases adsorb with respect to a first order reaction. In terms of results the kinetic adsorption rate constants for different adsorption pressures for both gases exhibited evidence of applicability to the IPD model for the 0.5 - 2.5 atm pressure range for DME and 0.5 - 2.0 atm for MeCl. Thereafter DME exhibited pseudo first order and second order kinetics at 3.0 and 3.5 atm, respectively whereas MeCl exhibited pseudo first order kinetics for the range 2.5 - 3.5 atm. The applicability to the IPD was no surprise since both adsorbates have molecular dimensions within the acceptable pore range for the highly microporous solid. In terms of DME, at high pressure (3.0 - 3.5 atm) the kinetics suggests pseudo first order then second order kinetics because the adsorbent approaches saturation meaning the IPD model can no longer apply. MeCl adsorption appears to exhibit pseudo first order kinetics from 2.5 - 3.5 atm however the R^2 for the IPD also demonstrated an equally high R^2 for the same range. The kinetic data supports the theory that initially the pores become filled with molecules, as adsorption proceeds molecules proceed to less active sites and the external surface owing to the different kinetic model applicability.

Although both gases exhibited evidence of pseudo first order and IPD kinetics it is evident that the gases for the entire isotherm adsorb via pseudo first order kinetics in terms of reaction then second order near saturation but largely dominated by IPD. Even though the model with the highest determination of coefficient is applicable to describe the adsorption kinetics if we assume pseudo first order kinetics applies then both gases appear to adsorb at a very similar rate. Assuming the pseudo second order model both start at a similar rate then decreases before rapidly rising again as the gases reach saturation. Assuming the IPD model applies both gases start at a similar rate constant value at 0.5 atm then both gases show an increase in the rate constant with pressure; of which DME exhibits the faster rate. The DME rate constant drop at 3.0 atm is a result of saturation of the solid as in isotherm figure earlier. The MeCl rate constant value increases in the range 3.0 - 3.5 atm due to continual adsorption behaviour as shown by the isotherm curve. The shape of the isotherm at the respective pressure shown in Fig. 5.6 explains the increasing rate constant value whilst there is also the possibility of adsorption on different adsorption sites due the high pressure as mentioned earlier which was reported by Kobayashi *et al.* [52].

On evaluation of the different kinetic models for 4A and 5A it can be seen that as suspected earlier, DME displays a faster rate due to the greater kinetic adsorption rate constants. This is believed to be due to its stronger base strength meaning it interacts with the surface with a greater affinity. Both gases exhibit similar trends according to each model, but in terms of reaction with the adsorbents adsorption proceeds as a pseudo second order reaction on 4A and pseudo first order

kinetics for 5A. Adsorption quantities on 4A were affected by low surface area, pore size and steric crowding through the presence of impurities with the rate being dependable upon the availability of functional groups for A-S interactions. On the other hand since 5A has such a high surface area and adequate pore size aperture for DME and MeCl, IPD occurs with DME adsorbing faster.

Fig. 5.13 shows the plots for the IPD versus surface resistance controlled adsorption mechanisms for pure component DME and MeCl on 4A from the adsorption isotherm data at 2.0 and 3.0 atm, respectively. Fig. 5.13a and c shows both mechanisms in the initial stages at the respective pressures for both adsorbates whilst Fig. 5.13b and d show the mechanisms over a longer time for the respective pressures. Where the data shows constant trends adsorbent saturation is achieved for the respective conditions.

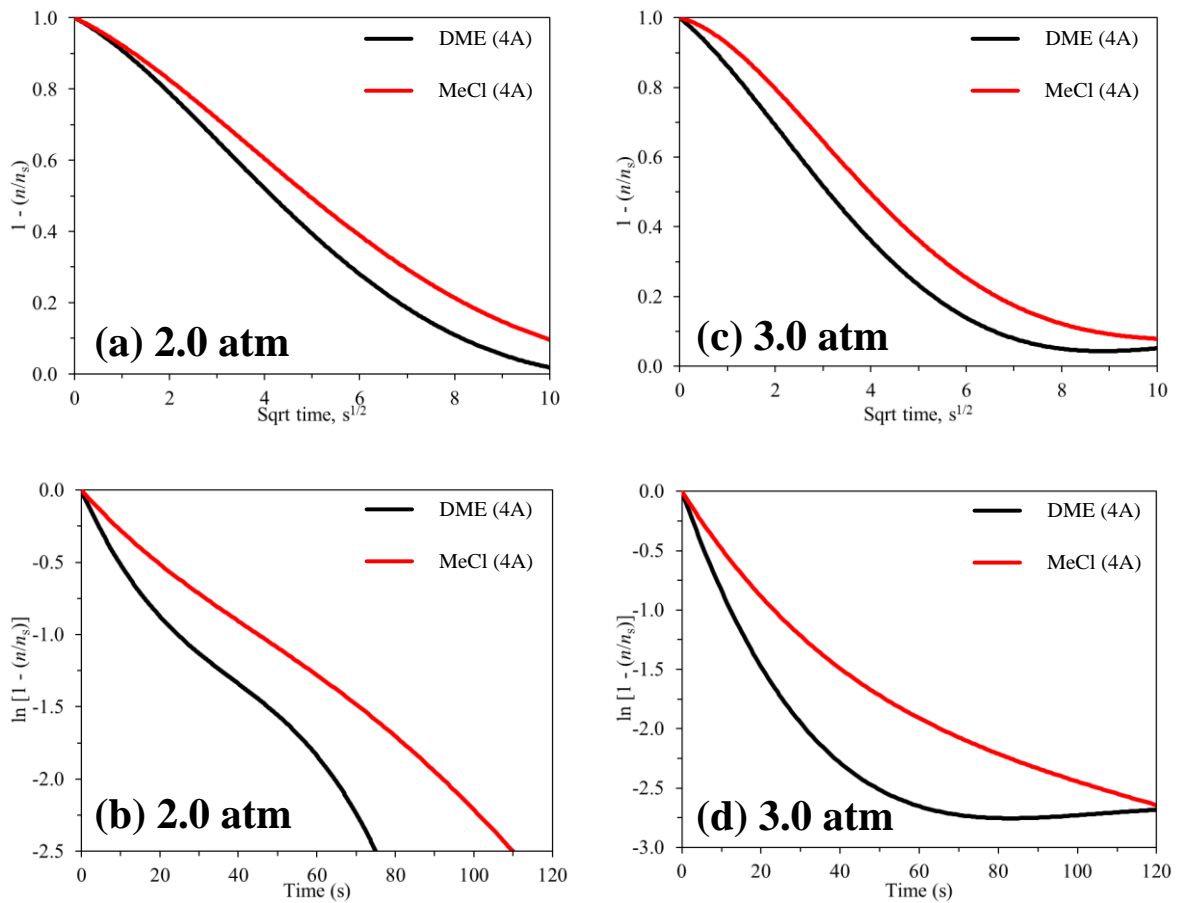


Fig. 5.13. Pure component adsorption mechanisms for DME and MeCl on zeolite 4A where a) and c) represents intracrystalline diffusion controlled adsorption in a short time scale and b) and d) represents surface resistance layering in a long time scale at 2.0 atm and 3.0 atm

Earlier the kinetic models eluded that DME exhibits a faster rate of adsorption into the adsorbent which was supported by the faster declining DME trend compared to MeCl. In the short time scale at 2.0 and 3.0 atm both gases exhibited greater linearity in the short time scale demonstrating evidence of IPD on 4A which was not the case particularly with DME in the longer time scale. Adsorption at 2.0 and 3.0 atm was pseudo second order for both gases according to the kinetic models but shows inconclusive evidence of the mechanism responsible. Due to the low surface area of the adsorbent the rate of adsorption appears to be slow and occur in stages i.e. trends exhibit linearity in stages.

In comparison at both pressures both DME and MeCl exhibit greater linearity for the initial longer time scale indicative of more surface resistance layering than IPD suggesting the former is the rate limiting step which is no surprise due to reasons mentioned earlier. At 2.0 atm both DME and MeCl exhibit linear trends in the earlier stages from 0 - 20 s and 0 - 60 s, respectively. The difference in time could be because MeCl can adsorb in pores as it has more adsorption sites to adsorb at therefore linearity for the longer time scale. It is worth noting that adsorption occurred in series in terms of data from an isotherm measurement and not a single run at each pressure on fresh adsorbent, therefore the impact of prior adsorption must be considered. The impact of such differences require further investigation however for the conditions considered particularly for 4A it is believed that the pressure gauge is not sensitive enough for the low surface area adsorbent particularly since substantially lesser quantities were adsorbed compared to adsorption on 5A. Nevertheless the kinetics models and mechanisms have supported the reported theories above but to some extent suggest that the adsorption mechanisms are more complicated as cautioned by Ruthven [39].

Fig. 5.14 shows the plots for the IPD versus surface resistance controlled adsorption mechanisms for pure component DME and MeCl on 5A from the adsorption isotherm data at 2.0 atm and 3.0 atm, respectively. On visual evidence for the conditions considered both gases appear to exhibit very similar trends, with the MeCl data declining marginally faster at 2.0 atm and DME declining slightly faster at 3.0 atm. The difference in behaviour can be attributed to the prior adsorption from the isotherm measurements at earlier pressure increments. At 2.0 atm it appears that both gases exhibit rapid IPD in two stages from 0.0 - 4.0 $s^{1/2}$ and 4.0 - 12.0 $s^{1/2}$ and some surface layering from 0 - 150 s most likely due to steric crowding. At 3.0 atm both gases show more definitive evidence of continual IPD (0.0 - 10.0 s) due to the high pressure but also surface layering adsorption due to most adsorption sites being already occupied. Comparatively it appears both mechanism support the earlier work and supports the isotherms and adsorption kinetic model data.

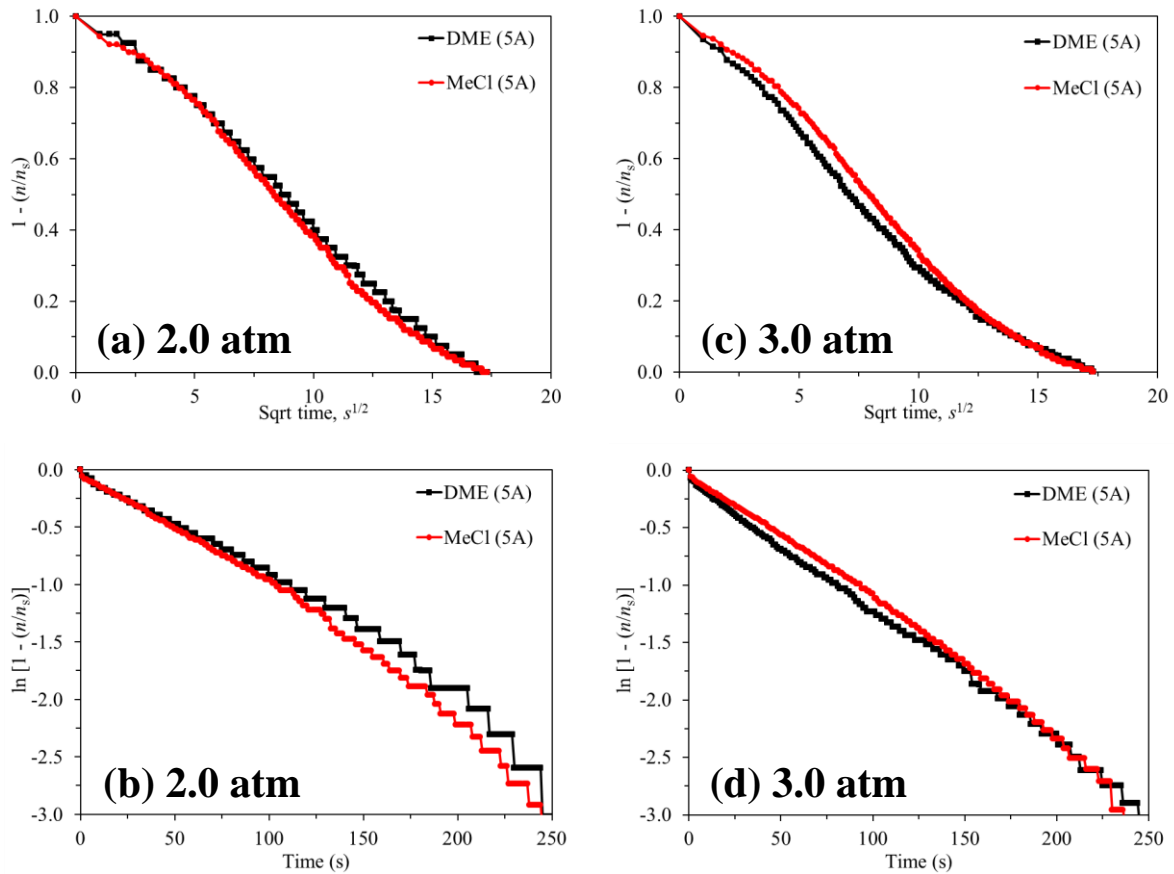


Fig. 5.14. Pure component adsorption mechanisms for DME and MeCl on zeolite 5A where a) and c) represents intracrystalline diffusion controlled adsorption in a short time scale and b) and d) represents surface resistance layering in a long time scale at 2.0 atm and 3.0 atm

5.3.1.6 Differential heat of adsorption

Fig. 5.15 compares the differential heat of adsorption for pure component DME and MeCl on zeolite 4A and 5A, respectively in terms of amount adsorbed (mol kg^{-1}). As it can be seen both gases exhibit very similar trends with a high initial heats of adsorption values of 30.11 and 44.77 kJ mol^{-1} for DME and MeCl on 4A then decreasing heat values with increasing coverage. On 5A DME exhibited a higher initial value of 29.81 kJ mol^{-1} compared to MeCl's 10.11 kJ mol^{-1} , thereafter MeCl resulted in two heat increases and DME exhibited one heat spike towards saturation (shown by an oval shape where blue is for DME and green for MeCl). Generally if the heat of adsorption value is constant this represents a homogenous surface however for the results obtained the trends indicate evidence of surface heterogeneity. Gallagher [117] reported that it is difficult to determine the nature of the adsorbed species using calorimetric data however the variation in differential heats of adsorption with coverage depicts quite clearly the distribution of surface sites and their reactivity to the respective adsorbates.

Typically differential heat of adsorption curves presents the following: an initial region which demonstrates adsorption onto the strongest adsorption sites thought to be of a Lewis type. The subsequent dropping trend with increasing coverage represents the adsorption onto one or more adsorption sites of intermediate strength. Whereas Yeo *et al.* [118] report that the initial decrease with increasing coverage can be considered to be a plateau where the heat of adsorption is constant (e.g. shown by dashed green (MeCl) and blue (DME) lines on 4A). The decrease with coverage is because the temperature was insufficient for full mobility therefore molecules adsorb simultaneously at strong and weak adsorption sites. The next region where heats decrease more or less steeply demonstrates the heterogeneity of the surface. For DME on 4A a slow heat rise (blue circles) was observed, which is indicative of interactions between adsorbed species i.e. DME-DME/MeCl-MeCl interactions or DME-H₂O/MeCl-H₂O interactions [52]. On the other hand, MeCl shows a subtle increase in differential heat when P/P_0 was 0.16 (0.08 mol kg^{-1}) and 0.48 (0.22 mol kg^{-1}). In terms of 5A, DME exhibits two heat rises from 0.32 - 1.23 mol kg^{-1} and a steeper heat rise at 1.73 - 2.19 mol kg^{-1} . Similarly MeCl exhibited heat rises from 0.41 - 0.99 mol kg^{-1} and 0.99 - 2.09 mol kg^{-1} . Although the heat rises are a result of A-A interactions there is a likelihood that some heat arises from A-H₂O interactions due to the already present molecularly adsorbed moisture. The saturation amount is the coverage where a quick drop in the calorimetric curve is observed to ensure sufficient adsorbate mobility when performed at a high enough temperature. When molecules have sufficient mobility they can move freely to adsorb in order of surface site strength. Although the heat data for both adsorbents showed evidence of heat decreases suspected to be due to the saturation of particular types of adsorption sites the corresponding isotherms were not so clear meaning the point of saturation was difficult to pinpoint [117].

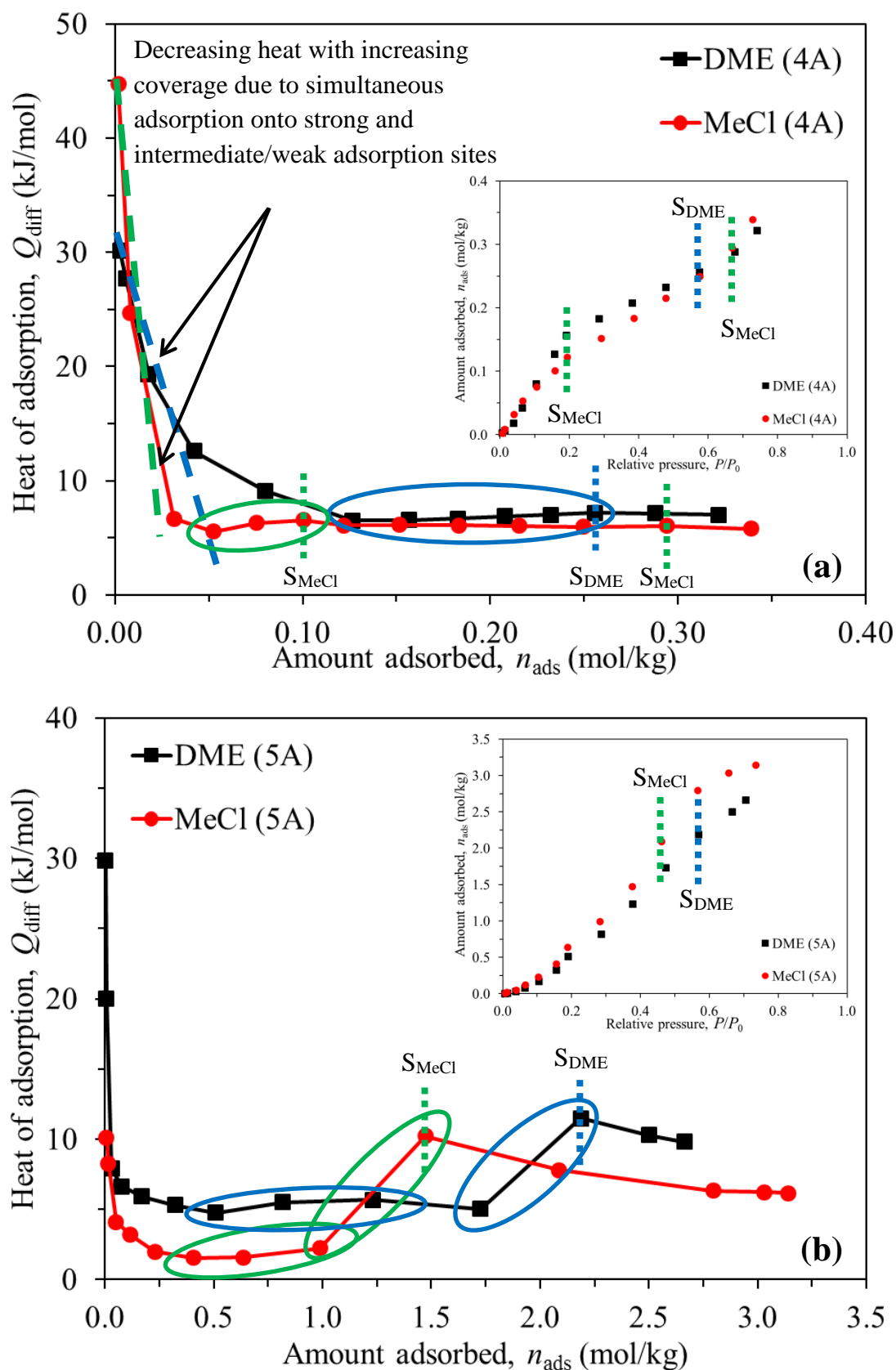


Fig. 5.15. Differential heat of adsorption for pure component DME and MeCl on a) 4A and b) 5A with corresponding isotherms to show adsorbent saturation points

With that being said the saturation point for MeCl on 4A was estimated to be 0.29 mol kg^{-1} (S_{MeCl}) demonstrated by the sharpest drop in heat value and shape of isotherm near saturation, thereafter the isotherm was relatively incomplete due to the inability to reach higher pressures [52]. Similarly for DME on 4A the saturation point was estimated to be at 0.26 mol kg^{-1} (S_{DME}) with adsorption continuing with pressure. In terms of 5A both saturation points were again difficult to determine from the isotherms but according to the differential heat data were reported to be 1.47 and 2.19 mol kg^{-1} for MeCl and DME, respectively. Although the values appear to be lower than expected it is important to recall the effect of already present moisture to the surface which causes steric crowding and therefore resulting in low saturation values. Gallagher [117] cites that a region at high coverage where the heat of adsorption approaches a nearly constant value is characteristic of hydrogen bonding or physisorption (VDW's forces) which is clearly visible especially on 4A, however the value depends on the adsorbate functional group. In the absence of a plateau of constant heat in the differential heat can either be a result of molecular interactions between molecules adsorbed at neighbouring sites or a true indication of differences between sites.

5.3.2 Pure component adsorption/desorption of dimethyl ether (DME) and methyl chloride (MeCl) on silica gels

5.3.2.1 Pure component adsorption isotherms

Below details the adsorption/desorption of both gases on the three different silica gels. Fig. 5.16 shows the adsorption isotherms in terms of relative pressure for pure component DME and MeCl on Si35-70, SiAmor and Si35-60. The adsorption capacities for DME and MeCl on the respective adsorbents in the same order were 3.49, 3.59, 2.56 and 3.12, 3.20, 2.29 mol kg⁻¹, respectively. The figures clearly show that both gases exhibited low solid-gas affinities at low pressure (< 0.15) due to the presence of molecularly adsorbed moisture and short equilibrium time like DME and MeCl adsorption on 5A then exhibit relatively linear isotherms trends towards saturation. Adsorption on SiAmor resulted in the largest adsorption capacity followed by Si35-70 and Si35-60, respectively. In term of SiAmor it is important to recognise that it is amorphous i.e. treated with water therefore more hydroxyls on the surface capable of dual site adsorption per acid site [52] which explains the larger adsorption capacity compared to Si35-70 even though the latter has a larger surface area. In terms of amount adsorbed DME exhibited a greater adsorption capacity on each silica gel for the incremental pressures. Such behaviour can be explained through comparisons with the respective studies for each adsorbate on silica gels; Robinson [100] and Ross and Kuo and Hines [48, 50].

In terms of DME adsorption the amount adsorbed on the silica gel with a similar surface area ~ 600 m² g⁻¹ (Si35-70 ~ 675 m² g⁻¹) was roughly half the amount reported by Robinson and Ross [100], however their conditions were more favourable for adsorption since the temperature was at its boiling point, after the adsorbent had been thermally pre-treated and with a longer automated equilibrium time. Similarly the amount adsorbed for MeCl on a silica gel with a similar surface area was reported to have doubled the capacity of the experimental data. This was a direct result of thermal pre-treatment to the adsorbent and adsorption for a longer equilibrium time. In terms of bonding, DME adsorbs through moderately strong hydrogen bonding [119] whereas MeCl adsorbs as a result of physical VDW's forces whereby adsorption follows the Dubinin pore filling mechanism.

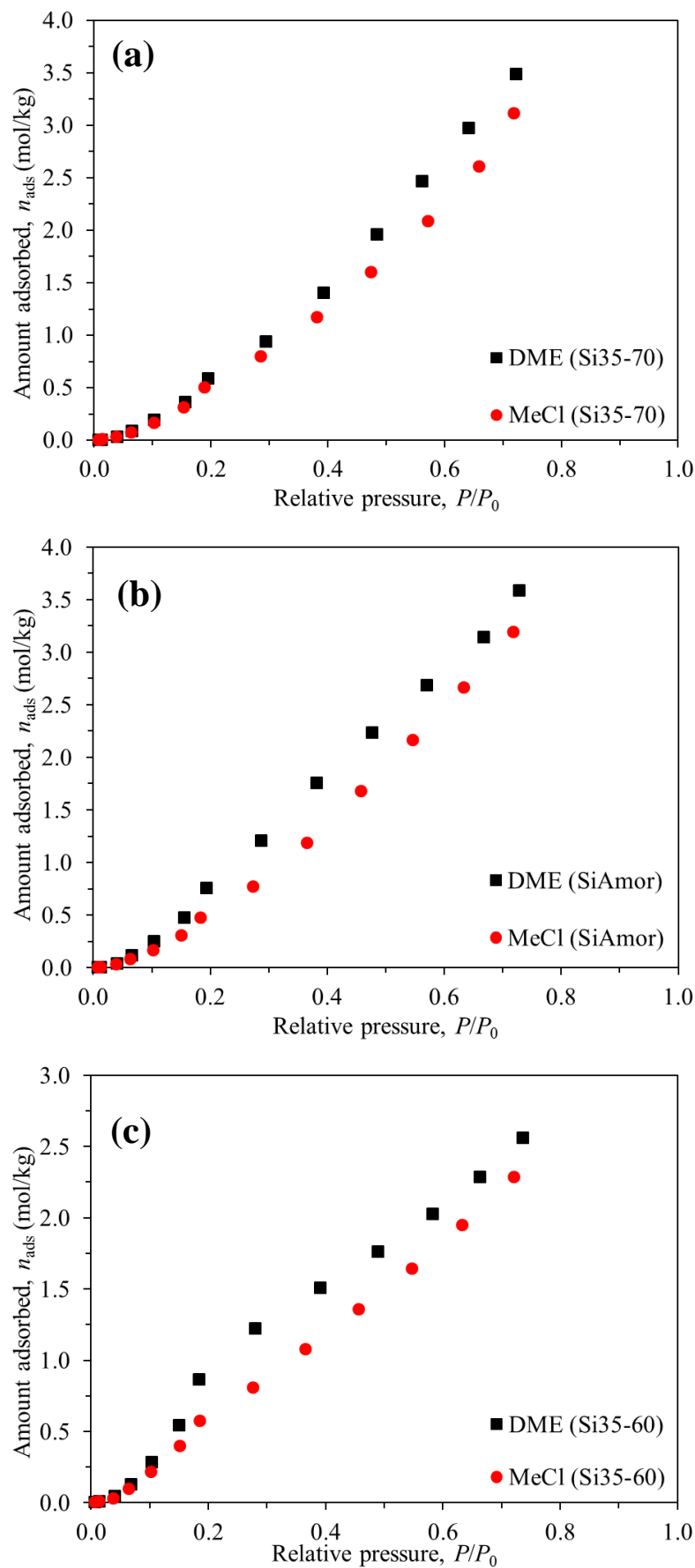


Fig. 5.16. Pure component adsorption isotherms for DME and MeCl on a) Si35-70, b) SiAmor and c) Si35-60

5.3.2.2 Pure component empirical adsorption models

Adsorption of DME and MeCl on each of the silica gels exhibited Type I behaviour due to a) the trend line depicted by each adsorbate on each adsorbent, b) each adsorbent being highly microporous and c) the adsorption uptake data for each combination towards high pressure indicative steady adsorption until saturation into plateau. Fig. 5.17 shows the adsorption uptake points for the isotherms shown in Fig. 5.16. It can be seen from the uptake points that adsorption is steady meaning the isotherm measurement is capable of continuing its trend line, thus indicating that the adsorbent is not fully saturated under the conditions considered. With that being said it is expected that towards a relative pressure near unity the adsorbent would become saturated and therefore result in a plateau for the isotherm curve. For Type I isotherms the models used earlier: Langmuir, Sips and Tóth are applicable, as are the DA and DR equations however for their applicability they require good low pressure adsorption data but as can be seen the conditions considered this was not the case. Therefore the data was fitted to the Freundlich model only. Table 5.7 shows the fitting parameters for DME and MeCl on all three silica gels. The data shows that all rate constants and heterogeneity parameters increased for each gas in the order of increasing surface area, which was expected since the larger the surface the greater the amount of respective adsorption sites. For each silica gel DME exhibited a larger adsorption rate constant and larger heterogeneity for the respective adsorbents. In terms of rate constants, DME demonstrated a wider variation (0.537 - 0.739) between values for the different silica gels where MeCl on the gels exhibited a smaller difference between values (0.418 - 0.498) suggesting the adsorption of the formers' rate constant are affected more by the surface area and or type of interactions.

Table 5.7. Freundlich empirical adsorption model parameters for pure component DME and MeCl on Si35-70, SiAmor and Si35-60

Parameters		Si35-70		SiAmor		Si35-60	
		DME	MeCl	DME	MeCl	DME	MeCl
Freundlich	<i>K</i>	0.537	0.418	0.722	0.437	0.739	0.498
	<i>t</i>	0.722	0.672	0.834	0.687	1.076	0.904
	<i>R</i> ²	0.999	0.999	0.999	0.999	0.995	0.999

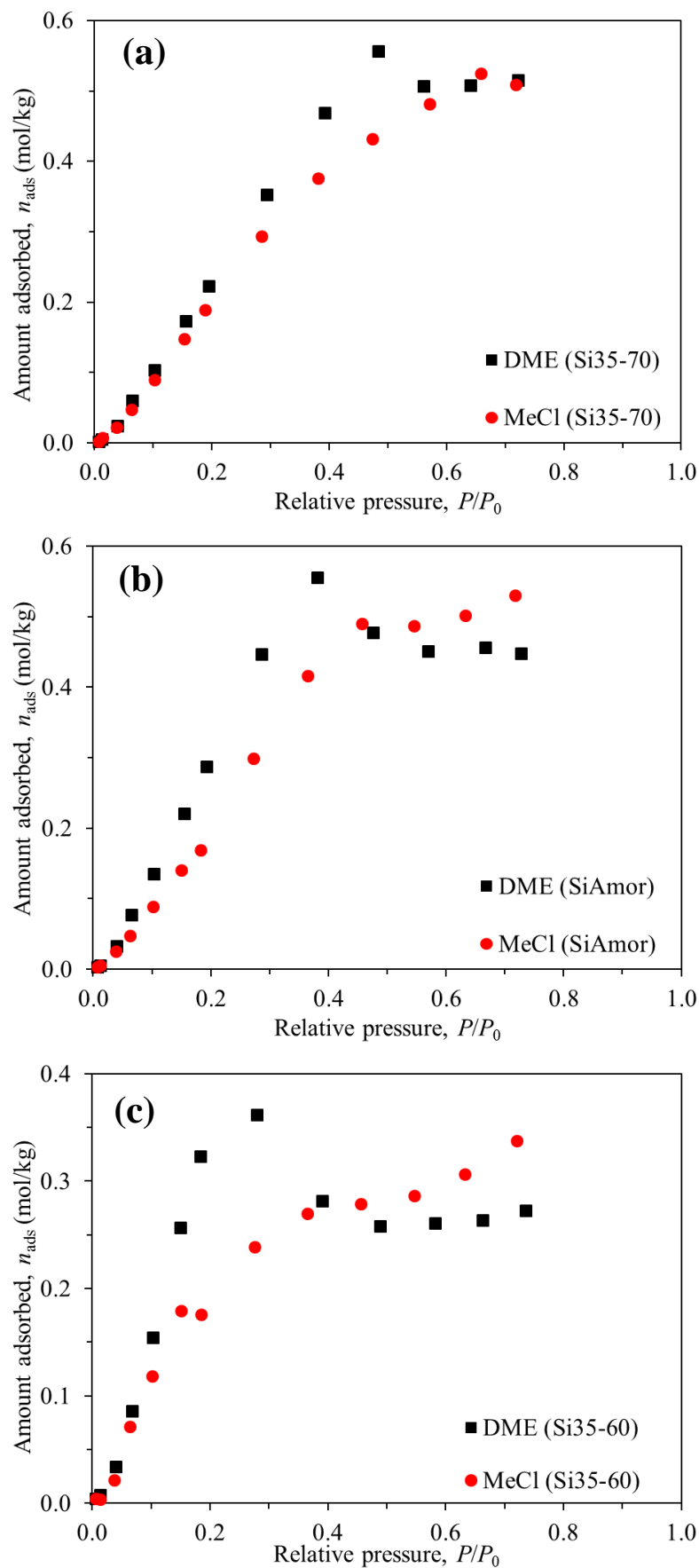


Fig. 5.17. Pure component adsorption uptake points for DME and MeCl on a) Si35-70, b) SiAmor and c) Si35-60

5.3.2.3 Pure component adsorption kinetics

Similar to the adsorption kinetics for zeolites, the kinetics for adsorption on the different silica gels was compared to determine the kinetic order of reaction and insight into the adsorption mechanism involved. Each of the A-S combinations was fitted to the four kinetic models with the parameters shown in Table 5.8 - Table 5.10. In terms of order of reaction adsorption of both DME and MeCl undergoes pseudo first order kinetics for both Si35-70 and SiAmor, respectively. On Si35-60 both gases exhibited pseudo first order kinetics from 0.5 - 1.5 atm then pseudo second order kinetics at > 2.0 atm. Although the IPD model applied at certain incremental pressures the model does not indicate the order of reaction like the pseudo models therefore utilised in conjunction with the pseudo models in the following section. As observed earlier with the zeolite 5A the applicability of the different kinetic models at different pressure is due to the presence of moisture and accumulation of prior adsorption thus promoting the impact of co-adsorption/competing effects which subsequently affects the rate.

On Si35-70 both gases exhibited pseudo first order kinetics throughout the isotherm measurements. With the exception of DME at 3.5 atm where there was a rapid rise due to second order kinetics. The steady kinetic behaviour can be explained by the adsorbent having the largest surface area available for adsorption and the solid not reaching saturation. On SiAmor MeCl exhibited pseudo first order kinetics throughout whereas DME exhibited first order kinetics from 0.5 - 2.5 atm then pseudo second order kinetics from 3.0 - 3.5 atm. Both gases demonstrated increasing trends with pressure. On Si-35-60 both gases exhibited pseudo first order kinetics from 0.5 - 1.5 atm then second order from 2.0 - 3.5 atm with DME exhibiting the largest deviations. In each case the behaviour in terms of changing order of reaction is due to a combination of effects: presence of some impurities, prior adsorption (isotherm measurement data) and physical and chemical properties of the gels. Although the kinetics are largely influenced by the respective functional groups of the adsorbates and adsorbents, the physical and other chemical properties of the adsorbents play an important role.

In terms of silica gel properties, Si35-60 has the lowest surface area but largest silica (Si) composition, ~ 29 % indicative of more silanols groups which are a cause of dual site adsorption/weaker mode of adsorption [52, 115]. Recall DME adsorbs through hydrogen bonding and MeCl through weak VDWs forces, the latter being weaker. The greater affinity of DME over MeCl to the silanol groups has already been shown therefore not a surprise with its increased rate constant (pseudo second order) behaviour on Si35-60. The second order behaviour is suspected to be because the adsorbent has the lowest surface area meaning fewer adsorption sites (approximately half of Si35-70), the highest Si composition; desirable for DME according to trends.

Table 5.8. Adsorption kinetic model parameters for pure component DME and MeCl on Si35-70

<u>DME on Si35-70</u>										
Adsorption pressure <i>atm</i>	<u>Pseudo first order</u>		<u>Pseudo second order</u>		<u>Elovich</u>			<u>IPD</u>		
	k'_{ads} (s ⁻¹)	R^2	k''_{ads} (mol kg ⁻¹ s ⁻¹)	R^2	α (mol kg ⁻¹ min ⁻¹)	β (kg mol ⁻¹)	R^2	k_{IPD} (mol kg ⁻¹ -mol ^{-1/2})	C_{IPD} (constant)	R^2
0.5	0.021	<u>0.977</u>	0.012	0.603	0.26	7.07	0.874	0.160	-0.037	0.960
1.0	0.018	0.979	0.018	0.800	0.36	5.92	0.828	0.198	-0.029	<u>0.984</u>
1.5	0.020	<u>0.996</u>	0.015	0.855	0.56	4.14	0.819	0.286	-0.030	0.992
2.0	0.021	<u>0.997</u>	0.016	0.901	0.73	3.44	0.795	0.350	-0.017	0.995
2.5	0.021	<u>0.999</u>	0.013	0.910	0.94	2.75	0.785	0.441	-0.016	0.996
3.0	0.024	<u>0.993</u>	0.021	0.956	1.07	2.94	0.715	0.429	0.032	0.984
3.5	0.043	<u>0.997</u>	0.039	0.982	1.21	3.44	0.615	0.386	0.083	0.935
<u>MeCl on Si35-70</u>										
Adsorption pressure <i>atm</i>	<u>Pseudo first order</u>		<u>Pseudo second order</u>		<u>Elovich</u>			<u>IPD</u>		
	k'_{ads} (s ⁻¹)	R^2	k''_{ads} (mol kg ⁻¹ s ⁻¹)	R^2	α (mol kg ⁻¹ min ⁻¹)	β (kg mol ⁻¹)	R^2	k_{IPD} (mol kg ⁻¹ -mol ^{-1/2})	C_{IPD} (constant)	R^2
0.5	0.018	0.937	0.025	0.712	0.19	10.62	0.839	0.109	-0.021	<u>0.966</u>
1.0	0.018	<u>0.996</u>	0.018	0.797	0.34	6.17	0.839	0.189	-0.028	0.983
1.5	0.020	0.981	0.007	0.872	0.22	5.95	0.944	0.140	-0.017	<u>0.993</u>
2.0	0.023	0.996	0.009	0.938	0.29	5.12	0.956	0.162	0.003	<u>0.997</u>
2.5	0.031	0.978	0.009	0.954	0.37	4.31	0.942	0.193	0.021	<u>0.989</u>
3.0	0.026	<u>0.994</u>	0.011	0.971	0.44	4.03	0.927	0.207	0.047	0.980
3.5	0.024	<u>0.997</u>	0.021	0.956	1.07	2.94	0.715	0.429	0.032	0.935

* R^2 values which are bold and underlined show that, that particular model is most applicable for the data analysis at that respective pressure/condition.

Table 5.9. Adsorption kinetic model parameters for pure component DME and MeCl on SiAmor

<u><i>DME on SiAmor</i></u>										
Adsorption pressure <i>atm</i>	<u>Pseudo first order</u>		<u>Pseudo second order</u>		<u>Elovich</u>			<u>IPD</u>		
	k'_{ads} (s ⁻¹)	R^2	k''_{ads} (mol kg ⁻¹ s ⁻¹)	R^2	α (mol kg ⁻¹ min ⁻¹)	β (kg mol ⁻¹)	R^2	k_{IPD} (mol kg ⁻¹ -mol ^{-1/2})	C_{IPD} (constant)	R^2
0.5	0.022	0.981	0.045	0.848	0.19	12.22	0.817	0.097	-0.010	<u>0.988</u>
1.0	0.027	0.970	0.032	0.914	0.41	6.30	0.785	0.192	-0.006	<u>0.993</u>
1.5	0.026	<u>0.991</u>	0.020	0.912	0.64	4.00	0.789	0.302	-0.011	0.991
2.0	0.029	<u>0.996</u>	0.020	0.940	0.90	3.14	0.754	0.391	0.009	0.980
2.5	0.041	<u>0.990</u>	0.039	0.979	1.13	3.51	0.628	0.374	0.073	0.935
3.0	0.044	0.957	0.057	<u>0.989</u>	1.38	3.71	0.543	0.372	0.115	0.895
3.5	0.057	0.993	0.076	<u>0.993</u>	1.52	4.12	0.486	0.349	0.134	0.867
<u><i>MeCl on SiAmor</i></u>										
Adsorption pressure <i>atm</i>	<u>Pseudo first order</u>		<u>Pseudo second order</u>		<u>Elovich</u>			<u>IPD</u>		
	k'_{ads} (s ⁻¹)	R^2	k''_{ads} (mol kg ⁻¹ s ⁻¹)	R^2	α (mol kg ⁻¹ min ⁻¹)	β (kg mol ⁻¹)	R^2	k_{IPD} (mol kg ⁻¹ -mol ^{-1/2})	C_{IPD} (constant)	R^2
0.5	0.019	<u>0.987</u>	0.047	0.796	0.13	15.96	0.843	0.073	-0.011	0.985
1.0	0.030	<u>0.992</u>	0.086	0.968	0.33	10.47	0.686	0.123	0.014	0.976
1.5	0.031	<u>0.999</u>	0.018	0.970	0.25	6.83	0.929	0.122	0.025	0.976
2.0	0.033	<u>0.999</u>	0.014	0.974	0.35	4.99	0.928	0.166	0.038	0.970
2.5	0.042	<u>0.996</u>	0.015	0.982	0.47	4.11	0.900	0.203	0.069	0.950
3.0	0.043	<u>0.993</u>	0.021	0.991	0.57	4.09	0.850	0.206	0.111	0.913
3.5	0.056	<u>0.993</u>	0.057	0.989	1.38	3.71	0.543	0.372	0.115	0.867

* R^2 values which are bold and underlined show that, that particular model is most applicable for the data analysis at that respective pressure/condition.

Table 5.10. Adsorption kinetic model parameters for pure component DME and MeCl on Si35-60

<u>DME on Si35-60</u>										
Adsorption pressure <i>atm</i>	<u>Pseudo first order</u>		<u>Pseudo second order</u>		<u>Elovich</u>			<u>IPD</u>		
	k'_{ads} (s ⁻¹)	R^2	k''_{ads} (mol kg ⁻¹ s ⁻¹)	R^2	α (mol kg ⁻¹ min ⁻¹)	β (kg mol ⁻¹)	R^2	k_{IPD} (mol kg ⁻¹ -mol ^{-1/2})	C_{IPD} (constant)	R^2
0.5	0.023	<u>0.983</u>	0.032	0.798	0.20	10.57	0.845	0.110	-0.016	0.982
1.0	0.025	0.991	0.032	0.929	0.49	5.65	0.762	0.218	0.000	<u>0.996</u>
1.5	0.032	<u>0.997</u>	0.036	0.960	0.70	4.51	0.707	0.278	0.024	0.963
2.0	0.051	0.978	0.093	<u>0.989</u>	0.92	5.79	0.528	0.240	0.079	0.881
2.5	0.045	0.951	0.159	<u>0.996</u>	1.19	7.08	0.414	0.215	0.104	0.828
3.0	0.036	0.888	0.134	<u>0.996</u>	1.33	6.19	0.422	0.245	0.116	0.840
3.5	0.044	0.937	0.201	<u>0.997</u>	1.36	7.83	0.366	0.203	0.113	0.798
<u>MeCl on Si35-60</u>										
Adsorption pressure <i>atm</i>	<u>Pseudo first order</u>		<u>Pseudo second order</u>		<u>Elovich</u>			<u>IPD</u>		
	k'_{ads} (s ⁻¹)	R^2	k''_{ads} (mol kg ⁻¹ s ⁻¹)	R^2	α (mol kg ⁻¹ min ⁻¹)	β (kg mol ⁻¹)	R^2	k_{IPD} (mol kg ⁻¹ -mol ^{-1/2})	C_{IPD} (constant)	R^2
0.5	0.020	0.974	0.047	0.849	0.17	13.07	0.821	0.091	-0.010	<u>0.991</u>
1.0	0.030	<u>0.991</u>	0.076	0.967	0.36	9.40	0.689	0.137	0.015	0.977
1.5	0.036	<u>0.995</u>	0.025	0.980	0.25	7.52	0.907	0.111	0.035	0.961
2.0	0.034	0.975	0.035	<u>0.993</u>	0.35	6.87	0.842	0.123	0.071	0.909
2.5	0.037	0.912	0.047	<u>0.996</u>	0.44	6.70	0.782	0.128	0.098	0.864
3.0	0.039	0.907	0.058	<u>0.997</u>	0.50	6.66	0.741	0.129	0.115	0.833
3.5	0.049	0.937	0.134	<u>0.996</u>	1.33	6.19	0.422	0.245	0.116	0.798

* R^2 values which are bold and underlined show that, that particular model is most applicable for the data analysis at that respective pressure/condition.

As discussed the IPD model only applied at some incremental pressures for the different adsorbate-silica gel interactions for reasons mentioned above. In terms of literature it has been observed that implementation of the IPD versus surface resistance controlled adsorption models have not been reported for silica gels. This is largely because characteristically silica gels have wider pore size distributions consisting of more than just micropores (macropores and/or mesopores) meaning adsorption is typically equilibrium driven and not kinetically. Nevertheless, for the conditions considered and consistency of analysis the two mechanisms were compared at 2.0 and 3.0 atm for information regarding the rate determining step. Shown by Fig. 5.18 - Fig. 5.20 adsorption of both gases on all silica gels appear to show greater linearity towards surface layering than IPD at 2.0 atm and 3.0 atm with both gases adsorbing at comparable rates. With that being said MeCl exhibited a slightly faster rate than DME through its faster declining slope on SiAmor and Si35-60, respectively. Surface resistance occurred due to the presence of molecularly adsorbed moisture and pre-adsorbed molecules from prior adsorption since results were from the isotherm measurements. The already present impurities and adsorbed molecules fill the strong adsorption sites meaning molecules from the bulk gas phase need more mobility and time to adsorb at weaker sites. Another impact of the impurities is that the time to reach equilibrium was affected due to competing effects and occupation of strong adsorption sites. This was particularly detrimental to a system with the above conditions since the adsorption of DME and MeCl on all three silica gels appears to be due to its thermodynamic equilibrium position rather than a faster kinetic rate or any molecular sieving effects.

On Si35-70 (Fig. 5.18) both gases linearity fitted to the longer time scale from ~ 0 -175 s for both pressures. In terms of the short time scale linearity was shown for both gases in three stages: $\sim 0 - 2.5$, $2.5 - 10$ and $10 - 20 \text{ s}^{1/2}$.

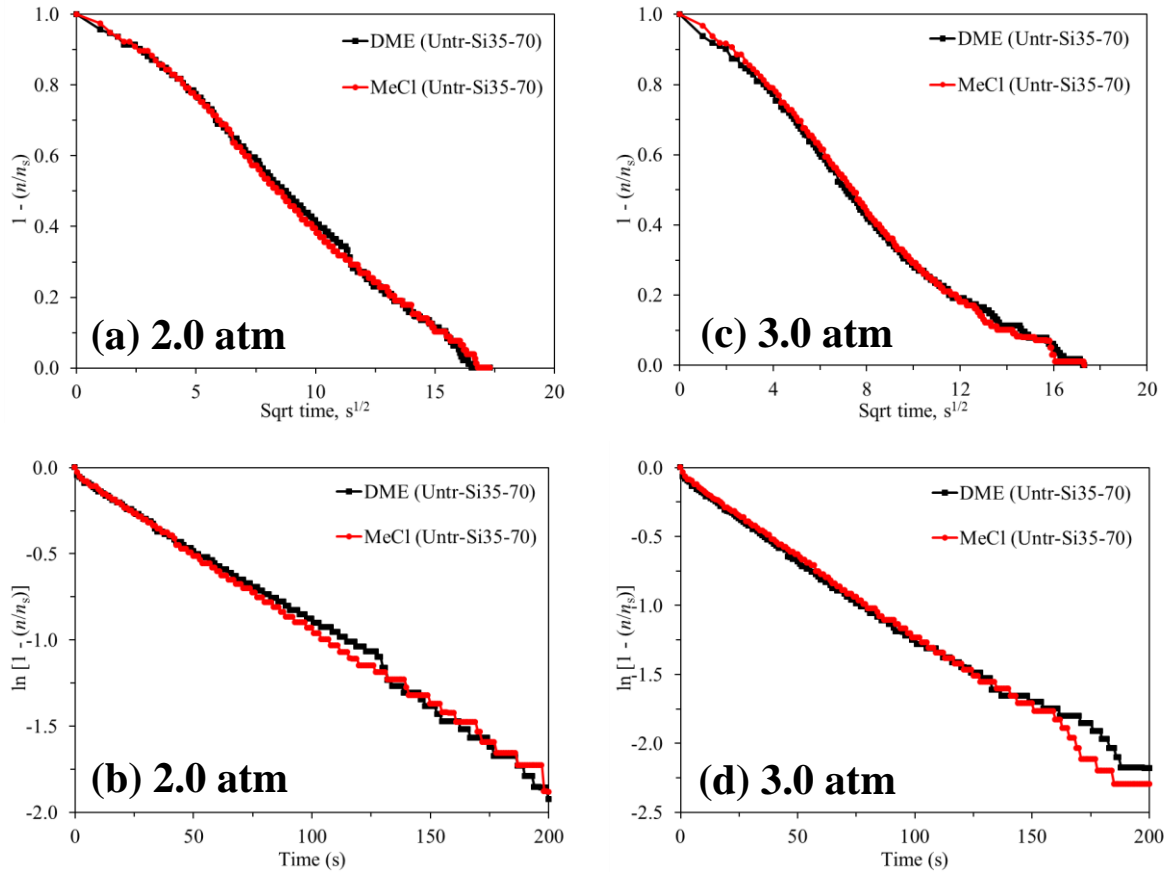


Fig. 5.18. Pure component adsorption mechanisms for DME and MeCl on Si35-70 where a) and c) represents intracrystalline diffusion controlled adsorption in a short time scale and b) and d) represents surface resistance layering in a long time scale at 2.0 atm and 3.0 atm

On SiAmor (Fig. 5.19) MeCl exhibited a faster rate at 2.0 atm but slower rate at 3.0 atm as shown in the longer time scale. The faster rate can be explained by MeCl being a more polar molecule and therefore weak VDW's forces occur quickly whereas DME adsorbs through more specific hydrogen bonding favoured by higher pressures i.e. greater energy to initiate interaction and subsequently reverse. Therefore in the long time scale MeCl adsorption slows down due to insufficient kinetic energy and DME continues to adsorb shown by its greater capacity in the isotherm and probable co-operative adsorption. At 3.0 atm DME exhibited a faster declining slope than MeCl due to the adsorption of DME on to the weaker Si groups meaning more available sites for adsorption with high kinetic energy resulting in the greater adsorption capacity. In the long time scale adsorption on SiAmor exhibited evidence of linearity in two stages at both pressures suggesting the presence of two different types of surface resistances: heat and mass resistances. Ruthven [1] reports that adsorbents which consist of microporous and macropores offer two

distinct resistances to mass transfer: micropore resistances of crystals or microparticles and the macropore diffusional resistance of the pellet. When adsorption occurs from a binary mixture (which in this case can be considered with the presence of molecularly adsorbed moisture) there may be an additional resistance to mass transfer associated through the laminar fluid boundary layer surrounding the particle. In the short time scale linearity on SiAmor was shown in two stages: $\sim 0 - 2.5$, $2.5 - 10 \text{ s}^{1/2}$ at both pressures.

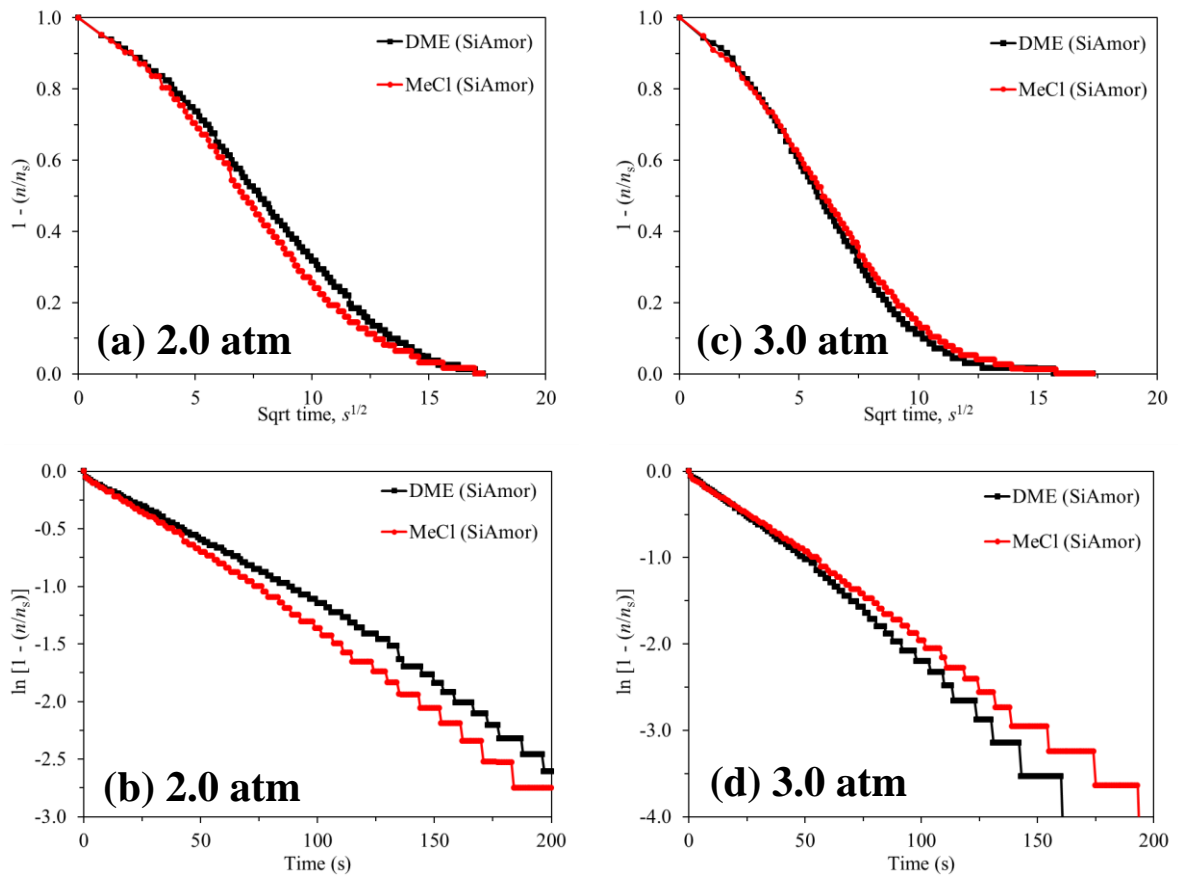


Fig. 5.19. Pure component adsorption mechanisms for DME and MeCl on SiAmor where a) and c) represents intracrystalline diffusion controlled adsorption in a short time scale and b) and d) represents surface resistance layering in a long time scale at 2.0 atm and 3.0 atm

On Si35-60 (Fig. 5.20) recall the adsorbent has the lowest surface area and the assumption that the strong hydroxyl groups are occupied with molecularly adsorbed moisture due to lack of thermal pre-treatment. This meant less adsorption sites were available and with the adsorbent having the largest Si group composition, collectively meaning DME adsorbed at a faster rate. In the long time scale linearity was shown from $\sim 0 - 150 \text{ s}$ with DME exhibiting the faster declining slope at 2.0 atm. At 3.0 atm the linearity in the long time scale was $\sim 0 - 75 \text{ s}$ symptomatic of more than one type of surface resistance as shown in the short time scale linearity. This was no surprise since this was the lowest surface area adsorbent therefore more sensitive to changes due to adsorption effects.

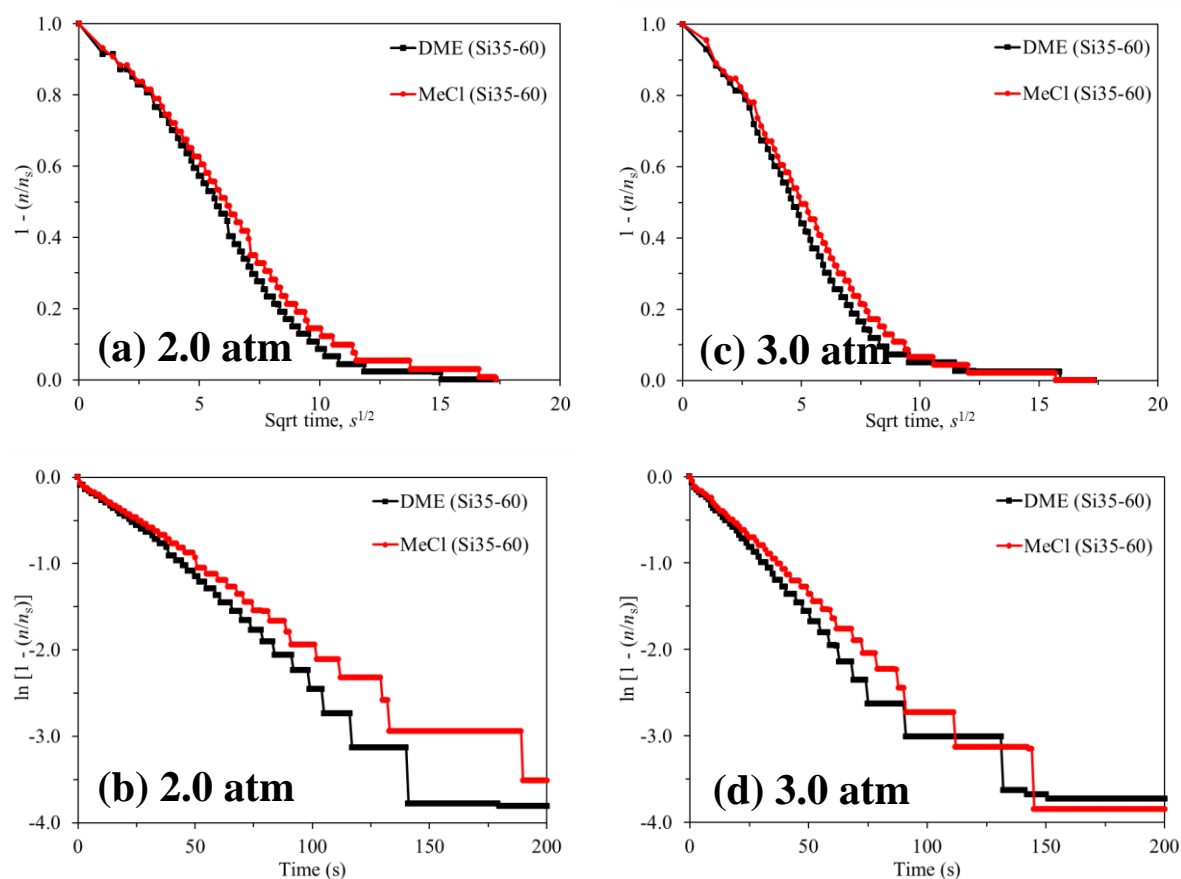


Fig. 5.20. Pure component adsorption mechanisms for DME and MeCl on Si35-60 where a) and c) represents intracrystalline diffusion controlled adsorption in a short time scale and b) and d) represents surface resistance layering in a long time scale at 2.0 atm and 3.0 atm

5.3.2.4 Pure component differential heat of adsorption

Fig. 5.21 compares the differential heats of adsorption for the pure component data of DME and MeCl on Si35-70, SiAmor and Si35-60, respectively. As can be seen on all three gels both gases exhibited very similar trends. DME on the gels exhibited a high initial differential heat (44.84, 45.54 and 33.31 kJ mol^{-1}) and a secondary heat spikes from 0.25 - 0.60 mol kg^{-1} whereas MeCl exhibited a high initial differential heat (46.14, 50.72 and 33.93 kJ mol^{-1}) then dropped before becoming constant with values $< 10 \text{ kJ mol}^{-1}$ on all silica gels. Apart from the initial A-S interactions all interactions trends thereafter were more constant i.e. homogenous adsorption behaviour. For both gases adsorption occurs due to physisorption interactions. Although it was reported that DME adsorbs due to strong hydrogen bonding and MeCl via weak VDW's forces this was not evident from the data obtained therefore difficult to qualitatively differentiate between the two gases.

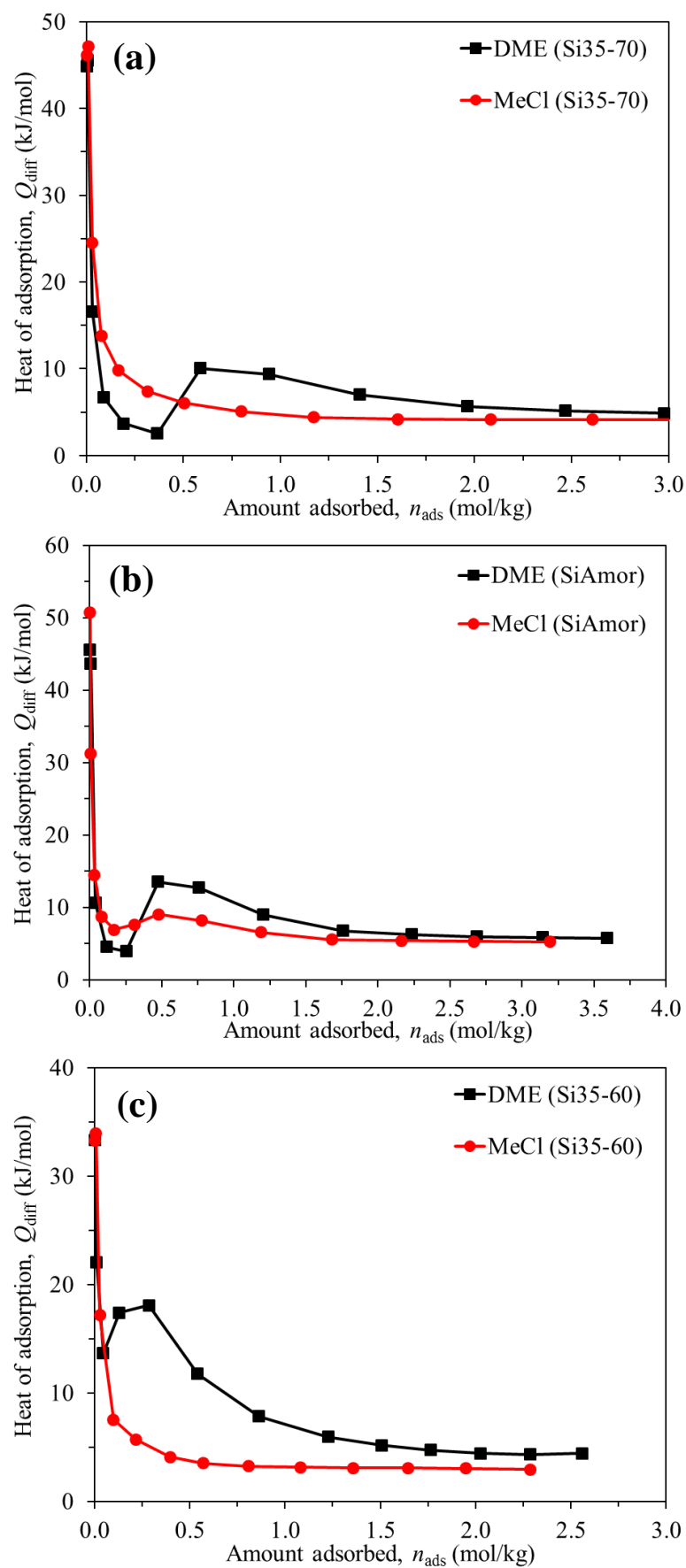


Fig. 5.21. Differential heat of adsorption for pure component DME and MeCl on a) Si35-70; b) SiAmor and c) Si35-60

Under the conditions considered the presence of moisture and impurities on the different silica gels influenced DME adsorption more strongly. Of the gels the SiAmor resulted in the highest initial value for both gases because of the greater hydroxyl groups responsible for hydrogen bonding. Adsorption on SiAmor aside, the initial differential heats for each respective adsorbate were decreasing with reducing surface area. Such behaviour was moderately attributed to the fact the lesser surface area adsorbent was closer to its equilibrium position (less adsorption sites to adsorb onto within the given equilibrium time) therefore when using the heat balance to determine the heat released in terms kJ mol^{-1} , if the uptake is not sufficient Q can be overestimated.

5.3.3 Pure component adsorption/desorption of dimethyl ether (DME) and methyl chloride (MeCl) on activated carbon

5.3.3.1 Pure component adsorption

Fig. 5.22 shows the adsorption isotherms at room temperature ($20\text{ }^{\circ}\text{C}$) in terms of relative pressure for pure component DME and MeCl on AC8-12. Within the conditions considered DME and MeCl had adsorption capacities of 4.12 and 4.71 mol kg^{-1} , respectively. Of all the adsorbents used, AC8-12 had the largest surface area and consists of mostly carbon, coupled with a moisture content of $\sim 4\%$. Compared to the adsorption isotherm trends on zeolite 5A and silica gels (all microporous) the adsorption behaviour of both gases on activated carbon resulted in a more definitive shapes to the trends.

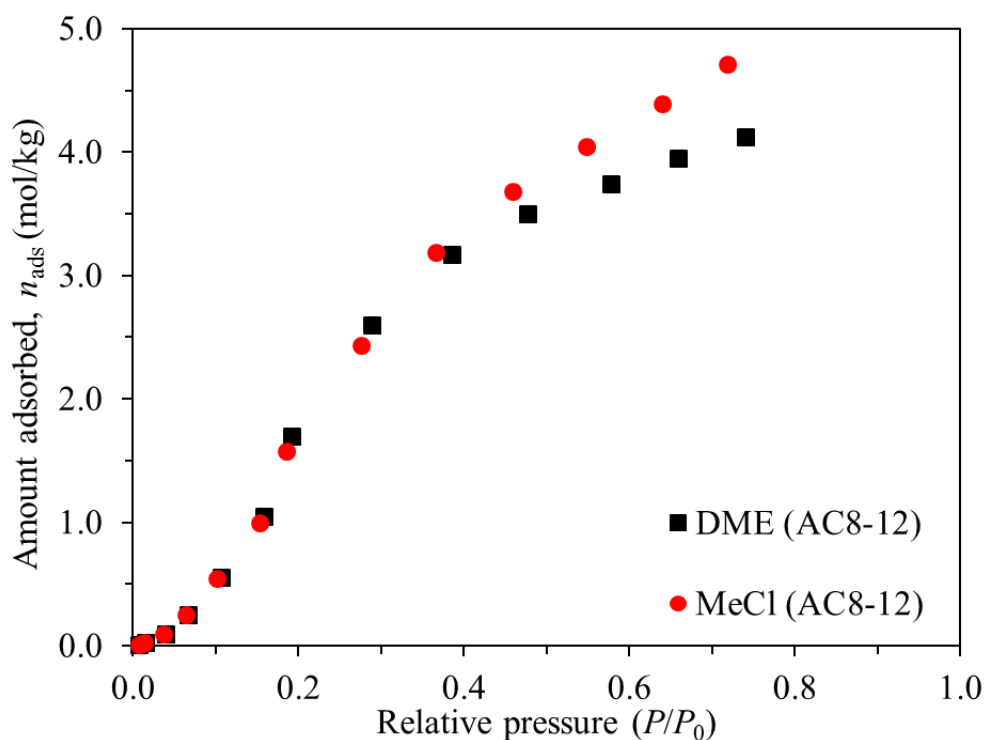


Fig. 5.22. Pure component DME and MeCl adsorption isotherms on AC8-12 at $20\text{ }^{\circ}\text{C}$

5.3.3.2 Pure component empirical adsorption models

It can be seen in Fig. 5.22 that both gases demonstrated Type I behaviour with MeCl exhibiting a larger adsorption capacity. Type I behaviour was depicted by the slow plateau at pressures towards saturation. Similar to the earlier isotherms on zeolite 5A and all silica gels, the low pressure behaviour is explained by the equilibrium position. Consequently the data was fitted to the Freundlich model as shown by Table 5.11. According to the model MeCl demonstrated a larger heterogeneity than DME and a rate constant which was around three times larger.

Table 5.11. Freundlich empirical adsorption model parameters for pure component DME and MeCl on AC8-12

	Parameters	Adsorbate	
		DME	MeCl
Freundlich	K	0.522	1.500
	t	0.818	1.126
	R^2	0.992	0.990

5.3.3.3 Pure component desorption isotherms

Fig. 5.23 shows the subsequent desorption isotherms for the respective adsorption data on AC8-12 for DME (a) and MeCl (b), respectively. As it can be seen both gases exhibited some hysteresis with reducing pressure. For the conditions considered part of the reason for hysteresis is suspected to be due to the short equilibrium time and potential implications of strongly bound moisture within the sample. The equilibrium time is responsible since desorption takes longer than adsorption due to reasons mentioned earlier. Moreover, impact of the impurities/moisture interacting with the respective adsorbates can result in stronger bonds being formed, therefore more energy needed to reverse adsorption.

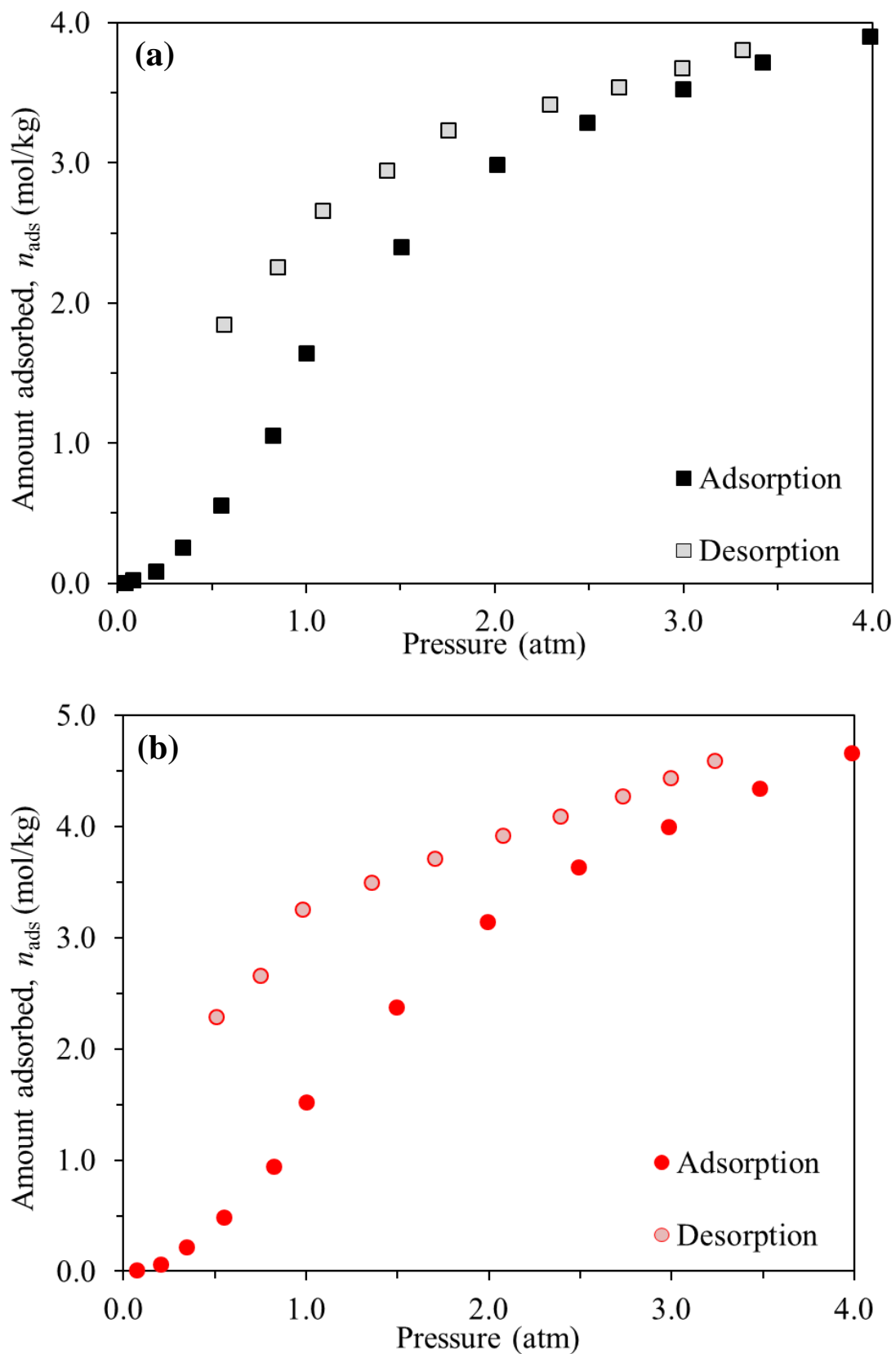


Fig. 5.23. Pure component adsorption and desorption isotherms at 20 °C for a) DME and b) MeCl on AC8-12

5.3.3.4 Pure component adsorption kinetics

Table 5.12 shows the fitting parameters for the respective kinetic models at increasing pressure increments. Of the four models the Elovich model fitted least for both gases as was the case with the other A-S interaction on the other adsorbent, with MeCl exhibiting the better fitting of the two adsorbates. According to the kinetic parameters both gases adsorbed exhibiting evidence of pseudo first order and IPD models for the selected pressures. However at higher pressures in both cases there was evidence of pseudo second order kinetics. Overall the DME data fitted to the pseudo first order model with an average R^2 value for the entire pressure range of 0.959 and 0.947 for the IPD model, respectively. MeCl on the other hand resulted in R^2 values of 0.961 and 0.971, respectively, in favour of the IPD model to the pseudo first order model. Due to the closeness of the values at this stage it is difficult to choose one model over the other for being largely responsible for the respective adsorption kinetics although both adsorb as first order reactions. It is worth recalling that AC8-12 has a high surface area and adequate pore size therefore IPD is highly likely. Of the two gases DME has the greater kinetic adsorption rate constant which increased by a factor of ~ 8 times faster from 2.0 - 3.5 atm.

Table 5.12. Adsorption kinetic model parameters for pure component DME and MeCl on AC8-12

<u>DME on AC8-12</u>										
Adsorption pressure <i>atm</i>	<u>Pseudo first order</u>		<u>Pseudo second order</u>		<u>Elovich</u>			<u>IPD</u>		
	k'_{ads} (s ⁻¹)	R^2	k''_{ads} (mol kg ⁻¹ s ⁻¹)	R^2	α (mol kg ⁻¹ min ⁻¹)	β (kg mol ⁻¹)	R^2	k_{IPD} (mol kg ⁻¹ -mol ^{-1/2})	C_{IPD} (constant)	R^2
0.5	0.023	<u>0.982</u>	0.014	0.769	0.397	5.19	0.853	0.222	-0.036	0.977
1.0	0.028	<u>0.992</u>	0.017	0.925	0.873	3.05	0.774	0.399	-0.005	0.988
1.5	0.037	<u>0.972</u>	0.015	0.950	1.379	2.15	0.735	0.577	0.029	<u>0.976</u>
2.0	0.052	<u>0.996</u>	0.037	0.987	1.946	2.52	0.553	0.541	0.159	0.892
2.5	0.058	0.917	0.144	<u>0.998</u>	2.695	4.65	0.336	0.352	0.213	0.776
3.0	0.053	0.889	0.136	<u>0.998</u>	2.836	4.81	0.325	0.347	0.215	0.779
3.5	0.075	0.952	0.400	<u>0.999</u>	3.093	8.14	0.240	0.226	0.175	0.700
<u>MeCl on AC8-12</u>										
Adsorption pressure <i>atm</i>	<u>Pseudo first order</u>		<u>Pseudo second order</u>		<u>Elovich</u>			<u>IPD</u>		
	k'_{ads} (s ⁻¹)	R^2	k''_{ads} (mol kg ⁻¹ s ⁻¹)	R^2	α (mol kg ⁻¹ min ⁻¹)	β (kg mol ⁻¹)	R^2	k_{IPD} (mol kg ⁻¹ -mol ^{-1/2})	C_{IPD} (constant)	R^2
0.5	0.020	<u>0.950</u>	0.017	0.792	0.372	5.71	0.840	0.204	-0.031	<u>0.982</u>
1.0	0.024	<u>0.993</u>	0.017	0.925	0.877	3.07	0.772	0.398	-0.004	<u>0.994</u>
1.5	0.031	<u>0.980</u>	0.005	0.949	0.647	2.39	0.946	0.347	0.027	<u>0.989</u>
2.0	0.039	<u>1.000</u>	0.009	0.985	0.847	2.33	0.899	0.358	0.129	0.945
2.5	0.055	0.981	0.026	<u>0.997</u>	1.011	3.18	0.755	0.270	0.230	0.845
3.0	0.063	0.995	0.049	<u>0.999</u>	1.058	4.09	0.666	0.215	0.241	0.779
3.5	0.050	0.941	0.136	<u>0.998</u>	2.836	4.81	0.325	0.347	0.215	0.779

* R^2 values which are bold and underlined show that, that particular model is most applicable for the data analysis at that respective pressure/condition.

For the IPD versus surface resistance layering diffusion models for pure component DME and MeCl at 2.0 atm and 3.0 atm it can be seen that the data supports the kinetic model data with the faster declining slope of DME indicative of faster adsorption. This is better shown in the long time scale which shows that DME reaches equilibrium faster than MeCl. It was reported that if the adsorption of MeCl on a carbon surface is operated at higher temperature the diffusivities increase and thus result in shorted equilibrium times. Ultimately, under the conditions considered there is non-favourable isotherm or kinetic evidence of one adsorbate gas being adsorbed substantially more or at an exploitable rate than the other.

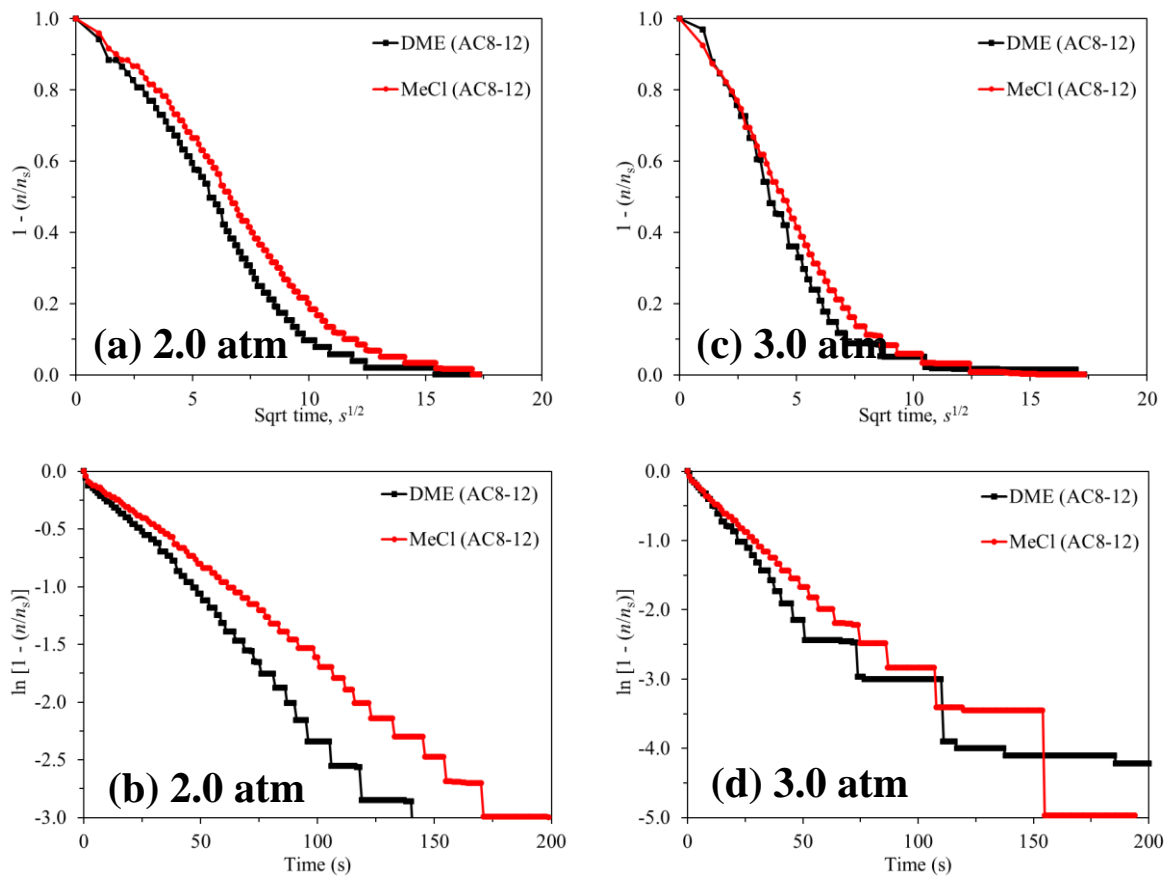


Fig. 5.24. Pure component adsorption mechanisms for DME and MeCl on AC8-12 where a) and c) represents intracrystalline diffusion controlled adsorption in a short time scale and b) and d) represents surface resistance layering in a long time scale at 2.0 atm and 3.0 atm

5.3.3.5 Pure component differential heat of adsorption

Fig. 5.25a compares the differential heat of adsorption for DME versus MeCl on AC8-12 in terms of amount adsorbed. Similarly Fig. 5.25b shows the data of the integral heats of adsorption to be in the same trend and magnitude as the differential heats.

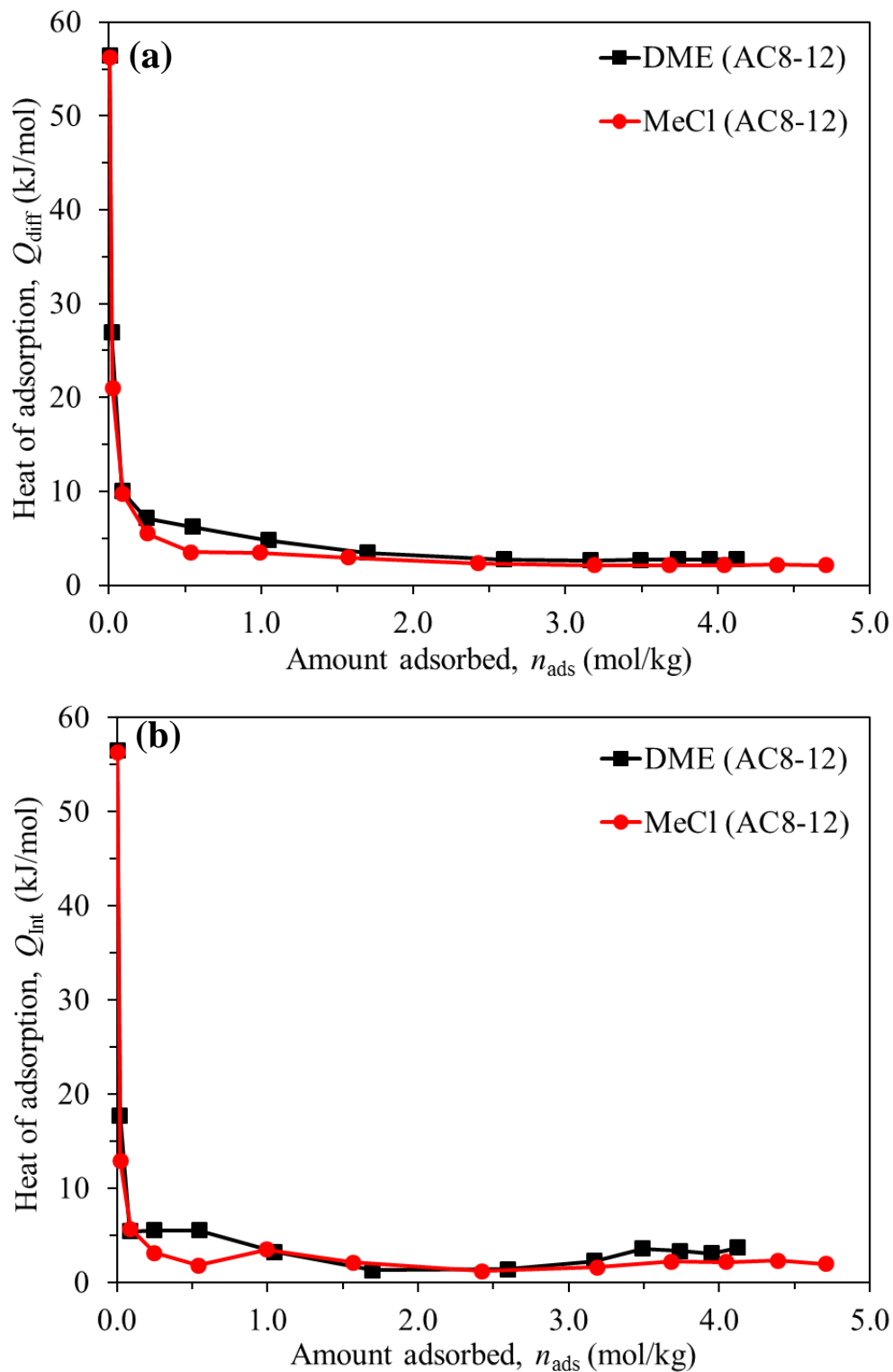


Fig. 5.25. a) Differential and b) integral heat of adsorption for pure component DME and MeCl on AC8-12 at 20 °C

As it can be seen by the differential heats both gases exhibited very similar trends with initial high heats of adsorption released with values of 56.42 and 56.27 kJ mol⁻¹ for DME and MeCl, respectively. Then the differential heats reduced to values in the range of 2.14 - 26.96 kJ mol⁻¹ until saturation. Initially the high differential heats of adsorption can be attributed to the interaction with the strong adsorption sites, and then adsorption proceeds to lesser ones. Based on the values it can be said that both gases adsorb onto the adsorbent via physisorption in a monolayer fashion. Similar to Kowalczyk *et al.* [120] the initial high differential heat arises from A-S interactions. They also report that depending upon the preparation of activated carbon if it is subjected to severe heating or oxidising atmospheres it can break up the micro-crystallites into their original crystallites. Therefore any chemisorbed oxygen or hydrogen imparts polar characteristics to the carbon solid thus influencing the adsorbents adsorption properties especially at low coverages. Moreover, the high initial differential heats of adsorption are a result of the short equilibrium time since the equilibrium position affects Q in the heat balance. At low coverages generally adsorption takes longer therefore the high initial differential heats are partly attributed to the incomplete equilibrium position [53]. It can be said if the equilibrium time is extended the differential heat values would decrease particularly since the adsorbent has a significantly large adsorption capacity.

5.3.4 Overall sorption error

Extensive sorption analysis was conducted initially for DME adsorption on zeolites 4A and 5A, respectively. This was to establish reference conditions for subsequent experiments using MeCl and other adsorbents. The adsorbents were selected due to their differences in surface area which gave an indication of the variation in error and consequently reveal the system's sensitivity to quantities of cumulative adsorption for small and large amounts adsorbed. As shown in Chapter I it was envisaged in the project proposal to carry out adsorption within a short residence time therefore a 5 min equilibrium time was selected at room temperature (20 °C). Triplicate adsorption experiments were conducted for DME on 4A and 5A to confirm reproducibility of runs for the two different adsorbents. Fig. 5.26 shows the percentage error for the adsorption isotherms for 1 h pre-treated zeolites 4A and 5A which were determined to be 1.32 % and 0.93 %, respectively. As it can be seen the error was so low that errors bars are barely visible and therefore confirming excellent reproducibility between experimental sets. Similar observations were made in terms of MeCl adsorption on the above.

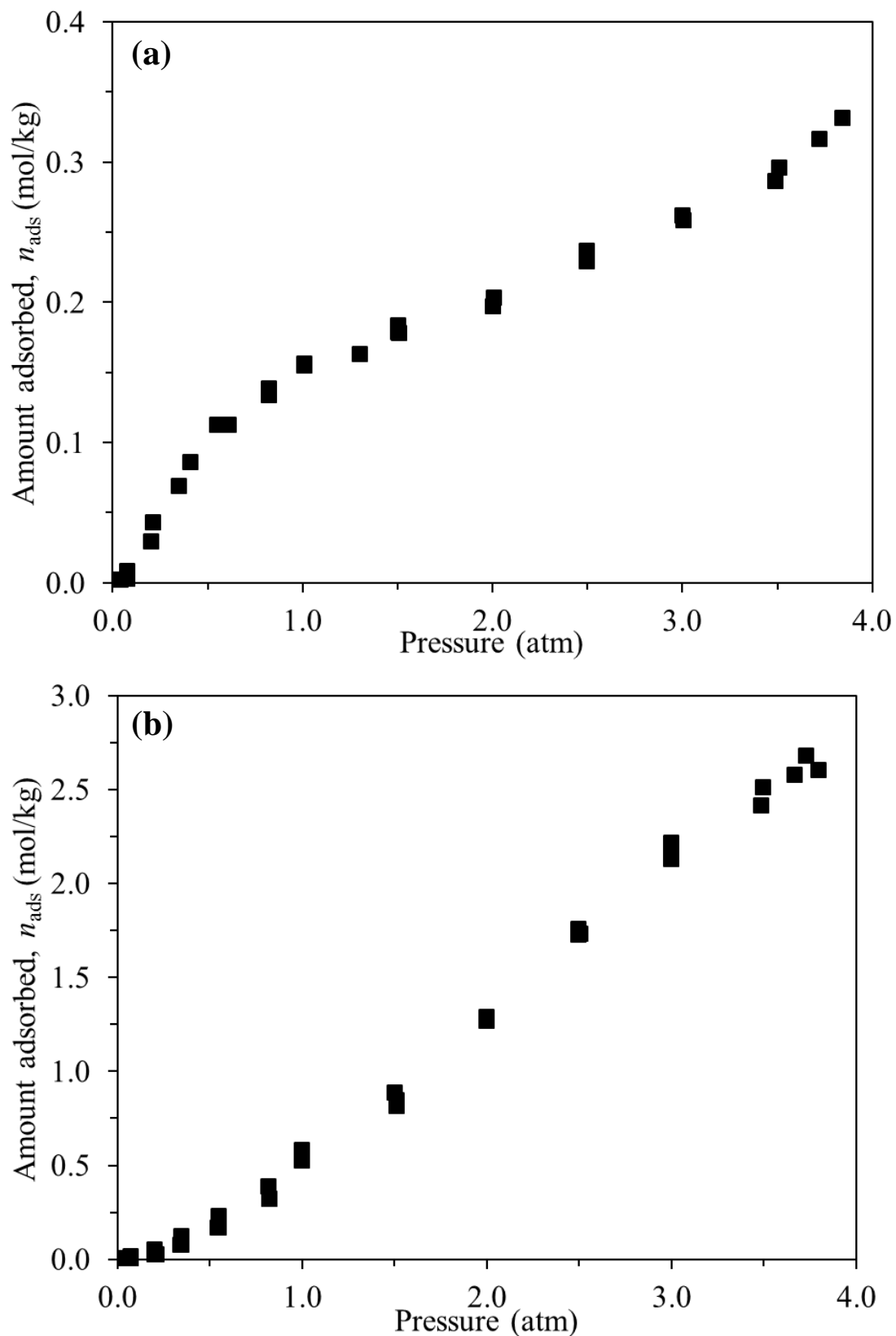


Fig. 5.26. Experiment error bars for pure component DME adsorption isotherms at room temperature, 20 °C on a) 4A and b) 5A

5.4 Summary

The following summarises the key findings from the chapter: For the pure component adsorption of DME and MeCl on zeolites 4A and 5A, respectively:

- DME and MeCl adsorbed with adsorption capacities of 0.32 and 0.34 mol kg⁻¹ exhibiting Type II and Type I classifications, respectively on 4A. According to the Langmuir and Freundlich rate constants, DME has a value over double to that of MeCl, suggesting a faster rate.
- The difference in isotherm type for adsorption on 4A clearly points towards the molecular dimensions of the molecules playing an important role. The adsorbent is microporous to the molecule capable of pore penetration whilst exhibiting limited porosity for DME due to its larger molecular size.
- Both DME and MeCl adsorbed with adsorption capacities of 2.66 and 3.14 mol kg⁻¹, respectively, both exhibiting a Type I classification on 5A. According to the Freundlich model MeCl has a larger rate constant (0.66 compared to 0.53) and a negligibly greater heterogeneity (0.83 compared to 0.82).
- On 4A, both DME and MeCl adsorbed according to the pseudo second order adsorption kinetics. DME adsorbed a little over 3.5 times faster at 1.0 atm than MeCl and generally more than twice as fast as MeCl in the 1.5 - 3.5 atm pressure range.
- On 4A, at 2.0 and 3.0 atm both DME and MeCl exhibited greater linearity for the initial longer time scale thus indicating surface resistance was the rate limiting step. Whereas on 5A both gases demonstrated evidence of IPD being the rate limiting step.
- On 4A, DME exhibited a lower initial heat of adsorption (30.11 kJ mol⁻¹) than MeCl (44.77 kJ mol⁻¹) with both gases exhibiting a rapid drop followed by a constant heat release with increasing coverage.
- On 5A DME exhibited a higher initial differential heat of adsorption value of 29.81 kJ mol⁻¹ compared to MeCl's 10.11 kJ mol⁻¹. Thereafter MeCl resulted in two heat increases and DME exhibited one towards saturation.

Pure component adsorption of DME and MeCl on Si35-70, SiAmor and Si35-60, respectively:

- On Si35-70, DME and MeCl adsorbed with adsorption capacities of 3.49 and 3.12 mol kg⁻¹, respectively, both exhibiting a Type I adsorption classification.
- On SiAmor DME and MeCl adsorbed with adsorption capacities of 3.59 and 3.20 mol kg⁻¹, respectively, both exhibiting a Type I adsorption classification.
- On Si35-60 DME and MeCl adsorbed with adsorption capacities of 2.56 and 2.29 mol kg⁻¹, respectively, both exhibiting a Type I adsorption classification.

- According to the Freundlich model all rate constants and heterogeneity parameters increased for each gas in the order of increasing silica gel surface area. For each silica gel DME exhibited a larger adsorption rate constant and larger heterogeneity for the respective adsorbents compared to MeCl.
- In terms of kinetics, both DME and MeCl undergo pseudo first order adsorption kinetics for both Si35-70 and SiAmor, respectively at similar rates.
- On Si35-60 both gases exhibited pseudo first order adsorption kinetics from 0.5 - 1.5 atm then pseudo second order kinetics from 2.0 - 3.5atm, at a similar rates.
- Diffusion models on all silica gels demonstrated linearity for both gases to the longer time scale at comparable rates. Surface resistance occurred due to the presence of molecularly adsorbed moisture and pre-adsorbed molecules from prior adsorption since results were from the isotherm measurements.
- Both gases adsorbed at similar rates on all three silica gels where adsorption was driven by thermodynamic equilibrium rather than a faster kinetic rate or any molecular sieving effects.
- Both gases exhibited very similar differential heat of adsorption trends. DME exhibited high initial differential heats of 44.84, 45.54 and 33.31 kJ mol⁻¹ and secondary heat spikes from 0.25 - 0.60 mol kg⁻¹. On the other hand, MeCl exhibited high initial differential heats of 46.14, 50.72 and 33.93 kJ mol⁻¹ then rapidly dropped before becoming constant with values < 10 kJ mol⁻¹ on Si35-70, SiAmor and Si35-60, respectively.

Pure component adsorption of DME and MeCl on AC8-12:

- DME and MeCl adsorbed with adsorption capacities of 4.12 and 4.71 mol kg⁻¹, respectively, with both exhibiting a Type I adsorption classification.
- According to the Freundlich model MeCl adsorbs with a rate constant three times larger than DME and with a greater heterogeneity.
- Both gases adsorbed exhibiting evidence of pseudo first order adsorption kinetics and IPD for the selected pressures. However at higher pressure in both cases there was evidence of pseudo second order kinetics.
- The diffusion models suggested DME adsorbed at a faster rate through the faster declining slope. In both cases a greater linearity was shown for the longer time scale.
- DME and MeCl adsorbed with initial differential heat of adsorption values of 56.42 and 56.27 kJ mol⁻¹, respectively, then both trends dropped rapidly to near constant values < 10.0 kJ mol⁻¹.

CHAPTER VI: EFFECT OF PRE-TREATMENT AND EQUILIBRIUM TIME ON ADSORPTION ISOTHERMS

6.1 Introduction

Sing *et al.* [121] report that prior to the determination of any adsorption isotherm some type of pre-treatment is essential. Any physisorbed species (impurities) should be removed from the surface and pores of the adsorbent via outgassing usually at elevated temperatures. Though thermal treatment to an adsorbent could potentially alter its properties it may be advisable to carry out each one independently then observe the actual effect of each pre-treatment method. It is recommended that in order to produce reproducible isotherms the outgassing conditions must be controlled and kept within the limits of the adsorption system. In some cases as opposed to exposing the adsorbent to high vacuum a simple flushing with an inert gas at high temperature can be adequate. If they are done under extreme conditions it can lead to changes in the surface composition e.g. decomposition of hydroxides or carbonates, irreversible changes in texture and or formation of surface defects. Therefore supported by the TGA which confirmed the presence of impurities all subsequent experiments were carried out following thermal pre-treatment to avoid contamination and competing adsorption effects.

Sorption mechanisms are driven by various kinetically controlled reactions or physical phenomena which have the largest variability of retention times from seconds to years [33, 63]. As shown earlier by Fig. 3.9 typically adsorption occurs rapidly within the first 30-60 s then slows down adsorbing at a gentle rate with time. This consequently means it can be very difficult to know if the true thermodynamic equilibrium position has been reached at a particular condition. Based on the adsorption and desorption analysis on adsorbents (as received subjected to 1 h vacuum pre-treatment) in Chapter V it was evident that the equilibrium time (5 min) was too short for complete adsorption at low pressures therefore increased to 15 min for each increment to allow adequate time for molecules to reach thermodynamic equilibrium. It is recognised that through various literature studies report longer equilibrium times up to 1-3 h for various A-S interactions but these were generally reported for automated systems. In terms of the results obtained measurements were carried out through manually dosed increments, thus meaning longer equilibrium times were not safe to conduct in the laboratory for health and safety reasons especially to obtain high resolution isotherms. The next section compares the effect of both thermal pre-treatment and thermal pre-treatment with extended equilibrium time on DME and MeCl isotherms on zeolites 4A and 5A, respectively. All thermally pre-treated adsorbents in vacuum were treated at 150 °C for 15 h. and defined as Pret-. All as received adsorbents pre-treated for 1 h vacuum only are defined by the abbreviated term "Untr-".

Although this work compares the work of relatively untreated and thermally pre-treated zeolites; with the latter to avoid contamination. It has been reported that wetting adsorbents such as zeolites with water to enhance or deter adsorption is detrimental to the adsorbent [92, 122]. Arnold [123] cautions that droplets of liquid water on zeolites can be unfavourable to adsorption as it can lead to the mechanical destruction of the zeolite. Though zeolites are hydrophobic, their binders which usually consist of clay are not. Therefore soaking of the particles can lead to them bursting during regeneration at high temperatures. Alternatively, too much moisture on can lead to condensation and recrystallization of the clay binders thus reducing the mesopore volume and transport properties.

6.2 Results and discussion

6.2.1 Effect of vacuum, thermal pre-treatment and longer equilibrium to pure component DME and MeCl adsorption isotherms on zeolites 4A and 5A

Fig. 6.1 shows the effect of longer vacuum and thermal pre-treatment to the zeolite isotherms and the combined effect of vacuum, thermal pre-treatment and extended equilibrium time for DME and MeCl on Pret-4A. As can be seen the effect thermal pre-treatment was significant especially at low pressure for both gases. The effect of longer vacuum and thermal pre-treatment with an extended equilibrium time resulted in an increase in adsorption capacity by 1.95 % and 20.37 % for DME and MeCl, respectively, when compared to the earlier values for 4A. Thermal pre-treatment in vacuum resulted in an increase in pore openings and removal of strongly bound volatiles and occluded moisture within the adsorbent structure thus allowing the adsorbate molecules to interact with the vacant surface sites without competition especially at low pressure; where molecules trend to adsorb in the pores at strong adsorption sites. Since the adsorbent has such a low surface area the impact of moisture with the surface was greater than the other microporous solids.

In terms of DME adsorption the effect of longer vacuum and thermal pre-treatment was more important at low pressure because the presence of moisture resulted in less adsorption sites being available due to steric crowding i.e. reducing the adsorption capacity at low pressure. The increase in equilibrium time allowed more time for more molecules to adsorb, particularly at low pressure as molecules had more time for mobility to adsorb at the different adsorption sites and subsequently reach its true thermodynamic equilibrium position unlike the earlier 5 min equilibrium time. Overall the effect of moisture made little difference to the DME isotherm but a significant impact to the MeCl isotherm.

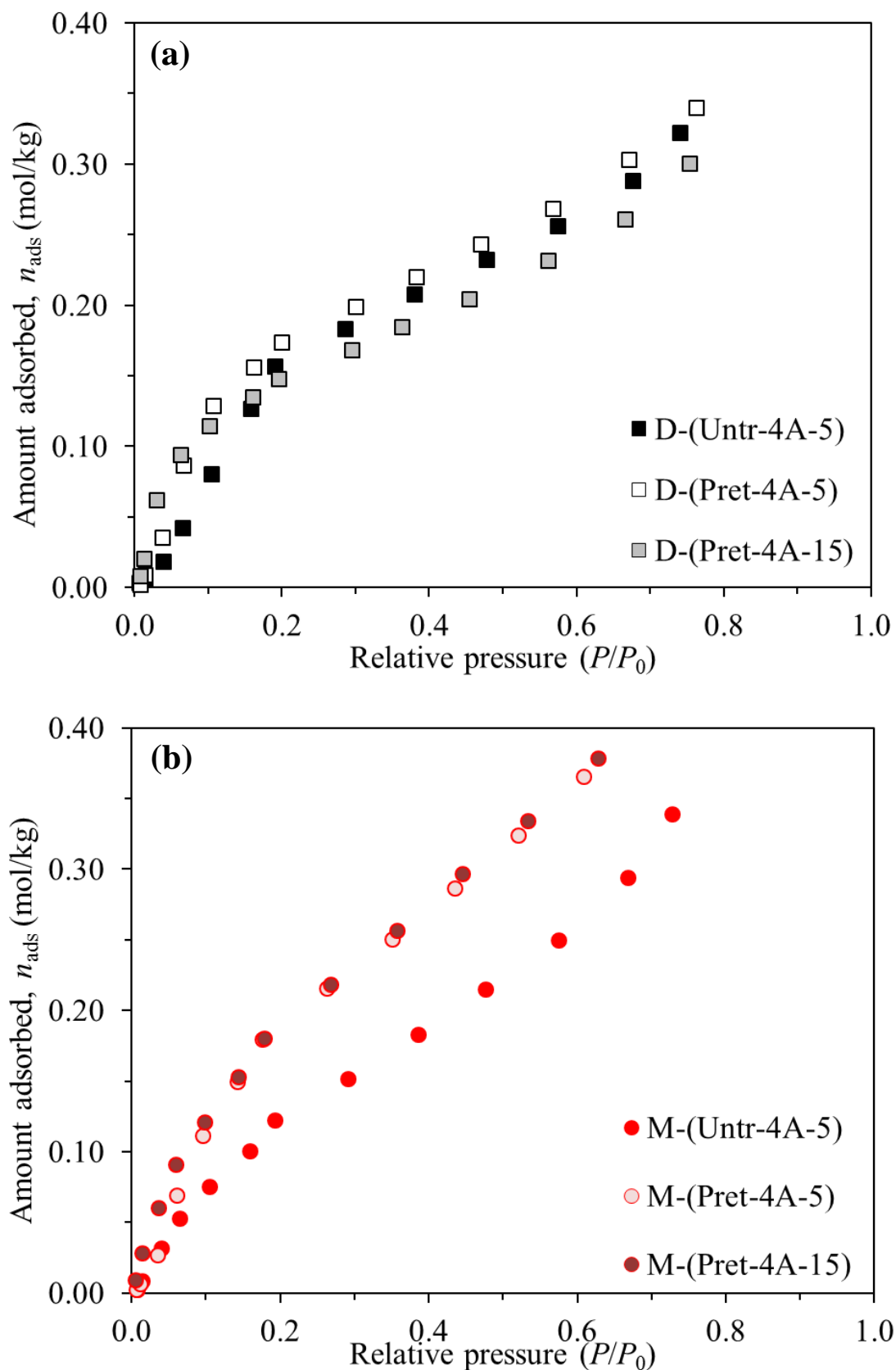


Fig. 6.1. Effect of longer vacuum and thermal pre-treatment with combined longer vacuum, thermal pre-treatment and extended equilibrium time for the pure component adsorption isotherms of a) DME and b) MeCl on Pret-4A

The thermal pre-treatment of the zeolite demonstrated substantially increased amounts adsorbed compared to 4A for the same equilibrium time (5 min). Whilst the extended equilibrium time for the thermally pre-treated isotherm resulted in a marginal increase in amount adsorbed. The substantial difference in isotherm shape and adsorption capacity for MeCl is essentially attributed to the effect of molecularly adsorbed surface and occluded moisture. Moisture played a huge role because its presence imparted a negative charge to the surface causing repulsive forces between moisture and polar adsorbate molecules resulting in limited sorption. It can be said that the thermal pre-treatment for the A-S interactions is imperative on the adsorbent, particularly in the case of MeCl. In the case of DME the effect of moisture was less because, water binds through hydrogen bonding and adsorption of DME on the zeolite is believed to be through DME, therefore adsorbs co-operatively.

The effect of longer vacuum and thermal pre-treatment and combined effect of longer vacuum and thermal pre-treatment with an extended equilibrium time for DME and MeCl on 5A is shown in Fig. 6.2. The thermal pre-treatment and longer equilibrium time resulted in an increase in adsorption capacities by 4.52 % and 6.69 % for DME and MeCl, respectively. As mentioned earlier the increased capacities are attributed to molecules being able to form a complete monolayer without the presence of steric crowding. Similar to Pret-4A the effect of longer vacuum, thermal pre-treatment and longer equilibrium had a greater impact for MeCl than with DME. The lesser impact of DME adsorption can be likened to comments earlier regarding co-operative DME adsorption with moisture whereas MeCl exhibits repulsive forces. Even though the adsorption capacities were slightly increased due to longer vacuum and thermal pre-treatment the effect of a longer equilibrium time was more pronounced. This is believed to be because the adsorbent is substantially more microporous with a greater surface area therefore more adsorption occurs subsequently requiring a longer equilibrium time; especially at low pressure where molecules do not have sufficient mobility to locate the strong adsorption sites i.e. take longer to locate. Compared to the results in section 5.3.1.1 for the as received isotherms, Fig. 6.2 demonstrates stronger evidence of Type I adsorption particularly at high pressure with evidence of plateau. The effect of a longer equilibrium time resulted in a shift left in the isotherms meaning more quantities were adsorbed at lower pressure meaning the adsorbent reached saturation quicker. Whilst the effect of thermal pre-treatment resulted in slightly increased adsorbed quantities at each pressure its impact is more likely to affect the kinetic rate of adsorption due to more sites being available for more and faster adsorption which is reported in the following sections.

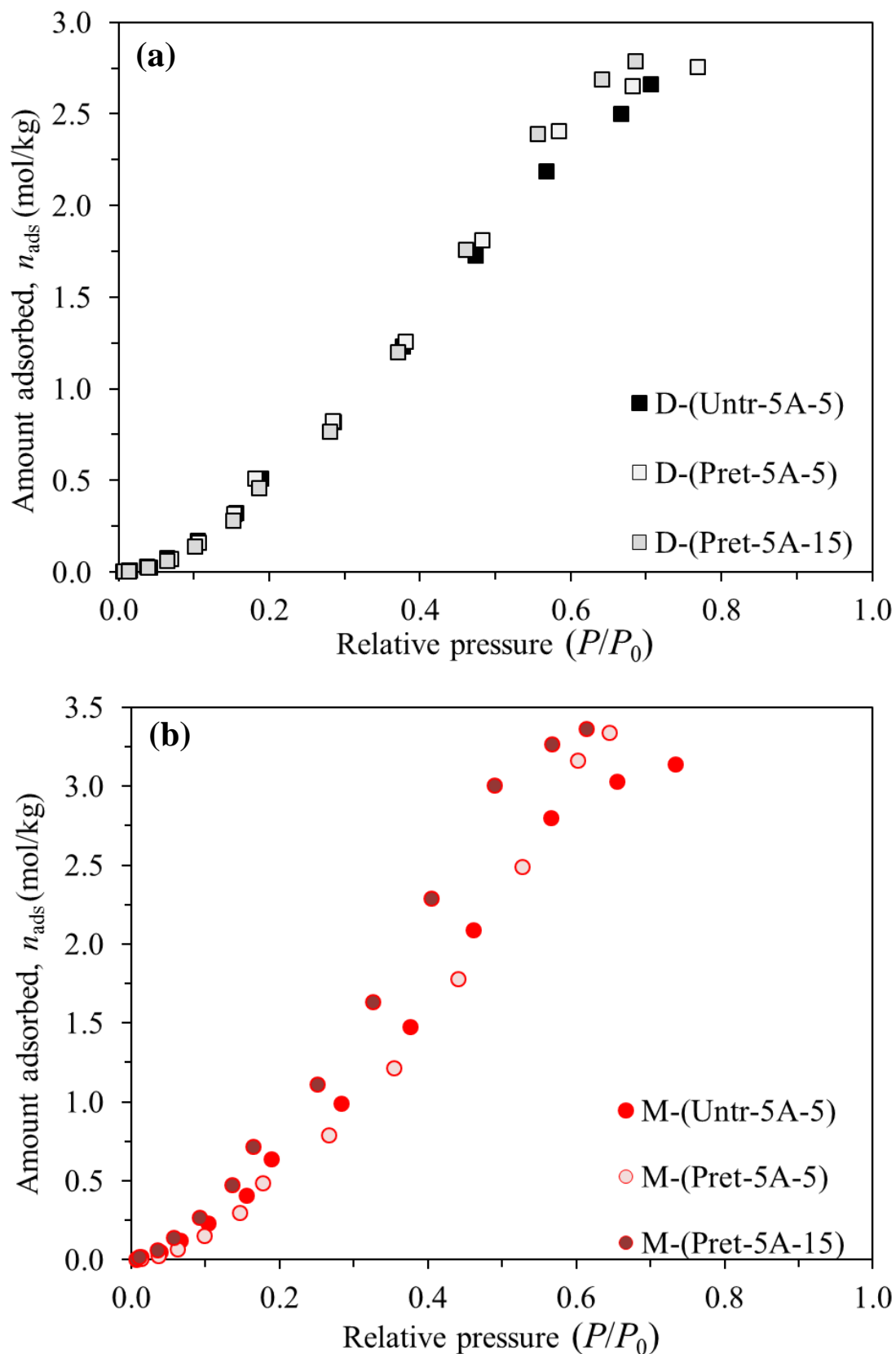


Fig. 6.2. Effect of longer vacuum and thermal pre-treatment with combined longer vacuum, thermal pre-treatment and extended equilibrium time for the pure component adsorption isotherms of a) DME and b) MeCl on Pret-5A

6.2.1.1 Pure component adsorption isotherms

Fig. 6.3 shows pure component adsorption isotherms for DME and MeCl on the vacuum and thermally pre-treated zeolites: Pret-4A and Pret-5A, respectively at constant room temperature (20 °C). Compared to the effects of vacuum and thermal pre-treatment and extended equilibrium time in the section above the pre-treated isotherms are compared in more detail for the respective 5 min and 15 min equilibrium time. As can be seen by the longer equilibrium time isotherms, with time more molecules were adsorbed. At low relative pressures on Pret-4A (< 0.1) DME exhibited a marginally larger adsorption capacity to MeCl suggesting a greater affinity to the strongest adsorption sites which is acknowledged to be because of the stronger base strength of O over Cl. For $P/P_0 = 0.1 - 0.7$, MeCl appears to exhibit a near linear increasing adsorption trend with more quantities adsorbed at each pressure than DME which exhibited slow increasing amounts adsorbed with pressure. For the conditions considered it is believed that adsorption of DME on the clean zeolite surface occurs mainly at the external surface adsorption sites whilst partially penetrating into the larger external pores (depending upon the molecules orientation) with the likelihood of partially blocking the pores. On the other hand, MeCl penetrates into the pores and adsorbs at the strongest adsorption sites then proceeds. Since the surface has no impurities it is able to adsorb naturally through its negatively charged Cl atom but at a slower rate than DME due to its weaker base strength.

Fig. 6.3b shows the results for adsorption of DME versus MeCl on Pre-5A for the different equilibrium times. As can be seen even with an extended equilibrium time it is not sufficient especially at low pressure (< 0.1) shown by concave shape before linearity to plateau. At low pressure molecules take longer to locate adsorption sites due insufficient mobility as mentioned earlier. In terms of the pore size, the 5A adsorbent has pore openings within the acceptable range for both DME and MeCl molecules, respectively thus showing relatively similar amounts adsorbed especially at low pressure. With the extended equilibrium time the plateau point shifts to lower pressures as expected. The greater amount of MeCl adsorbed can be attributed to either physically adsorbed multilayers due to VDW's forces and or adsorption onto different adsorption sites; which does not appear to occur with DME.

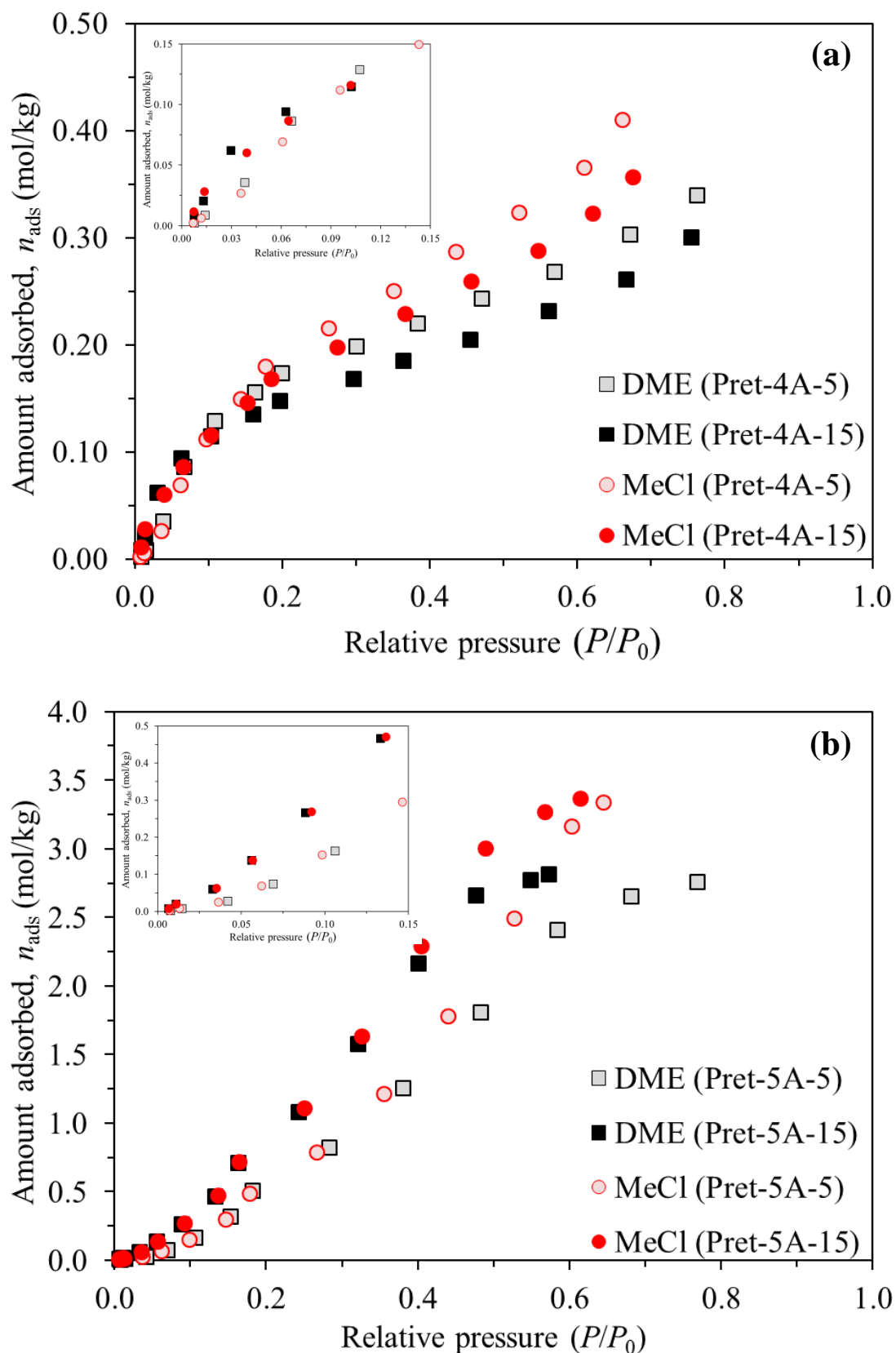


Fig. 6.3. Pure component adsorption isotherms for DME and MeCl at 20 °C for 5 min versus 15 min equilibrium time on a) Pret-4A and b) Pret-5A

6.2.1.2 Pure component empirical adsorption models

Fig. 6.4 shows Langmuir, Freundlich, Sips and Tóth empirical adsorption models applied to DME and MeCl adsorption on zeolites 4A and 5A, respectively in terms of pressure (see section 2.5 for overall model equations). As discussed with the respective DME and MeCl isotherms on 4A and 5A the isotherm exhibited much definitive trends following thermal pre-treatment in vacuum with an extended equilibrium time. For the respective A-S interactions DME adsorbs according to a Type II classification whereas MeCl exhibits a Type I classification on Pret-4A. Both DME and MeCl adsorption isotherms on Pret-5A clearly exhibited Type I behaviour although there was still evidence of a low solid-gas affinity at low pressure, but this is due to reasons mentioned earlier. Compared to the isotherms obtained for the same adsorbates on the 1 h vacuum pre-treated zeolites (Fig. 5.5 and Fig. 5.6) the isotherm shapes were more definitive and conclusive in terms of determining the classification.

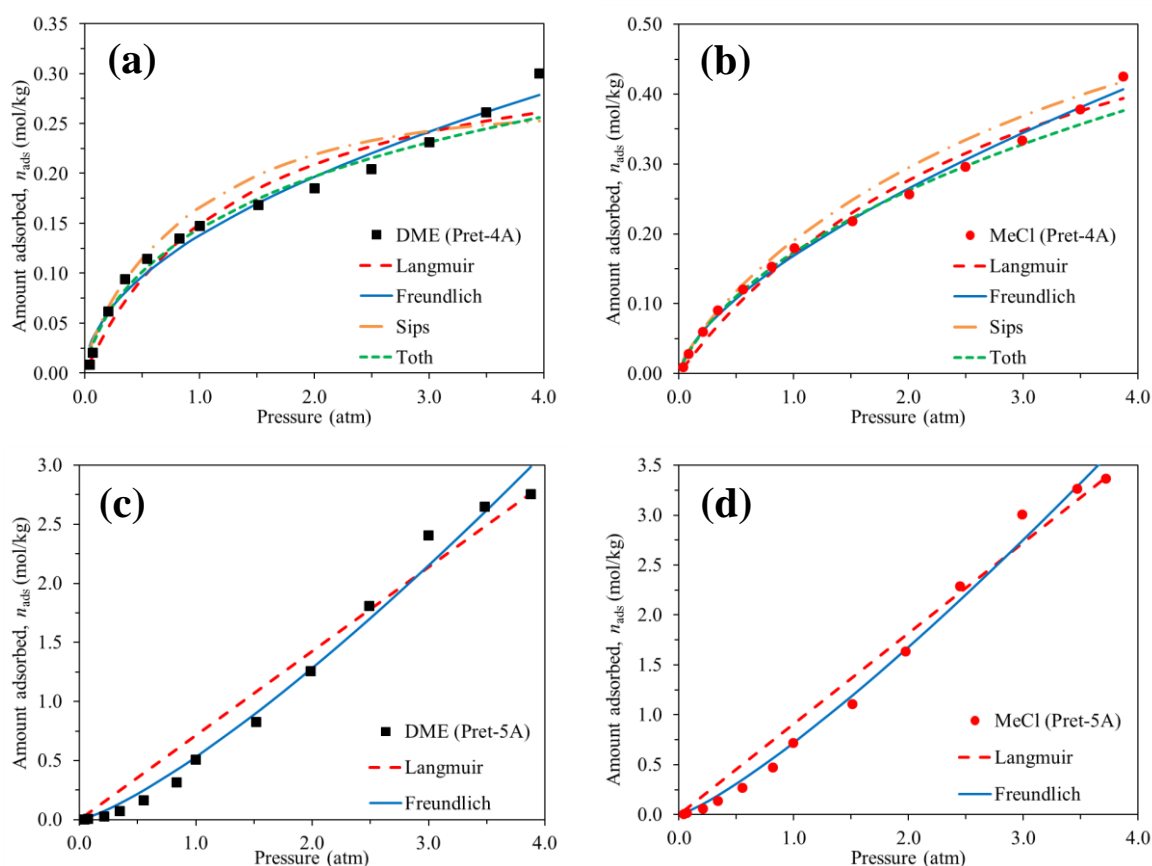


Fig. 6.4. Pure component empirical adsorption models at 20 °C for a) DME on Pret-4A; b) MeCl on Pret-4A; c) DME on Pret-5A and MeCl on Pret-5A

Table 6.1 shows the fitting parameters for DME and MeCl adsorption on Pret-4A to the Langmuir, Freundlich, Sips and Tóth fitting models and Fig. 6.4 shows the corresponding fitting curves for the longer time equilibrium data. Like the adsorption on 4A both the DME and MeCl experimental data was fitted to all four empirical adsorption models on Pret-4A following a 15 min equilibrium time. All models fitted relatively well to the data with high R^2 values (> 0.990). The Sips and Tóth

models appear to fit well but gave high n_s values suggesting an over exaggeration of the value. According to the Langmuir rate constant, DME has a value over double to that of MeCl, suggesting a faster rate. The Freundlich model resulted in the best fitting chiefly due to its moderate pressure applicability. According to the model the adsorbent has a greater heterogeneity for DME than MeCl with values of 1.96 and 1.54, respectively whilst MeCl adsorption has a larger rate constant. As can be seen by R^2 values DME did not fit as precisely to the data as MeCl because of the Type II classification. Its behaviour is not applicable for the models which generally apply to Type I isotherms. Nevertheless the models can still be used to compare with the MeCl data. Due to the poor low pressure adsorption behaviour for DME and MeCl on Pret-5A, this resulted in poor fitting parameters for the Langmuir model which resulted in an extremely exaggerated value of n_s . Similarly the Sips and Tóth models were not applicable due to the data at both pressure limits. On comparison of the two gases to the Freundlich model on Pret-5A; MeCl has a larger rate constant and greater heterogeneity for the system.

Table 6.1. Empirical fitting parameters for pure component DME and MeCl adsorption isotherms on Pret-4A and Pret-5A

Parameters		Pret-4A		Pret-5A	
		DME	MeCl	DME	MeCl
Langmuir	b	0.741	0.311	5.84×10^{-4}	7.86×10^{-4}
	n_s	0.350	0.721	1222.18	1158.11
	R^2	0.990	0.996	0.984	0.990
Freundlich	K	0.138	0.169	0.530	0.721
	t	1.959	1.538	0.784	0.820
	R^2	0.994	0.999	0.994	0.994
Sips	b	0.265	0.096	-	-
	n_s	0.523	1.152	-	-
	c	1.466	1.352	-	-
	R^2	0.996	0.999	-	-
Tóth	b	1.299	0.187	-	-
	n_s	0.852	4.783	-	-
	c	0.365	0.292	-	-
	R^2	0.996	0.999	-	-

6.2.1.3 Pure component adsorption kinetics

Table 6.2 and Table 6.3 show the fitting parameters for the pseudo first order, pseudo second order, Elovich and IPD kinetic models (see section 2.6 for the respective model equations) when applied to DME and MeCl adsorption on vacuum and thermally pre-treated zeolites 4A and 5A, defined as Pret-4A-5 and Pret5A-5, respectively with the 5 min equilibrium time. Table 6.4 and Table 6.5 show the same data but following the 15 min equilibrium time, Pret-4A-15 and Pret5A-15, respectively. Compared to the earlier as received zeolites subjected to 1 h vacuum pre-treatment it can be seen the rate constants are much more consistent especially MeCl at different pressures for the entire range suggesting more simple kinetics. On the Pret-4A-15 both DME and MeCl exhibited pseudo second order kinetics indicative of rapid adsorption due to the limited adsorption sites available for both adsorbates. Over the entire isotherm measurements, DME exhibited a rate constant nearly double that of MeCl suggesting a faster rate of adsorption at any given pressure in the range (0.0 - 4.0 atm). Compared to the shorter equilibrium time it is clear that if the equilibrium is not reached this can lead to a mis-interpretation of the kinetic order at a particular pressure and potential failure when designing a sorption system. This was particularly depicted by the trends shown by the rate constant values and the near perfect R^2 values for Pret-4A-15 compared to Pret-4A-5.

As shown by Table 6.5 both gases exhibited pseudo first order kinetics for adsorption on Pret-5A-15 for the pressure range 0.0 - 2.5 atm then pseudo second order kinetic from 3.0 - 3.5 atm. The second order behaviour is suspected to be due to the adsorbent reaching saturation therefore the concentration of the bulk gas phase was comparable to the fractional uptake divided by the coverage at equilibrium. Compared to the as received zeolites the kinetic rate constants for both gases after vacuum and thermal pre-treatment and longer equilibrium time were effectively halved with more definitive increasing trends for the rate constant value with pressure. Similarly the data Pret-5A-5 resulted in marginally lesser rate constant values for pseudo first order kinetics meaning the effect of impurities was small and as expected following a longer equilibrium time the rate constant was smaller. Following thermal pre-treatment in the shorter equilibrium time both gases exhibited high R^2 values for the IPD model thus suggesting both adsorbates undergo some IPD especially when the adsorption at each pressure was relatively incomplete compared to the longer equilibrium time isotherms. In both cases over the entire isotherm, adsorption preceded at a steady rate then as the adsorbent reaches saturation the adsorption kinetic order changes. The change in kinetic order could be a result of cumulative adsorption from the isotherm measurement and not adsorption at that pressure (high) on a fresh adsorbent; on a fresh adsorbent at high pressure adsorption would be so rapid due to molecules having more than adequate energy and mobility to adsorb on all adsorption sites simultaneously.

Table 6.2. Adsorption kinetic model parameters for pure component DME and MeCl on Pret-4A-5

<u>DME on Pret-4A-5</u>										
Adsorption pressure <i>atm</i>	<u>Pseudo first order</u>		<u>Pseudo second order</u>		<u>Elovich</u>			<u>IPD</u>		
	k'_{ads} (s ⁻¹)	R^2	k''_{ads} (mol kg ⁻¹ s ⁻¹)	R^2	α (mol kg ⁻¹ min ⁻¹)	β (kg mol ⁻¹)	R^2	k_{IPD} (mol kg ⁻¹ -mol ^{-1/2})	C_{IPD} (constant)	R^2
0.5	0.026	0.961	0.198	0.951	0.106	28.46	0.726	0.044	0.002	<u>0.978</u>
1.0	0.027	0.839	0.897	<u>0.991</u>	0.199	48.35	0.388	0.033	0.017	0.830
1.5	0.030	0.796	0.993	<u>0.996</u>	0.441	39.30	0.289	0.044	0.030	0.758
2.0	0.093	0.985	1.172	<u>0.997</u>	0.633	41.21	0.237	0.045	0.034	0.713
2.5	0.052	0.936	1.319	<u>0.999</u>	0.792	35.84	0.228	0.053	0.041	0.701
3.0	0.043	0.749	1.352	<u>0.991</u>	0.596	20.59	0.344	0.081	0.045	0.827
3.5	0.044	0.633	1.423	<u>0.999</u>	1.471	34.80	0.177	0.059	0.053	0.652
<u>MeCl on Pret-4A-5</u>										
Adsorption pressure <i>atm</i>	<u>Pseudo first order</u>		<u>Pseudo second order</u>		<u>Elovich</u>			<u>IPD</u>		
	k'_{ads} (s ⁻¹)	R^2	k''_{ads} (mol kg ⁻¹ s ⁻¹)	R^2	α (mol kg ⁻¹ min ⁻¹)	β (kg mol ⁻¹)	R^2	k_{IPD} (mol kg ⁻¹ -mol ^{-1/2})	C_{IPD} (constant)	R^2
0.5	0.022	0.993	0.198	0.950	0.104	29.51	0.725	0.043	0.002	<u>0.988</u>
1.0	0.023	0.800	0.700	<u>0.991</u>	0.172	41.78	0.455	0.036	0.015	0.868
1.5	0.035	0.905	0.234	<u>0.997</u>	0.133	29.20	0.702	0.030	0.030	0.823
2.0	0.034	0.844	0.303	<u>0.998</u>	0.179	28.83	0.619	0.031	0.039	0.757
2.5	0.100	0.985	0.604	<u>0.998</u>	0.252	34.44	0.483	0.027	0.045	0.639
3.0	0.024	0.679	0.447	<u>0.998</u>	0.277	28.33	0.508	0.033	0.052	0.664
3.5	0.031	0.789	0.315	<u>0.991</u>	0.596	20.59	0.344	0.081	0.045	0.827

^a R^2 values which are bold and underlined show that, that particular model is most applicable for the data analysis at that respective pressure/condition.

Table 6.3. Adsorption kinetic model parameters for pure component DME and MeCl on Pret-5A-5

<u>DME on Pret-5A-5</u>										
Adsorption pressure <i>atm</i>	<u>Pseudo first order</u>		<u>Pseudo second order</u>		<u>Elovich</u>			<u>IPD</u>		
	k'_{ads} (s ⁻¹)	R^2	k''_{ads} (mol kg ⁻¹ s ⁻¹)	R^2	α (mol kg ⁻¹ min ⁻¹)	β (kg mol ⁻¹)	R^2	k_{IPD} (mol kg ⁻¹ -mol ^{-1/2})	C_{IPD} (constant)	R^2
0.5	0.024	0.951	0.062	0.798	0.104	20.55	0.840	0.057	-0.008	<u>0.982</u>
1.0	0.020	0.991	0.047	0.902	0.255	10.01	0.786	0.121	-0.005	<u>0.997</u>
1.5	0.023	<u>0.995</u>	0.026	0.895	0.417	5.89	0.801	0.204	-0.012	0.993
2.0	0.024	<u>0.993</u>	0.020	0.909	0.603	4.22	0.791	0.286	-0.012	0.993
2.5	0.026	<u>0.992</u>	0.017	0.913	0.774	3.32	0.787	0.364	-0.012	0.991
3.0	0.025	<u>0.990</u>	0.018	0.951	1.149	2.60	0.731	0.477	0.026	0.973
3.5	0.033	0.939	0.085	<u>0.992</u>	1.156	5.21	0.500	0.275	0.100	0.883
<u>MeCl on Pret-5A-5</u>										
Adsorption pressure <i>atm</i>	<u>Pseudo first order</u>		<u>Pseudo second order</u>		<u>Elovich</u>			<u>IPD</u>		
	k'_{ads} (s ⁻¹)	R^2	k''_{ads} (mol kg ⁻¹ s ⁻¹)	R^2	α (mol kg ⁻¹ min ⁻¹)	β (kg mol ⁻¹)	R^2	k_{IPD} (mol kg ⁻¹ -mol ^{-1/2})	C_{IPD} (constant)	R^2
0.5	0.022	0.979	0.054	0.787	0.111	18.83	0.844	0.062	-0.010	<u>0.980</u>
1.0	0.022	<u>0.997</u>	0.045	0.900	0.257	9.76	0.794	0.124	-0.006	0.995
1.5	0.026	0.982	0.012	0.921	0.190	7.37	0.958	0.112	-0.004	<u>0.996</u>
2.0	0.025	0.987	0.008	0.927	0.274	5.19	0.958	0.160	-0.003	<u>0.995</u>
2.5	0.025	0.990	0.007	0.932	0.362	4.04	0.952	0.205	0.002	<u>0.996</u>
3.0	0.025	0.990	0.006	0.937	0.457	3.26	0.952	0.255	0.007	<u>0.996</u>
3.5	0.037	<u>0.986</u>	0.018	0.951	1.149	2.60	0.731	0.477	0.026	0.973

^a R^2 values which are bold and underlined show that, that particular model is most applicable for the data analysis at that respective pressure/condition.

Table 6.4. Adsorption kinetic model parameters for pure component DME and MeCl on Pret-4A-15

<u>DME on Pret-4A-15</u>										
Adsorption pressure <i>atm</i>	<u>Pseudo first order</u>		<u>Pseudo second order</u>		<u>Elovich</u>			<u>IPD</u>		
	k'_{ads} (s ⁻¹)	R^2	k''_{ads} (mol kg ⁻¹ s ⁻¹)	R^2	α (mol kg ⁻¹ min ⁻¹)	β (kg mol ⁻¹)	R^2	k_{IPD} (mol kg ⁻¹ -mol ^{-1/2})	C_{IPD} (constant)	R^2
0.5	0.008	0.639	0.565	<u>0.992</u>	0.092	59.533	0.593	0.0152	0.020	0.731
1.0	0.025	0.977	0.807	<u>0.999</u>	0.110	54.367	0.577	0.0167	0.023	0.721
1.5	0.018	0.897	0.783	<u>0.999</u>	0.231	41.080	0.464	0.0231	0.039	0.631
2.0	0.013	0.496	0.819	<u>0.999</u>	0.313	37.606	0.419	0.0256	0.048	0.590
2.5	0.014	0.595	0.646	<u>0.999</u>	0.288	35.493	0.448	0.0269	0.047	0.619
3.0	0.015	0.656	0.599	<u>0.999</u>	0.311	30.275	0.467	0.0312	0.053	0.631
3.5	0.027	0.646	0.784	<u>1.000</u>	0.403	26.011	0.443	0.0365	0.066	0.606
<u>MeCl on Pret-4A-15</u>										
Adsorption pressure <i>atm</i>	<u>Pseudo first order</u>		<u>Pseudo second order</u>		<u>Elovich</u>			<u>IPD</u>		
	k'_{ads} (s ⁻¹)	R^2	k''_{ads} (mol kg ⁻¹ s ⁻¹)	R^2	α (mol kg ⁻¹ min ⁻¹)	β (kg mol ⁻¹)	R^2	k_{IPD} (mol kg ⁻¹ -mol ^{-1/2})	C_{IPD} (constant)	R^2
0.5	0.0111	0.9093	0.390	<u>0.997</u>	0.083	46.544	0.699	0.019	0.019	0.808
1.0	0.0061	0.6588	0.454	<u>0.994</u>	0.125	48.519	0.570	0.019	0.026	0.721
1.5	0.0076	0.5531	0.348	<u>0.996</u>	0.249	34.132	0.487	0.028	0.044	0.660
2.0	0.0052	0.4881	0.376	<u>0.994</u>	0.321	32.498	0.441	0.030	0.052	0.618
2.5	0.0063	0.5606	0.428	<u>0.997</u>	0.352	29.335	0.446	0.033	0.057	0.617
3.0	0.0070	0.6088	0.426	<u>0.998</u>	0.385	27.726	0.439	0.035	0.062	0.611
3.5	0.0076	0.6604	0.350	<u>0.998</u>	0.354	25.435	0.475	0.037	0.062	0.645

^a R^2 values which are bold and underlined show that, that particular model is most applicable for the data analysis at that respective pressure/condition.

Table 6.5. Adsorption kinetic model parameters for pure component DME and MeCl on Pret-5A-15

<u>DME on Pret-5A-15</u>										
Adsorption pressure <i>atm</i>	<u>Pseudo first order</u>		<u>Pseudo second order</u>		<u>Elovich</u>			<u>IPD</u>		
	k'_{ads} (s ⁻¹)	R^2	k''_{ads} (mol kg ⁻¹ s ⁻¹)	R^2	α (mol kg ⁻¹ min ⁻¹)	β (kg mol ⁻¹)	R^2	k_{IPD} (mol kg ⁻¹ -mol ^{-1/2})	C_{IPD} (constant)	R^2
0.5	0.010	<u>0.994</u>	0.040	0.967	0.098	16.310	0.949	0.0505	0.007	0.974
1.0	0.012	<u>0.990</u>	0.028	0.980	0.202	8.848	0.925	0.0934	0.025	0.957
1.5	0.012	<u>0.995</u>	0.024	0.987	0.339	5.975	0.892	0.1392	0.055	0.935
2.0	0.014	<u>0.997</u>	0.022	0.991	0.480	4.572	0.868	0.1825	0.089	0.915
2.5	0.015	<u>0.996</u>	0.023	0.993	0.625	3.849	0.835	0.2172	0.128	0.884
3.0	0.015	0.940	0.046	<u>0.998</u>	0.770	4.486	0.721	0.1909	0.181	0.801
3.5	0.017	0.833	0.289	<u>1.000</u>	0.951	11.468	0.435	0.0831	0.152	0.599
<u>MeCl on Pret-5A-15</u>										
Adsorption pressure <i>atm</i>	<u>Pseudo first order</u>		<u>Pseudo second order</u>		<u>Elovich</u>			<u>IPD</u>		
	k'_{ads} (s ⁻¹)	R^2	k''_{ads} (mol kg ⁻¹ s ⁻¹)	R^2	α (mol kg ⁻¹ min ⁻¹)	β (kg mol ⁻¹)	R^2	k_{IPD} (mol kg ⁻¹ -mol ^{-1/2})	C_{IPD} (constant)	R^2
0.5	0.010	<u>0.975</u>	0.034	0.957	0.094	16.231	0.961	0.051	0.004	0.980
1.0	0.010	<u>0.998</u>	0.025	0.976	0.199	8.753	0.933	0.095	0.021	0.969
1.5	0.011	<u>0.991</u>	0.019	0.982	0.323	5.736	0.918	0.144	0.043	0.954
2.0	0.012	<u>0.994</u>	0.017	0.988	0.479	4.290	0.890	0.194	0.079	0.938
2.5	0.013	<u>0.993</u>	0.014	0.989	0.612	3.405	0.884	0.244	0.105	0.926
3.0	0.016	0.992	0.019	<u>0.994</u>	0.789	3.118	0.826	0.268	0.165	0.876
3.5	0.016	0.692	0.186	<u>1.000</u>	1.081	6.864	0.517	0.133	0.211	0.654

^a R^2 values which are bold and underlined show that, that particular model is most applicable for the data analysis at that respective pressure/condition.

Although the IPD model did not apply for Pre-4A it was important to analyse the mechanisms in more detail to observe for any surface layering resistance and or give more kinetic information. Fig. 6.5 shows the plots for the IPD versus surface resistance controlled adsorption mechanisms for pure component DME and MeCl on Pret-4A-15 from the adsorption isotherm data at 2.0 atm and 3.0 atm, respectively. As can be seen from the data the rate of adsorption of both gases is relatively rapid at a similar rate (rate in declining slope) shown by the longer time scale.

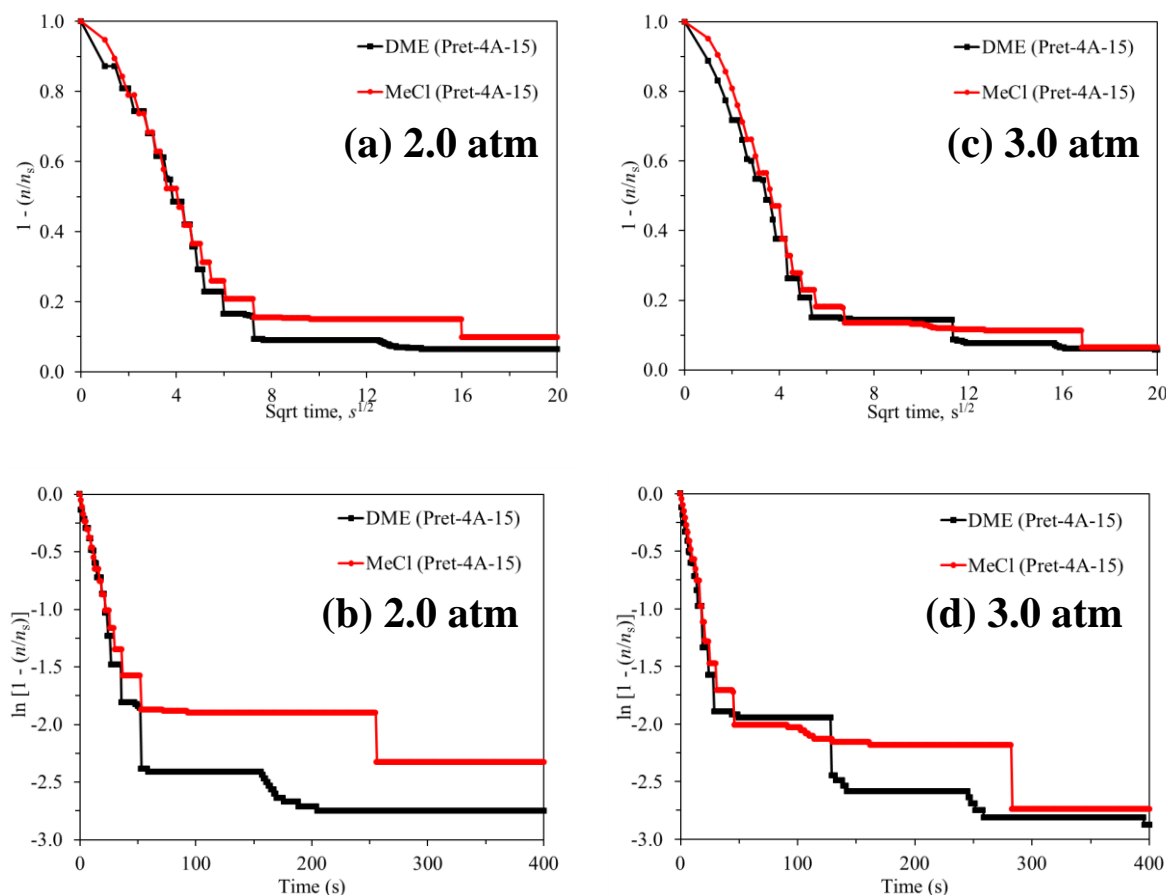


Fig. 6.5. Pure component adsorption mechanism for DME and MeCl on Pret-4A-15 where a) and c) represents IPD controlled adsorption in a short time scale and b) and d) represents surface resistance layering in a long time scale

When compared to the Pret-5A data shown by Fig. 6.6, rapid adsorption occurred within 60 s whereas adsorption on the microporous 5A adsorbent took much longer due to the presence of more adsorption sites. The data on Pret-4A demonstrated poorer sensitivity in results due to limited adsorption sites, meaning the effect of adsorption was less fluid compared to Pret-5A where molecules continued to locate adsorption sites. In terms of adsorption on Pret-4A at both pressures it appears that both gases show greater linearity for the longer time scale from 0-40 s and 0-30 s where rapid adsorption occurred for DME and MeCl at 2.0 atm and 3.0 atm, respectively. Thereafter molecules required more energy to locate lesser adsorption sites. For the conditions considered especially the low surface area adsorbent it is believed that a more sensitive

pressure detector is required in order to obtain more steady dropping pressure readings. In terms of rate of decline on Pret-4A both gases appear to be declining at a similar rate with negligible visual evidence suggesting DME adsorbs marginally faster. For the conditions considered on Pret-5A, DME appears to adsorb slightly faster due to reasons mentioned earlier. At 2.0 atm both gases showed more linearity towards the longer time scale indicative of surface layering resistance which occurred in two stages from 0 - 100 s then from 100 - 400 s. In terms of the shorter time scale both gases exhibited similar trends; slow from 0 - 3 s^{1/2} then steady decrease up to 15 s^{1/2}. At 3.0 atm no linearity was shown in the short time scale suggesting no IPD which makes sense since typically pore adsorption occurs at low pressure and the IPD did not typically apply for the pressure. In the longer time scale both gases demonstrated evidence of surface layering resistance due to competing adsorption between molecules for the remaining adsorption sites and the adsorbent reaching its saturation capacity.

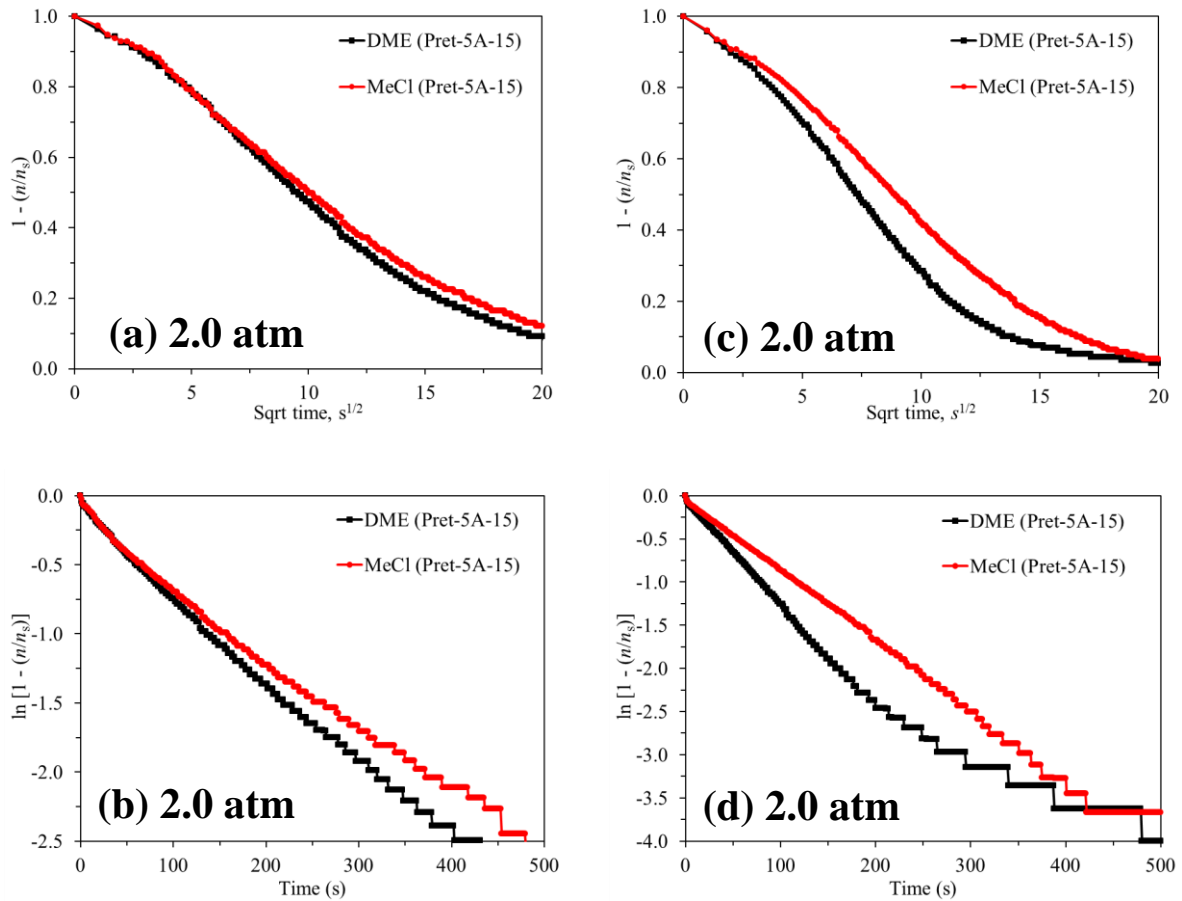


Fig. 6.6. Adsorption mechanism for pure component DME and MeCl on Pret-5A-15 where a) and c) represents IPD controlled adsorption in a short time scale and b) and d) represents surface resistance layering in a long time scale

6.2.1.4 Pure component differential heat of adsorption

Fig. 6.7a and c compares the differential heat of adsorption for pure component DME and MeCl on Pret-4A and Pret-5A, respectively in terms of amount adsorbed. As it can be seen both gases exhibited relatively constant heat values for their respective isotherms with DME exhibiting two heat spikes. The initial differential heats were 23.30 and 10.21 kJ mol⁻¹ for DME and MeCl, respectively on Pret-4A. With increasing coverage DME exhibited evidence of adsorption onto different sites with heat drops at 0.06 and 0.19 mol kg⁻¹. For increasing coverage the differential heats released were in the range 26.98 - 16.55 kJ mol⁻¹. Similar to the published work earlier [114], the heat of adsorption is in the range to that for the heat of condensation of DME (21.50 kJ mol⁻¹) indicative of physisorption binding energy arising from weak VDW's forces between the A-S [114, 120].

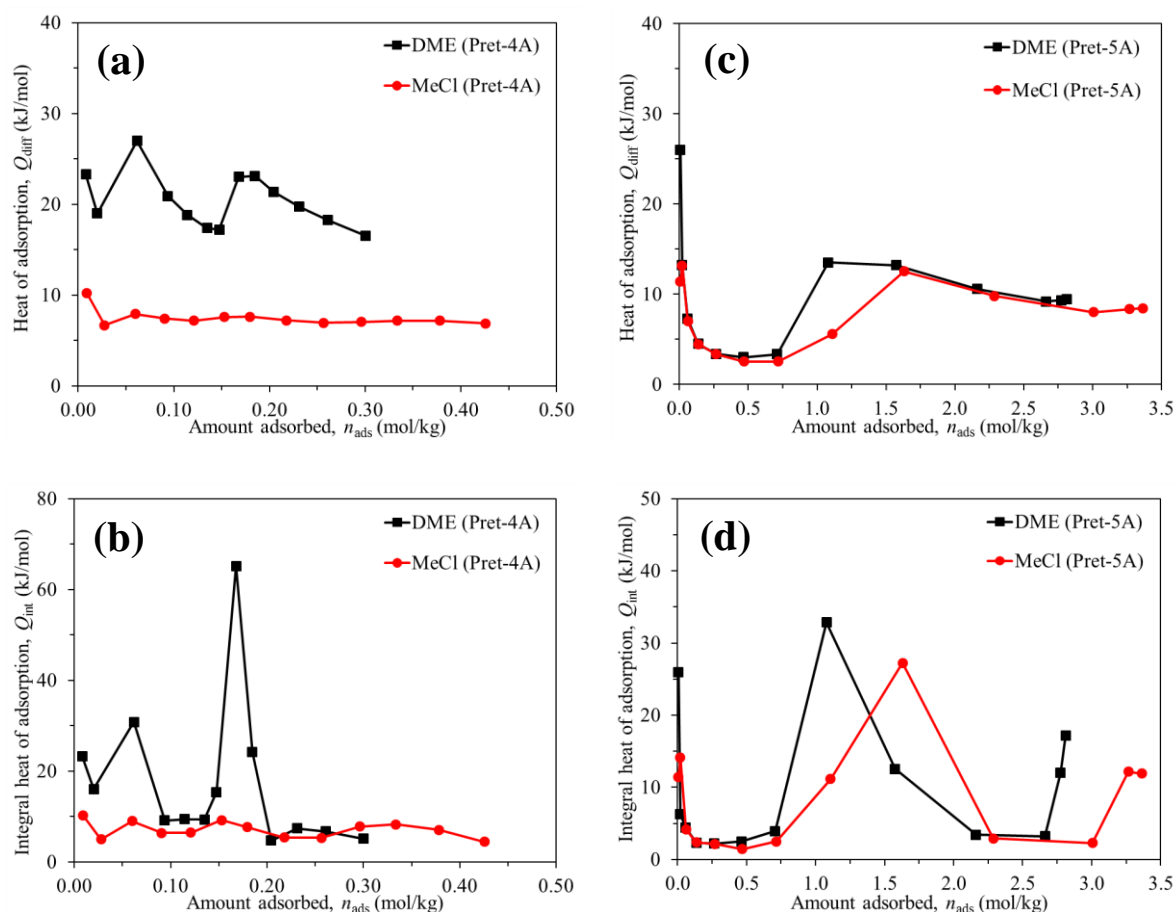


Fig. 6.7. Heat of adsorption for DME and MeCl where a) and c) represents differential heats and b) and d) represent integral heats for Pre-4A and Pret-5A

Apart from the initial heat value, MeCl exhibited differential heats of adsorption in the range of 7.94 - 6.68 kJ mol⁻¹ suggesting extremely weak adsorptive behaviour for increasing coverage. In both cases the adsorption compared to untreated resulted in more homogenous adsorption behaviour with relatively constant heats being released due to the removal of impurities and

molecules reaching their true equilibrium position under the respective conditions. With DME on Pret-4A there were two definitive heat drops indicative of adsorption at different sites. On the other hand the heat drop values for MeCl were too close to acquire definitive conclusions regarding the adsorption sites except for that the adsorption is extremely weak and homogenous. In addition, Fig. 6.7b shows supporting integral heat of adsorption which suggests DME exhibits stronger A-A interactions than A-S interactions with increasing coverage.

In terms of Pre-5A, Fig. 6.7b and Fig. 6.7d shows the differential and integral heats of adsorption for pure component DME and MeCl. Unlike Pret-4A both gases exhibited very similar trends with evidence of initial A-S interactions with differential heat values of 25.96 and 13.17 kJ mol⁻¹ for DME and MeCl, respectively. With increasing coverage both gases exhibited evidence of A-A interactions ~ 1.0 - 1.75 mol kg⁻¹ for DME and MeCl, respectively. Similarly, the integral heat plots showed similar trends with DME exhibiting higher A-A interactions than MeCl at a lower coverage. On comparison to Pret-4A, again MeCl exhibited a very low heat of adsorption with values suggesting a much weaker mode of interaction compared to DME; the latter again indicative of values close to that for its heat of condensation. Of the zeolites, Pret-5A clearly demonstrated evidence of greater heterogeneity which is no surprise considering its substantially larger surface area. For the conditions considered the impact of the ether group has a greater heat release compared to the Cl with both adsorbent surfaces. From the collective data it is evident DME exhibited the stronger mode of interaction due to hydrogen bonding as postulated and reported earlier. On the other hand MeCl adsorbs via weak interactions most likely dipole-dipole interactions. Although the latter is reported earlier to be significantly less in terms of magnitude of strength this has not been reflected in the values obtained. It is believed that similar to the sensitivity of the pressure gauge for results obtained using zeolite 4A it would be more accurate to have a more sensitive temperature control and recorder but more so due to more accurate methods to measure the heat losses in and around the system. It is worth noting that the Pret-4A-5 and Pret-5A-5 differential and integral data resulted in larger heat value due to the equilibrium position thus affecting the value, Q from the heat balance.

6.3 Summary

The following summarises the overall findings for the chapter for pure component adsorption of DME and MeCl on vacuum and thermally pre-treated adsorbents (zeolites 4A and 5A) and combined vacuum and thermally pre-treated adsorbents with an extended equilibrium time:

- The effect of thermal pre-treatment in vacuum (150 °C for 15 h) and extended equilibrium time (5 to 15 min) resulted in increased adsorption capacities by 1.95 % and 20.37 % for DME and MeCl, respectively on Pret-4A compared to adsorption on 4A. Similarly, the adsorption capacities on Pret-5A increased by 4.52 % and 6.69 % for DME and MeCl, respectively.
- The effect of moisture made little difference to the DME isotherm but significant impact to the MeCl plot on 4A because moisture imparted a negative charge to the surface causing repulsive forces between moisture and polar adsorbate molecules resulting in limited sorption whereas DME was less effected since moisture and DME both bind through hydrogen bonding therefore probably adsorb co-operatively.
- On Pret-4A, DME and MeCl adsorbed according to a Type II and Type I classification, respectively which was the same classification for the as received adsorbents subjected to 1 h vacuum pre-treatment.
- According to the Freundlich model on Pret-4A the adsorbent has a greater heterogeneity for DME than MeCl with values of 1.96 and 1.54, respectively whilst MeCl adsorption has a larger rate constant (0.17 compared to 0.14).
- On Pret-5A both gases adsorbed via a Type I classification. In terms of the Freundlich model MeCl had a larger rate constant (0.72 compared to 0.53) and marginally greater heterogeneity (0.82 compared to 0.78).
- Compared to the as received zeolites the kinetic rate constants for both gases after thermal pre-treatment and longer equilibrium time (Pret-) were effectively halved with more definitive increasing trends for the rate constants due to the respective equilibrium position of the respective A-S interactions.
- On the Pret-4A both DME and MeCl exhibited pseudo second order adsorption kinetics. With DME exhibiting a rate constant nearly double that of MeCl thus suggesting a faster rate of adsorption at any given pressure in the 0-3.5 atm range.
- On Pret-5A both gases exhibited pseudo first order adsorption kinetics from 0.0-2.5 atm then pseudo second order adsorption kinetics from 3.0-3.5 atm due to the adsorbent reaching saturation.
- On Pret-4A, at 2.0 and 3.0 atm both gases demonstrated linearity for the longer time scale indicative of surface resistance a consequent of limited adsorption sites. Both gases

fractional uptake trends declined at a similar rate with negligible visual evidence suggesting DME adsorbs marginally faster.

- On Pret-5A, DME appears to adsorb slightly faster with both gases exhibiting a greater linearity for the longer time scale (surface resistance).
- On Pret-4A DME exhibited a higher initial differential heat of adsorption ($23.30 \text{ kJ mol}^{-1}$) than MeCl ($10.21 \text{ kJ mol}^{-1}$). With increasing coverage DME demonstrated two heat spikes whereas MeCl values remained constant $< 10.0 \text{ kJ mol}^{-1}$. DME adsorbed heterogeneously whilst MeCl adsorbed homogeneously.
- On Pret-5A, DME exhibited a higher initial differential heat of adsorption ($25.96 \text{ kJ mol}^{-1}$) than MeCl ($13.17 \text{ kJ mol}^{-1}$). With increasing coverage both gases demonstrated evidence of A-A interactions.

CHAPTER VII: BINARY ADSORPTION OF MECL: DME MIXTURES ON DIFFERENT ADSORBENTS

7.1 Binary gas adsorption literature

For an effective application of adsorptive separation the process fundamentally depends on suitable developments of adsorption cycles and accurate equilibrium data. Both single and multicomponent data over a wide range of temperature and pressure are necessary for design. Since the collection of experimental data can be tedious and time consuming predictions using thermodynamic models is preferable, particularly single component data to predict multicomponent behaviour. Bakhtyari and Mofarahi [124] caution that the predicted binary model from pure component data should be checked against at least one set of multicomponent experimental data for reliability and accuracy. It is widely reported that it is possible to separate mixtures by fundamentally understanding the behaviour between molecules and the surface. Thereafter molecular simulations can provide a useful insight into molecular behaviour within the system which is unavailable from experiments alone [125].

Binary gas adsorption involves three degree of freedom: pressure, temperature and compositions [126]. The amount of competition and capacity for trace compounds depends on the nature/background of the compound, its concentration and the characteristics of the adsorbent. The concentration is important since it affects how much of the component can be adsorbed. When the concentration of the adsorbed phase is low the bulk concentration remains constant. At higher concentrations, sorption may be driven by competition between several species that affect the composition of the bulk. Moreover the measurement method can have a big influence particularly if operation is using a flow-through or closed AC [33]. In multicomponent systems molecules with a lower volatility, increased polarity and greater degree of unsaturation are more tightly held. Ruthven [1] reports that the electrostatic interactions such as polarization, dipoles and quadruples between adsorbate and adsorbents are only significant for adsorbents with ionic structures, however zeolites do contain cations, therefore charge interactions must be considered. Volatile compounds are especially susceptible to displacement because they are weakly adsorbed and diffuse rapidly. Competitive adsorption occurs where the components in the mixture may induce the adsorption of others, co-adsorb or even compete to adsorb, but this depends on the adsorbates [18].

In terms of the problem at hand, DME has a lower volatility thus capable of displacing competing MeCl molecules. DME is more polarizable since it has a C-C bond unlike MeCl, but MeCl has a greater polarity. The higher the polarizability the greater the momentary shift the of the molecule thus increasing the likelihood of an interaction with the adsorbent surface [127]. MeCl adsorption

is influenced by the number and position of the chlorine atoms whilst it is through the O bond with DME. The number of molecules of any ether adsorbed at or near saturation is influenced by the cross-sectional area and the covering power per molecule. Therefore at higher pressures more adsorption occurs especially of smaller molecules, which is what was observed with the pure component isotherm analysis, whereas the more complex molecules can become highly adsorbed.

From the pure component data of all the adsorbents used for the separation of DME from MeCl mixtures, Pret-4A demonstrated the largest potential for MeCl purification. With this in mind, it has been observed that the adsorbent is widely used for various mixture separations especially since it can selectively adsorb and separate molecules based on their shape, size, polarity, high selectivity and high transportability [125, 128, 129]. Perez and Armenta [128] reported that the adsorption rate and capacity for CO₂, ethylene and ethane on 4A decreased in the order of decreasing quadruple moment and increasing critical diameter of the gas molecules and not solely the molecular dimensions. It is reported that one of the most important industrial applications of zeolites is the 4 Å molecular sieve because there are two interconnecting three dimensional channels: *a*) connected α -cages or supercages, 11.4 Å in diameter, separated by 4.2 Å apertures and *b*) β -cages or sodalite cages, 6.6 Å in diameter alternating with the α -cages separated by 2.2 Å apertures [74]. Recall Ruthven [1] claims that the effects of vibration of both the diffusing molecule and crystal lattice during adsorption means molecules can penetrate the free diameter windows of the zeolite with greater critical diameters than the free diameter itself, which is what is suspected with DME on zeolite 4A.

Grande *et al.* [129] reported that for the equilibrium binary adsorption of propane/propylene on 4 Å it took three days for equilibrium to be reached, whilst experiments for 3 h equilibrium time showed a large difference in amount adsorbed to the former. Since kinetic selectivity is measured by the ratio of micropore diffusivities for the components as shown earlier. Differences in diffusion rates between molecules of comparable molecular weight become large enough to provide a useful separation only when steric effects hinder diffusion. Molecular sieve separations, which depend on the exclusion of larger adsorbate molecules from the micropores, are less common than separation based on differences in adsorption equilibrium or diffusivity. This is because stringent geometric requirements are necessary for selective adsorption and the kinetic rate of the unwanted component needs to be essentially zero. Separation by sieving can in principle provide an extremely high selectivity for molecules of different shapes and size i.e. CO₂/N₂ separation by a ETS-4 molecular sieve [130]. Reid *et al.* [131] reported the kinetics and size exclusion of molecules for selective adsorption using CMS's. They reported that the adsorption kinetics for probe molecules is a complex function of their size, shape and electronic structure. Therefore the following factors must be considered a) size exclusion by selective

porosity b) diffusion through the selective porosity c) diffusion along the pores and d) adsorbate-adsorbent interactions. The selective porosity provides the barrier to the diffusion of molecules into the porous structure and in the case of larger molecules, leads to exclusion. They reported that for the same micropore volume, planer and tetrahedral molecules were adsorbed. Different adsorbates with the same tetrahedral structure were virtually excluded from the bulk of the microporous structure to the same extent. In contrast the linear molecules were adsorbed without any significant exclusion.

The separation of N₂ and O₂ in industry is a kinetic based separation through size exclusion. When N₂ is in close proximity to the exposed cations of the zeolite crystal, a charge induced dipole forms and the N₂ is attracted into the zeolite crystal. N₂ is more polarisable than O₂ and therefore the zeolite selectively adsorbs N₂ allowing the O₂ gas to pass unrestricted. Due to the modified zeolite used the cage structures were designed to allow only O₂ to pass through and exclude the larger N₂ molecules. That is, the holes in the side of the zeolite dice were large enough to allow O₂ entry but small enough to exclude N₂. The heat of adsorption for N₂ and O₂ was ~ 24.0 and ~ 15.0 kJ mol⁻¹, respectively. However N₂ exhibited a steeper decrease with coverage therefore heterogeneously adsorbed while O₂ only slightly heterogeneously adsorbed with a relatively constant heat of adsorption [126]. Bakhtyari and Mofarah [124] reported the binary adsorption of methane (CH₄) and N₂ on a 5 Å zeolite. Zeolite 5 Å is a truncated octahedron with a central cavity pore of 11.4 Å. The Na⁺ cations typically found in 4 Å are exchanged with Ca²⁺ or Mg²⁺ cations to form larger apertures. With a Si/Al ratio of one and suitable apertures it allows for the transport of molecules with a kinetic diameter of ≤ 4.9 Å. The type-A zeolite used commercially has a high selectivity for N₂ in air separation due to interactions between the cations and the quadruple moment in N₂. However due to the stronger polarizability of CH₄ than N₂ it causes stronger interactions with the former [124, 127, 132]. Mulgundmath [132] reported that N₂ adsorption at a fixed pressure and temperature increased its selectivity even with a lower gas composition, moreover separation of mixtures was favoured by higher temperatures, but resulted in reduced adsorption quantities.

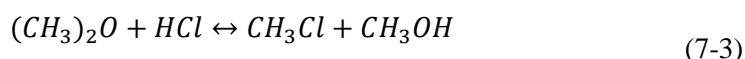
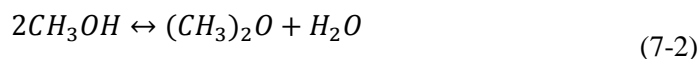
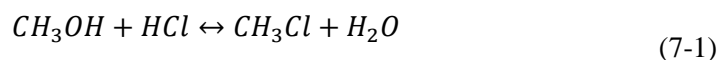
7.1.1 Reported dimethyl ether (DME) and methyl chloride (MeCl) desorption

There is one reported study on desorption of a binary mixture containing DME and MeCl on microporous adsorbents with another brief study written in Russian which requires translation. Saburina and Begun [133] in the short Russian article reported that the most promising adsorbents with the higher selectivity coefficients for their purpose was silica gel KSMG and zeolite CaX when compared to activated carbon. They used nitrogen as a desorbing agent in a multicyclic

adsorption-regeneration experiment at 30 °C. MeCl desorbed off silica more efficiently than from the zeolite after it had been flushed for 30 min with N₂. After 60 min, 90 % of the DME was desorbed from the silica. Interestingly, they concluded that the silica gel KSMG was recommended for industrial application under multicyclic operating conditions for regeneration and separation of MeCl and DME.

7.1.2 Reported dimethyl ether (DME) conversion to methyl chloride (MeCl)

According to Schmidt *et al.* [134] in the presence of a alumina or zinc chloride catalyst supported on pure alumina MeOH reacts with HCl giving MeCl and water. The only side product (DME) can be further reacted with HCl to form more MeCl. It was reported that only a few studies on the kinetics have been published however most of them only consider Eq. (7-1) and that the other two were negligible from a kinetic point of view. The reaction scheme is shown below:



7.2 Experimental

Binary adsorption was carried out at constant room temperature at various pressures through single run experiments on thermally pre-treated adsorbents. Since there was no online gas analysis and the manifold could not be dosed with subsequent mixtures the analysis was conducted at a specified condition with incremental manual gas sampling from the manifold and AC outlet, respectively.

7.2.1 Gas chromatography and mass spectrometry (GC-MS) analysis

The Hewlett Packard series II 5890 plus gas chromatography with a 5972 series mass spectrometer was used to quantify separation of DME and MeCl mixtures. In this study, two different GC columns were installed and used for quantifiable binary mixtures analysis. The first column (GC-Col-1) was a RTX-1 dimethyl polysiloxane 30 m x 0.32 mm x 5 µm column capable of separation based on volatility. Although separation through volatility of these gases is extremely difficult it was understood that if parameters such as column flow rate and sample size were varied separation might be possible. The GC-MS analysis was conducted using 10 µl sample injections with isothermal operation at 30 °C, a column flow rate of 1.50 ml min⁻¹ and a fixed split ratio of 13:1. The second column (GC-Col-2) used was a PoraPLOT U 25 m x 0.25 mm x 8 µm recommended for the separation of polar and apolar volatile compounds. The analysis was

also conducted using 10 μl sample injections but with isothermal operation at 120 $^{\circ}\text{C}$. The column flow rate was 0.539 ml min^{-1} with a fixed split ratio of 33:1.

7.2.2 Quantification and calibration curves

Although quantitative analysis was achievable using the GC-MS spectrums it was essential to determine the relationship between the magnitudes of the peaks for the gases particularly the impurity for a known amount of DME in MeCl. Both the GC and MS spectrum data were used to quantify the results obtained per injection. Different concentrations of DME (0 - 40 vol. %) were injected into the GC-MS and calibrated for qualitative and quantitative analysis. High concentration of MeCl could not be calibrated because the points fell outside the calibration range; particularly with the MeCl concentration frequently being > 95 vol. %. Nevertheless MeCl quantities were quantified by other means, shown later. Since the primary objective of this study was to remove DME from MeCl, different concentrations of DME as the impurity in MeCl were prepared and injected into the GC-MS thus allowing two calibration curves to be obtained for the GC and MS, respectively. The MS was used initially to identify each component in each mixture and support the quantification obtained using the GC. However, it was observed that with DME concentrations (< 2.0 vol. %) numerical peak areas were unavailable therefore the MS was calibrated at lower concentrations. For cases where the impurity concentration of DME in the mixture was too low for GC quantification the MS data was used.

7.2.2.1 GC quantification

The actual concentrations (C_{act}) of DME were determined using the external calibration method. For different concentrations of DME the numerical peak areas were plotted against the actual concentrations thus resulting in a trendline. The subsequent calibration curve was then used to determine the DME concentration at the manifold and AC outlet prior to and post adsorption. In each case the predicted concentration mixture using Ideal gas laws was compared to the GC quantification value to ensure relative concordance between concentrations obtained. MeCl was quantified in terms of the ratio of GC peak response to the initial concentration peak response for the component (prior to adsorption). The method was implemented since the high concentration quantities could not be calibrated and it was impossible to inject precisely 10 μl per sample due to human error. During adsorption the MeCl peak response reduced therefore logically quantified in terms of detected quantity to the initial quantity. As a result of the quality and limitations of the equipment two things were of prime interest which were sought out from the results a) confirmation of purification behaviour of a mixture through the removal of DME or MeCl from the mixture i.e. decreasing or vanishing peaks with adsorption time indicative of adsorption and

b) determine the impact if any on the other adsorbate gas even if it was relatively more quantitative rather than qualitative.

7.2.2.2 MS quantification

During the ionisation stage in the MS molecules become fragmented and split into different fragments. As an example Fig. 7.1 demonstrates some typical fragmentations of DME due to the ionisation process. Generally to quantify a component, the total of all its fragments would be summated to determine the overall quantity of the component. However due to the quality and sensitivity of the equipment and analysis from preliminary data an altered approach was used to quantify MeCl and DME, respectively. For the MS calibration points the sum of 45 and 46 m/z ions were used for DME whilst the 50-52 m/z ions were used for MeCl from each GC peak maximum at each retention time. It is important to recognise that the 45 and 46 ions for DME were selected due to their continuous pattern of appearing in similar quantities consistently during pure component and binary analysis. On the other hand, for MeCl the 50-52 ions were predominantly visible in high abundance. Although other peaks such as 15 m/z were observed these were ignored since they could be a result of methyl groups from either adsorbate. Therefore to be sure of the respective component detected only the plausible ions responsible for each adsorbate were used. It is postulated that since the MeCl has a higher polarity the atoms are more strongly held to the carbon whereas DME is more susceptible to ionisation fragmentation due to its larger electron cloud. It is accepted that although the technique may not be considered one hundred percent, the chief objective was to observe for any purification behaviour. Nevertheless, the method has been confidently applied to qualitatively quantify separation behaviour between MeCl and DME.

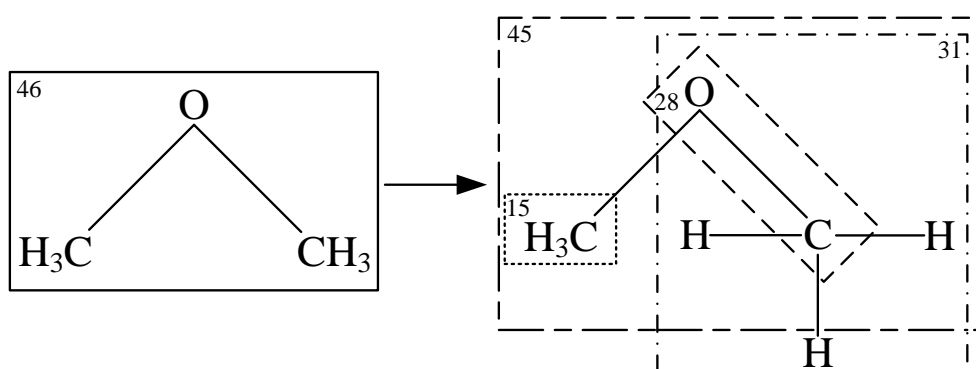


Fig. 7.1. An illustrative example of the DME fragmentation in a MS

system was vacuumed again. Next the system was flushed twice with some MeCl to ensure all DME was removed then filled the manifold with MeCl to a particular pressure. The syringed DME was then injected into the MeCl stream. Thereafter mixtures were allowed to settle for 1 h to ensure complete mixing before analysis.

7.2.3.2 Predicting concentrations of binary mixtures

Below is an example calculation for the determination of a binary mixture stream for the adsorption on Pret-4A. The manifold was dosed to ~ 23.0 psiA (1.57 atm) and contained at a temperature of 22.4 °C. Using a sample lock syringe 1 ml of DME was syringed from the manifold and added to the MeCl to create the mixture:

$$\text{Moles of DME in 1ml} = 1.565 * 0.001 / 0.999 * 0.0821 * 295.95 = 6.52 \times 10^{-5} \text{ mol}$$

The manifold was then pressurised with MeCl to 29.4 psiA (2.00 atm) and contained at a temperature 22.4 °C. The number of moles of MeCl contained within the manifold was:

$$\text{Mole of MeCl in manifold} = 2.001 * 0.0202 / 0.999 * 0.0821 * 295.95 = 1.69 \times 10^{-3} \text{ mol}$$

Once the 1 ml quantity of DME was added to the manifold containing MeCl, the total number of moles of the binary mixture was:

$$\text{Total moles of MeCl + DME} = 1.69 \times 10^{-3} + 6.52 \times 10^{-5} = 1.75 \times 10^{-3} \text{ mol}$$

The concentrations of DME and MeCl in mol L⁻¹ were:

$$\text{Total concentration} = 1.75 \times 10^{-3} / 0.0202 = 8.65 \times 10^{-2} \text{ mol L}^{-1}$$

$$\text{MeCl concentration} = 1.69 \times 10^{-3} / 0.0202 = 8.33 \times 10^{-2} \text{ mol L}^{-1}$$

$$\text{DME concentration} = 6.52 \times 10^{-5} / 0.0202 = 3.22 \times 10^{-3} \text{ mol L}^{-1}$$

Therefore the binary mixture contained the following volume split:

$$\text{MeCl} = (1.69 \times 10^{-3} / 1.75 \times 10^{-3}) * 100 = \mathbf{96.28 \text{ vol. \%}}$$

$$\text{DME} = (6.52 \times 10^{-5} / 1.75 \times 10^{-3}) * 100 = \mathbf{3.72 \text{ vol. \%}}$$

7.2.4 Batch mode fixed bed binary adsorption

For batch adsorption the manifold was dosed with the binary gas mixture to ~ 25.0 psiA (~ 1.7 atm) pressure. The system was then allowed to equilibrate by opening valve MV₅ (Fig. 3.3) located between the manifold and the AC. Gas samples were taken manually at different time intervals (15 min, 30 min and 45 min) from sample points SP1 at the manifold and SP2 at the AC outlet and the pressure in the system was continuously recorded. This procedure allowed for

observing the changes in pressure as well as the gas composition while adsorption proceeded from different regions of the adsorption system.

7.2.4.1 Batch mode blank binary expansion experiment

In order to validate the experimental rig for batch mode binary gas adsorption the system was tested by expanding a binary mixture into an empty AC. This was to ensure both sample points gave consistency in quantification, no adsorption occurred and consequently both regions equilibrated quickly due to no adsorption effects.

7.2.5 Continuous flow binary adsorption

For continuous flow experiments, the manifold was dosed to ~ 40.0 psiA (~ 2.7 atm) with the binary gas mixture and then allowed to flow from the manifold through the packed AC before being released to the atmospheric discharging line. All the experiments were carried out at room temperature around 20 ± 3 °C. Each run was initiated by $\frac{1}{4}$ - $\frac{1}{2}$ opening valve MV₅ (Fig. 3.3) and fully opening valve MV₈ at the discharge line. Valve MV₅ was partially opened accordingly to ensure slow gas flow through the AC, hence, longer gas residence and contact time between the adsorbate molecules and adsorbent.

Experimentally the pressure in the system was observed to drop down to atmospheric pressure typically after ~ 7 min. Beyond that, the driving force for flow between the two regions (i.e. pressure difference) diminished as the system pressure approached atmospheric pressure (~ 14.7 psiA). Subsequently, any drop in the pressure thereafter was mainly attributed to steady state adsorption while the system approached equilibrium. The system was in steady state since there was no primary degree of freedom dominating a particular mode of adsorption i.e. PSA or TSA. The changes in the gas composition at the feeding manifold and at the AC outlet were sampled and analysed by the GC-MS system at given time intervals between 30 s and 50 min. The system pressure was also recorded during each experiment. Samples were taken at 5 min interval and not at closer intervals because each sample injection took 5 min to analyse using the GC-MS.

7.2.5.1 Continuous flow blank experiment

For validation of the procedure and analysis method one continuous flow blank experiment was conducted using the same above procedure but with the AC packed with non-adsorbing glass beads.

7.3 Results and discussion

Below presents the calibration curves for the GC and MS respectively, which were used to qualitatively quantify adsorption and desorption of DME and MeCl, respectively. This is followed by the results from batch and continuous flow adsorption for different concentration mixtures containing DME in MeCl mixtures on the different vacuum and thermally pre-treated adsorbents.

7.3.1 Calibration curves

Calibration curves were determined for quantitative analysis using both GC-Col-1 and GC-Col-2. Preliminary analysis was conducted using GC-Col-1 where only the MS data could be calibrated due to poor GC peak separation. Since GC-Col-2 resulted in better peak separation different concentrations of DME were calibrated using both the GC and MS, respectively. It is accepted that the means used to quantify particularly the MS was not ideal therefore it was important to compare the MS trend with the GC trend and observe for an equally feasible relationship in a similar order of magnitude which could be used to gain confidence and subsequently support validation of the former. Ultimately a method was successfully implemented to measure the magnitude of adsorption for DME in terms of concentration.

7.3.1.1 GC-Col-1

Fig. 7.3 shows the GC and MS spectrums for an analysed mixture containing 40: 60 vol. % (D: M) using GC-Col-1. The top spectrum in the figure shows the GC signal spectrum with the x -axis giving the retention time and the y -axis giving the relative abundance. The bottom spectrum in the figure shows the MS peak response to the GC data in terms of m/z versus the relative abundance at a manually selected GC retention time. As can be seen both DME and MeCl retain in close proximity at retention times of 2.21 and 2.23 min, respectively, which resulted in the peaks being conjoined. Although the MeCl peak max was 2 s later, the peak starting point overlaps the ending of the DME peak thus causing a crossover of peaks. Having said that even with the overlapping of peaks the respective peak maximums and numerical peaks were still available thus numerical quantification. The subsequent MS spectrum shows the magnitude of peaks at the conjoined intersection which shows 45 and 46 m/z ions for DME and 50-52 m/z ions for MeCl. Since low concentrations were of prime interest the column was tested for peak separation at lower concentrations of DME. However as Fig. 7.4 shows that the DME peak exhibited shouldering on the MeCl peak which resulted in no visible peak max or numerical GC quantification. This meant apart from visual peak separation no qualitative quantification was possible. Due to the manual sampling procedure an air peak was visible on the GC spectrums at 1.25 min. The air peak confirmed by the MS was frequently observed in a similar order of

magnitude. Since the system was regularly leak tested and a stringent dosing procedure was used this peak was not suspected to be a result of any other impurity.

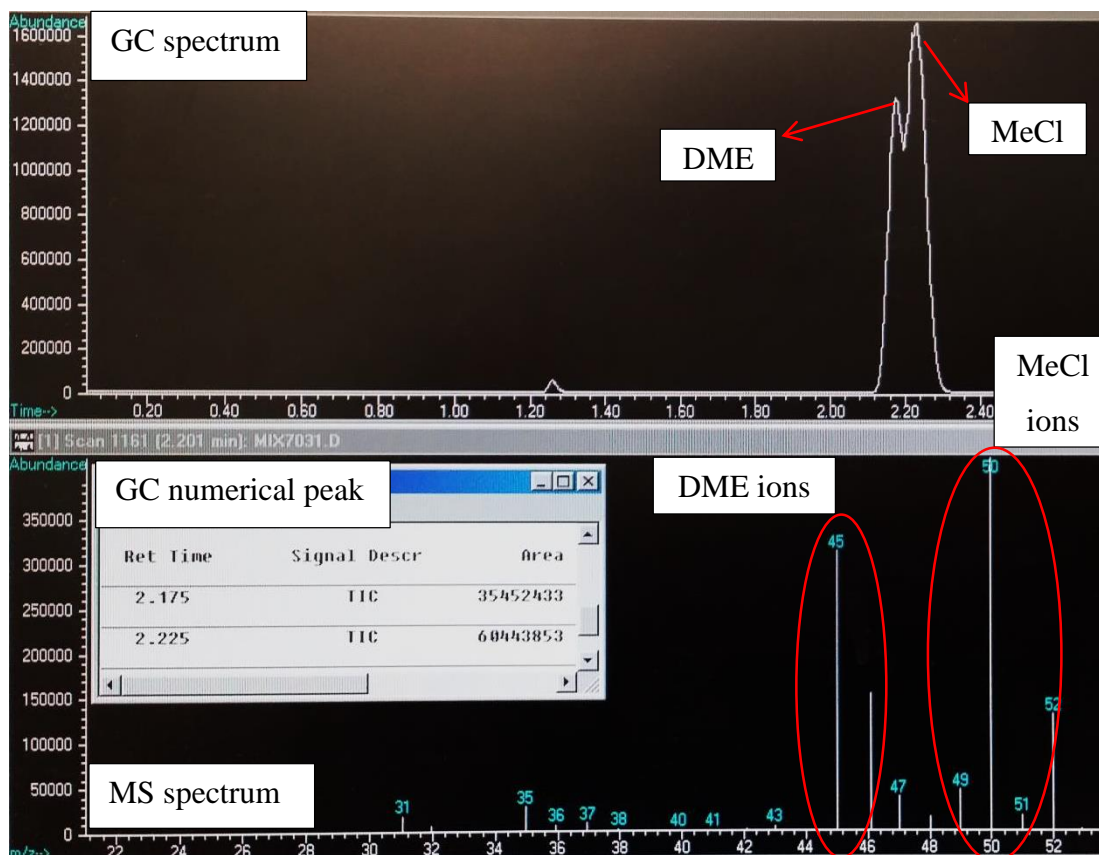


Fig. 7.3. MeCl and DME peak separation using GC-Col-1

As shown by the red circle around the GC numerical data in Fig. 7.4 no numerical peak area was available for DME due the overlapping of peaks. As a result in order to achieve some kind of quantification method the pure components of both gases were injected and used to determine the actual peak retention times. These respective retentions times were then used to quantify each component using the MS. Through knowledge of the retention times the maximum GC peak points for DME and MeCl, respectively were obtained. Then by analysing the MS data at the respective GC peak maximums the total responses were quantified. Since GC-Col-1 could not be calibrated for GC numerical quantification for the necessary low concentrations of DME, the above method was implemented for different concentrations of DME in MeCl and calibrated using the MS quantification method only. Fig. 7.5 shows the MS calibration curve for DME in the concentration range 0.4-20.0 vol. %. As can be seen the trend demonstrated a linear fit with a R^2 of 0.994. The resulting plot was used to determine the different concentrations of the binary mixtures pre and post adsorption for the batch fixed bed adsorption analysis. Although the calibration did not give a 100 % accurate concentration the method was used successfully to at

least give quantification in terms of the magnitude of the decreasing DME peaks due to adsorption/desorption.

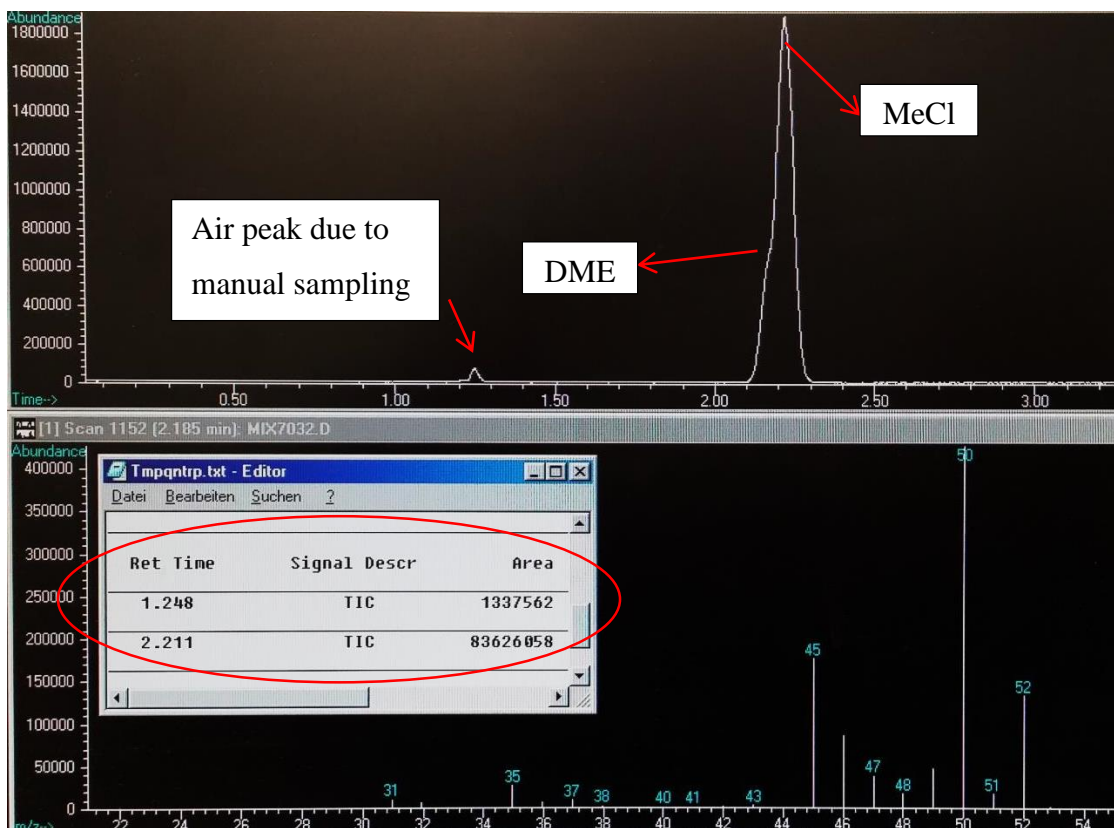


Fig. 7.4. DME shouldering on MeCl GC peak response using GC-Col-1

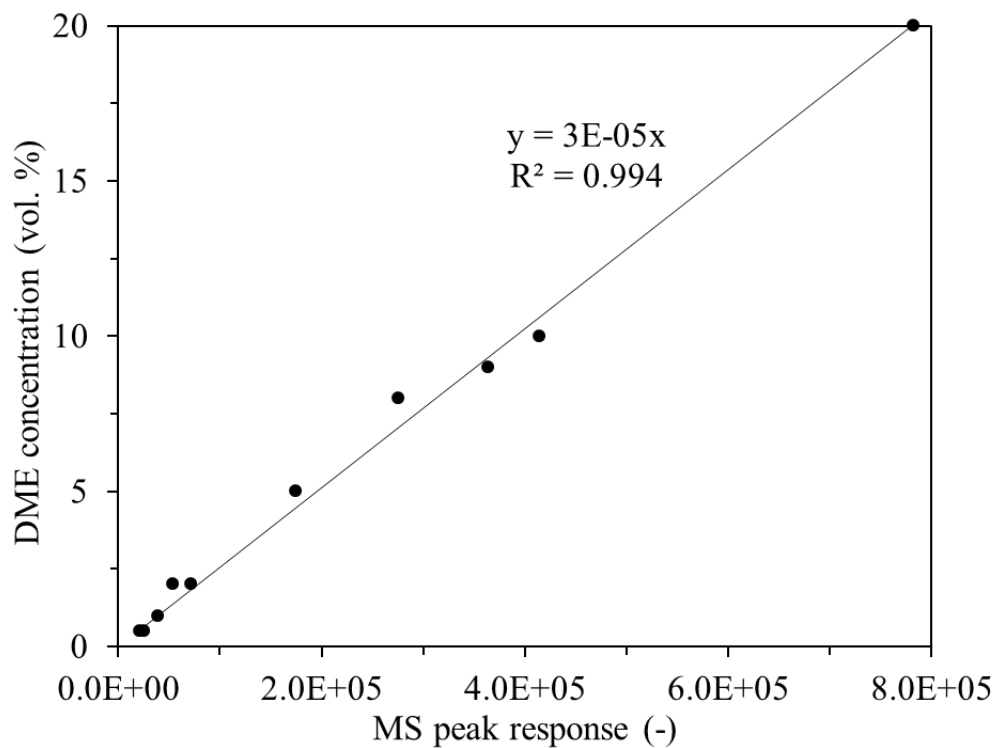


Fig. 7.5. MS calibration curve for DME on GC-Col-1

7.3.1.2 GC-Col-2

The bulk of the GC-MS analysis in this chapter has been carried using GC-Col-2. The GC signal provided clear detection and distinct peaks for MeCl and DME, respectively at different retention times and was quantified using the numerical area under each detected peak where possible, which was calculated by the system using each respective relative abundance value. Similarly the MS also provided a clear detection with a corresponding abundance value at the respective gas retention time. This data allowed for calibration of the GC and MS data against concentrations by relating the recorded numerical peak areas and relative abundances for each individual component in the sample against the actual mixture composition.

Fig. 7.6 shows the GC and MS spectrums, respectively for an analysed mixture containing 5: 95 vol. % (D: M). It can be seen peak separation of MeCl and DME using GC-Col-2 was better than the GC-Col-1. MeCl and DME retained at 4.01 and 4.22 min, respectively thus allowing the peaks to separate along the chromatogram with no overlap. Although both the GC and the MS could be calibrated, analysis using GC-Col-2 displayed only visual peaking but no numerical quantification at DME concentrations < 2.0 vol. % due to poor equipment sensitivity. Therefore the MS was calibrated to more points at low concentrations (0.41 - 2.0 vol. %) to achieve greater accuracy in calibration and subsequent concentration readings. Fig. 7.7 shows the deviation between the predicted and actual values for the GC and MS, respectively compared to a $y=x$ plot. Following injections it was important to compare the predicted concentrations with the actual concentrations obtained using both calibration curves. It can be seen that the DME concentrations for actual versus predicted deviated more at higher concentrations from the $y=x$ line whilst demonstrating more concordance between the two at the relevant low DME concentrations.

For the mixture injected in Fig. 7.6 the predicted concentration was 5.25 vol. % whereas the GC peak response corresponded to a concentration of 5.30 vol. %; the rest of the mixture being MeCl. Similarly, the corresponding MS peak response for DME extrapolated to a concentration of 5.40 vol. %, thus showing excellent concordance. It is important to note that the actual concentrations were expected to be greater than the predicted ones since the MeCl stream already contained DME before the subsequent binary mixture quantity was added. Additional quantities were added to the MeCl streams to obtain quantifiable mixtures for qualitative analysis. Fig. 7.8 and Fig. 7.9 show the respective GC and MS calibration curves for DME using GC-Col-2. As it can be seen both calibrations exhibit linear trends with high coefficients of determination.

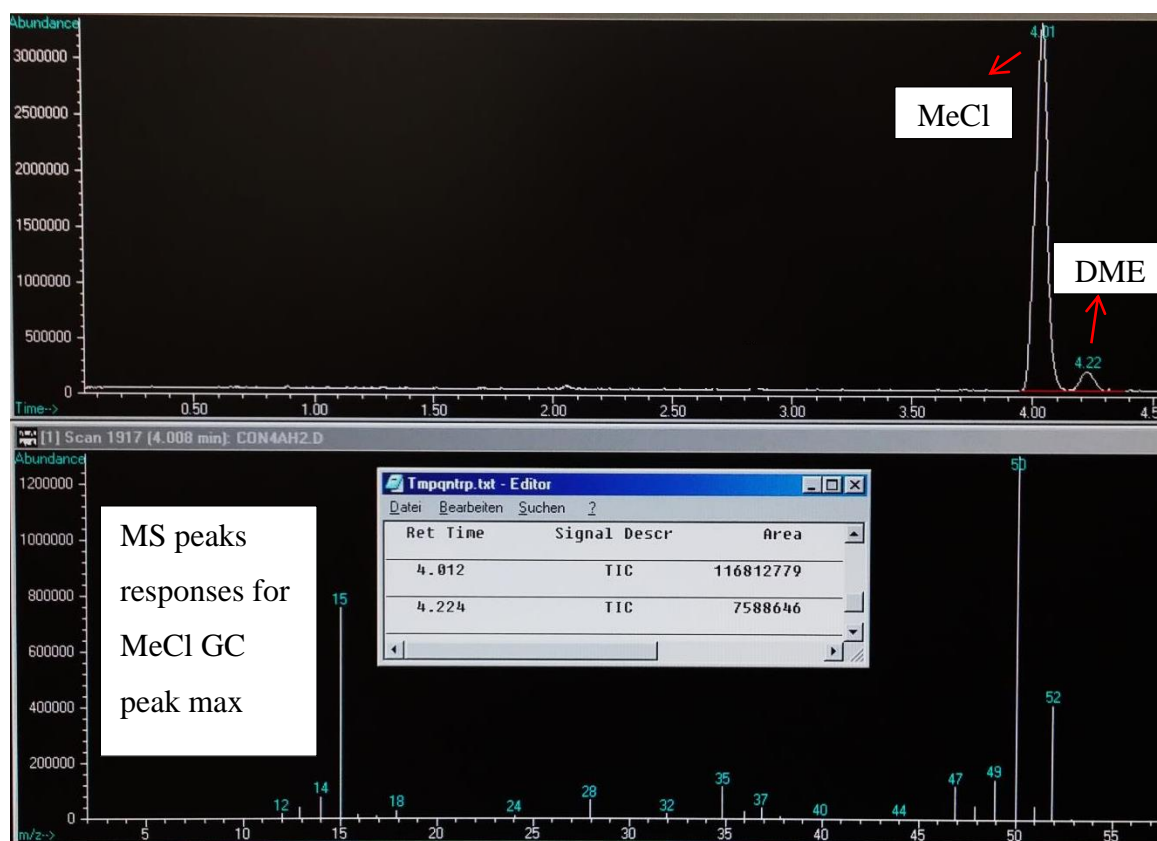


Fig. 7.6. MeCl and DME peak separation using GC-Col-2

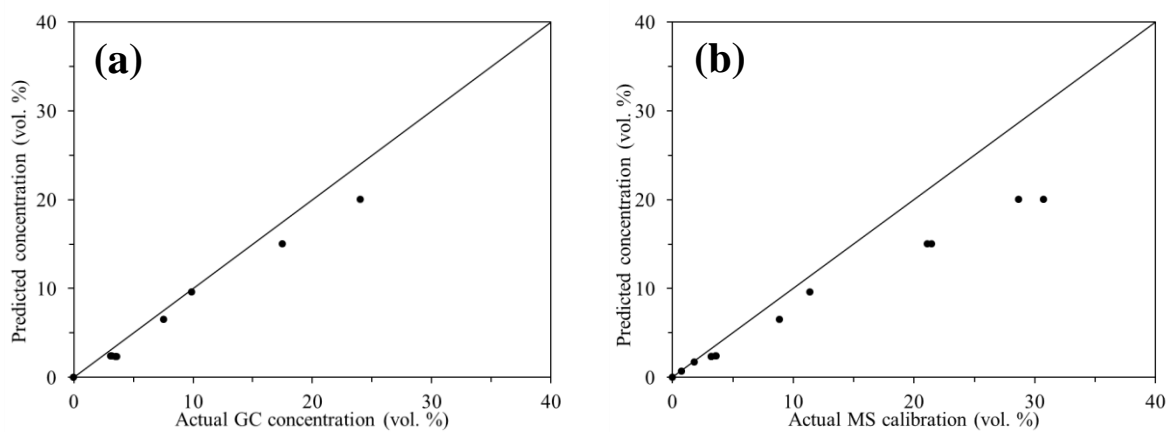
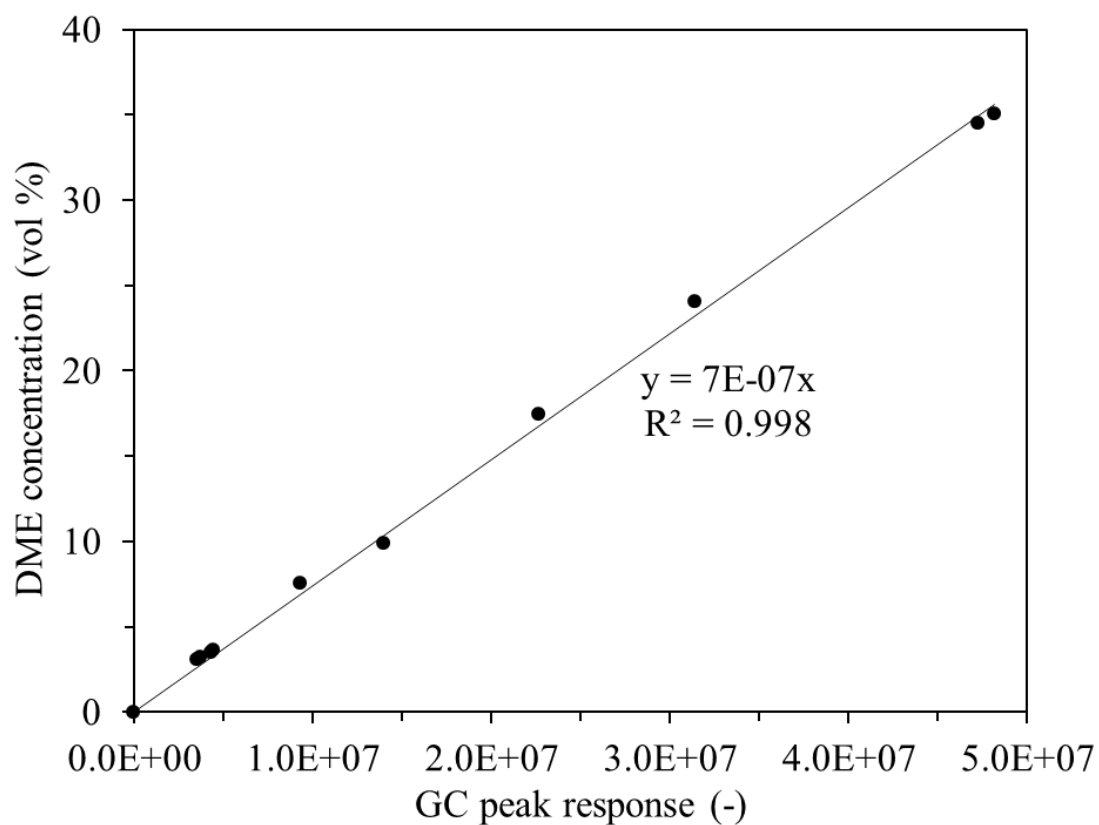
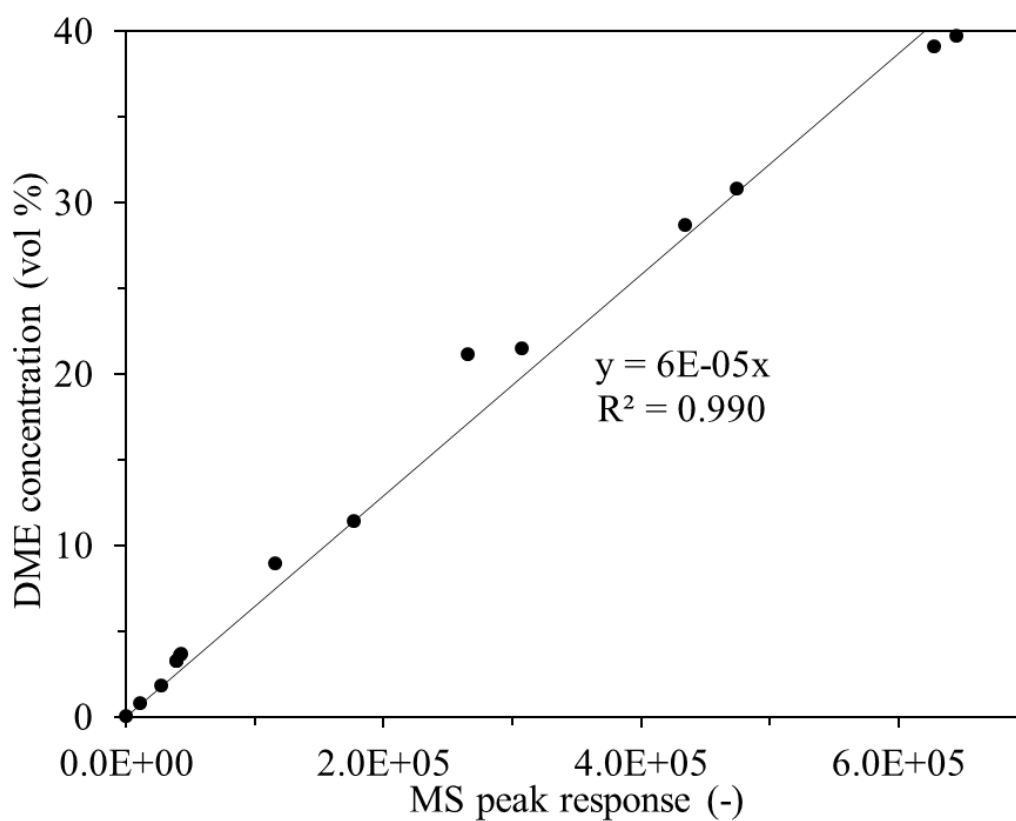


Fig. 7.7. Actual concentration versus predicted concentration (vol. %) for a) GC and b) MS

**Fig. 7.8.** GC calibration curve for GC-Col-2**Fig. 7.9.** MS calibration curve for GC-Col-2

7.3.2 Batch binary mixture expansion into an empty adsorption cell (AC)

Before carrying out binary adsorption on the different adsorbents it was important to test and validate the rig under empty AC conditions in order to ensure the concentrations of the mixture were relatively concordant at both sample points with respect to time following gas expansion from one region to the next. Fig. 7.10 shows the concentration of DME and ratio of MeCl in the manifold and AC outlet before and during expansion. The concentration of DME was determined using the MS calibration curve and the MeCl quantified in terms of the ratio of the MS peak response per injection to the initial manifold MS peak response. This is because the manifold initially begins at a high pressure with a given amount of molecules contained. Then as the charged manifold is released to the empty AC region the pressure drops and subsequently the number of molecules in the manifold reduces until equilibrium is reached. As the figure shows, following batch expansion of the mixture into an empty AC the concentration of both components were concordant at both sample points after 15 and 30 min. Initially the manifold contained 13.0 vol. % DME from SP1, then the concentration at SP2 after 15 and 30 min was 12.9 and 12.8 vol. %, respectively. Similarly, the ratio of MeCl at both sample points remained above 0.92 demonstrating detection of measurable quantities at both sample points. Both components behaved as expected thus validating the set-up and method. This was because no adsorption occurred therefore molecules equilibrated with the empty volume quickly and thus appeared in similar concentrations at both sample points.

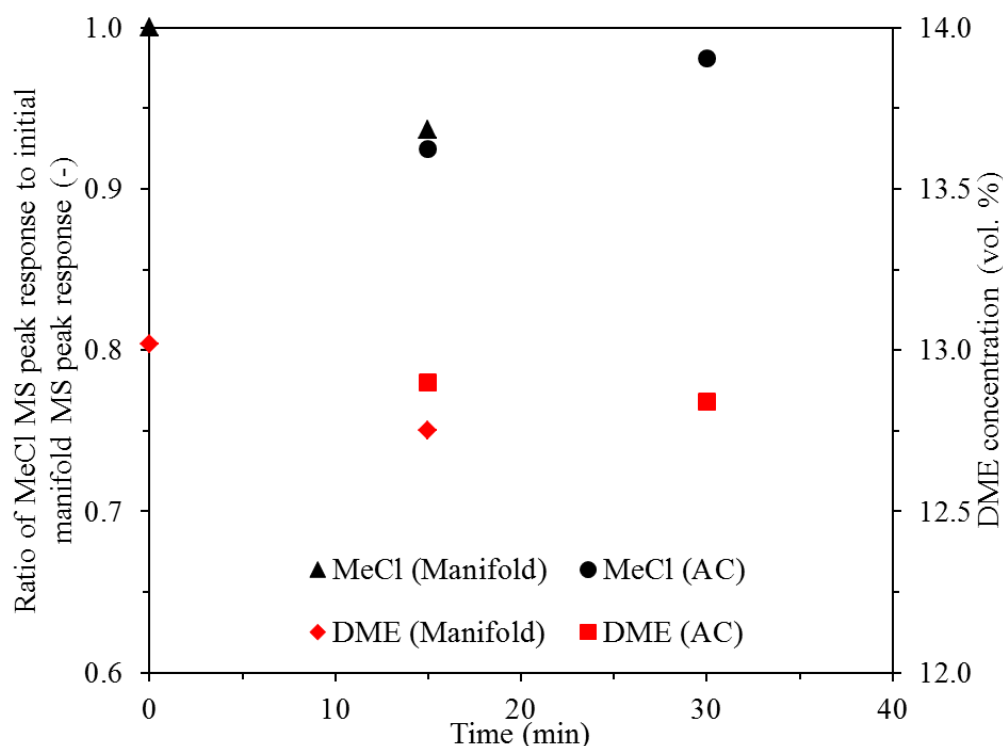


Fig. 7.10. Ratio of MeCl outlet peak response to the initial manifold peak response and DME concentrations at manifold and AC outlet following batch mode binary mixture expansion in an empty AC

7.3.3 Continuous flow of a binary mixture into an adsorption cell (AC) filled with glass beads

Following batch fixed bed binary mixture expansion into the empty AC the system was tested using a continuous flow of a binary mixture through the AC filled with glass beads. Glass beads were used as a reference run before using adsorbents since they are non-porous and non-adsorbing. The purpose of this experiment was to ultimately validate the procedure for continuous flow and see if the concentrations at both sample points were relatively concordant with respect to residence time and if differences were observed with the different adsorbents were due to adsorption effects and not experimental error. Since the outlet was released to atmosphere via a check valve and the manifold started at ~2.5 - 3.5 atm and continuous flow only occurred for ~ 7 min. Therefore the experiment was particularly important to observe the behaviour of the mixture once the flow reached atmospheric pressure. Gas samples were taken from both sample points at different time intervals to observe for concentration changes resulting from continuous flow (0 – 7 min) where the driving factor was pressure then due to thermodynamic equilibrium effects (6 – 30 min) where no pressure and temperature adsorption driving factors were present.

Fig. 7.11 shows the concentration of DME and ratio of MeCl in the manifold and AC outlet before and during continuous flow analysis. Where the AC results correspond to the right y-axis and the manifold readings correspond to the left y-axis. Initially the concentration of DME in the manifold was 2.60 %. Following continuous flow the DME concentration at the outlet after 0.5 and 7 min was 2.04 and, 2.19 %, respectively. After the initial 7 min of continuous flow the DME concentration at 18 and 29 min continued to increase slowly to 2.31 and 2.40 %, respectively. Under ideal conditions the DME concentration would have been the same at both sample points within 1 min, however due to non-ideal conditions and factors such as temperature, pressure, sample injection size and calibration, the concentration of DME behaved as expected with a slow increasing concentration at the AC slowly; which was within an acceptable deviation of the initial concentration. On the other hand, the ratio of MeCl dropped after being expanded to the AC region, but then remained constant thus showing a consistency for the intensity of molecules at both sample points through the experiment. As stated earlier the drop is when the high pressure manifold is released to the AC region the pressure drops and subsequently the number of molecules in the manifold reduces.

During expansion of the mixture from the manifold through the glass beads loaded AC molecules equilibrate more readily between the two regions than when loaded with a microporous adsorbent. With glass beads adsorbate molecules pass through the interparticle voids easily without physically or chemically interacting with the solid particles and as a result the adsorbate molecules

remain in the bulk gas phase whilst filling the empty volume in the same concentration. Contrastingly in the presence of microporous adsorbents, molecules are expected to rapidly become adsorbed into the solid and thus reduce the concentration of the bulk gas phase. Ultimately the above blank tests results demonstrate the non-adsorption behaviour of the mixture using glass beads and thus validate the experimental procedure for adsorption on different adsorbents.

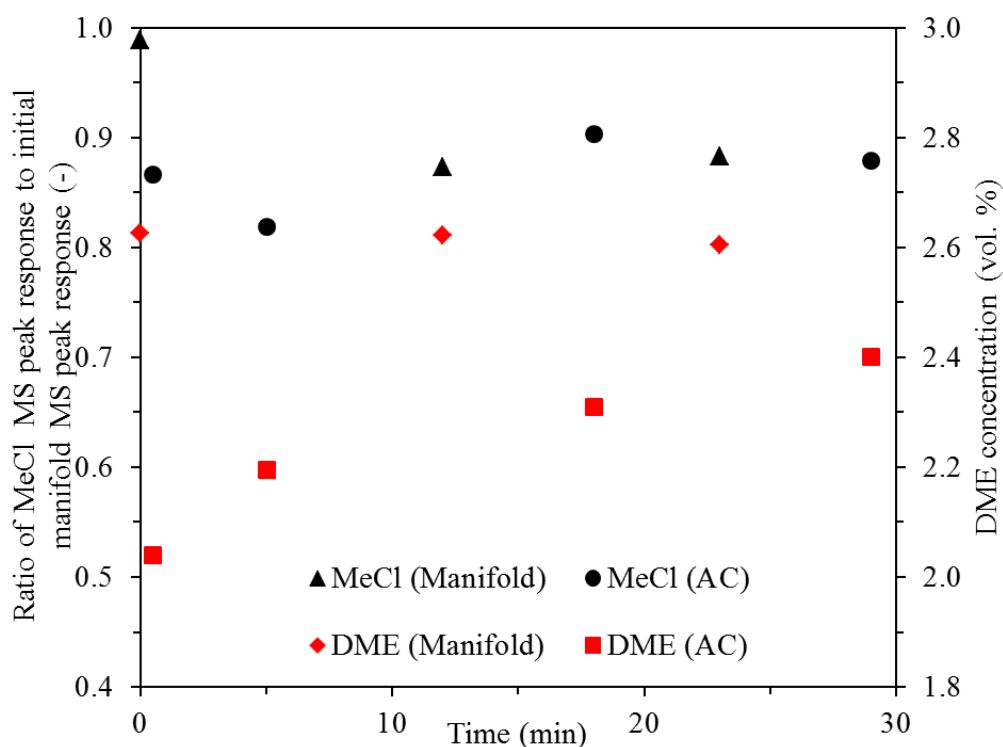


Fig. 7.11. Ratio of MeCl outlet peak response to the initial manifold peak response and DME concentrations at manifold and AC outlet following a continuous flow of a binary mixture through an AC filled with glass beads

7.3.4 Batch fixed bed binary gas adsorption

Since the experimental system was validated for binary mixtures using an empty and glass beads filled AC the subsequent experiments were carried out by loading the AC with the different adsorbents in batch mode. The pure component analysis showed that zeolite 4A exhibited the largest separation difference between MeCl and DME but in much lesser quantities (mol kg^{-1}) than the other microporous adsorbents. The following demonstrates the binary adsorption behaviour for different concentration mixtures on the different adsorbents. The following results from batch mode binary adsorption were obtained using data from GC-Col-1.

7.3.4.1 Zeolite 4A

Two batch fixed bed binary adsorption experiments were conducted on Pret-4A. The conditions for each experiment are shown in Table 7.1.

Table 7.1. Conditions for batch fixed bed adsorption of binary mixtures on Pret-4A

	Pret-4A-B1	Pret-4A-B2
Initial manifold pressure, <i>psiA</i>	21.2	24.9
Temperature, °C	21.5	21.9
Mass of adsorbent, g	2.60	2.80
DME MS calibration conc. (vol. %)	6.11	2.63

Fig. 7.12 shows the DME concentration at the manifold and AC outlet (figures on the left) and the ratio of MeCl at the outlet and manifold to the initial manifold peak response (figures on the right) for experiments Pret-4A-B1 (Fig. 7.12a and b) and Pret-4A-B2 (Fig. 7.12c and d), respectively at different time intervals.

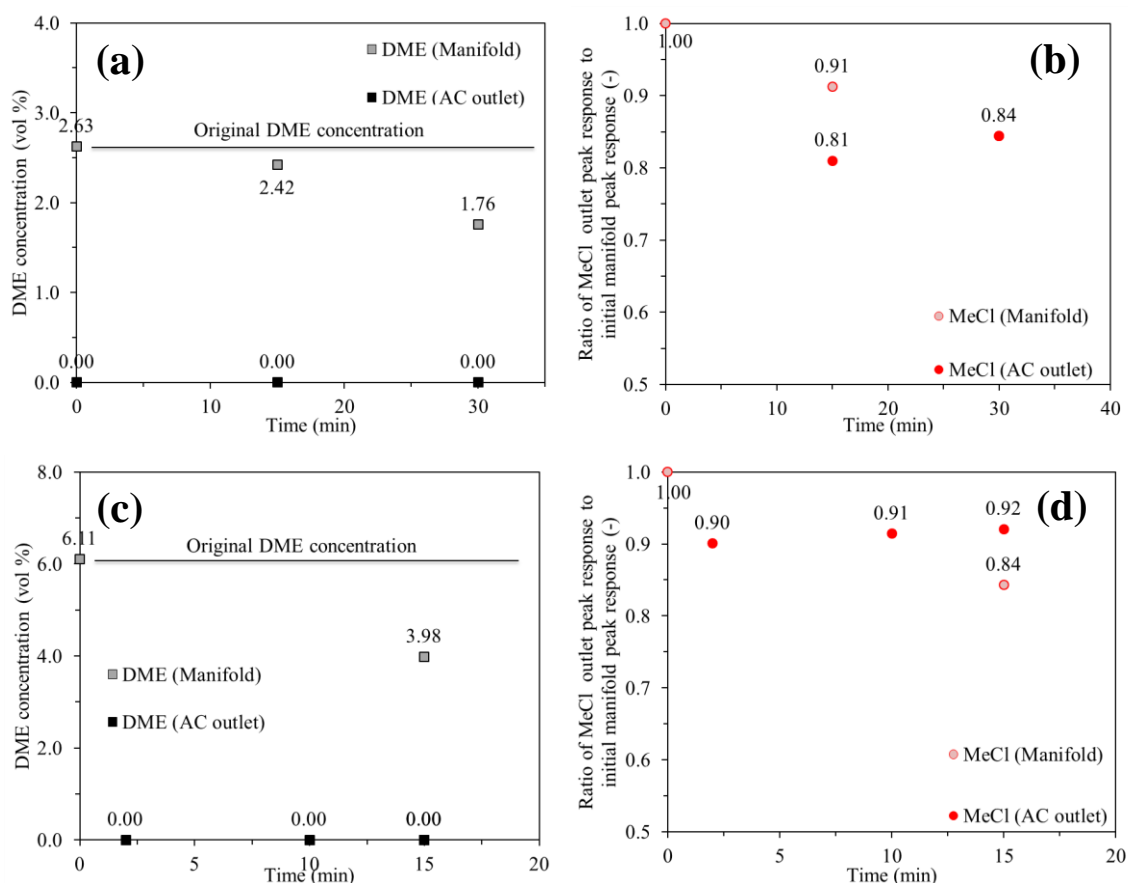


Fig. 7.12. DME concentration in manifold and AC outlet [left figures: a and c] and ratio of MeCl peak response at manifold and AC outlet to initial manifold peak [right figures: b and d] at different time intervals following batch fixed bed binary adsorption on Pret-4A-B1 and Pret-4A-B2

As can be seen both experiments show no DME at the outlet even at after 30 min. In both cases the subsequent DME concentration in the manifold reduced to just over half the initial

concentration suggesting slow adsorption due to competing MeCl adsorption and or potential MeCl displacement. The ratio of MeCl at both sample points remained at a value greater than 0.8 throughout each analysis. Although collectively there is strong evidence to suggest purification of DME from batch MeCl streams. In order to quantify the amounts adsorbed below the binary adsorption for both cases are quantified using Ideal gas laws in the following sub-section.

7.3.4.1.1 Quantification of batch fixed bed binary gas adsorption on zeolite 4A

For experiment: Pret-4A-B1 the moles of MeCl and DME in the manifold at the conditions specified in Table 7.1 were:

Moles of MeCl: 7.61×10^{-3} mol.

Moles of DME: 1.59×10^{-4} mol.

Total: 1.57×10^{-3} mol. – 97.96: 2.04 vol. % [Ideal gas laws]. According to the DME calibration curve the DME concentration was determined to be 2.63 vol. %, after 30 min equilibrium the DME concentration using the calibration curve went down to 1.76 vol. % meaning 0.87 vol. % DME was adsorbed. The vol. % adsorbed can be converted to mol.:

The 0.87 vol. % DME adsorbed (mol.): 5.26×10^{-4} mol.

DME adsorbed per mass of adsorbent (mol kg^{-1}): $5.26 \times 10^{-4} / 2.60 \times 10^{-3} = \mathbf{0.020 \text{ mol kg}^{-1}}$

After equilibrium the final conditions were:

12.7 psiA (0.864 atm) and 21.8 °C, void volume (0.02824 L), therefore the total amount of binary mixture in the non-adsorbed gas phase within system:

$$n = PV / RT = 0.864 * 0.02824 / 0.08205 * 294.95 = 1.01 \times 10^{-3} \text{ mol.}$$

The total amount adsorbed by the adsorbent was calculated from the initial manifold moles of binary gas minus the total moles of binary gas contained within the system at the final equilibrium conditions:

$$\text{Total adsorbed into adsorbent (mol.)} = 1.57 \times 10^{-3} - 1.01 \times 10^{-3} = 5.60 \times 10^{-4} \text{ mol.}$$

$$\text{Amount of MeCl adsorbed by difference (mol.): } 5.60 \times 10^{-4} - 5.26 \times 10^{-4} = 5.07 \times 10^{-4} \text{ mol.}$$

$$\text{MeCl adsorbed (mol kg}^{-1}\text{)} = 5.07 \times 10^{-4} / 2.60 \times 10^{-3} = \mathbf{0.195 \text{ mol kg}^{-1}}$$

$$\text{Total MeCl and DME adsorbed (mol kg}^{-1}\text{)} = 5.60 \times 10^{-4} / 2.60 \times 10^{-3} = \mathbf{0.216 \text{ mol kg}^{-1}}$$

$$\text{Percentage of DME adsorbed at saturation (\% mol kg}^{-1}\text{)} = 0.020 / 0.216 = \mathbf{9.65 \%}$$

$$\text{Percentage of MeCl adsorbed at saturation (\% mol kg}^{-1}\text{)} = 0.195 / 0.216 = \mathbf{90.35 \%}$$

Along with the percentage of adsorbent saturation for each component the overall adsorption efficiency of removing each component with respect to its original concentration can be determined by Eq. (7-4):

$$\text{Efficiency} = \frac{\text{moles of component adsorbed}}{\text{Initial moles of component in mixture}} \times 100 \quad (7-4)$$

Therefore the efficiency of removing DME from original concentration in terms of moles since no DME was observed at AC outlet and the reduced concentration at the manifold:

$$= (5.26 \times 10^{-5} / 1.59 \times 10^{-4}) \times 100 = \mathbf{33.08 \%}$$

Efficiency of removing MeCl from the original mixture concentration in terms of moles:

$$= (5.07 \times 10^{-4} / 7.61 \times 10^{-3}) \times 100 = \mathbf{6.66 \%}$$

Similarly for experiment: Pret-4A-B2 the moles of MeCl and DME in the manifold at the conditions specified in Table 7.1 were:

Moles of MeCl: 1.26×10^{-3} mol.

Moles of DME: 8.26×10^{-5} mol.

Total: 1.34×10^{-3} mol. – **93.86: 6.14 vol. % [Ideal gas laws]**. According to the DME calibration curve the DME concentration was determined to be **6.11 vol. %**. According to the DME calibration curve the DME concentration was determined to be 3.98 vol. % after 15 min equilibrium. Therefore the amount of DME adsorbed was 2.13 vol. %. In terms of moles adsorbed per mass of adsorbent:

The 2.13 vol. % DME adsorbed (mol.): 2.88×10^{-5} mol.

DME adsorbed (mol kg⁻¹): $2.88 \times 10^{-5} / 2.80 \times 10^{-3} = \mathbf{0.010 \text{ mol kg}^{-1}}$

After equilibrium the final conditions were:

10.5 psiA (0.714 atm) and 22.7 °C, void volume (0.02824 L), therefore the total amount of binary mixture in the non-adsorbed gas phase within system:

$$n = PV / RT = 0.714 \times 0.02824 / 0.08205 \times 295.85 = 8.31 \times 10^{-4} \text{ mol.}$$

The total amount adsorbed by the adsorbent:

$$\text{Total adsorbed into adsorbent (mol.)} = 1.34 \times 10^{-3} - 8.31 \times 10^{-4} = 5.09 \times 10^{-4} \text{ mol.}$$

Amount of MeCl adsorbed by difference (mol.): $5.09 \times 10^{-4} - 2.88 \times 10^{-5} = 4.80 \times 10^{-4}$ mol.

MeCl adsorbed (mol kg^{-1}) = $4.80 \times 10^{-4} / 2.80 \times 10^{-3} = \mathbf{0.172 \text{ mol kg}^{-1}}$

Total MeCl and DME adsorbed (mol kg^{-1}) = $5.09 \times 10^{-4} / 2.80 \times 10^{-3} = \mathbf{0.182 \text{ mol kg}^{-1}}$

Percentage of DME adsorbed at saturation ($\% \text{ mol kg}^{-1}$) = $0.010 / 0.182 = \mathbf{5.50 \%}$

Percentage of MeCl adsorbed at saturation ($\% \text{ mol kg}^{-1}$) = $0.172 / 0.182 = \mathbf{94.50 \%}$

Efficiency of removing DME from original concentration in terms of moles:

$$= (2.88 \times 10^{-5} / 8.26 \times 10^{-5}) * 100 = \mathbf{34.87 \%}$$

Efficiency of removing MeCl from the original mixture concentration in terms of moles:

$$= (4.80 \times 10^{-4} / 1.26 \times 10^{-3}) * 100 = \mathbf{38.10 \%}$$

For the above examples, the cases cannot be exactly compared due to differences in pressure and DME composition but collectively analysed to comprehend the binary adsorption behaviour. It can be seen that although the entire manifold quantity is not adsorbed by the adsorbent mainly due to saturation and insufficient molecule mobility with time. For the combined quantities adsorbed at equilibrium (0.216 and 0.182 mol kg^{-1} for the respective conditions at B1 and B2, respectively are in close proximity to the quantities adsorbed by the pure component isotherms of DME and MeCl respectively at the corresponding pressures. From the adsorption efficiency calculations it is clear that the adsorbent is effective at removing over one third of the original DME concentration from the manifold (without its presence at the AC outlet), whilst adsorbing up to 40 % of the initial MeCl concentration for the conditions considered. With that being said, where the MeCl adsorption efficiency was less (6.66 %) for B1 the equilibrium time was longer, thus meaning a longer time for potential DME displacement of MeCl. Under the conditions considered there is evidence of competitive adsorption of DME and MeCl on the adsorbent with potential displacement of the latter, which require some more investigation. In terms of a scientific explanation of the above is as follows:

- A-S interactions occur simultaneously yet independently between DME and MeCl and the respective adsorption sites.
- Both gases compete for sites, with MeCl adsorbing more due to suspected co-operative adsorption with more fellow molecules in the bulk gas phase. DME being in a smaller concentration adsorbs with respect to mobility and availability of adsorption sites.
- DME potentially displaces MeCl with time due to MeCl being more volatile and susceptible to displacement; this theory requires some further investigation.

- The adsorbent is saturated at equilibrium with quantities of both components with respect to the operating conditions. Adsorption is slow with time since molecules have less mobility to adsorb i.e. insufficient activation energy to adsorb and whilst most adsorption sites are occupied.
- DME is not observed at the AC outlet due to steric effects of the molecule being larger than the acceptable pore openings and as the adsorbent becomes saturated from the top of the bed down, molecules are unable to penetrate/diffuse through easily within the conditions considered.

7.3.4.2 Zeolite 5A

Batch mode binary gas adsorption on Pret-5A was initially carried out using 3.0 g of pre-treated adsorbent like the quantity used for pure component experiments. However the single batch run quantity of binary gas at moderate pressure dropped quickly due to rapid uptake by the solid as shown earlier in Fig. 3.9, therefore reduced quantities were (0.3 – 0.5 g) used for subsequent microporous adsorbent experiments. The adsorption behaviour was because there were less moles of gas contained in the manifold than the adsorbent capacity. Furthermore, as the dosed manifold was released to the fresh adsorbent in the AC this meant molecules adsorbed more rapidly onto the vacant adsorption sites compared to adsorption at the same pressure during an isotherm measurement. GC and MS samples taken from the AC outlet at earlier incremental times showed poor quantification of either gas even before equilibrium. This was also because as adsorption preceded the majority of molecules in the bulk phase depleted (generally < 1 min) therefore by the time equilibrium was reached there was no quantity of gas in the bulk that was feasible for GC-MS sampling or analysis (i.e. equilibrium pressure ~ 5.2 psiA). Similarly, the outlet demonstrated minimal quantities of gas due to the lack of penetration of the mixture through the bed which was due to rapid adsorption by the solid. With that being said samples were still taken at different time intervals from the different sample points to gain as much information as possible.

Table 7.2 shows the conditions for three binary gas adsorption experiments carried out on the adsorbent under varying conditions. Each experiment was operated at constant room temperature with the pressure in the range of 1-5 - 2.0 atm and DME concentration (< 4.0 vol. %). In each case there was evidence that DME was detected in traceable amounts at the AC outlet. This was no real surprise as the adsorbent adsorbed the majority of the mixture and some non-adsorbed molecules were able to reach SP2 due to both molecules being within the acceptable pore opening range for molecular sieving effects. In all cases MeCl was present in greater amounts than DME at the outlet due its high concentration within the mixtures. Samples taken after the 15 min equilibrium time at SP1 showed small peaks for both gases, this was because adsorption

proceeded more slowly with time due to molecules having insufficient energy to adsorb. Ultimately, unlike batch fixed bed binary mixture adsorption on Pret-4A the adsorption on Pret-5A was less favourable and did not demonstrate sufficient evidence for purification behaviour.

Table 7.2. Conditions and data for batch fixed bed adsorption of binary mixtures on Pret-5A

	Pret-5A-1	Pret-5A-2	Pret-5A-3
Temperature, °C	22.6	23.0	22.8
Mass of adsorbent, g	3.0	0.50	0.50
DME concentration in mixture using GC-Col-1, vol. %	3.95	1.10	3.85
Initial manifold pressure, <i>psiA</i>	25.2	29.5	28.7
Equil. pressure after 2 min, <i>psiA</i>	5.8	10.4	10.5
Equil. pressure after 15 min, <i>psiA</i>	0.7	4.4	4.9
Comments	DME detected at AC outlet in small amounts (0.4 vol. % after 7 min).	DME detected at AC outlet in trace amounts after 2 and 15 min. (0.20 vol. % after 2 min).	DME not detected at 10 min and 15 min but traces present after 20 min (0.30 vol. % after 2 min).

7.3.4.3 Si35-70

Si35-70 was selected. Table 7.3 shows the initial and final conditions for a batch mode binary gas adsorption experiment carried out on Pret-Si35-70.

Table 7.3. Conditions and data for batch binary gas analysis on Pret-Si35-70

	Pret-Si35-70-B1
Temperature, °C	22.8
Mass of adsorbent, g	0.35
DME concentration in mixture using GC-Col-1, vol. %	1.63
Initial manifold pressure, <i>psiA</i>	22.9
Equil. pressure after 2 min, <i>psiA</i>	10.3
Equil. pressure after 15 min, <i>psiA</i>	9.7

Fig. 7.13a shows the DME concentration at the manifold and AC outlet and the ratio of MeCl at the AC outlet and manifold to the initial manifold peak response (Fig. 7.13b) for batch fixed bed binary adsorption on Pret-Si35-70 at different time intervals. Similar to binary adsorption on the zeolites DME demonstrated a decreasing concentration trend in the manifold due to adsorption which was fast within the first 15 min then slow for the next 15 min due to adsorbent saturation. Though there was evidence of DME adsorption, it was able to penetrate the outlet in small

quantities even after 15 min thus demonstrating a lack of suitability for the objective coupled by the fact that silica gels do not typically purify by means of molecular sieving. On the contrary the ratio of MeCl at both sample points was > 0.80 throughout the analysis. Ultimately, although there is evidence of DME adsorption collectively that data does not support sufficient purification behaviour for the adsorbent to be considered for separation under the conditions considered.

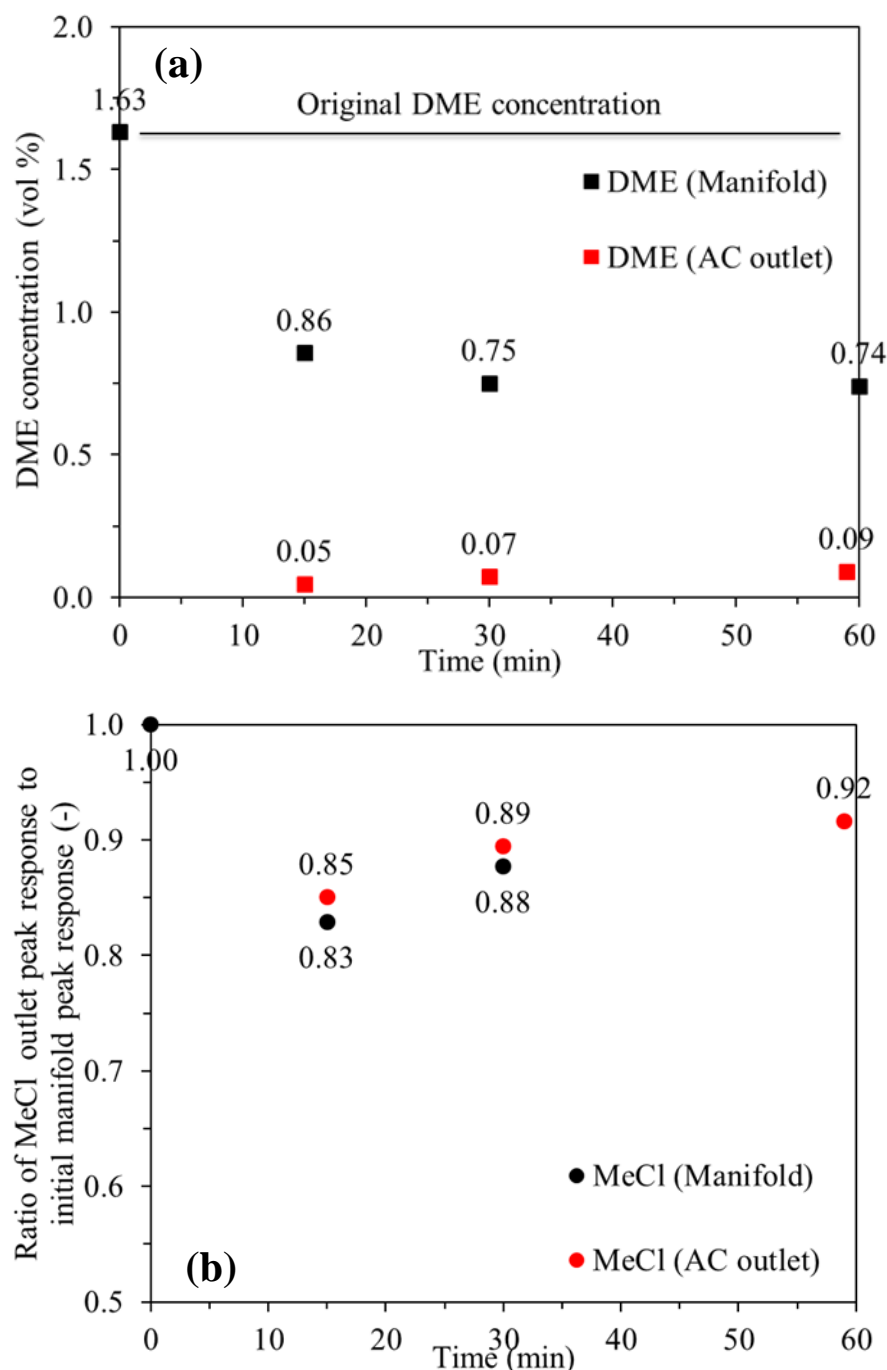


Fig. 7.13. a) DME concentration in manifold and AC outlet and b) ratio of MeCl peak response at manifold and AC outlet to initial manifold peak at different time intervals following batch fixed bed binary adsorption on Pret-Si35-70

7.3.5 Continuous flow of binary mixtures

The following demonstrates the continuous flow adsorption behaviour of different concentration binary mixtures on the different adsorbents. It is important to stress that the continuous flow analysis was carried out for up to 50 min and flow of the mixture only occurred for the first 7 min then the system was allowed to equilibrium in a steady state with no real adsorption driving force whilst taking samples from the two samples points at different time intervals.

7.3.5.1 Zeolite 4A

Three experiments with different DME concentrations were conducted on zeolite 4A, which are summarized along with the operating conditions in Table 7.4.

Table 7.4. Conditions for continuous flow adsorption of binary mixtures on Pret-4A

	Pret-4A-C1	Pret-4A-C2	Pret-4A-C3
Initial manifold pressure, <i>psiA</i>	41.2	39.2	42.2
Temperature, °C	22.5	22.7	23.1
Mass of adsorbent, <i>g</i>	2.65	2.65	2.65
DME GC calibration conc. (vol. %)	N/A	6.27	9.99
DME MS calibration conc. (vol. %)	0.66	6.56	10.82

Fig. 7.14 show the GC and MS spectrums for samples taken from experiment Pret-4A-C1 at the AC outlet after 1 min and 7 min, respectively. As can be seen by both figures DME does not appear in the GC or MS spectrums at the respective times. Such behaviour was observed with all the other runs on this adsorbent. On the contrary shown by the GC peak at 4.01 min MeCl was always present in measurable amounts with a significant abundance and numerical peak area from each sample analysis. Fig. 7.15 shows the outlet concentrations for DME from 0–50 min for the three experiments. All experiments show no DME at the outlet for the first 7 min from the commencement of flow with negligible quantities detected afterwards; due to the adsorbent being saturated. Similarly, Fig. 7.16 demonstrates the ratio of the MeCl peak response at the AC outlet with respect to the initial manifold values. It is evident that the ratios are close to unity for each of the experiments at the start of runs, thus confirming high quantities of MeCl at the AC outlet even after 30 s (Pret-4A-C2 and C3). The slow rising ratio in Pret-4A-C1 was due to the very slow release of the gas controlled by having the valve between the manifold and the AC only quarterly opened, whereas in the other two experiments this valve was half opened.

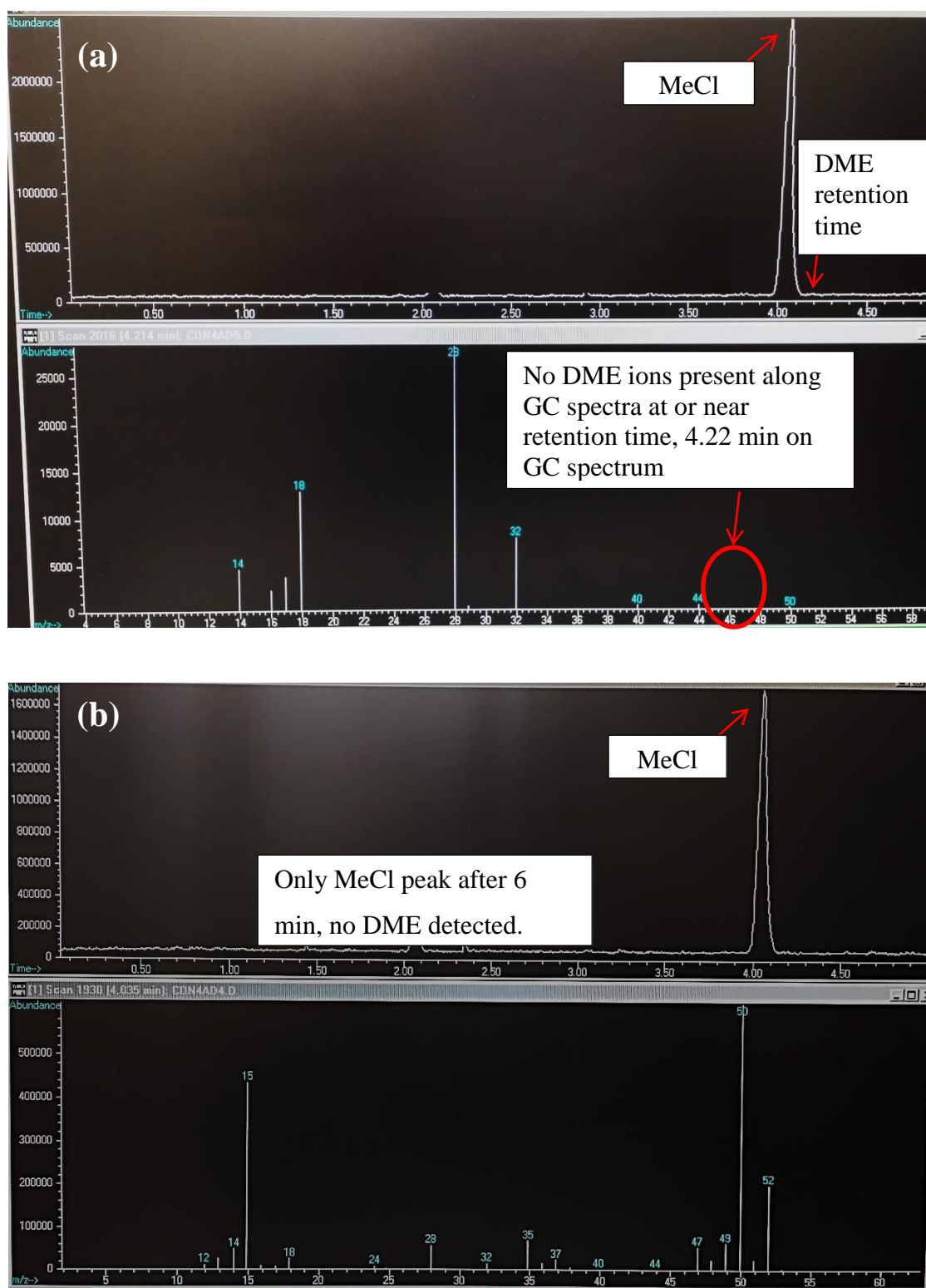


Fig. 7.14. GC and MS spectrums for AC outlet concentration for Pret-4A-C1, a) after 1 min and b) after 7 min from commencement of binary mixture flow

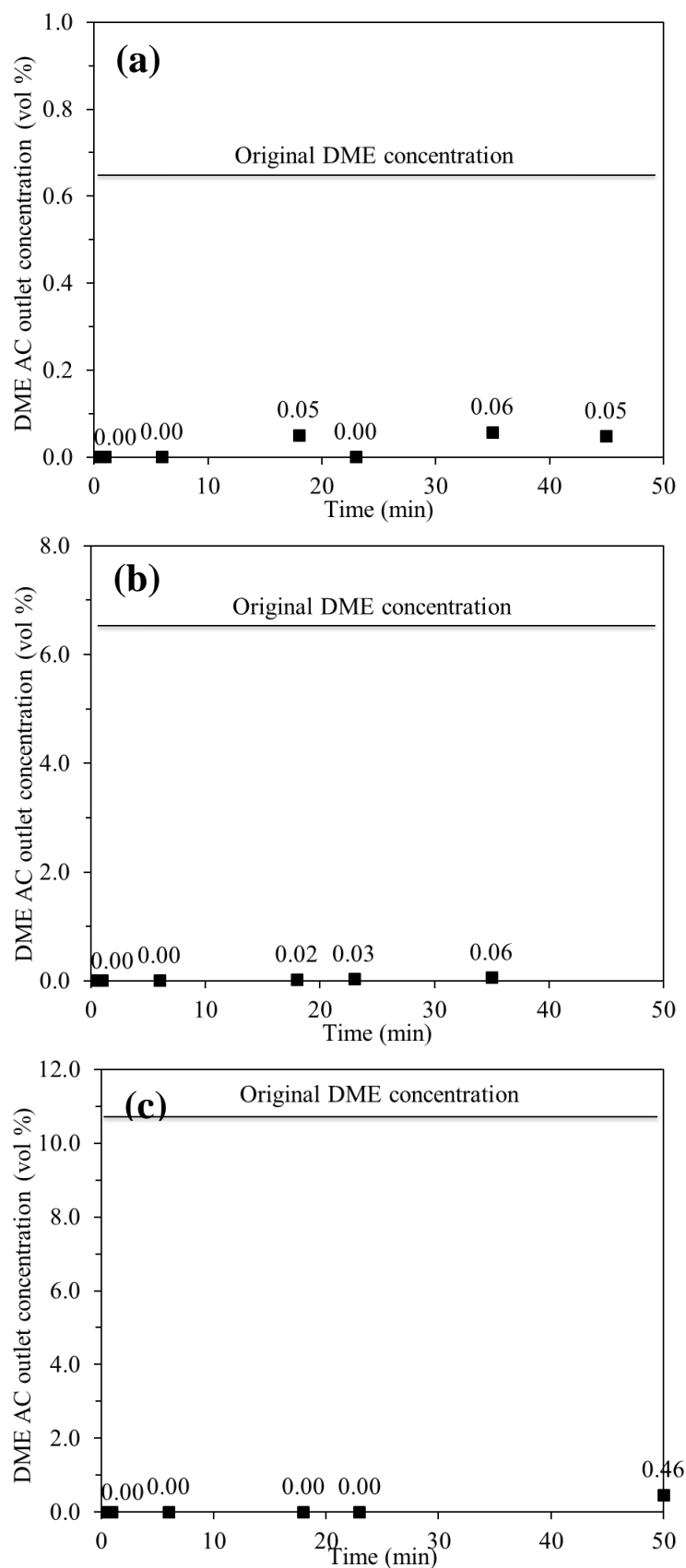


Fig. 7.15. DME AC outlet concentration following continuous flow experiments of binary mixtures on Pret-4A where (a) C1 (b) C2 and (c) C3

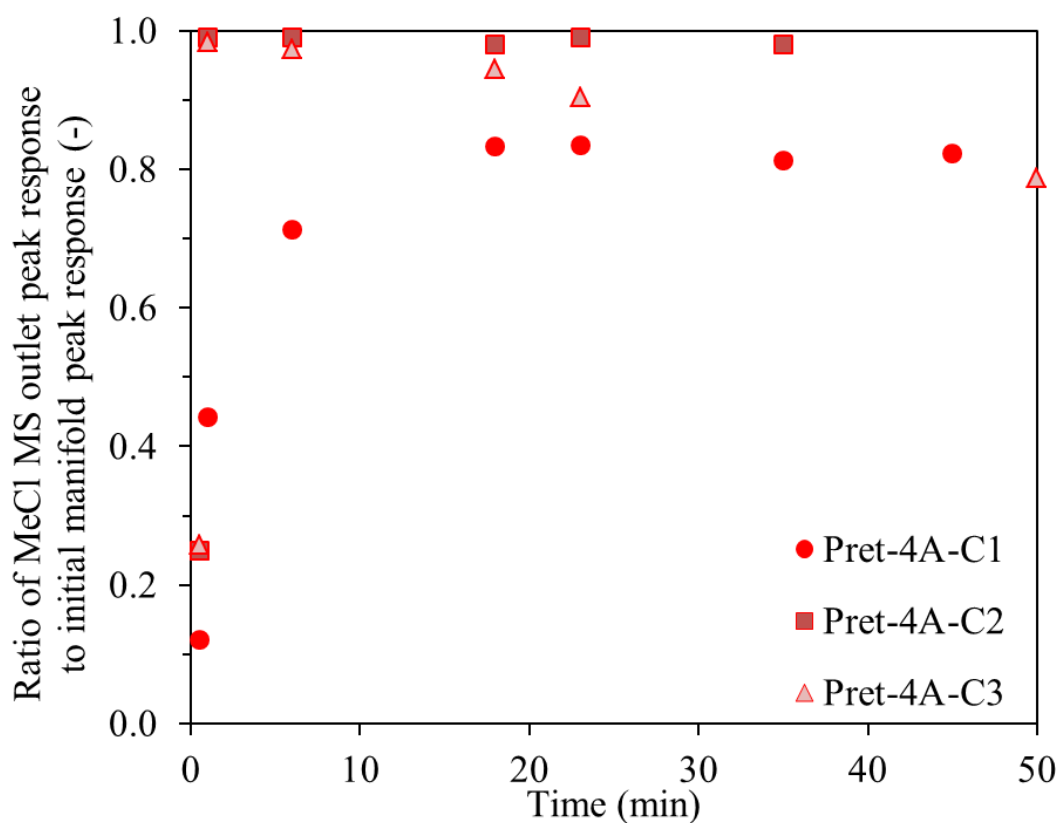


Fig. 7.16. Ratio of MeCl outlet peak response to the initial manifold peak response following continuous flow experiments of binary mixtures on Pret-4A

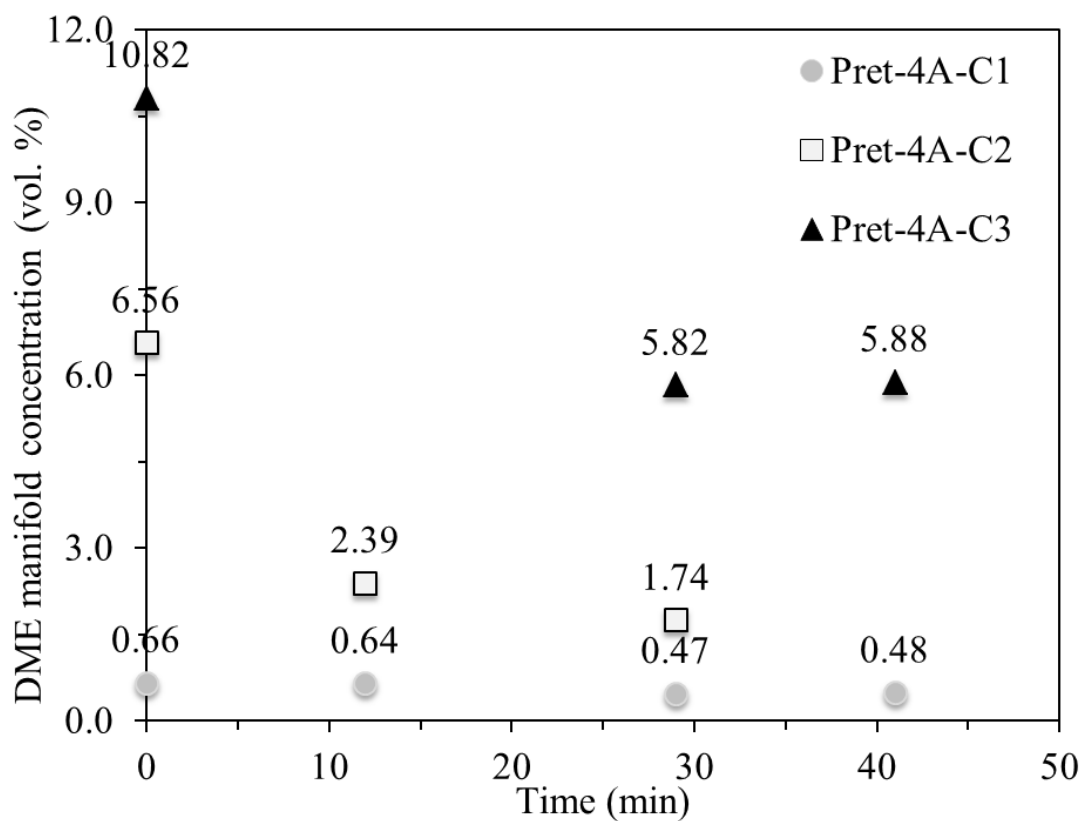


Fig. 7.17. DME manifold concentration following continuous flow experiments of binary mixtures on Pret-4A

Fig. 7.17 shows respective DME concentrations in the manifold at different time intervals following continuous flow of the binary mixtures. As can be seen with time in each case the DME concentration drops due to adsorption uptake by the adsorbent with the overall trend favouring a greater DME concentration for increased uptake. From the collective data it is clear that although the entire mixture was not adsorbed by the solid there was strong evidence to support competing adsorption and molecular sieving effects in favour of the overall project aim. For this to be true it is assumed that the bed is well packed with minimal voidage and that once the gas mixture flows through the packed bed all adsorbate molecules interact with some at least part of the adsorbent particles. This is because it is believed that no one adsorbate molecule would pass through the bed without contacting any part of any adsorbent particle. By which point as the bed saturates top down, it becomes harder for larger molecules to penetrate towards the outlet within the conditions considered. The molecular sieving effects are plausible since MeCl has the molecular dimensions to penetrate through pores whereas DME becomes excluded. It is accepted that for molecular sieving effects to occur the molecular geometry of the molecules must be precise to the dimensions of the pore opening with the consideration of interparticle void spaces but theoretically and through literature this is realistic for the case considered. Moreover, if we recall the adsorbent is a low surface area solid with its function depicted by its name (zeolite molecular sieve) therefore from the commencement of flow the adsorbent becomes saturated top down. As a result the slow drop in DME concentration with time (after 10 min) can be explained by the slow penetration of the DME into the adsorbent towards the bottom region of the bed. This would make sense because the continuous flow of the mixture reached a relative steady after 7 min meaning there was no definitive adsorption driving force in terms of pressure, temperature or concentration.

Ultimately the binary adsorption results on Pret-4A provided concrete evidence of selective adsorptive separation of DME from MeCl-DME binary mixtures even at DME concentrations as low as 0.66 vol. % (within the range of the industrial gas under investigation). This confirms the suitability of molecular sieve 4 Å for the purification of DME from MeCl streams. The following scientific explanation on how and why this selective adsorptive separation occurs is summarised below through the experimental results obtained and applied theoretical knowledge:

- Initially from the commencement of flow the mixture flows rapidly at high pressure meaning the A-S contact time is very short owing to the adsorbent cage like structure therefore not all molecules have enough contact time to actually adsorb at a particular adsorption site. Consequently molecular sieving effects occur because MeCl molecules pass through the bed via pores/voids to the AC outlet whereas DME penetrates the solid where possible but is excluded from the pores due to its large size.

- Simultaneously DME and MeCl molecules adsorb with former adsorbing faster due to its faster adsorption kinetics meaning MeCl takes double the time to adsorb the same amount within the same time frame;
- MeCl adsorbs through very weak dipole-dipole interactions therefore depending upon the pressure of the incoming mixture MeCl molecules potentially adsorb/desorb with the oncoming mixture whereas DME adsorbs more strongly through mainly hydrogen bonds;
- Some MeCl displacement by DME is feasible but favourable with an increased DME concentration for greater competing effects particularly since MeCl is more volatile therefore more susceptible for displacement;
- The adsorbent is saturated at the equilibrium time with respect to the conditions. The adsorbent has a greater adsorption capacity if operated at a higher pressure as shown by the respective pure component isotherms. But the reason the adsorbent becomes saturated and adsorption is slow with time is because molecules have less mobility to adsorb at weaker adsorption sites i.e. insufficient activation energy to adsorb.

7.3.5.2 Zeolite 5A

Two experiments with different DME concentration were conducted on zeolite molecular sieve 5A, which are summarized along with the operating conditions in Table 7.5.

Table 7.5. Conditions for continuous flow adsorption of binary mixture on Pret-5A

	Pret-5A-C1	Pret-5A-C2
Initial manifold pressure, <i>psiA</i>	38.5	43.7
Temperature, °C	23.1	22.6
Mass of adsorbent, <i>g</i>	0.35	0.35
DME GC calibration conc. (vol. %)	1.60	5.70
DME MS calibration conc. (vol. %)	1.65	5.76

Fig. 7.18 show the GC and MS spectrums for samples taken from the AC outlet after 1 min and 7 min, respectively from experiment Pret-5A-C2. As can be seen by both figures unlike with Pret-4A DME appears in the GC or MS spectrums at the respective times. Similar behaviour was observed with other experiments using this adsorbent with DME present at the outlet within the first 7 min of flow. Shown by the GC peak at 4.01 min MeCl was always present in measurable amounts with a significant abundance and numerical peak area at each sample time.

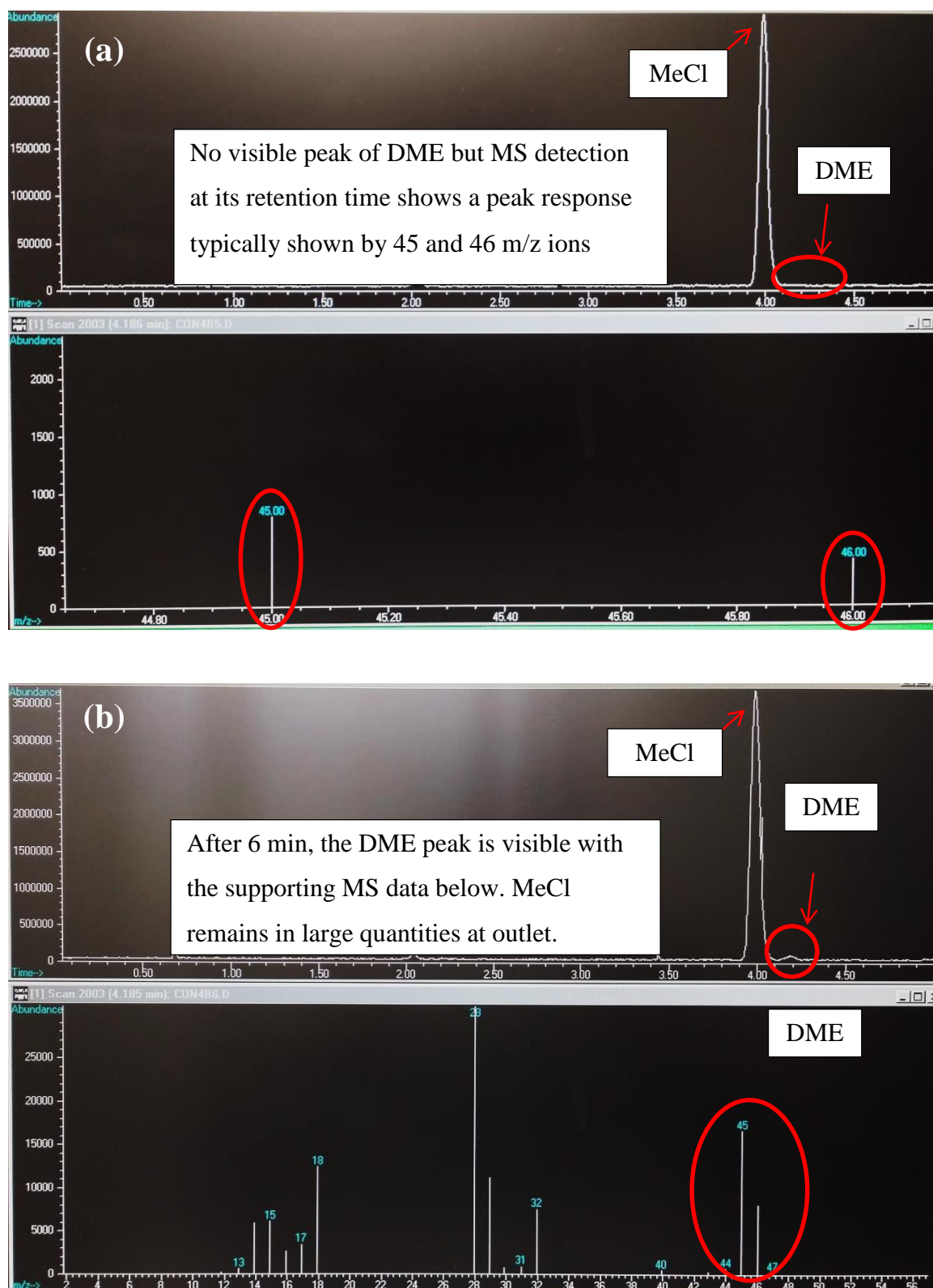


Fig. 7.18. GC and MS spectrums for AC outlet concentration for Pret-5A-C2, a) after 1 min and b) after 7 min from commencement of binary mixture flow

Fig. 7.19 shows the AC outlet concentrations for DME from 0–50 min for the two experiments. In both cases it can be seen that DME was detectable at the outlet following commencement of flow especially within the first 7 min of flow where the pressure was the main adsorption driving

force. After 7 min the concentration of DME reduced which was due to its release to vent. Unlike continuous binary flow on Pret-4A adsorption on Pret-5A exhibited non adsorptive separation behaviour. Similarly, Fig. 7.20 quantifies the ratio MeCl at the outlet to the initial manifold peak response at different time intervals. It is evident that unlike Pret-4A the ratios are much lower largely due more adsorption occurring on the highly microporous solid.

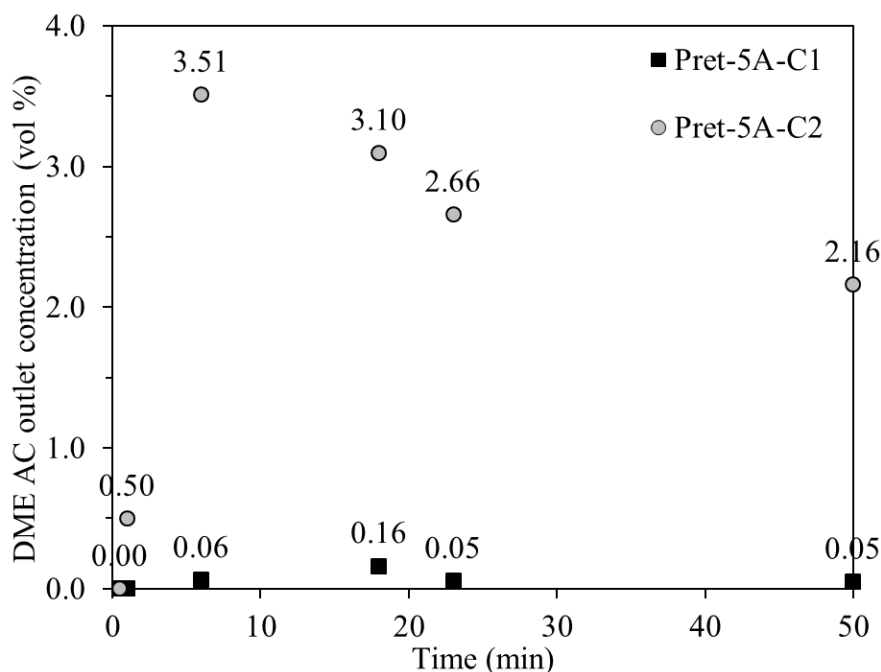


Fig. 7.19. DME manifold concentrations for two continuous flow run experiments on Pret-5A where (a) C1 and (b) C2

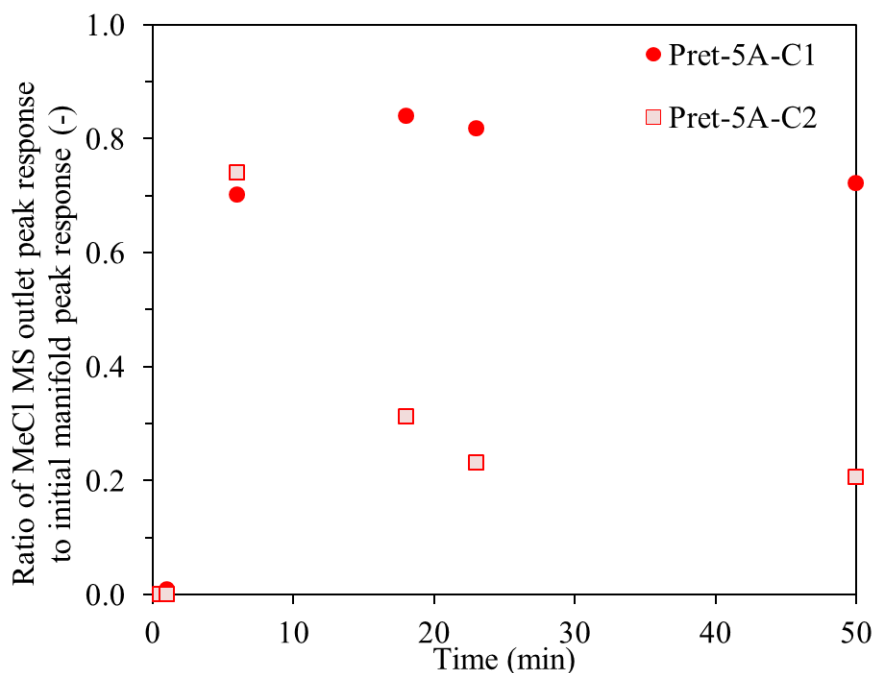


Fig. 7.20. MeCl MS AC outlet peak ratio to initial manifold peak following continuous flow of binary mixture on Pret-5A where (a) C1 and (b) C2

It is believed that in both cases initially the mixture is rapidly adsorbed whilst some molecules pass through pores/voids to the AC outlet. As the adsorbent becomes saturated more molecules pass through the adsorbent bed and or diffuse through to the outlet. Adsorption on this adsorbent occurs simultaneously due to the respective A-S interactions and some molecular sieving effects, especially the former. In conclusion following binary mixture continuous flow adsorption on the adsorbent there is evidence of competing DME and MeCl adsorption but no proof in terms of being able to exploit the parameters/conditions for separation of the mixture.

7.3.5.3 Si35-70

Two experiments with different DME concentrations were conducted on Pret-Si35-70; the largest surface area of all silica gels used. Table 7.6 shows the respective operating conditions.

Table 7.6. Conditions for continuous flow adsorption of a binary mixture on Pret-Si35-70

	Pret-Si35-70-C1	Pret-Si35-70-C2
Initial manifold pressure, <i>psiA</i>	41.2	41.1
Temperature, °C	22.5	22.0
Mass of adsorbent, <i>g</i>	0.35	0.35
DME MS calibration conc. (vol. %)	0.66	5.30

Fig. 7.21 shows the DME outlet concentration with time, Fig. 7.22 shows the ratio of MeCl at the outlet to the initial manifold quantity and Fig. 7.23 demonstrates the DME manifold concentration with time. In both experiments it can be seen that DME was detected at the outlet after at least 18 min even with a DME concentration in a mixture as low as 0.66 vol. %. The slow appearance at the outlet is explained by a lack of mobility of particularly DME molecules in the mixture and dominant MeCl adsorption into the pores due to its high concentration. The adsorbent becomes saturated from the top of the bed down therefore with time during steady state equilibrium (> 7 min) the non-adsorbed molecules pass through the interparticle voids towards the outlet. As the adsorbent becomes saturated with co-operatively adsorbed MeCl molecules there are fewer free adsorption sites for the DME molecules as a result molecules require more energy to adsorb onto weaker sites and consequently penetration to the outlet. As shown by the ratio of MeCl at the outlet the ratio is much lower, than that of the zeolite due to greater adsorption and no molecular sieving effects. Fig. 7.23 shows that a lower concentration of DME in the mixture has less competing effects for its uptake, which was observed with all adsorbents. With a higher concentration the molecules are able to compete with other MeCl molecules for adsorption sites unless given time for potential displacement. Ultimately for the conditions considered on the adsorbent there appears to be some evidence of a concentration gradient of DME across the bed due to reasons mentioned above but no definitive adsorptive separation. Although there is some evidence of mixture separation during continuous flow further investigations are required which are proposed in Chapter IX.

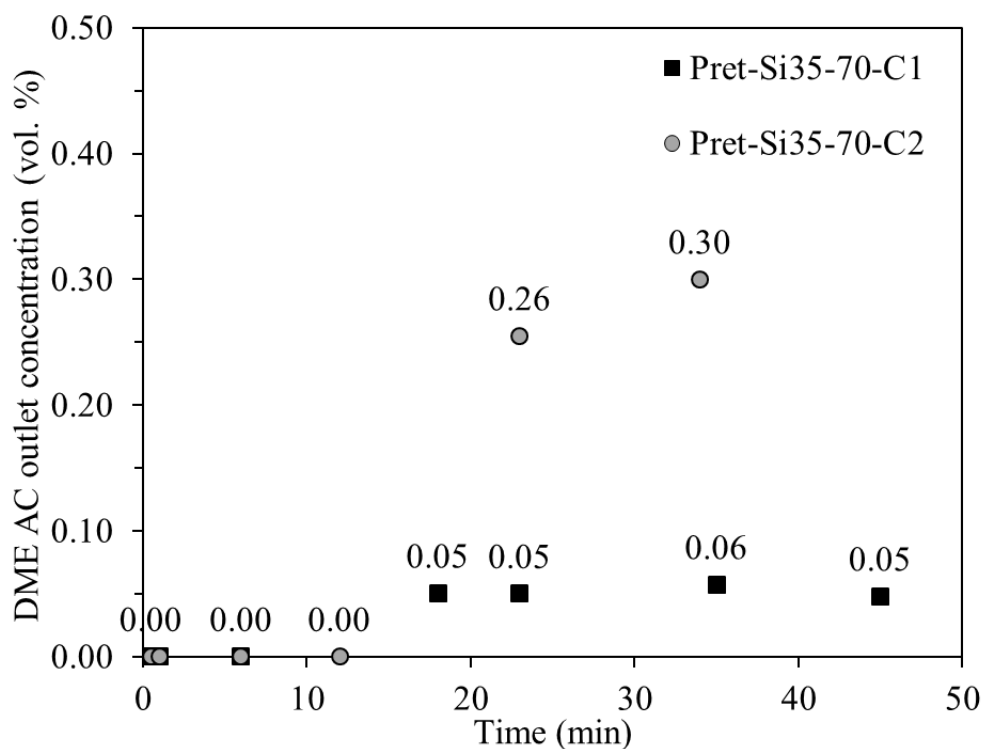


Fig. 7.21. DME AC outlet concentration following continuous flow experiments of binary mixtures on Pret-Si35-70

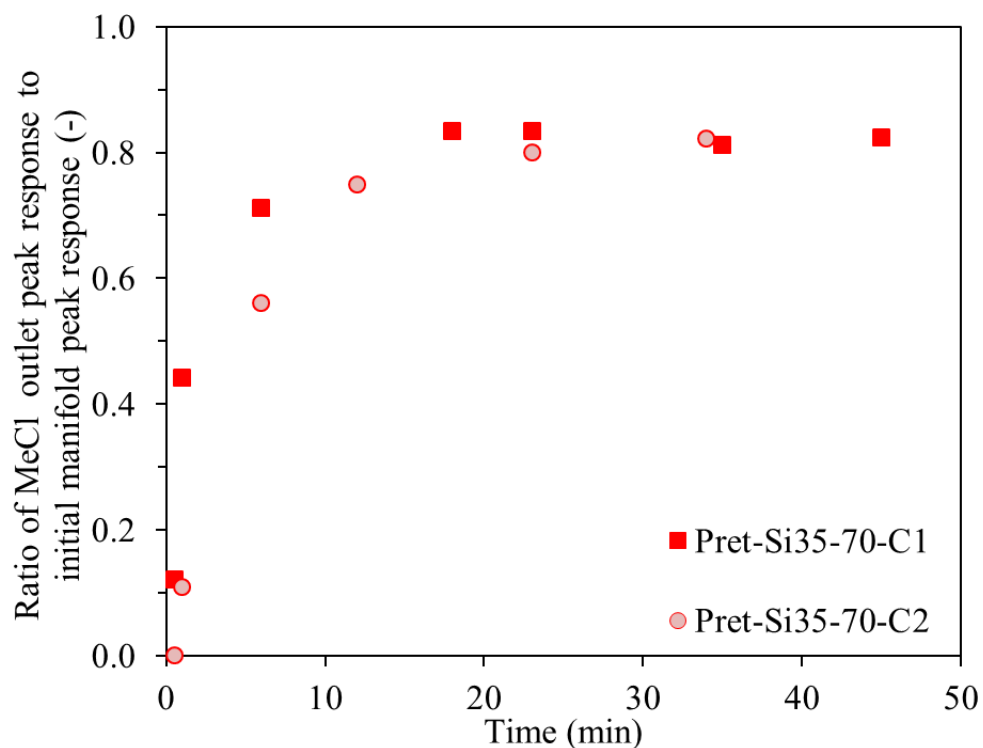


Fig. 7.22. Ratio of MeCl outlet peak response to the initial manifold peak response following continuous flow experiments of binary mixtures on Pret-Si35-70

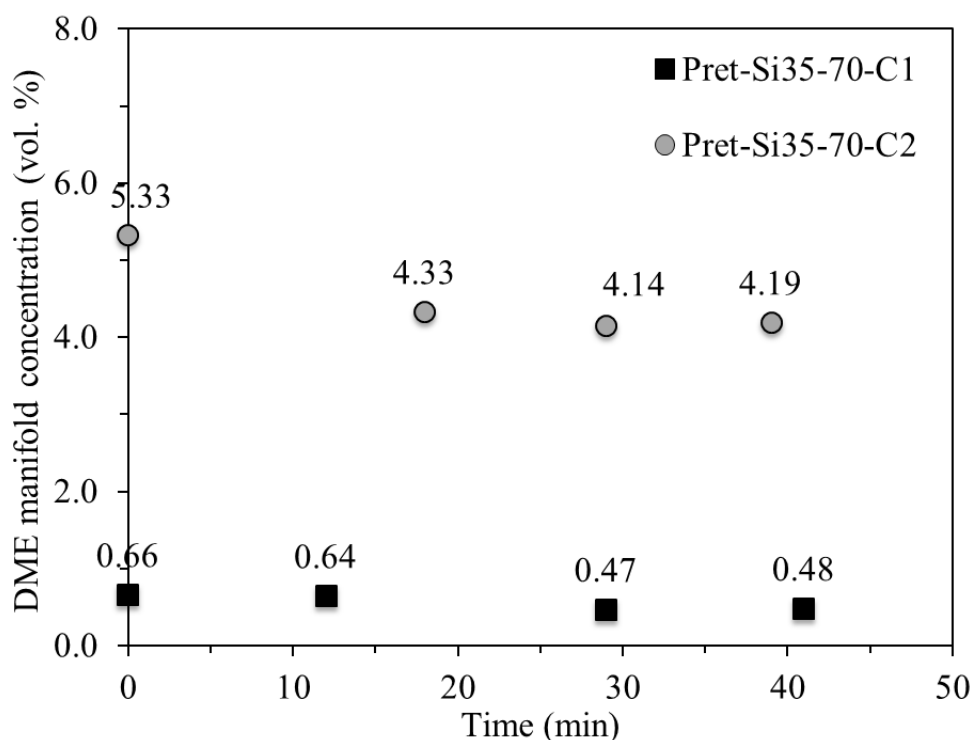


Fig. 7.23. DME manifold concentration following continuous flow experiments of binary mixtures on Pret-Si35-70

7.3.5.4 SiAmor

Two experiments with different DME concentrations were conducted on Pret-SiAmor, which are summarized along with the operating conditions in Table 7.7. Fig. 7.24 shows the AC outlet concentrations for DME from 0–50 min for the two experiments. In both cases it can be seen that for the concentrations of DME considered a consistent quantity was detectable at the outlet after at least 18 min following the commencement of flow. In both cases no DME was detected at the outlet during at least the first 12 min. On the other hand, MeCl was detectable in measurable quantities at the outlet even after 30 s (Pret-SiAmor-C2). The lower ratio of Pret-SiAmor-C1 was due to the reduced opening of the inlet valve. As shown by Fig. 7.26 the DME manifold reduces slowly due to slow adsorption meaning adsorption is dominated with bulk MeCl. It is believed adsorption follows the same adsorption behaviour as Pret-35-70 for reasons mentioned earlier.

Table 7.7. Conditions for continuous flow adsorption of binary mixture on Pret-SiAmor

	Pret-SiAmor-C1	Pret- SiAmor -C2
Initial manifold pressure, <i>psiA</i>	39.0	39.4
Temperature, °C	21.7	22.2
Mass of adsorbent, <i>g</i>	0.45	0.35
DME MS calibration conc. (vol. %)	1.52	2.06

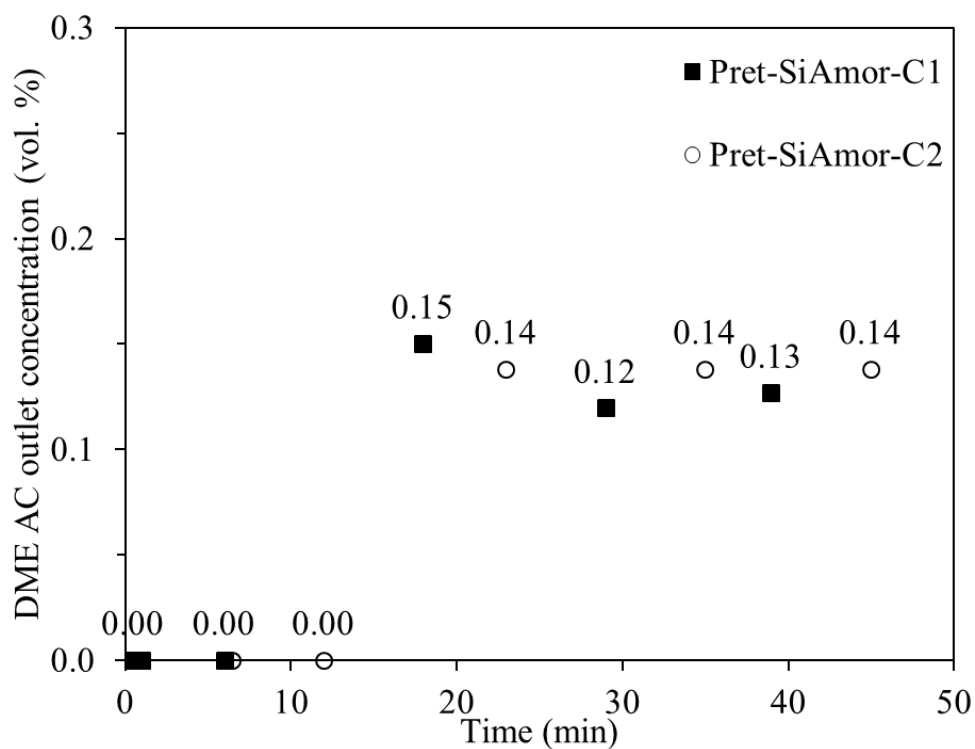


Fig. 7.24. DME AC outlet concentration following continuous flow experiments of binary mixtures on Pret-SiAmor

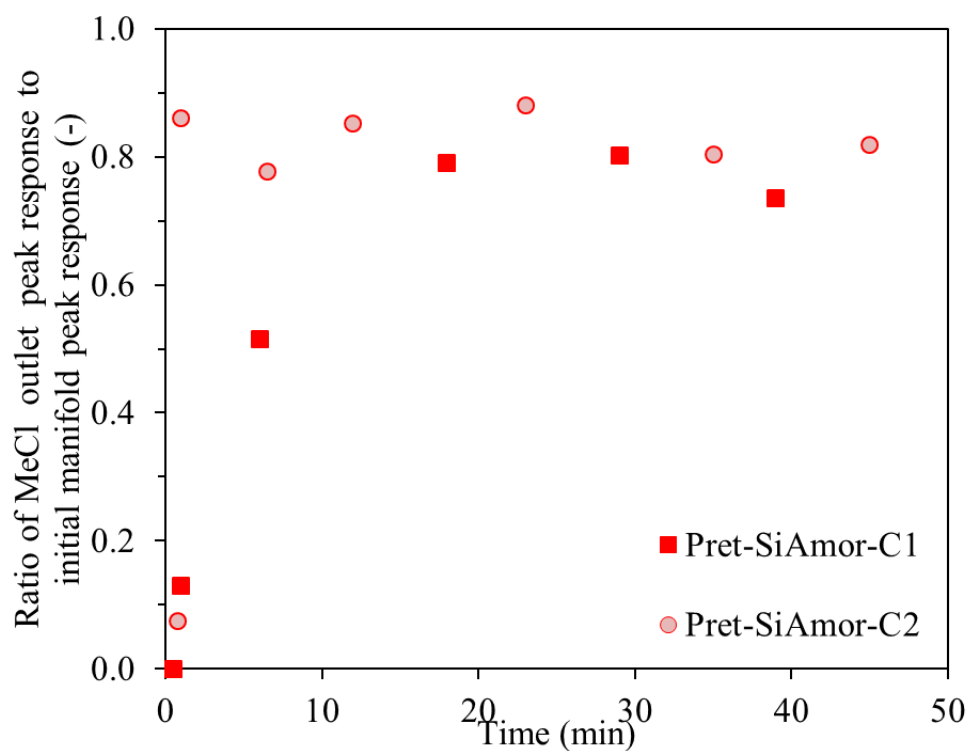


Fig. 7.25. Ratio of MeCl outlet peak response to the initial manifold peak response following continuous flow experiments of binary mixtures on Pret-SiAmor

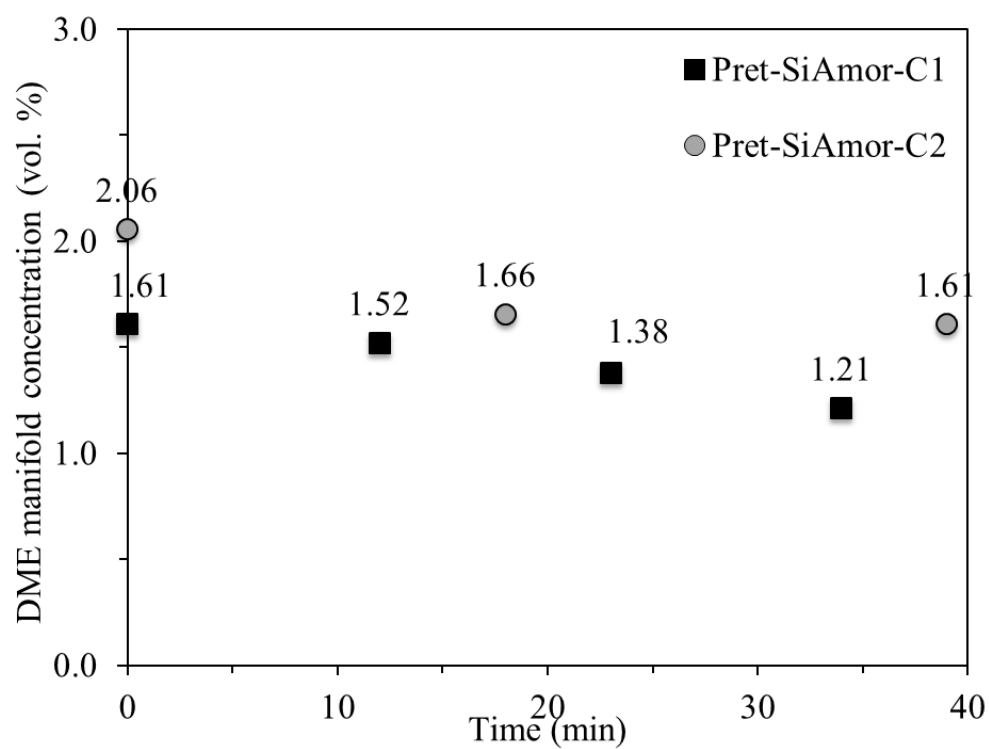


Fig. 7.26. DME manifold concentration following continuous flow experiments of binary mixtures on Pret-SiAmor

7.3.5.5 Si35-60

One experiment with a DME concentration of 1.49 vol. % in a MeCl stream was analysed for binary adsorption on Pret-Si35-60. The initial manifold pressure was 41.0 psiA at a temperature of 22.2 C adsorbed onto 0.35 g of adsorbent. Fig. 7.27 shows the MeCl outlet ratio to the initial quantity on the left y-axis and the DME outlet concentration on the right y-axis. As can be seen DME was detected at the outlet after at least 18 min at a concentration > 0.11 vol. %. No DME was detected during the initial continuous flow of the mixture. The DME manifold concentration was 1.28 vol. % after 40 min suggesting limited DME adsorption due to bulk MeCl adsorption. The lack of DME adsorption and lack of presence in the early stages is due to reasons explained earlier with the above silica gels regarding molecules mobility and competing effects.

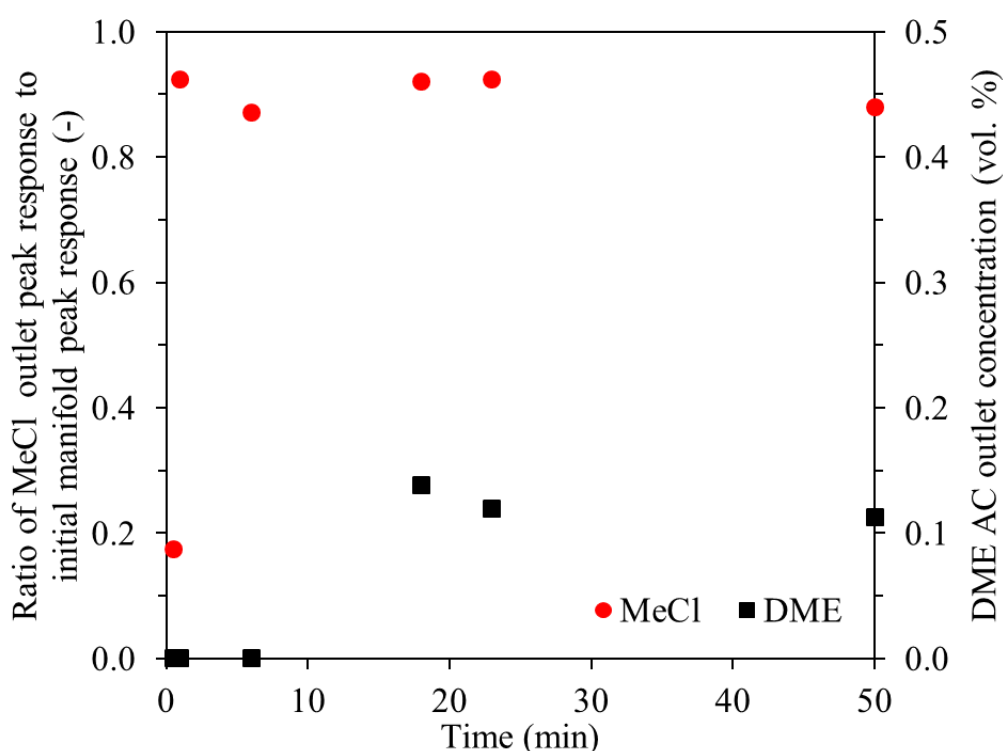


Fig. 7.27. MeCl MS AC outlet peak ratio to initial manifold peak (left y-axis) and DME outlet concentration following a continuous flow of binary mixture on Pret-Si35-60 (right y-axis)

7.3.6 Desorption

7.3.6.1 Zeolite 4A

TSD and PSD experiments were carried out on the aforementioned adsorption experiments following adsorption analysis. For TSD analysis after equilibrium the AC region was heated and the manifold DME concentration was analysed at different temperature increments. The fundamental issue with the above was since there was no constant pressure control, molecules desorbed due to the increase in temperature and consequential increasing in pressure. On the other hand, PSD was carried out by isolating the two regions following equilibrium then manually removing a portion of the manifold quantity using the MV; thereafter the regions were allowed to equilibrium. Whilst the temperature increased MeCl quantities were seen to increase through the MS peak response however the magnitude of desorption could not be qualitatively quantified. Fig shows the TSD analysis following continuous flow adsorption of a mixture initially containing 0.41 vol %.

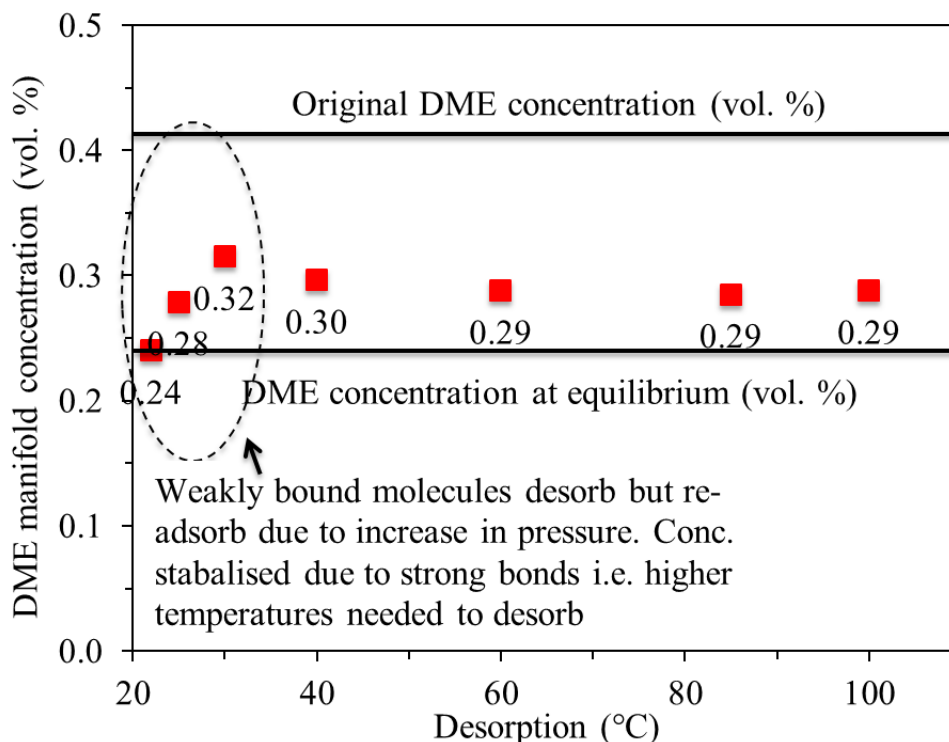


Fig. 7.28. TSD analysis from 20-100 °C for DME manifold concentration using Pret-4A

Following equilibrium the manifold concentration of DME was 0.24 vol. % due to lack of adsorption sites/mobility and due to the adsorbent being saturated with MeCl. Nevertheless the AC was heated up to 100 °C whilst measuring the DME concentration in the manifold at different temperature increments. As can be seen with increasing temperature up to 30 °C (0.32 vol. %) some DME initially became desorbed thus increasing its concentration of molecules within the manifold. However as the temperature increased so did the pressure, this meant both adsorbates

desorbed and potentially re-adsorbed. It is plausible that the MeCl desorbed more easily due to weaker bonds therefore vacated some sites for re-adsorption of DME. With increasing temperature the concentration of DME remained relatively constant from 40 - 100°C meaning adsorption of DME on the adsorbent was dominated by much stronger interactions at strong adsorption sites meaning higher temperatures are required for complete removal.

Fig. 7.29 shows the PSD analysis of the DME concentration in the manifold when the initial DME manifold concentration was 2.06 vol. % and the final equilibrium concentration of DME in the manifold was 1.61 vol. %. With PSD the trend was expected to increase in terms of concentration but due to the system limitations this meant by removing a portion of the manifold quantity the overall DME desorbed quantity could not be qualitatively quantified. By removing a portion of the gas from the manifold in order to carry out pressure swing, this resulted in both MeCl and DME leaving the bulk consequently affecting the overall concentration with respect to the initial concentration and total number of moles.

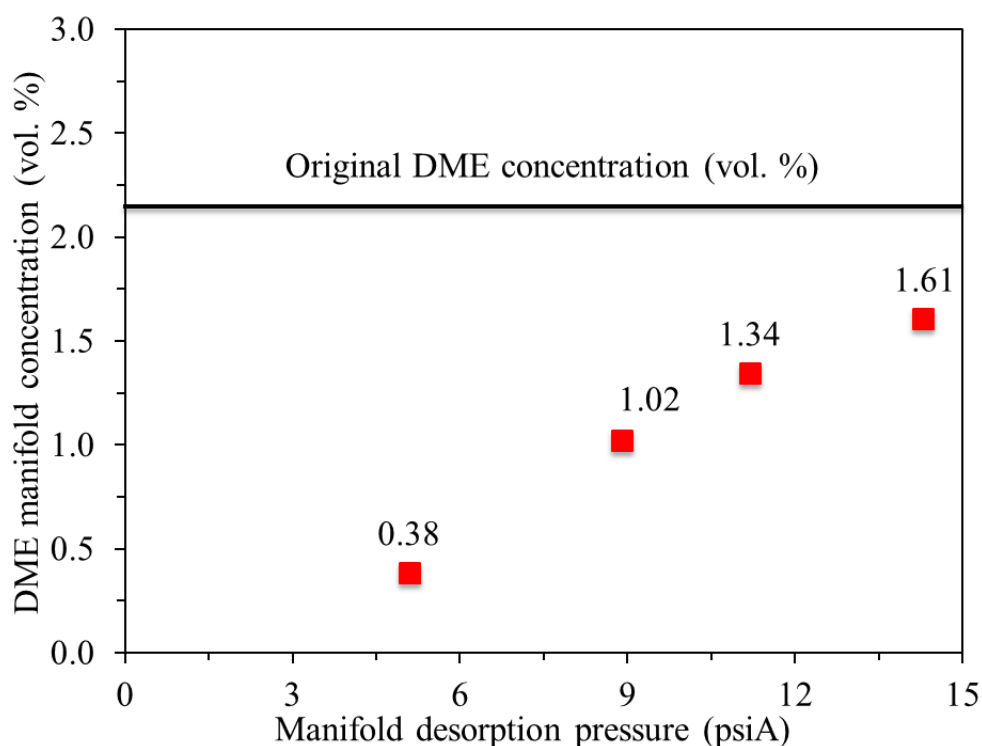


Fig. 7.29. PSD analysis for DME manifold concentration using Pret-4A

7.4 Summary

The following summarises the key findings from the chapter. For the batch fixed bed mode binary gas mixture adsorption on Pret-4A:

- The adsorbent demonstrated clear purification behaviour of a MeCl stream containing DME with no DME outlet detection after 15 or 30 min whereas MeCl was detectable in measurable amounts.
- The adsorption efficiency of experiments demonstrated the adsorbent was effective at removing over one third of the original DME concentration with the rest being MeCl, with respect to the conditions.
- Some evidence of MeCl displacement with DME was observed over a longer equilibrium time however the observation requires further analysis.
- Although both DME and MeCl both adsorb onto the solid, DME was not observed at the outlet due to steric effects with the molecule being larger than the acceptable pore openings. Furthermore since the adsorbent becomes saturated from the top of the bed down, molecules were unable to penetrate/diffuse through easily within the conditions considered.

Batch fixed bed binary mixture adsorption on Pret-5A:

- All experiments demonstrated evidence of small quantities of DME and large amounts of MeCl at the AC outlet. This was due to both molecules adsorbing and being within the acceptable pore opening range for molecular sieving effects, thus demonstrating lack of suitability for purification through steric effects.

Batch fixed bed binary mixture adsorption on Pret-Si35-70:

- DME was detected in small quantities at the outlet with large amounts of MeCl thus demonstrating lack of suitability for adsorptive separation. Here adsorption was driven by thermodynamic equilibrium over kinetic or steric effects.

Continuous flow of a binary mixture adsorption on Pret-4A:

- The GC and MS revealed adsorptive purification of DME from MeCl streams through the presence of the MeCl peak and vanishing of DME peak at the AC outlet at different time intervals for up to at least 12 min.
- Strong evidence of selective adsorptive separation of DME from MeCl-DME binary mixtures was observed even at DME concentrations as low as 0.66 vol. %; within the range of the industrial gas under investigation.

- Trace DME quantities were detected at the outlet after 18 min following continuous flow of mixture believed to be due to slow penetration of the gas through the interparticle voids and lack of a driving degree of freedom (P , T , C).
- Purification of MeCl occurs because of adsorption and steric effects. Whilst both adsorbates adsorb due to the respective physisorption bonds, DME is more strongly bound at a faster rate whilst being excluded from the pores meaning it is unable to reach the outlet.
- In a continuous flow process with a short A-S contact time it is believed that MeCl would pass through the bed adsorbing minimally whereas DME would adsorb due to the faster kinetics and stronger heat of adsorption.

Continuous flow of a binary mixture adsorption on Pret-5A:

- There was evidence of competitive co-adsorption of DME and MeCl but no proof in terms of exploitable parameters/conditions for separation a mixture. Similar to the batch mode adsorption both molecules adsorbed and penetrated through the pores especially at earlier time intervals, ~ 1 min, thus confirming the adsorbent's lack of suitability for the purpose.

Binary gas adsorption on Pret-Si35-70, Pret-SiAmor and Pret-Si35-60:

- In each case, DME was observed to be at the AC outlet after at least 18 min with increasing quantities thereafter. Whilst DME was not detected at earlier intervals this was believed to be due to rapid adsorption into the solid and the presence of large concentrations of MeCl.
- Similar to batch mode adsorption, adsorption on these adsorbents is driven by equilibrium and not kinetic or steric effects therefore unsuitable under the conditions considered.

Binary gas desorption analysis on Pret-4A:

- TSD and PSD resulted in evidence of some DME desorption from the adsorbent into the manifold region. However due to system limitations qualitative quantification of both gases was un-obtainable. Recommendations to overcome such issues are listed in the following chapter.

Whilst binary adsorption on the zeolite 5A and silica gels demonstrated co-adsorption of both molecules it is feasible for separation through selective desorption or exploitation of the kinetics or strength of interactions. The aforementioned would however require further study.

CHAPTER VIII: CONCLUSIONS

This research was mainly focused on the experimental adsorption/desorption to investigate the potential purification of MeCl streams containing DME impurities using various types of adsorbent materials. Irrefutably, there was strong evidence to propose zeolite molecular sieve 4 Å for adsorptive MeCl purification. From the pure component analysis on both as received and thermally pre-treated adsorption isotherms DME and MeCl exhibited evidence of Type II and I isotherm classifications on zeolite 4A. As reported the difference in type was attributed to the molecular dimensions of the molecules playing a key role. It was also recognised that the presence of moisture within the zeolites framework resulted in repulsive forces towards MeCl due to the adsorbates polarity. On the other hand, DME adsorbed relatively co-operatively in the presence of moisture due to the adsorption being dominated by hydrogen bonding. Irrespective of thermal pre-treatment, DME was observed to have faster adsorption kinetics than MeCl whilst adsorbing heterogeneously with a stronger strength of interaction whereas MeCl adsorbed homogeneously. In addition the empirical model parameters for the Langmuir and Freundlich models supported the reported behaviour through obtained parameters i.e. DME had a larger rate constant than MeCl on 4A.

The results from the pure component adsorption data was further supported by the results obtained from the batch and continuous flow binary gas adsorption experiments. It was observed through the batch and continuous flow binary gas adsorption experiments that competitive co-adsorption of DME and MeCl occurs with molecular sieving effects whereby the larger DME molecules were excluded from penetrating the pore opening and consequently resulting in purified MeCl to appear at the AC outlet. Of the tested mixtures, from the adsorption efficiency calculations it was clear that the adsorbent was effective at removing over one third of the original DME concentration from the manifold (without its presence at the AC outlet), whilst adsorbing up to 40 % of the initial MeCl concentration for the conditions considered. The lack of adsorption of the binary mixture in the manifold was due to the equilibrium time and insufficient mobility of adsorbate molecules to adsorb at weaker adsorption sites. Furthermore, it was believed that the adsorbent bed became saturated from the top down as expected which resulted in the pores becoming occupied and or blocked meaning suitably DME was unable to the AC outlet within the conditions considered.

It is postulated that for a binary mixture flowing through a packed bed of vacuum and thermally pre-treated zeolite 4A MeCl molecules penetrate through the pores to the outlet whilst adsorbing minimally due to the weak dipole-dipole interactions. As a result the strength of interactions are so weak that a simple flush with more inlet gas at high pressure (or vacuum) could potentially

desorb some molecules and adsorb further. On the other hand, DME is suitably unable to penetrate through the adsorbent bed due to the steric effects but adsorbs via stronger hydrogen bonding whilst diffusing into the solid at least twice as fast as MeCl.

In terms of comparison to industry and potential of scale up, DME and MeCl adsorption can be closely likened to the industrial kinetic based separation of N₂/O₂ mixtures on a zeolite 4A whereby DME and N₂ are alike and MeCl and O₂ are alike:

- N₂ is the larger molecule and is excluded from the pores whilst this is the case with DME. Consequently O₂ is smaller therefore passes through the zeolite cages to the outlet as observed with MeCl.
- N₂ is more polarisable than O₂ as is the case with DME over MeCl.
- N₂ has a faster diffusion rate into the solid than O₂; ~ 3 - 4 times faster whereby DME adsorbs at least twice as fast as MeCl.
- N₂ adsorbs more strongly ~ 24 kJ mol⁻¹ with a similar value for DME on Pret-4A and O₂ adsorbs ~ 15 kJ mol⁻¹ whereby MeCl adsorbs with a less value ~ 10 kJ mol⁻¹.

Along with the aforementioned conclusions the following conclusions have been made with respect to the overall project objectives:

- A self-designed, constructed and commissioned gas purification rig capable of pure component and binary gas adsorption/desorption analysis was successfully used to investigate the purification of DME from mixtures containing MeCl.
- The different adsorbents used were characterised using BET, TGA, SEM and EDXA analyses.
- Pure component adsorption/desorption was carried out for DME and MeCl on six different adsorbents namely: zeolite molecular sieves 4 Å and 5 Å; silica gels: amorphous, 35-70 mesh and 35-60 mesh and granular activated carbon 8-12 mesh following different pre-treatment conditions.
- All pure component results were chiefly analysed through adsorption/desorption isotherms, empirical adsorption modelling, adsorption kinetics and diffusion models and calorimetric heat of adsorption analysis.
- Binary gas adsorption was investigated on the different thermally pre-treated adsorbents in batch fixed bed and continuous flow mode for various concentration mixtures containing DME (0.4 - 10.0 vol. %) as the low concentration impurity in MeCl streams.
- Qualitative and quantitative binary adsorption analysis was carried out using a calibrated GC-MS system for the DME concentration in the manifold and AC outlet at different

time intervals. Similarly, MeCl was quantified through its detected peak response at the respective time to the initial peak response prior to adsorption.

- Essentially the overall project objective was satisfied with respect to the original task in terms of reaching strong favourable conclusions and starting from nothing into constructing a novel sorption rig capable of various analyses.

The following conclusions are defined with the view to satisfy the company objectives:

- Compared to the current technology used to purify MeCl, a potential adsorption/desorption process using the promising zeolite 4 Å molecular sieve would typically require a single batch of adsorbent capable of numerous regenerations. As opposed to transporting large acid and waste quantities over long distances.
- Only DME and MeCl gases were used in this process with no potential implications of toxic side products. Furthermore, the adsorbent could in theory adsorb trace quantities of MeOH and water; typically found in MeCl streams, which is highly favourable for the silicone industry.
- A potential adsorption/desorption technology has fewer associated costs to the process than the existing technology i.e. re-usable adsorbent, no CO₂ emissions, no toxic side products or waster products. More importantly with a separate DME stream this could allow Dow Corning to sell or utilise a highly useful gas for hydrogen gas production or react using a γ-alumina catalyst to produce more MeCl [134].
- A potential adsorption/desorption process would be substantially greener than the existing purification process since the process uses only two key components the MeCl stream and the solid adsorbent i.e. << 2 tonnes CO₂ / tonne of DME removed.
- An adsorption/desorption process is highly suitable for large scale processing but dependent upon the amount of adsorbent required with respect to regenerations. For this further investigations are required especially for binary desorption products.

CHAPTER IX: FUTURE WORK AND RECOMMENDATIONS

Overall this study investigated a wide range of adsorbents (zeolites, silica gels and activated carbon) and demonstrated for the first time potential to purify MeCl streams containing DME impurities using adsorption/desorption separation under different adsorbent pre-treatment and adsorption operating conditions. The study also revealed for the first time the adsorption isotherms, empirical and kinetic models and heats of adsorption for the respective A-S interactions. The following recommendations are made with respect to improve the experimental aspects of the work carried out. Implementation of the following would result in more accurate qualitative quantification of adsorption/desorption:

- **Online GC-MS/TCD:** this would be ideal to especially determine molecular sieving effects when passing a mixture stream over the adsorbent for different run times. On the other hand, would be useful for PSD and TSD, since the system was sensitive to small changes in conditions.
- **The custom built heating and cooling block for the FlowCat AC with a heater/chiller and circulating fluid:** more sensitive temperature control would allow more accurate temperature control during sorption and used for obtaining isotherms over a wider temperature range (-20 - 100 °C). Moreover the custom built block would minimise heat losses, which are detrimental for calorimetric measurements.
- **A more sensitive pressure gauge in manifold and additional pressure gauge for AC line:** this would allow for more accurate quantification of amounts adsorbed. The additional pressure gauge would allow for the true equilibrium position to be recognised between the two regions.
- **Mass flow meter at inlet and outlet:** could be used to accurately determine flow rates, effect of adsorption, saturation and use for recycles streams.
- **Operation in fluidised/circulating fluidised mode:** would improve the heat and mass transfer of adsorbate molecules with the adsorbent.

Whilst it has been proven that DME can effectively be completely removed from a mixture of MeCl and DME. To ultimately determine the viability of this as a commercial process the following points are addressed with the view to satisfy the company's key concerns/points:

- **Adsorbent capacity,**
 - **Optimal conditions for maximizing adsorption capacity:**
 - Thermally pre-treat adsorbent at higher temperature (~ 250 °C) in vacuum.

- Conduct adsorption/desorption at lower temperatures, as close to the boiling points of the gases as possible.
- Have less adsorption isotherm points but have a longer equilibrium time (30 min) especially for $P/P_0 < 0.2$.
- Increasing adsorbent surface area by crushing particles to observe for increased adsorption/molecular sieving effects.
- Ion exchanging the Ca^+ cations within the zeolite 5A adsorbent framework with Na^+ cations and thus reduce the pore diameter whilst substantially increasing the adsorbent surface area.
- Increasing the adsorption temperature could potentially increase the adsorption rate/diffusivity and reduce the equilibrium time however would decrease the capacity.
- **Composition of material adsorbed on adsorbent,**
 - **Optimal conditions for minimizing MeCl adsorbed:**
 - The effect of surface moisture was shown to reduce the MeCl adsorbed quantities, however presence of moisture results in an unwanted impurity and different A-S and A-A interactions.
 - Experimental batch adsorption/desorption experiments with varying concentrations of DME (0.5, 1.0, 2.0, 3.0, and 5 vol. %) and operating at ~ 1.5 and 3.5 atm. Using ideal gas laws to determine amounts sorbed and taking GC-MS samples at different time intervals.
 - Carry out similar experiments to above with less adsorbent.
 - **Understanding whether MeCl once adsorbed can be displaced by DME:**
 - Experimentally saturate adsorbent with MeCl then pass a flow of DME through the bed to observe the effect.
 - Similarly saturate adsorbent with DME and then pass a flow of MeCl through and compare the behaviour.
 - Further insight into displacement would be obtained from the above batch experiments whereby the DME concentration trend could be analysed for increasing displacement behaviour with increasing DME concentration and equilibrium time.
- **Desorption evaluation,**
 - **Can adsorption mechanism be used to affect differential desorption:**
 - Carry out single batch experiments and vary concentration of DME in mixtures (~ 0.5 - 5.0 vol. %) and operate at different pressures (~ 1.5 - 3.5 atm). Followed by subsequent desorption then quantify using Ideal gas laws and gas analysis for quantification.

○ **Conditions required for effective desorption:**

- Carry out PSD of pure components analysis, whilst observing the rate.
- PSD analysis following single batch binary mixture adsorption with online gas analysis.
- Saturate adsorbent with each respective gas at different pressures then carry out TSD to compare each pure component data at 1.0 - 3.0 atm.
- Carry out TSD experiments from batch binary experiments with different concentrations of DME in the mixture and using online gas analysis. However if the pressure is not controlled it would be raised resulting in simultaneous TSD and PSD.

The final recommendations are highlighted with respect to furthering the knowledge gap and potential exploitable avenues in and around this research:

- Since silanol groups favour DME over MeCl, by thermally pre-treating a silica gel adsorbent in vacuum (~ 1000 °C) it would result in a silanol groups (only) containing solid. Therefore the adsorbent could be potentially used to adsorb only/more DME than MeCl at a faster rate.
- For longer equilibrium time analysis less adsorption points (low resolution isotherm) could be used but for longer incremental equilibrium times in a manually operated volumetric adsorption/desorption system.
- DME and MeCl adsorption on all three silica gels appears to be due to its thermodynamic equilibrium position rather than a faster kinetic rate or any molecular sieving effects. Nevertheless according to the study by Saburina and Begun [133] simply flushing an inert gas could potentially separate the respective components due to the strength of interactions.
- Any chemisorbed O_2 or hydrogen imparts polar characteristics to the carbons thus influencing the adsorbents adsorption properties especially at low coverages therefore pre-treatment of the surface with the above then observing for adsorption/desorption behaviour for DME and MeCl, respectively.
- Adsorption on thermally pre-treated activated carbon at higher temperature to observe the effect of kinetic diffusivity and equilibrium for both adsorbates since it was reported that increasing the temperature increases the rate of MeCl adsorption [68].
- Carry out adsorption on CMS's with the same pore range since they have similar functions as a zeolite molecular sieve (4A).

REFERENCES

1. Ruthven, D.M., *Principles of adsorption and adsorption processes*. A Wiley-Interscience Publication. 1984, Canada: John Wiley & Sons, Inc.
2. Yang, R.T., *Adsorbents Fundamentals and Applications*. 2003, New Jersey: John Wiley & Sons, Inc.
3. Kowalewicz, A., Wojtyniak, M., *New alternative fuels for I.C. engines - A review*. Journal of KONES internal combustion engines, 2004. **11**: p. 358-368.
4. Kasaie, M., Sohrabi, M., *Kinetic study on methanol dehydration to dimethyl ether applying clinoptilolite zeolite as the reaction catalyst*. Journal of The Mexican Chemistry Society, 2009. **53**(4): p. 233-238.
5. Galvita, V.V., Semin, G.L., Belyaev, V.D., Yurieva, T.M., Sobyenin, V.A., *Production of hydrogen from dimethyl ether*. Applied Catalysis A: General, 2001. **216**: p. 85-90.
6. Semelsberger, T.A., Ott, K.C., Borup, R.L., Greene, H.L., *Generating hydrogen-rich fuel-cell feeds from dimethyl ether (DME) using physicochemical mixtures of a commercial Cu/Zn/Al₂O₃ catalyst and several solid-acid catalysts*. Applied Catalysis A: General, 2006. **65**: p. 291-300.
7. Faungnawakij, K., et al., *Hydrogen production from dimethyl ether steam reforming over composite catalysts of copper ferrite spinel and alumina*. Applied Catalysis B: Environmental, 2007. **74**(1-2): p. 144-151.
8. Gazsi, A., Ugrai, I., Solymosi, F., *Production of hydrogen from dimethyl ether on supported Au catalysts*. Applied Catalysis A: General, 2011. **391**: p. 360-366.
9. Wang, T., Li, Y., Ma, L., Wu, C., *Biomass to dimethyl ether by gasification/synthesis technology - an alternative biofuel production route*. Energy, 2011. **5**(3): p. 330-339.
10. Liu, D., Yoo, C., Zhanga, J., Fanga, D., Chenb, D., *Catalytic dehydration of methanol to dimethyl ether over modified γ -Al₂O₃ catalyst*. Fuel, 2011. **90**: p. 1738-1742.
11. Tan, Y., et al., *Modification of Cu-based methanol synthesis catalyst for dimethyl ether synthesis from syngas in slurry phase*. Catalysis Today, 2005. **104**(1): p. 25-29.
12. El-Nahas, A.M., Uchimaru, T., Sugie, M., Tokuhashi, K., Sekiya, A., *Hydrogen abstraction from dimethyl ether (DME) and dimethyl sulphide (DMS) by OH radical: A computational study*. Journal of Molecular Structure: THEOCHEM, 2005. **722**(1-3): p. 9-19.
13. Harper, K., Minofar, B., Sierra-Hernandez, M.R., Casillas-Ituarte, N.N., Roeselova, M., Allen, H.C., *Surface residence and uptake of methyl chloride and methyl alcohol at the air/water interface studied by vibrational sum frequency spectroscopy and molecular dynamics*. Journal of Physical Chemistry A, 2009. **113**: p. 2015-2024.
14. Lof, A., Wallen, M., Bard, J., *Methyl chloride*, in *Concise International Chemical Assessment 2000*, World Health Organization: Switzerland. p. 1-45.
15. McInroy, A.R., Lundie, D.T., Winfield, J.M., Dudman, C.C., Jones, P., Lennon, D., *Improved atom efficiency via an appreciation of the surface activity of alumina catalysts: Methyl chloride synthesis*. Applied Catalysis B: Environmental, 2007. **70**: p. 606-610.
16. Wei, Y.Z., D.; Liu, Z.; Su, B-L., *Mechanistic elucidation of chloromethane transformation over SAPO-34 using deuterated probe molecule: A FTIR study on the surface evolution of catalyst*. Chemical Physics Letters, 2007. **444**: p. 197-201.
17. Deng, S., *Sorbent technology*, in *Encyclopedia of chemical processing*. 2006, Taylor & Francis.
18. Parida, S.K., Dash, S., Patel, S., Mishra, B.K., *Adsorption of organic molecules on silica surface*. Advances in Colloid and Interface Science, 2006. **121**(1-3): p. 77-110.
19. Richards, J.R., *Adsorption*, in *APTI 415: Control of gaseous emissions*. 2000.
20. Miller, T.M., *Atomic and molecular polarizabilities*. CRC Handbook of Chemistry and Physics, 2000. **77**: p. 193-202.
21. Ertan, A., *CO₂, N₂ and Ar adsorption on zeolites*, in *Chemical Engineering*. 2004, Izmir: Izmir Institute of Technology.
22. Sircar, S., Myers, A.L., *Gas separation by zeolites*, in *Handbook of zeolite science and technology*. 2003, Marcel Dekker, Inc: New York.

23. Itodo, A.U., Itodu, H.U., Garfar, M.K., *Estimation of specific surface area using Langmuir isotherm method*. Journal of Applied Science Environmental Management, 2010. **14**: p. 141-145.
24. Itodo, A.U., Itodu, H.U., *Estimation of surface area using Langmuir isotherm methods*. Journal of Applied Science Environmental Management, 2010. **14**: p. 141-145.
25. Thomas, W.J., Crittenden, B.D., *Adsorption Technology and Design*. Technology and Engineering, ed. Butterworth-Heinemann. 1998, Oxford: Reed Educational and Professional Publishing Ltd.
26. Cuhadaroglu, D., Uygun, O.A., *Production and characterization of activated carbon from a bituminous coal by chemical activation*. African Journal of Biotechnology, 2008. **7**(20): p. 3703-3710.
27. Soto, M.L., Moure, A., Dominguez, H., Parajo, J.C., *Recovery, concentration and purification of phenolic compounds by adsorption: a review*. Journal of Food Engineering, 2011. **105**: p. 1-27.
28. Do, D.D., *Adsorption Analysis: Equilibria and Kinetics*, ed. R.T. Yang. 1999, Imperial College, UK: Imperial College Press.
29. Ackley, M., Rege, S., Saxena, H., *Application of natural zeolites in the purification and separation of gases*. Microporous and Mesoporous Materials, 2003: p. 25-42.
30. Bowen, T.C., et al., *Driving Force for Pervaporation through Zeolite Membranes*. Journal of Membrane Science, 2003. **225**: p. 165-176.
31. Oh, S.H., *Surface area, pore volume and pore size distribution from the gas sorption isotherm*. 2009. p. 1-33.
32. Ho, Y., Porter, J., McKay, G., *Equilibrium isotherm studies for the sorption of divalent metal ions onto Peat: Copper, Nickel and Lead single component systems*. Water, Air and Soil Pollution, 2002. **144**: p. 1-33.
33. Limousin, G.G., J-P.; Charlet, L.; Szenknect, S.; Barthes, V.; Krimissa, M., *Sorption isotherms: A review on physical bases, modeling and measurement*. Applied Geochemistry, 2007. **22**: p. 249-275.
34. Goldberg, S., Criscenti, L.J., *Modeling adsorption of metals and metaloids by soil components*, in *Processes of heavy metals and metalloids in soil environments*, A. Violante, Huang, P M., Gadd, G.M., Editor. 2008, John Wiley & Sons, Inc.
35. Toreci, I., Tezel, F.H., Yong, Y., Sayari, A., *Adsorption separation of methyl chloride from nitrogen using ZSM-5 and mesoporous SBA-15*. Adsorption Science and Technology, 2006. **24**(1): p. 79-99.
36. Toreci, I., *Adsorption separation of methyl chloride from air*, in *Chemical Engineering*. 2004: University of Ottawa.
37. Yao, C. and T. Chen, *A new simplified method for estimating film mass transfer and surface diffusion coefficients from batch adsorption kinetic data*. Chemical Engineering Journal, 2015. **265**(0): p. 93-99.
38. Klaewkla, R., Arend, M., Hoelderich, W.F., *A Review of Mass Transfer Controlling the Reaction Rate in Heterogenous Catalytic Systems*, in *Mass Transfer - Advanced Aspects*, H. Nkajima, Editor. 2011.
39. Ruthven, D.M., *Diffusion in type A zeolites: New insights from old data*. Microporous and Mesoporous Materials, 2012. **162**(0): p. 69-79.
40. Idris, S.A., et al., *Adsorption kinetic study: Effect of adsorbent pore size distribution on the rate of Cr (VI) uptake*. Microporous and Mesoporous Materials, 2013. **165**(0): p. 99-105.
41. Pandey, P.K., Sharma, S.K., Sambi, S.S., *Kinetics and equilibrium study of chromium adsorption on zeolite NaX*. International Journal of Environmental Science and Technology, 2010. **7**(2): p. 395-404.
42. Ho, Y.S., McKay, G., *Application of kinetic models to the sorption of copper(II) on to peat*. Adsorption Science and Technology, 2002. **20**(8): p. 797-814.
43. Romero-Gonzalez, J., Gardea-Torresdey, J.L., Perlta-Videa, J.R., Rodriguez, E., *Determination of equilibrium and kinetic parameters of the adsorption of Cr(III) and*

- Cr(VI) from aqueous solutions to agave lechuguilla biomass*. Bioinorganic Chemistry and Applications, 2005. **3**(1-2): p. 55-68.
44. Qui, H., Lv, L., Pan, B.-c., Zhang, Q.-j., Zhang, W.-m., Zhang, Q.-x., *Critical review in adsorption kinetic models*. Journal of Zhejiang University Science A, 2009. **10**(5): p. 716-724.
45. Al-Meshragi, M., Ibrahim, H.g., Aboabboud, M.M. *Equilibrium and kinetics of chromium adsorption on cement kiln dust*. in *Proceedings of the World Congress on Engineering and Computer Science*. 2008. San Francisco.
46. Cheung, O., et al., *Adsorption kinetics for CO₂ on highly selective zeolites NaKA and nano-NaKA*. Applied Energy, 2013. **112**(0): p. 1326-1336.
47. Nguyen, C., Do, D.D., *Heat of desorption measure by means of electrical heat excitation*. Langmuir, 2001. **17**: p. 2287-2290.
48. Kuo, S.-L., Hines, A.L., *Adsorption of chlorinated hydrocarbon pollutants on silica gel*. Separation Science and Technology, 1988. **23**(4&5): p. 293-303.
49. Ramirez, D., Qi, S., Rood, M.J., *Equilibrium and heat of adsorption of organic vapors and activated carbons*. Environmental Science Technology, 2005. **39**: p. 5864-5871.
50. Kuo, S.-L., Hines, A.L., Dural, N.H., *Correlation of methyl chloride, methylene chloride, chloroform, and carbon tetrachloride adsorption data on silica gel*. Separation Science and Technology, 1991. **26**(8): p. 1077-1091.
51. Goyal, M., R. Dhawan, and M. Bhagat, *Adsorption of dimethyl sulfide vapors by activated carbons*. Colloids and Surfaces A: Physicochemical and Engineering Aspects, 2008. **322**(1-3): p. 164-169.
52. Kobayashi, Y., et al., *Adsorption isotherms of methanol and dimethyl ether on SAPO-34 measured together with differential adsorption heat measurement*. Chinese Journal of Catalysis, 2013. **34**(12): p. 2192-2199.
53. Garbacz, J.K., Rychlicki, G., Terzyk, A.P., *A comparison of isosteric and differential heats of gas adsorption on microporous active carbons*. Adsorption Science and Technology, 1994. **11**: p. 15-29.
54. Cavalcante, J.C., *Industrial adsorption separation processes: fundamentals, modelling and application* Latin America Applied Research, 2000: p. 357-364.
55. Rezaei, F., Webley, P., *Structured adsorbents in gas separation processes*. Separation and Purification Technology, 2010. **70**: p. 243-256.
56. Leofanti, G., et al., *Catalyst characterization: characterization techniques*. Catalysis Today, 1997. **34**(3-4): p. 307-327.
57. Chilver, C.H., Pentchev, I., Weinberger, B., Lamari, F.D., *A comparison between the different methods for measurement of an excess adsorption of pure gases on porous adsorbents at high pressure*. Journal of the University of Chemical Technology and Metallurgy, 2007. **42**: p. 77-84.
58. Webb, P.A., *Introduction to chemical adsorption analytical techniques and their applications to catalysis*. MIC Technical Publications, 2003: p. 1-10.
59. Mulgundmath, V.P., Kunkel, M., Tezel, F.H., Golden, T.C., Mogan, J., Morin, B., *Adsorption equilibrium parameters of trace impurities*. Separation Science and Technology, 2009: p. 874-893.
60. Keller, J.U., Staudt, R., *Experimental Methods and Adsorption Isotherms*. 2005, Boston, USA: Springer Science + Business Media Inc.
61. Webb, P.A., *Volume and density for particle technologists*. Micrometrics Instrument Corp., 2001. **6**: p. 1-22.
62. Rouquerol, J., Avnir, D., Fairbridge, C.W., Everett, D.H., Haynes, J.H., Pernicone, N., Ramsay, J.D.F., Sing, K.S.W., Unger, K.K., *Recommendations for the characterization of porous solids*. International Union of Pure and Applied Chemistry, 1994. **66**: p. 1739-1758.
63. Malbrunot, P., Vidal, D., Vermesse, J., *Adsorbent helium density measurement and its effect on adsorption isotherms at high pressure*. Langmuir, 1997. **13**: p. 539-544.

64. Ozdemir, E., *Chemistry of the adsorption of carbon dioxide by argonne premium coals and a model to simulate CO₂ sequestration in coal seams*, in *School of Engineering*. 2004, University of Pittsburgh.
65. Setoyama, N., Kaneko, K., *Density of He adsorbed in micropores at 4.2K*. Adsorption, 1995. **1**: p. 165-173.
66. Bae, Y.-S., Yazaydm, A.O., Snurr, R.Q., *Evaluation of the BET method for determining surface areas of MOFs and zeolites that contain ultra-micropores*. Langmuir, 2010. **26**(8): p. 5475-5483.
67. Zarchy, A.S., Maurer, R.T., Chao, C.C., *Process for separation and recovery of methyl chloride from vent streams containing isobutane*. 1995, Uop: U.S.A. p. 1-6.
68. Mariwala, R.K., Foley, H.C. , *Calculation of micropore sizes in carbogenic materials from the methyl chloride adsorption isotherm*. Industrial & Engineering Chemistry Research, 1994. **33**: p. 2314-2321.
69. Cousins, D.S., Laesecke, A., *Sealed gravitational capillary viscometry of dimethyl ether two next-generation alternative refrigerants*. Journal of Research of the National Institute of Standards and Technology, 2012. **117**: p. 231-256.
70. Smith, J., Van Ness, H., Abbott, M., *Introduction to Chemical Engineering Thermodynamics*. Chemical International Edition. 2005, New York: McGraw-Hill
71. Sudibandriyo, M., Pan, Z., Fitzgerald, J.E., Robinson-Jr, R.L., Gasem, K.A.M., *Adsorption of methane, nitrogen, carbon dioxide and their binary mixtures on dry activated carbon at 318.2 K and pressures up to 13.6 MPa*. Langmuir, 2003. **19**: p. 5323-5331.
72. Kumar, A., *Adsorption of methane on activated carbon by volumetric method*, in *Chemical Engineering*. 2011, National Institute of Technology, Rourkela: India.
73. Geldart, D., *Gas Fluidization Technology*, ed. Wiley. 1986, New York.
74. Walker, P.L., Lamond, T.G., Metcalfe, J.E., *The preparation of 4A and 5A carbon molecular sieves*. Carbon and Graphite, 1966: p. 7-12.
75. Triebe, R.W., Tezel, F.H., Khulbe, K.C., *Adsorption of methane, ethane and ethylene on molecular sieve zeolites*. Gas Separation & Purification, 1996. **10**(1): p. 81-84.
76. Purewal, J., *Hydrogen adsorption by alkali metal graphite intercalation compounds*. 2010, Institute of Technology Pasadena: California.
77. Semelsberger, T.A., *Steam reforming of dimethyl ether for generating hydrogen-rich fuel-cell feeds*, in *Chemical Engineering*. 2005, Case Western Reserve.
78. Atkins, P., Paula, J.D., *Physical chemistry*. Vol. 8. 2006, Oxford: University Press.
79. Jaumain, D. and B.-L. Su, *Monitoring the Brønsted acidity of zeolites by means of in situ FT-IR and catalytic testing using chloromethane as probe molecule*. Catalysis Today, 2002. **73**(1-2): p. 187-196.
80. Choma, J., kloske, M., Jaroniec, M., *An imporved methodology for adsorption characterization of unmodified and modified silica gels*. Journal of Colloid and Interface Science, 2003. **226**: p. 168-174.
81. Goldstein, J.I., Newbury, D.E., Joy, D.C., Echlin, P., Lifshin, E., Sawyer, L., Michael, J.R., *Scanning electron microscopy and x-ray microanalysis*. 3e ed. 2003, New York: Plenum Press.
82. Hossain, M.A., Kumita, M., Mori, S., *SEM characterization of the mass transfer of Cr(VI) during the adsorption on used black tea leaves*. African Journal of Pure and Applied Chemistry, 2010. **4**(7): p. 135-141.
83. Zholobenko, V., Garforth, A., Dwyer, J., *TGA-DTA study on calcination of zeolitic catalysts*. Thermochimica Acta, 1997. **294**: p. 39-44.
84. Wang, X.L., Chua, H.T., Gao, L.Z., *A thermogravimetric analyzer for condensible gas adsorption under subatmospheric conditions*. Journal of Thermal Analysis and Calorimetry, 2007. **90**: p. 935-940.
85. Tabirizy, V.A., Denoyel, R., Hamouda, A.A., *Characterization of wettability alteration of calcite, quartz and kaolinite: surface energy analysis*. Colloids and Surfaces A: Physicochemical and Engineering Aspects, 2011. **384**: p. 98-108.

86. Wei, Y., et al., *Mechanistic elucidation of chloromethane transformation over SAPO-34 using deuterated probe molecule: A FTIR study on the surface evolution of catalyst*. Chemical Physics Letters, 2007. **444**(1-3): p. 197-201.
87. Khaleel, A., I. Shehadi, and A. Al-Marzouqi, *Catalytic conversion of chloromethane to methanol and dimethyl ether over mesoporous γ -alumina*. Fuel Processing Technology, 2011. **92**(9): p. 1783-1789.
88. Jiang, X.Z., *In-situ FTIR studies of dimethyl ether adsorption on H-ZSM-5 zeolites*. Chinese Journal of Chemistry, 1996. **14**: p. 497-505.
89. Forester, T.R., Howe, R.F., *In situ FTIR studies of methanol and dimethyl ether in ZSM-5*. Journal of the American Chemical Society, 1987. **109**: p. 5076-5082.
90. Anderson, J.A., Rochester, C.H., *Infrared study of the adsorption of 1,2-Dimethoxyethane on silica*. Journal of the Chemical Society, Faraday Transactions 1, 1989. **85**(10): p. 3505-3512.
91. Knowlton, G.D., White, T.R., *Thermal study of types of water associated with clinoptilolite* Clays and Clay Minerals, 1981. **29**: p. 403-411.
92. Zhuravlev, L.T., *The surface chemistry of amorphous silica. Zhuravlev model*. Colloids and Surfaces A: Physicochemical and Engineering Aspects, 2000. **173**: p. 1-38.
93. Lamia, N., Granato, M., Gomes, P., Grande, C., Wolff, I., Leflaive, P., *Propane/Propylene separation by simulated moving bed II. Measurement and prediction of binary adsorption equilibria of Propane, Propylene, Isobutane and 1-Butene on 13X zeolite*. Separation Science and Technology, 2009. **44**: p. 1485-1509.
94. Post, H.W., von Plessen, H., Lendle, W., , *Process for the removal of dimethyl ether in methyl chloride*. 1988.
95. Roth, P., Leistner, E., Haverkamp, H., Wendal, W., Kleiber, M. , *Process for the separation of dimethyl ether and chloromethane mixtures*. 1999: U.S.A. p. 1-5.
96. Kobayashi, Y., et al., *Species surface concentrations on a SAPO-34 catalyst exposed to a gas mixture*. Chinese Journal of Catalysis, 2014. **35**(3): p. 430-436.
97. Reyes, S.C., Krishnan, V.V., Demartin, G.J., Sinfelt, J.H., Strohmaier, K.G., Santiesteban, J.G., , *Separation of methanol, ethanol and/or dimethyl ether from hydrocarbon mixtures*. 2005.
98. Nagji, M.M., Corvini, G., *Process for the removal of dimethyl ether contained as an impurity in liquid olefinic C3-C5 feeds*. 1987.
99. Smith Jr. L.A.; Jones, E.M., Hearn, D., *Method for removal of dimethyl ether and methanol from C4 hydrocarbon streams*. 1992: U.S.A. p. 1-6.
100. Robinson, E., Ross, R.A., *Sorption of dimethyl ether on silica gel*. Canadian Journal of Chemistry, 1970. **48**: p. 13-16.
101. Brown, K.A., Ho, W., *The interaction of methyl chloride and Si(100)2 x 1*. Surface Science, 1995. **338**: p. 111-116.
102. Woelke, A., Imanaka, S., Watanabe, S., Goto, S., Hashinokuchi, M., Okada, M., Kasai, T., *Dissociative adsorption of methyl chloride on Si(001) studied by scanning tunneling microscopy*. Journal of Electron Microscopy, 2005: p. 21-24.
103. Bugyi, L. and F. Solymosi, *Adsorption and dissociation of dimethyl ether on clean and oxygen-dosed Rh(111)*. Surface Science, 1997. **385**(2-3): p. 365-375.
104. Farkas, A.P., Solymosi, F., *Adsorption and reaction of dimethyl and diethyl ethers on Mo2C/Mo(100)*. Surface Science, 2008. **602**: p. 1497-1506.
105. Kasahara, T. and K. Itoh, *Infrared reflection absorption spectroscopic study of the adsorption structures of dimethyl ether and methyl ethyl ether on Cu(100) and Ag(100)*. Surface Science, 2007. **601**(4): p. 1054-1063.
106. Leuty, G.M., Abu-Nada, A., Tsige, M., *Multilayer adsorption of methane and chloromethane on the Molybdenum (100) surface*. The Journal of Physical Chemistry C, 2012. **116**: p. 14514-14525.
107. Pearce, J.N., Reed, G.H., *The heat of adsorption of certain organic vapours by charcoal at 25°C and 50°C*. Journal of American Chemistry Society, 1924: p. 905-914.
108. Pearce, J.N., Johnstone, H.F., *The adsorption of the vapors of methane and its chlorine derivatives by activated charcoal*. Journal of Physical Chemistry, 1926: p. 1260-1279.

109. Wu, J., Ma, L., Zhao, H., Wang, Z., *The separation of chloromethane mixtures and the recovery of dichloromethane, chloroform and carbon tetrachloride by activated carbon fibre*. Adsorption Science and Technology, 2002. **20**(2): p. 169-177.
110. Ali, A.-K., M., Saleh, J.M., Hikmat, N.A., *Adsorption, decomposition and surface reactions of methyl chloride on metal films of iron, nickel, palladium, lead, gold and copper*. Journal of Chemical Society, 1987. **83**(8): p. 2391-2406.
111. Borgmann, W., Kunkel, J., Fritz, H., Lauermann, G., Walzl, R., Muller, K., *Methods for separating dimethyl ether from an olefin-containing product stream*. 2003: USA.
112. Tamagawa, K., et al., *Molecular structure of dimethylether as determined by a joint analysis of gas electron diffraction and microwave spectroscopic data*. Journal of Molecular Structure, 1984. **125**(1-2): p. 131-142.
113. Preuss, M., Schmidt, W.G., Seino, K., Bechstedt, F., *Methylchloride adsorbed on Si(001): an ab initio study*. Applied Surface Science, 2004. **234**: p. 155-161.
114. Lad, J.B. and Y.T. Makkawi, *Adsorption of dimethyl ether (DME) on zeolite molecular sieves*. Chemical Engineering Journal, 2014. **256**(0): p. 335-346.
115. Kobayashi, Y., Li, Y., Wang, Y., Wang, D. , *Adsorption isotherms of methanol and dimethyl ether on SAPO-34 measured together with differential heat measurement*. Chinese Journal of Catalysis, 2013. **34**: p. 2192-2199.
116. Azizian, S., *Kinetic models of sorption: a theoretical analysis*. Journal of Colloid and Interface Science, 2004. **276**(1): p. 47-52.
117. Gallagher, P.K., *Handbook of thermal analysis and calorimetry*, ed. P.K. Gallagher. Vol. 5. 2008, The Netherlands: Elsevier.
118. Yeo, Y.Y., Vattuone, L., King, D.A., *Calorimetric heats for CO and oxygen adsorption and for the catalytic CO oxidation reaction on Pt{111}*. Journal of Physical Chemistry, 1997. **106**(1): p. 392-401.
119. McDonald, R.S., *Surface functionality of amorphous silica by infrared spectroscopy*. Journal of American Chemistry Society, 1958. **62**: p. 1168-1178.
120. Kowalczyk, H., Rychlicki, G., Terzyk, A.P., *Low coverage adsorption of methanol, ethanol and carbon tetrachloride on homo and heterogeneous surface. Differential heat and integral molar entropy*. Polish Journal of Chemistry, 1993. **67**: p. 2019-2028.
121. Sing, K.S., Everett, D.H., Haul, R.A.W., Moscou, L., Pierotti, R.A., Rouquerol, J., Siemieniewsha, T., *Reporting physisorption data for gas/solid systems with special reference to the determination of surface area and porosity*. Pure Applied Chemistry, 1985. **57**: p. 603-619.
122. Belyakova, L.A., Varvarin, A.M., *Surfaces properties of silica gels modified with hydrophobic groups*. Colloids and Surfaces A: Physicochemical and Engineering Aspects, 1999. **154**: p. 285-294.
123. Arnold, C., *Zeolites in VOC abatement and industrial waste gas purification*, in *Zeolites in Chemical Engineering*, A. Chemie-Bertung, Editor. 2014.
124. Bakhtyari, A.M., M., *Pure and binary adsorption equilibria of methane and nitrogen on zeolite 5A*. Journal of Chemical Engineering Data, 2014. **59**: p. 626-639.
125. Wu, J.Y.L., Q.L.; Xiong, Y.; Zhu, A.M.; Chen, Y., *Molecular simulation of water/alcohol mixtures' adsorption and diffusion in zeolite 4A membranes*. Journal of Physical Chemistry B, 2009. **113**: p. 4267-4274.
126. Mofarahi, M.S., M., *Pure and binary adsorption isotherms of nitrogen and oxygen on zeolite 5A*. Journal of Chemical Engineering Data, 2009. **54**: p. 916-921.
127. Harlick, P.J.E., Tezel, F.H., *Adsorption of carbon dioxide, methane and nitrogen: pure and binary mixture adsorption by ZSM-5 with SiO₂/Al₂O₃ ratio of 30*. Separation Science and Technology, 2002. **31**(1): p. 33-60.
128. Romero-Perez, A., Aguilar-Armenta, G., *Adsorption kinetics and equilibria of carbon dioxide, ethylene, and ethane on 4A (CECA) zeolite*. Journal of Chemical Engineering Data, 2010. **55**: p. 3625-3630.
129. Grande, C.A., Gigola, C., Rodrigues, A.E., *Propane-propylene binary adsorption on zeolite 4A*. Adsorption 2003. **9**: p. 321-329.

130. Shang, J.L., G.; Singh, R.; Gu, Q., Nairn, K.M.; Bastow, T.J.; Medhekar, N.; Doherty, C.M.; Hill, A.J.; Liu, J.Z.; Webley, P.A., *Discriminative separation of gases by a "Molecular Trapdoor" mechanism in chabazite zeolites*. Journal of American Chemistry Society, 2012. **134**: p. 19246-19253.
131. Reid, C.R., ; Thomas, K.M., *Adsorption kinetic and size exclusion properties of probe molecules for the selective porosity in a carbon molecular sieve used for air separation*. Journal of physical Chemistry B, 2001. **105**: p. 10619-10629.
132. Mulgundmath, V.P., Tezel, F.H., Hou, F., Golden, T.C., *Binary adsorption behaviour of methane and nitrogen gases*. Journal of Porous Material, 2012. **19**: p. 455-464.
133. Saburina, E.B., Begun, L.B., *Desorption of methyl chloride and dimethyl ether from microporous adsorbents by an inert gas*. Zhurnal Prikladnoi Khimii, 1989. **62**: p. 847-849.
134. Schmidt, S.A., Kumar, N., Reinsdorf, A., Eranen, K., Warna, J., Murzin, D.Y., Salmi, T., *Methyl chloride synthesis over Al_2O_3 catalyst coated microstructured reactor- Thermodynamics, kinetics and mass transfer*. Chemical Engineering Science, 2013. **95**: p. 232-245.